Final Report 930-307

FATIGUE OF DIAPHRAGM-GIRDER CONNECTIONS

Prepared by

J. Michael Stallings
Thomas E. Cousins
J. W. Tedesco

APRIL 1996

TECHNICAL REPORT STANDARD TITLE PAGE

1. Report No.	2. Government Accession No.	3. Recipient's Catalog No.
4. Title and Subtitle Fatigue of Diaphragm-Girder Connections		5. Report Date April 1996 6. Performing Organization Code
7. Author(s) Stallings, J. Michael, Cousins, Thomas E., Tedesco, J. W.		8. Performing Organization Report No.
9. Performing Organization Name and Address Auburn University Highway Research Center 238 Harbert Engineering Center Auburn, AL 36849-5337		10. Work Unit No. 11. Contract or Grant No. 930-307 13. Type of Report and Period Covered Final
12. Sponsoring Agency Name and Address Alabama Department of Transportation Research and Development Bureau 1409 Coliseum Boulevard Montgomery, AL 36130-3050		14. Sponsoring Agency Code
15. Supplementary Notes		

16. Abstract

Distortion-induced fatigue cracking has occurred at hundreds of diaphragm-girder connections in multi-girder steel bridges in Birmingham, Alabama in recent years. The research goal was an improved maintenance strategy for repair and maintenance of the bridges so the potential for future cracking is minimized. The investigation included field measurements of distortion-induced stresses at connections, field measurements of the effects of removing diaphragms from two in-service bridges, structural evaluations of typical bridge designs, Finite Element Method analyses of typical bridge designs, and laboratory testing of bolted connections.

Results indicate interior diaphragms can be removed from many existing bridges without significant negative effects. Guidelines for evaluating candidate bridges were developed for both simple spans and continuous spans. A bolted connection was designed, installed in the field, and tested. Tests confirmed the new design performed better than the original design.

17. Key Words	18. Distribution Statement
Bridges, fatigue, tests, diaphragms, load distribution	No Restriction

19. Security Classif. (of this report)	20. Security Classif. (of this page)	21. No. of Pages	22. Price
None	None	327	

Form DOT F 1700.7 (8-69)

ACKNOWLEDGEMENT

The material contained herein was obtained or developed in connection with a research project, "Fatigue of Diaphragm-Girder Connections," RP 930-307, conducted by the Highway Research Center at Auburn University. The research project was sponsored by the Alabama Department of Transportation (ALDOT) and the Federal Highway Administration (FHWA). Traffic control, bridge inspection vehicles, test load vehicles and operators for the field testing, and manpower and equipment for removal of diaphragms from existing bridges were provided by the Alabama Department of Transportation Maintenance Bureau and Third Division. Fatigue testing equipment was purchased with funding from the sponsors. The support, interest, cooperation, and assistance of many personnel from ALDOT and FHWA is gratefully acknowledged. Much work by graduate students Matthew D. Bell, Daniel G. Davis, David A. Lower, Nathan M. Porter, Thomas E. Stafford, and Dennis Tow is gratefully acknowledged.

DISCLAIMER

SUMMARY

Construction of the interstate highway system through downtown Birmingham began in the late 1960's, and multi-girder steel bridges were used extensively. In most bridges, rolled W-shapes were used for girders and rolled channels for the diaphragms. The diaphragm-girder connections were typically made of a flat plate shop welded to the girder web and field welded to the diaphragm. The diaphragm connection plates were not attached to the girder flanges because welding to a tension flange was discouraged in common design practice at that time.

Over the last six years bridge inspectors have discovered distortion-induced fatigue cracks in the welds, connection plates, diaphragms, and girder webs at hundreds of the diaphragm-girder connections in the Birmingham bridges. Repairs included removing cracked welds, drilling holes at crack tips, and replacing welded connections with a bolted angle connection. Subsequent bridge inspections revealed that holes drilled at crack tips were ineffective at some connections, and fatigue cracks had initiated in many of the bolted connection angles after only two years in-service.

The project goal was to develop an improved maintenance strategy for repairing diaphragm-girder connections and maintaining the bridges so that the potential for future cracking is minimized. The following options were investigated: continued use of holes drilled at the tips of web cracks, removal of interior diaphragms to eliminate diaphragm-girder connections, and redesign of the bolted connection angle to improve the fatigue life. The investigations included field measurements of distortion-induced stresses at connections, field measurements of the effects of removing diaphragms from two in-service bridges, structural evaluations of typical bridge designs, Finite Element

Method analyses of typical bridge designs to evaluate the effects of removing diaphragms, and laboratory testing of bolted diaphragm-girder connections.

Results of the research indicate interior diaphragms can be removed from existing bridges without significant negative effects. Guidelines for evaluating candidate bridges were developed for both simple spans and continuous spans. Evaluations of five typical designs were performed which indicate that all interior diaphragms can be remove from the (two) simple span bridges investigated and approximately half the interior diaphragms can be removed from the (three) continuous span bridges investigated.

The cause of the fatigue cracking in the original bolted connection angles used in repairs was identified, and a new design was developed. Laboratory tests and field measurements confirmed that the fatigue performance of the new design was better than that of the original design. The new design is proposed for use at connections where diaphragms are not removed.

TABLE OF CONTENTS

List of Figures

List of Tables

CHAPTER ONE

INTRODUCTION

BACKGROUND

Multi-girder steel bridges are common along the state and interstate highway systems throughout the United States. The steel girders span in the direction of traffic flow from bent to bent and serve as the primary load carrying members. The structural system is tied together by a reinforced concrete deck slab and transverses steel members, or diaphragms, that are connected to the girders. Diaphragms at the girder supports provide resistance to transverse traffic and wind loadings. Interior diaphragms stabilize the girders during construction and placement of the deck, and also serve to some extent to distribute traffic loads transversely among the girders.

Construction of the interstate highway system through downtown Birmingham began in the late 1960's, and multi-girder steel bridges were used extensively. Primarily rolled W-shapes were used for girders and rolled channels for the diaphragms as shown in Figure 1.1. The diaphragm-girder connection in the original construction typically consisted of a plate field welded to the channel diaphragm and shop welded to the girder web. A typical connection is shown in Figure 1.2. Some connections were made using an angle welded to the girder web instead of a flat plate. The diaphragm connection plates were not attached to the girder flanges because welding to a tension flange was discouraged in common design guides at that time.

Over the last six years bridge inspectors have discovered fatigue cracking in the welds and base metal in many of the welded diaphragm-girder connections. Cracks have been discovered in the welds connecting the diaphragm to the connection plate,

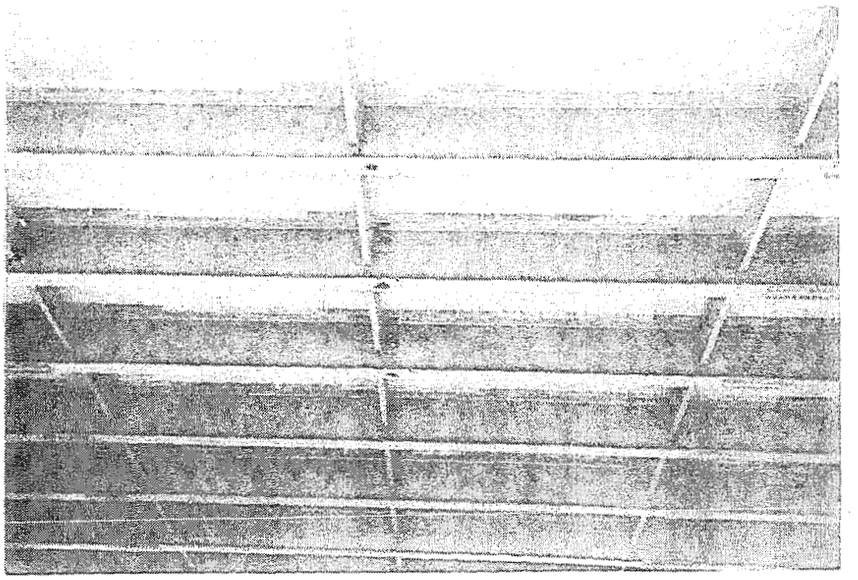

Figure 1.1. Typical Lines of Channel Diaphragms

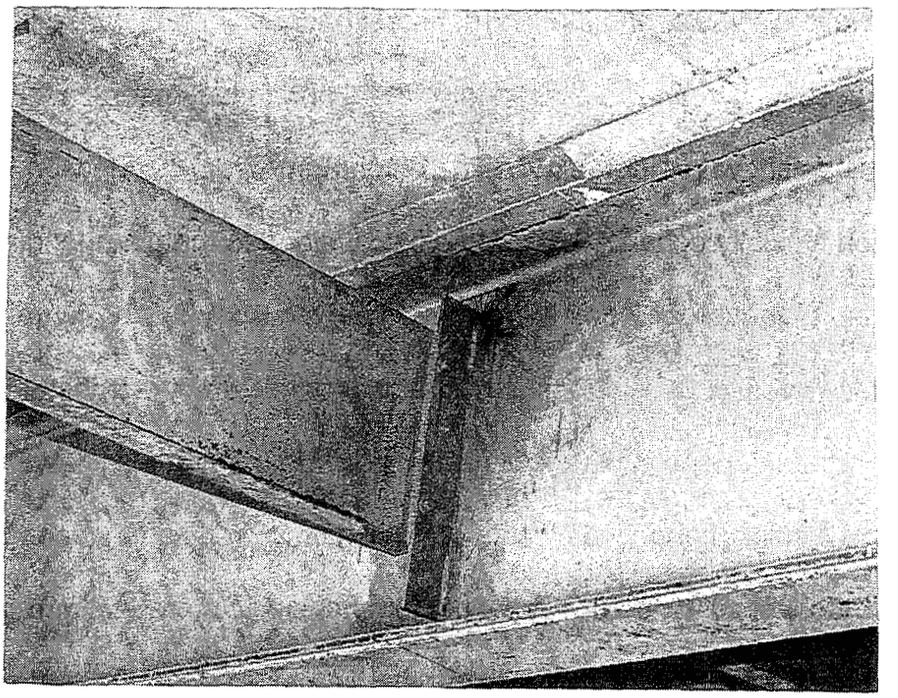

Figure 1.2. Welded Plate Diaphragm-Girder Connection

in the welds connecting the connection plate to the girder web and in the girder web. Cracking in the girder web, as illustrated in Figure 1.3, poses the greatest threat to the longevity of the bridges. Fatigue cracks develop at diaphragm-girder connections due to secondary live load forces created by differential deflections between the girders. These secondary live load forces cause out-of-plane distortion of the girder web which leads to distortion-induced stresses in the web and in the welds of the connection.

In the past the Alabama Department of Transportation (ALDOT) used three basic techniques to repair fatigue cracking at diaphragm-girder connections. Short cracks in welds were removed by grinding. More extensive weld cracks and cracked connection plates were repaired by removing the original welded connection and installing an angle bolted to the diaphragm and girder web as shown in Figure 1.4. Subsequent bridge inspections revealed cracking in many of these angles, as illustrated in Figure 1.5, due to bending of the angle leg bolted to the girder web. Distortion-induced cracks in the girder web were repaired by drilling a 19 mm to 25 mm diameter hole to remove the crack tips. This was ineffective at some locations as illustrated in Figure 1.6 by the fatigue cracks which have extended beyond the holes. Connections with significant weld cracks and web cracking were repaired by a combination of drilling holes in the web at crack tips and replacing the connection with a bolted angle connection.

Total repair costs for fatigue cracking at diaphragm-girder connections were approximately $8 million at the time this research project started. This large maintenance cost resulted from fatigue cracking at hundreds of connections. The cost of repairs, recognition that hundreds of additional connections may experience similar

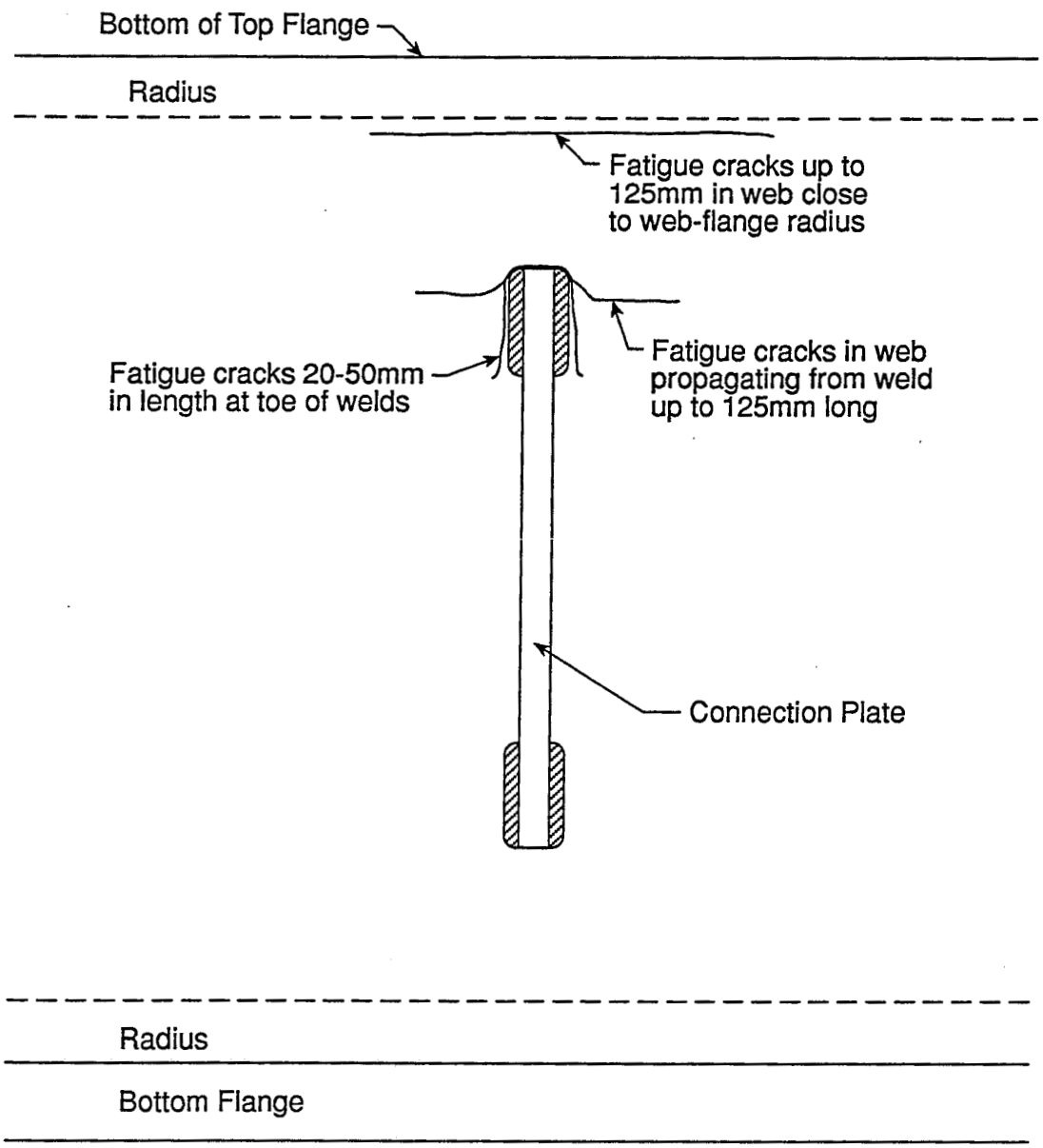

Figure 1.3. Typical Web Gap Cracks

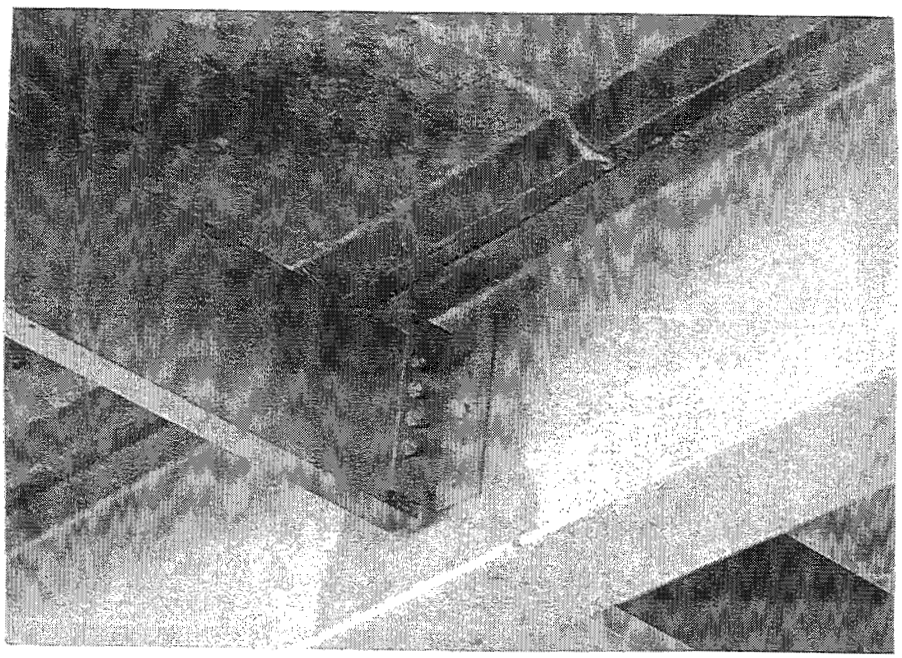

Figure 1.4. Bolted Angle Connection

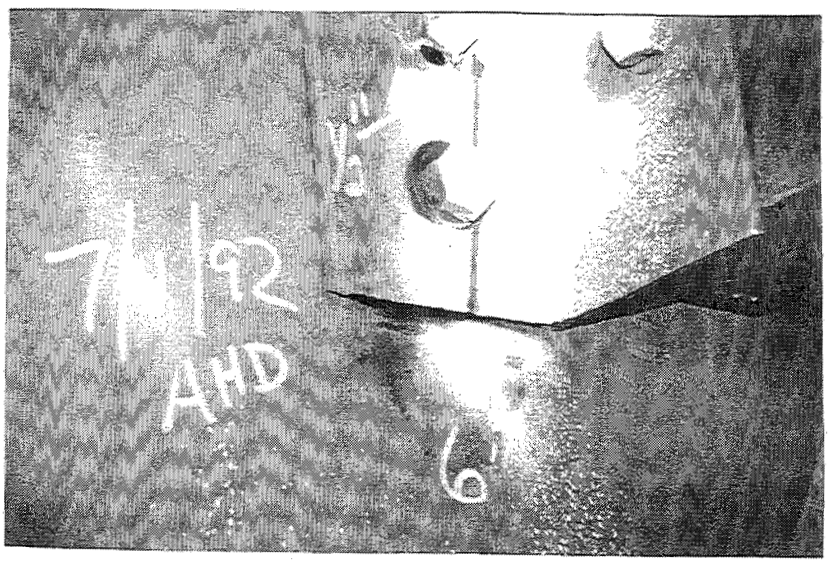

Figure 1.5. Typical Fatigue Crack in Existing Bolted Connection Angles

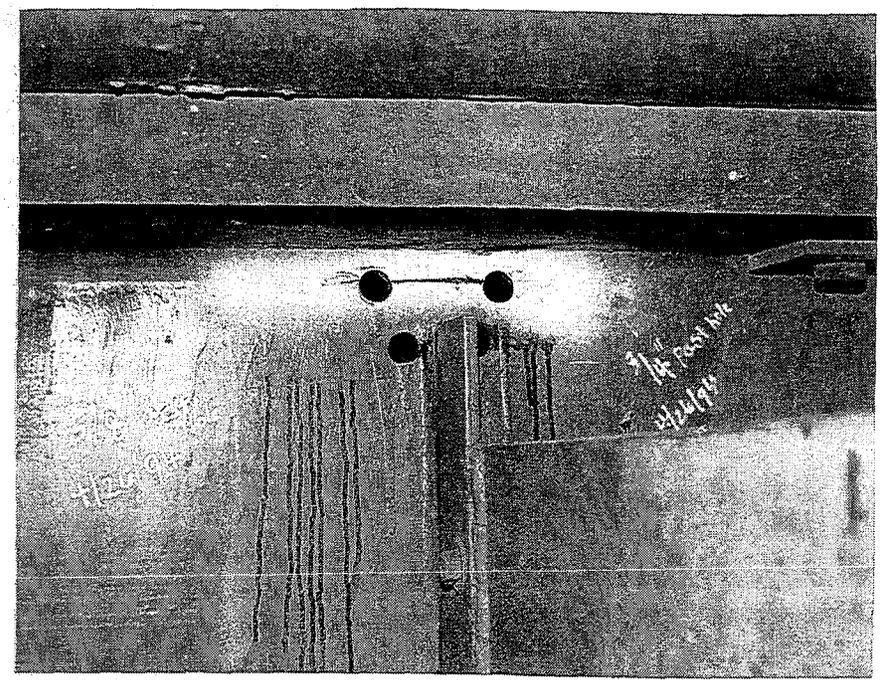

Figure 1.6. Web Cracks at Welded Plate Connection with Drilled Hole Repair

problems, and concern that the repairs being performed were not permanent provided motivation for this research.

PROJECT OBJECTIVES

The overall goal of this project was to develop a maintenance strategy for repairing fatigue cracking at diaphragm-girder connections and maintaining the bridges so that the potential for future fatigue cracking is minimized. Specific objectives were to investigate the following maintenance options: complete or partial removal of interior diaphragms, continued use of hole drilling to repair web cracks, and relocation and/or redesign of bolted connection angles. A description of the options is given below along with the methodology used to evaluate each one.

Holes Drilled at Crack Tips

Past laboratory tests by Fisher et al. (1990) indicate that drilling a hole at the tip of a distortion-induced fatigue crack is an effective repair under certain stress conditions. Inspections of bridges in Birmingham just prior to the start of this project revealed cracks propagating beyond the holes at approximately five percent of the connections where holes were drilled. This could result from missing the crack tip when the hole was drilled or from re-initiation of the crack as a result of very high distortion-induced stresses. One objective of this project was to use field measurements of stresses at several connections to evaluate the potential for successful permanent arrest of distortion-induced web cracks. The evaluation was performed using field measurements of distortion-induced stresses at 13 different welded connections in various bridges around the Birmingham area. A summary of the field measurements and evaluations is provided in Chapter Two of this report and more complete details are given in an Interim Report, Stallings et al. (1995).

Diaphragm Removal

Diaphragms have been required in multi-girder steel bridges at a spacing no greater than 7.6 m since 1944 by the American Association of State Highway and Transportation Officials' *Standard Specifications for Highway Bridges* (1944). The 7.6 m limit was apparently an arbitrary limit which was possibly based on construction requirements. Early experts such as Newmark (1948) recognized that diaphragms had only a small effect on the performance of a bridge after the concrete deck was completed.

The goal here is to identify conditions where diaphragms can be removed from existing bridges to eliminate diaphragm-girder connections where fatigue cracking is a problem. By eliminating the connection, the fatigue problem is solved.

Several parallel efforts were undertaken to investigate the effects of diaphragm removal. Structural evaluations were performed for five typical bridges. These evaluations, reported in Chapter Four, included a load rating analysis, wind load analysis, and a lateral-torsional buckling analysis for continuous span bridges. The results of the evaluations illustrate the effects of diaphragm removal with standard engineering calculations. The structural evaluations provide a methodology for evaluating other bridges where diaphragm removal is desirable. Appendix A and B outline the methods and provide example calculations.

Effects of diaphragm removal were also investigated by field tests. Load tests were performed on two bridges, a long simple span and a three span continuous bridge, before and after all the interior diaphragms were removed. The field tests and results are discussed in Chapters Five and Six. To extend the investigation beyond the practical limits of field tests, Finite Element Method (FEM) analyses were performed on eight bridges which cover a wide range of typical bridge geometries. FEM analyses and results are discussed in Chapter Seven.

Relocation of Diaphragms and Redesign of Bolted Connections

The possibility that complete diaphragm removal may not be feasible for all bridges was recognized before the project began. Results early in the project illustrated that complete removal was not always possible. Logical alternatives include moving the diaphragms to locations where the potential for cracking is minimized and

redesigning the connections to improve the fatigue life. Trade-offs between the costs of moving lines of diaphragms and expected improvements in the fatigue life of proposed new connections narrowed the focus of the research to improving the performance of bolted diaphragm-girder connections.

Field observation of numerous cracked connection angles, such as the one shown in Figure 1.5, indicated that the fatigue crack initiated at the outside surface of the angle in front of the bottom bolt. Fatigue cracks were observed to initiate at the edge of an indentation created by the nut or bolt head during tightening as shown in Figure 1.7, or a short distance in front of the bolt as shown in Figure 1.8. The fatigue crack propagated inward and lengthwise along the angle as illustrated by the shape of the fatigue crack in Figure 1.8. The inward crack propagation resulted from a tensile bending stress at the outside face of the angle caused by the diaphragm pushing on the bottom of the angle. Subsequent field and laboratory test data confirm this conclusion and show this is possible due to the existence of a gap between the inside face of the angle and the girder web as shown in Figure 1.9. The width, or size, of the gap limits how much the diaphragm can push the angle to close the gap, and places a limit on the maximum possible magnitude of the tensile stress range which causes fatigue cracking.

A truck crossing a bridge can cause the diaphragm to push or pull on the bottom of a connection angle based on where the connection is relative to the loaded traffic lane. Generally, all connections undergo some pushing and pulling from truck traffic distributed among the traffic lanes. Field measurements of stresses in angles of the original design show that very heavy trucks pull (or pry) on the bottom of the angle

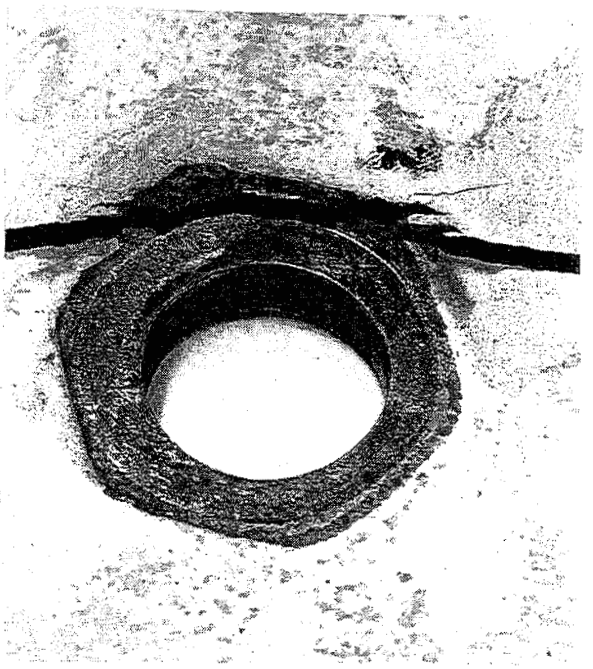

Figure 1.7. Fatigue Crack at Indentation Caused by Bolt Head

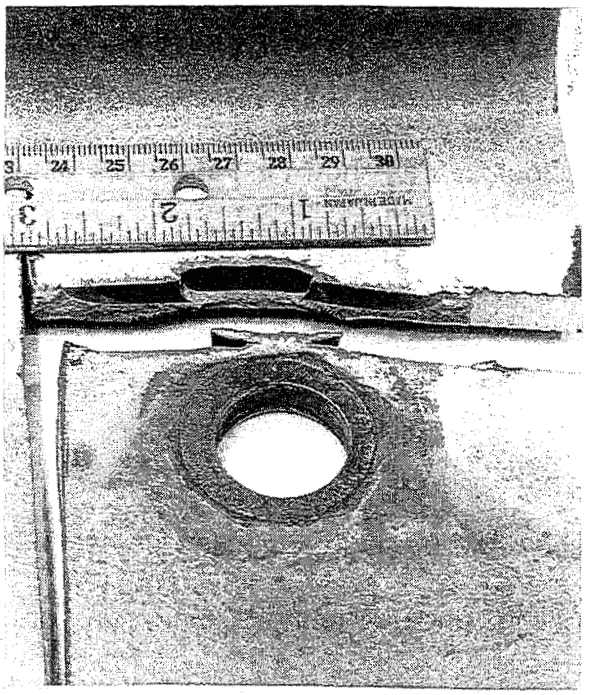

Figure 1.8. Fatigue Crack In Front of Bolt

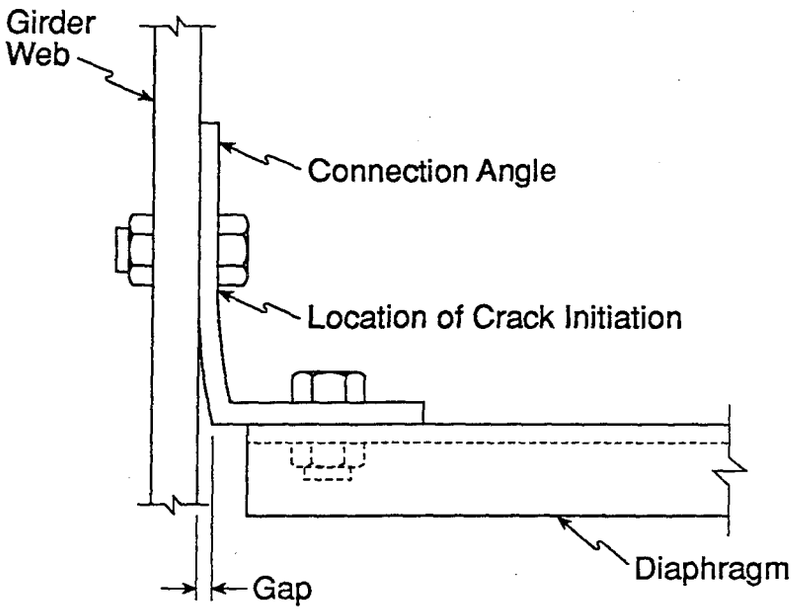

Figure 1.9. Gap Between Connection Angle and Girder Web

sufficiently to cause yielding in front of the bottom bolt. This yielding results in a permanent increase in the width of the gap between the angle leg and the girder web which accelerates fatigue crack initiation.

Based on the observed causes of the cracking and preliminary field and lab test results, a proposed new connection angle design was chosen. The angle leg bolted to the girder web was lengthened to decrease the stress in front of the bottom bolt. The yield strength of the angle was increased from 36 ksi to 50 ksi to limit the size gap that can be created by yielding of the angle. And, a specific installation sequence was developed. By tightening the bolts on the girder web first the gap width between the angle and the girder web is minimized. Tightening the bolts between the diaphragm

and the angle first can create a significant gap when the bolts connecting the angle to the girder web are tightened.

Subsequently, field and laboratory tests were performed as part of this project to evaluate the performance of the new angle relative to former designs. A discussion of the field tests and results is included in Chapter Two. The laboratory tests are discussed in Chapter Three.

CHAPTER TWO

FIELD EVALUATION OF FATIGUE CRACKING

INTRODUCTION

Field tests were conducted during the summers of 1993 and 1994. The first goal of the field tests conducted during the summer of 1993 was to measure typical distortion-induced stresses and girder deflections in multi-girder bridges on the interstate-highways in Birmingham. This information was used to design laboratory tests of bolted diaphragm-girder connections. The second goal was to investigate whether or not fatigue cracking should be expected at previously uncracked web gaps and connection angles. This was accomplished by comparing the measured stresses at uncracked connections with estimated fatigue limits. The next goal was to examine the effectiveness of using holes drilled at the tips of distortion-induced web cracks to stop crack propagation. Stresses measured at uncracked connections were compared to laboratory test results by Fisher et al. (1990) to determine if hole drilling would be effective at these connections. Lower (1995) presents full details of the field investigation conducted during the summer of 1993.

Connections in eight different multi-girder bridges in the Birmingham area were selected for instrumentation and testing. Measurements of girder deflections and distortion-induced stresses and deformations at diaphragm-girder connections were made at each test site. Data were recorded as trucks in normal traffic flow and as calibration trucks (trucks of known size and weight) crossed the bridges.

During the summer of 1994 one of the eight bridges was retrofitted with a new connection angle design. The new angle design was chosen to reduce the magnitude

of stresses in the girder web above the connection and the magnitude of the stresses in the angles which have caused premature failures in other angle designs. By reducing these stresses the service life of the angle is prolonged and the likelihood of the initiation of fatigue cracks in the girder web is reduced. The goal of testing the new connection angle design during the summer of 1994 was to determine if the new connection angle design performed as expected.

Measurements of girder deflections, and distortion-induced stresses and deformations at the new diaphragm-girder connections were made. Data were recorded as trucks in the normal traffic flow and as calibration trucks crossed the bridge. Stafford (1996) presents full details of the field investigation conducted during the summer of 1994.

BRIDGE DESCRIPTIONS

The behavior of diaphragm-girder connections at eight bridge test sites in Birmingham was investigated during the summer of 1993. The types of connections instrumented are illustrated in Figure 2.1. From one to four connections were instrumented at each test site. The first six sites were chosen because they were along segments of the interstate where fatigue cracking was common and contained connections similar to welded plate and bolted angle connections that had already cracked (types A, B, C, and D in Figure 2.1). One design for bolted angle replacement (type D) was used by ALDOT at the first six test sites in previous repairs. The last two test sites were at bridge locations where the design of the replacement connection angles was significantly different (types E and F) from that used at the first six test

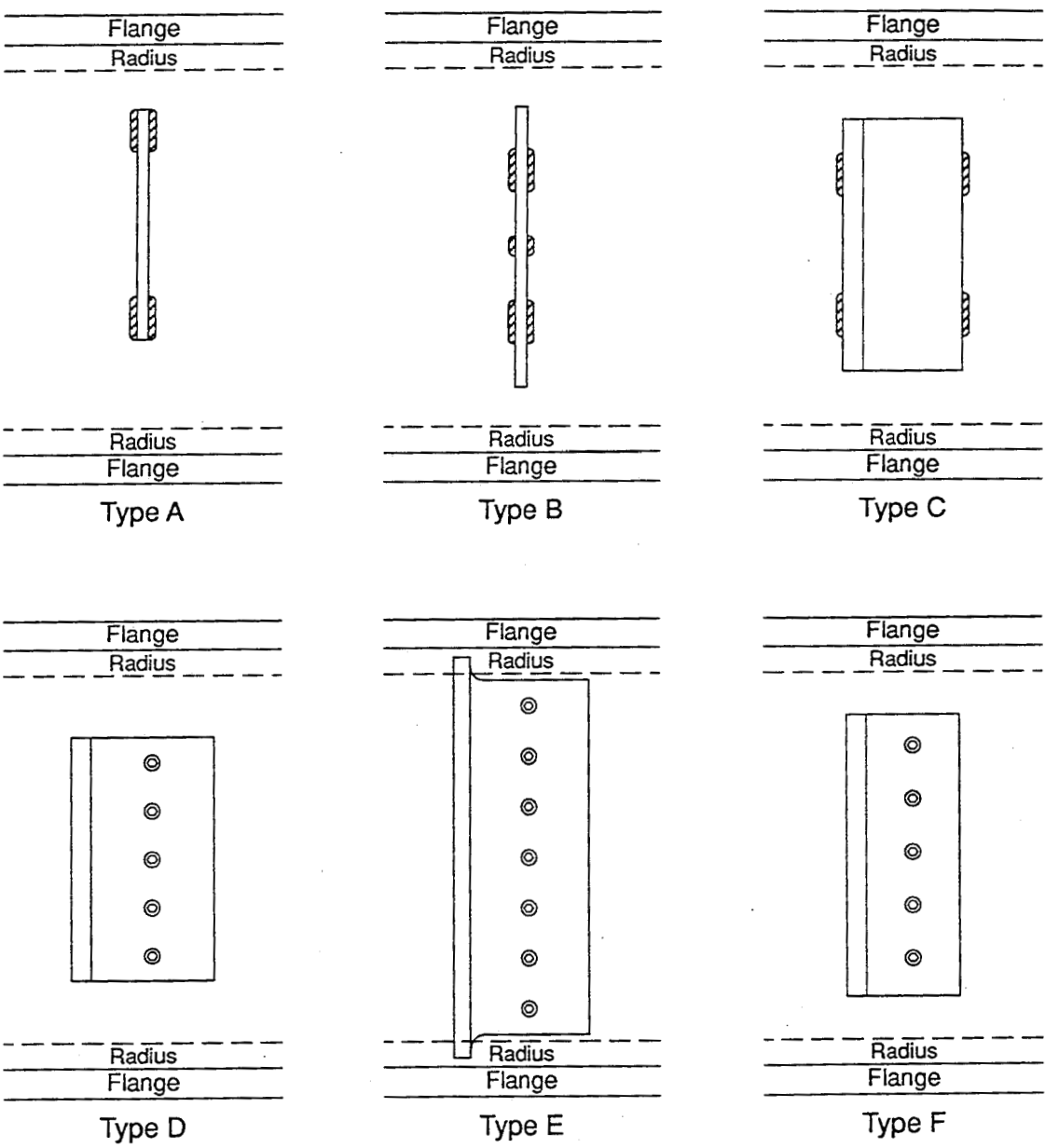

Figure 2.1. Reference Connection Types for Summer of 1993

sites, and no cracking of the replacement angles at the last two test sites has been discovered to date.

Only connections with no fatigue cracks were instrumented. Once cracking has occurred, the stress field in a connection changes and the stress ranges that caused cracking can not be measured. Visual inspections and in some cases dye penetration tests were performed before each connection was instrumented to ensure no fatigue cracks were present.

During the summer of 1994 existing connections and diaphragms were removed and replaced with a new connection angle (type G) at one of the eight test sites instrumented during the summer of 1993. The type G connection is shown in Figure 2.2. The type G connection angle was a L 203 x 152 x 9.52 (mm) by 0.484 m long and was bolted to the girder web at a distance of either 89 mm or 178 mm below the girder top flange.

The eight test sites are given in Table 2.1, and a list of the connection types instrumented at each test site is shown in Table 2.2. Test site number 6 was the location of the testing of the type G connection angles during the summer of 1994. A brief description of each of these testing locations and the corresponding traffic history follows. The traffic histories are based on traffic count data supplied by ALDOT.

The first four test sites were located on the bridge called the I-65 Railroad Viaduct which is located on I-65 in downtown Birmingham. The northbound bridge starts as two simple spans at Second Avenue South and continues North about 1 km as a series of three span continuous, five span continuous, and simple span segments over a network of railroad tracks. The bridge ends with two simple span bridges over

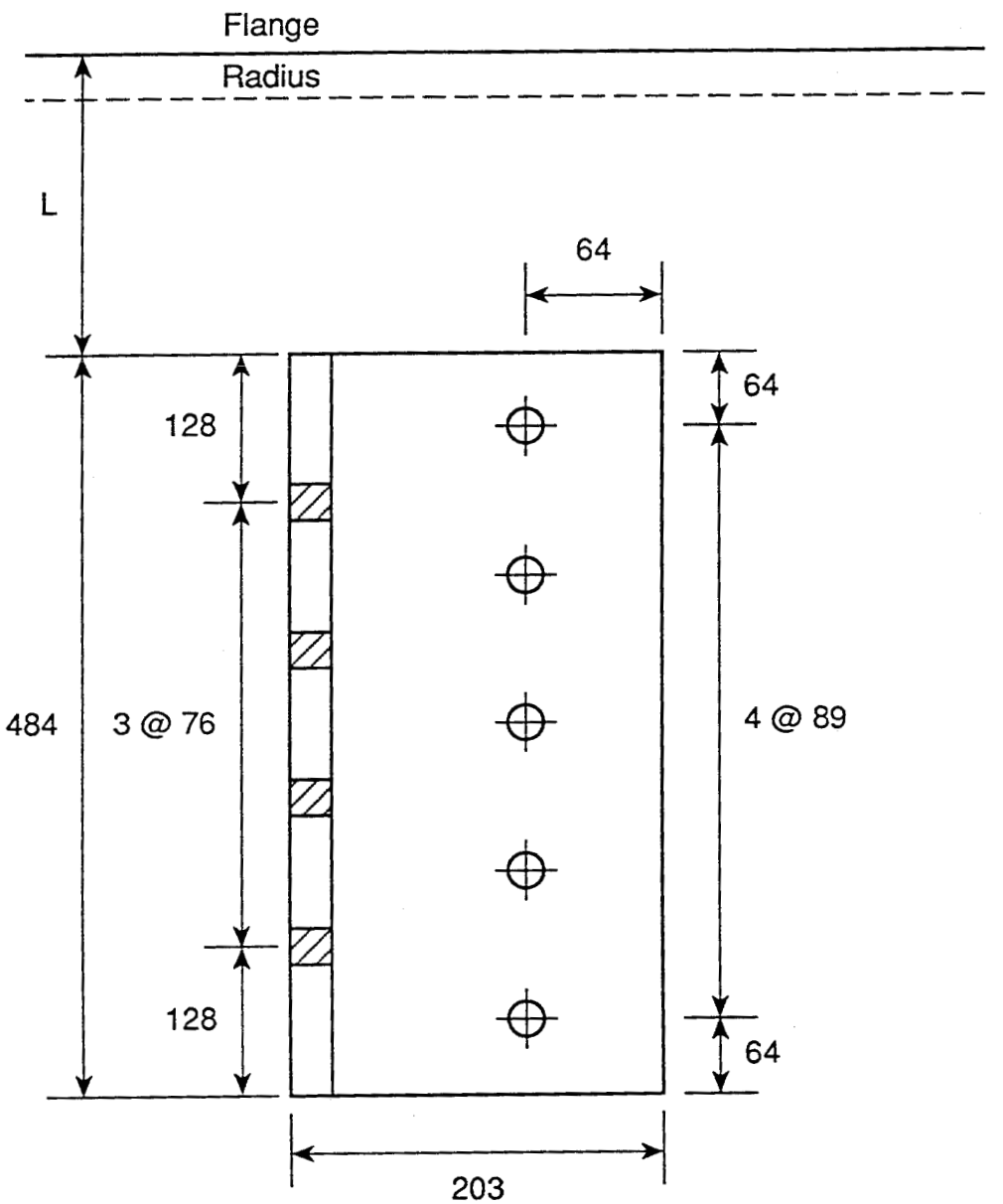

All dimensions in millimeters

Figure 2.2. Type G Connection Angle (L 203 x 152 x 12.7 mm by 0.484 m Long)

Table 2.1. Location of Bridge Test Sites

Location	Interstate	Bridge Name	Length of Span Tested (m)	Girder Spacing (m)	Girder Size	Diaphragm Size	Type of System (Span Lengths, m)
1	I-65	Railroad Viaduct 2nd Av. S to 1st Av. N	20.3	2.44	W920 x 271	MC460 x 63	5 Span Cont. (20, 20, 20, 20, 20)
2	I-65	Railroad Viaduct 2nd Av. S to 1st Av. N	20.4	2.44	W920 x 201	MC460 x 63	5 Span Cont. (20, 20, 20, 20, 20)
3	I-65	Railroad Viaduct 2nd Av. S to 1st Av. N	24.7	2.44	W920 x 289	MC460 x 63	Simply Supported (25)
4	I-65	Railroad Viaduct 2nd Av. S to 1st Av. N	18.8	2.44	W920 x 253	MC460 x 63	5 Span Cont. (19, 19, 19, 19, 19)
5	I-65	16th Avenue S Overpass	26.2	2.21	W920 x 289	MC460 x 63	3 Span Cont. (17, 26, 14)
6	I-59/ I-20	CBD Interchange 19th St. N. to 27th St. N.	22.1	2.52	W920 x 289	MC460 x 63	3 Span Cont. (22, 32, 22)
7	I-65	Rocky Ridge Road Overpass	26.5	2.31	Plate Girder	MC460 x 63	3 Span Cont. (27, 35, 23)
8	I-59	Red Oak Road Overpass	14.3	2.15	W840 x 176	MC460 x 63	Simply Supported (15)

Table 2.2. Connection Types Instrumented at Each Test Site

Test Site	Type Connection *						
	A	B	C	D	E	F	G
1	2			1			
2	1			2			
3	2			1			
4	1		1	1			
5	2		1	1			
6		2		1			8*
7					1		
8	1					1	

*Connection angles tested during summer of 1994

First Avenue North. The I-65 Railroad Viaduct was originally constructed in the late 1960's and was opened to traffic in 1969. The original multi-girder bridge was designed to allow for expansion, and in the late 1980's one lane each was added to the northbound and southbound bridges. The lane was supported by adding two girders to the inside portion of each bridge and was opened to traffic in 1988. A total system of eighteen girders (nine per bridge) support five northbound lanes and five southbound lanes.

Approximately 14 million heavy commercial vehicles (in each direction) have crossed the I-65 Railroad Viaduct since it was opened. The average daily traffic for this time period has steadily increased. Since the opening of the fifth lane in 1988, approximately 275 more trucks are using the Railroad Viaduct on an average daily basis. The average number of heavy vehicles per day has increased by 875 over the past ten years.

The fifth test site instrumented during the summer of 1993 was the 16th Avenue South Overpass which is approximately one half mile south of the Railroad Viaduct on I-65. The overpass is skewed and has staggered diaphragms. This overpass consists of a three span continuous multi-girder bridge for the southbound traffic and one for the northbound traffic. Each bridge has eight girders.

The 16th Avenue Overpass Bridges were constructed in the late 1960's and were opened to two lane traffic in the northbound and southbound directions in 1970. After the addition of two girders (per bridge) to the original six girder bridges in the late 1980's, the bridges were opened in 1988 to an additional lane for both directions. The traffic history of these bridges indicates a steady increase of commercial vehicle use over the past ten years. From 1984 to 1994, the number of average daily heavy commercial vehicles has increased from 961 to 2,711 trucks. A difference of approximately 1,750 truck crossings per day. Throughout the life of the bridge, approximately 17 million heavy commercial vehicles have crossed in one direction over the 16th Avenue North Overpass.

Test site 6 was located in downtown Birmingham on the Central Business District (CBD) Interchange of Interstate I-59/I-20. The CBD Interchange starts at 16th Street North and winds west through town over a series of three span continuous and simple span multi-girder bridges until it ends at 27th Street North. This one mile long interchange has three entrance ramps and three exit ramps. The test site at the CBD Interchange is located between 18th Street North and 19th Street North adjacent to the Alabama School of Fine Arts.

The CBD interchange was constructed in the early 1970's, and was opened to four lane traffic, both westbound and eastbound, in 1972. The average daily number of heavy commercial vehicles that cross these bridges are considerably higher than for any other bridges investigated during the summer of 1993. Approximately 3,907 heavy commercial vehicles cross this interchange per day at the present time. Over the life of the bridge roughly 23 million heavy commercial vehicles (one direction) have used this interchange.

The I-65 Rocky Ridge Road Overpass approximately eight miles south of downtown Birmingham was the bridge instrumented for test site 7. These dual three span continuous bridges were constructed of eleven built-up plate girders. Both the northbound and southbound multi-girder bridges were built in the mid 1970's, and were opened to four lanes of traffic in each direction in 1977.

Like the other bridges instrumented, the traffic history for the Rocky Ridge Overpass shows a general steady increase of heavy commercial vehicles over life of the bridge. Approximately 1,649 more heavy commercial vehicles cross the bridge per day in 1994 than in 1984. Since 1979, roughly 9.5 million heavy commercial vehicles have crossed the Rocky Ridge Overpass in each direction.

The multi-girder bridge investigated at test site 8 is on I-59 just outside of Centerpoint, Alabama, which is roughly eight miles northwest of downtown Birmingham. The Red Oak Road Overpass on I-59 consists of twin multi-girder bridges. Each bridge has three simply supported spans and six girders per direction. Because the overpass is slightly skewed to the interstate, the diaphragm-girder connections are slightly offset from girder to girder. In the early 1970's the Red Oak

Road Overpass was constructed to accommodate two lanes for the northbound traffic and two lanes for the southbound traffic. These four lanes were opened to traffic in 1975.

Unlike the other traffic histories, the average daily heavy commercial traffic at the I-59 Red Oak Road Overpass has generally remained constant over the past ten years, estimated at 1,018 vehicles. Roughly 6 million heavy commercial vehicles have crossed the I-59 Red Oak Road Overpass.

DIAPHRAGM-GIRDER CONNECTION DESCRIPTIONS

At the eight test sites the diaphragm-girder connections fall into seven categories and were labeled connection types A through G. Diagrams of the connection types are provided in Figures 2.1 and 2.2. Three of these connection types are the original welded connections, while the other four are bolted connections used in repair. A description of each connection type follows.

The type A connection consists of a connection plate which is welded to the web of the girder, and the plate is cut short of both the tension and compression flanges. The 9 mm transverse fillet welds which connect the plate and web terminate not more than 7 mm from the end of the plate. The type A connection was the primary diaphragm-girder connection used in the original construction of these bridges. Nine type A connections were instrumented during the summer of 1993.

The second welded connection, type B, is very similar to the type A connection because the type B connection also consists of a connection plate welded to the girder web, and the welds are the same size. However, the welds of this type connection terminate approximately 75 mm from the ends of the connection plate and include

short welds near the middle of the plate. Two type B connections, both at test site 6, were instrumented during the summer of 1993.

The type C connection consisted of an L 127 x 88.9 x 9.53 (mm) by 0.711 m long angle with the 88.9 mm leg attached to the girder by 9 mm fillet welds. The welds terminated about 75 mm from the ends of the angle. Two type C welded angle attachments were instrumented.

The first of the bolted connections investigated was the type D connection. This was the predominant replacement angle connection used in downtown Birmingham. Also, cracks have been discovered in many of this type of angle. Five bolts are used to connect one leg of an L 152 x 152 x 9.52 (mm) by 0.482 m long angle to the web of a girder. The vertical location of the diaphragm on the out-standing leg of the angle varied, but there were always four bolts used to attach the diaphragm to the connection angle. A total of seven type D bolted connections were instrumented.

One type E bolted connection was instrumented at test sight seven. The L 152 x 102 x 12.7 (mm) by 1.11 m long angle used at this connection extended from flange to flange of the girder but was not attached to either flange. A space of approximately 3 mm was left between the top and bottom of the angle and the corresponding girder flange. Seven bolts were used to attach the 102 mm leg of the angle to the web of the girder.

The type F connection was similar to the type D connection. The type F connection was an L 152 x 102 x 15.9 (mm) by 0.66 m long angle connected to the web of a girder. The main difference between the type D and type F connection is the size and the thickness of the angles. The type D connection consists of a 152 mm by

152 mm, 9.53 mm thick angle, while the type F connection consists of a 102 mm by 152 mm angle which is 15.9 mm thick. There was one type F connection investigated during the summer of 1993 at test site 8.

Eight of the type G connection angles were instrumented at test site 6 during the summer of 1994. The web gaps were instrumented at four of these connections. To this point, the type G connections have been used in the field only as part of this project. The geometry of the type G design is illustrated in Figure 2.2. All the connection angles except the type G were made of steel with a yield strength of 250 MPa. The yield strength of the type G angles is 345 MPa.

CONNECTION WEB GAP LENGTHS

The web gap is the area of the girder web between the top of the connection plate or angle and the bottom of the girder top flange. The distortion-induced stresses in the web that can cause fatigue cracking are related to the size of the web gap. Figures 2.3 and 2.4 show sketches of the web gap area for six of the connection types instrumented. The web gap area for the type G connection is shown in Figure 2.2. Table 2.3 lists the location, measured web gap length (L), and radius size for all instrumented web gaps. The distance from the bottom of the top flange to the nearest weld for welded plate connections and to the top of the connection angle for bolted connections is reported as the web gap length in Table 2.3. Since many of the connections instrumented were on interior girders with straight diaphragms, the web gap length (L) for the connections on each face of the web are included in Table 2.3.

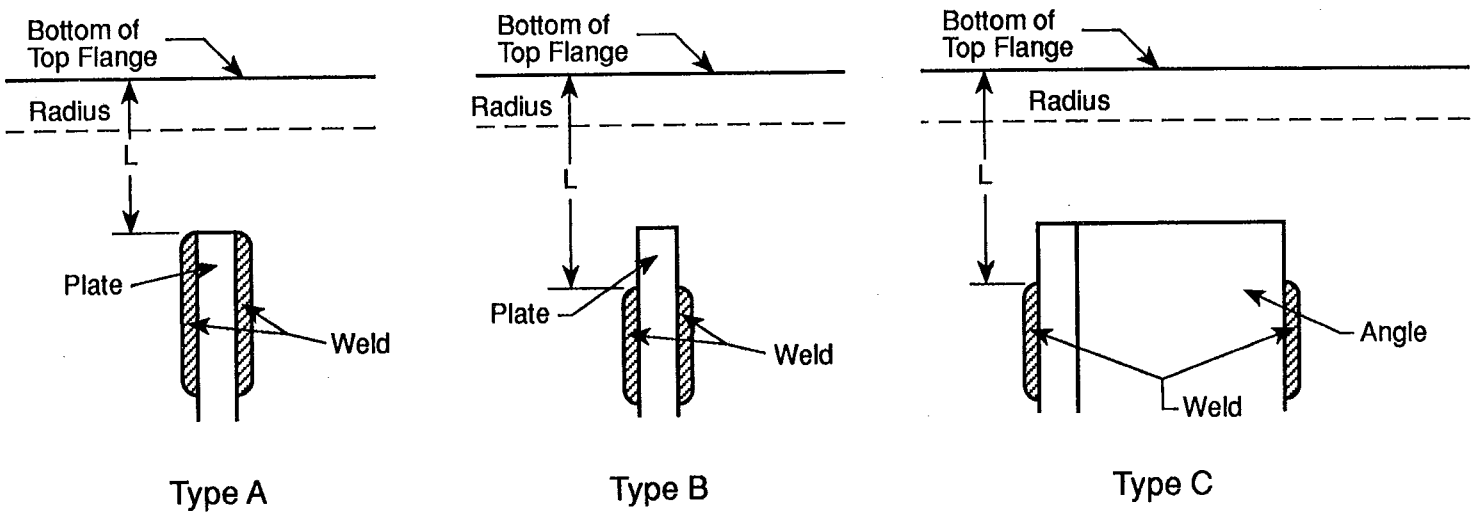

Figure 2.3. Typical Web Gap Regions for Welded Connections

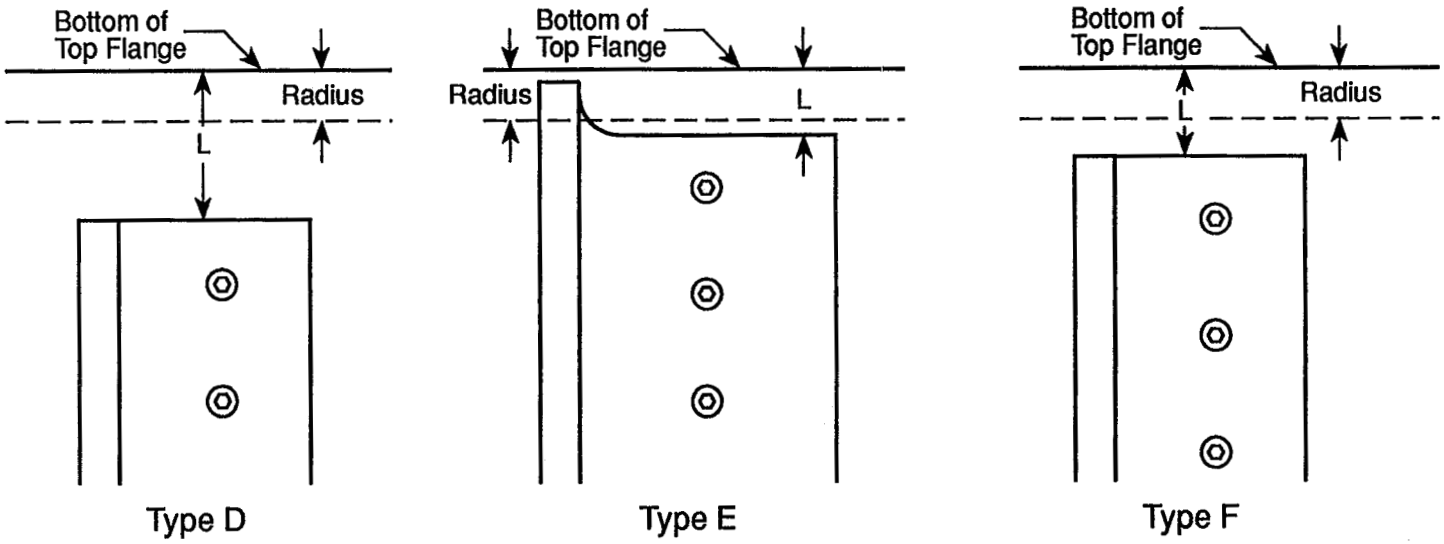

Figure 2.4. Typical Web Gap Regions for Bolted Connections

Table 2.3. Web Gap Lengths

Test Site (connection designation)	Connection Types	Web Gap, L[1] (mm)	Radius (mm)
Summer of 1993			
1 (a)	A/A	45/46	20
(b)	A/A	42/45	20
(c)	D/D	13/133	20
2 (a)	D/A	102/53	20
(b)	A/A	51/51	20
(c)	D/D	95/96	20
3 (a)	A/A	42/30	18
(b)	A/D	41/205	18
(c)	D/D	80/90	18
4 (a)	A/A	44/49	20
(b)	D/D	103/191	20
(c)	C/C	120/119	15
5 (a)	A[2]	35	20
(b)	A[2]	47	8
(c)	D[2]	116	15
(d)	C[2]	122	15
6 (a)	D/D	87/82	18
(b)	B/B	116/128	18
(c)	B[3]	99	18
7 (a)	E/E	23/28	14
8 (a)	A[2]	60	18
(b)	F[2]	35	18
Summer of 1994			
6 (d)	G/G	178/178[4]	24
(e)	G/G	178/178[4]	30
(f)	G/G	89/89[4]	30
(g)	G/G	89/89[4]	24
(h)	G/G	178/178	24
(i)	G/G	178/178	30
(j)	G/G	89/89	30
(k)	G/G	89/89	24

[1] Instrumented face of web/reverse face of web
[2] Staggered diaphragms
[3] Exterior connection
[4] Strain gages not placed in web gap at this location

INSTRUMENTATION AND DATA ACQUISITION

Instrumentation

The instrumentation included electrical resistance strain gages, for measuring surface strains on the girders and diaphragms, and Linear Variable Differential Transformers (LVDTs) for measuring out-of-plane displacements of the connection plates and angles. In addition, deflectometers were used for measuring vertical girder deflections.

The strain gages were self temperature compensating foil gages with polyamide encapsulation and preattached lead wires. The majority of the gages had a nominal resistance of 350 ohms, but due to lack of available gages at the start of the project several gages at test site 1 were 120 ohms. The gage factors varied from approximately 2.0 to 2.1.

All out-of-plane displacements were measured with LVDTs that were manufactured by Lucas-Schaevitz, Inc. The LVDTs had a dynamic measurement range of approximately +/- 6.35 mm with a resolution of 0.00254 mm. Each LVDT was mounted using a magnetic base and adjustable arm (Figure 2.5).

Deflectometers (Figure 2.6) which are essentially calibrated cantilever beams were used to measure the vertical deflection of the girders. Each deflectometer had four strain gages, mounted two per side, and wired as a full bridge on a 508 mm long by 88.9 mm wide by 6.35 mm thick aluminum plate. One end of the aluminum plate was attached to the underside of the girder using C-clamps. At the other end of the plate, a wire was stretched from an eye hook in the aluminum plate to the ground where the wire was tied to a weight. The cantilever device was then pre-deflected by

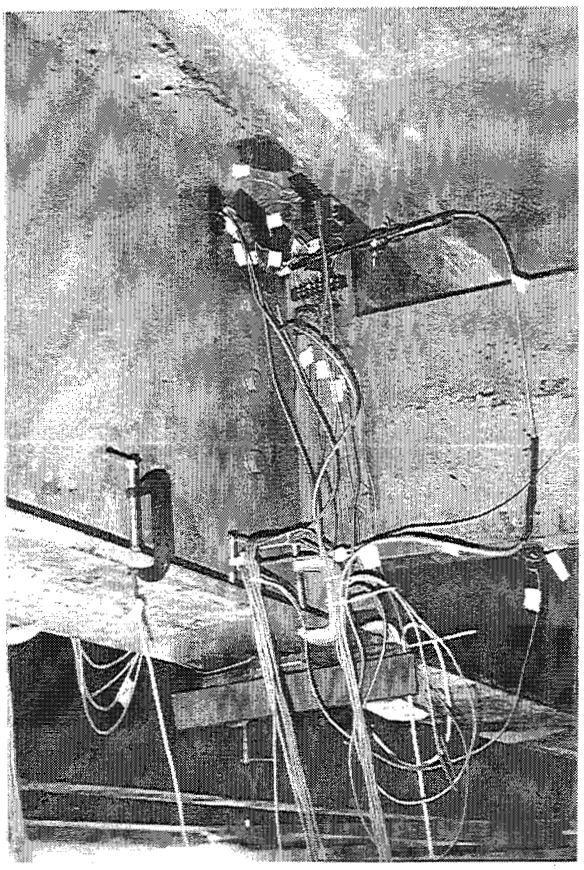

Figure 2.5. Linear Variable Differential Transducer Mounted on the Magnetic Base with Adjustable Arm

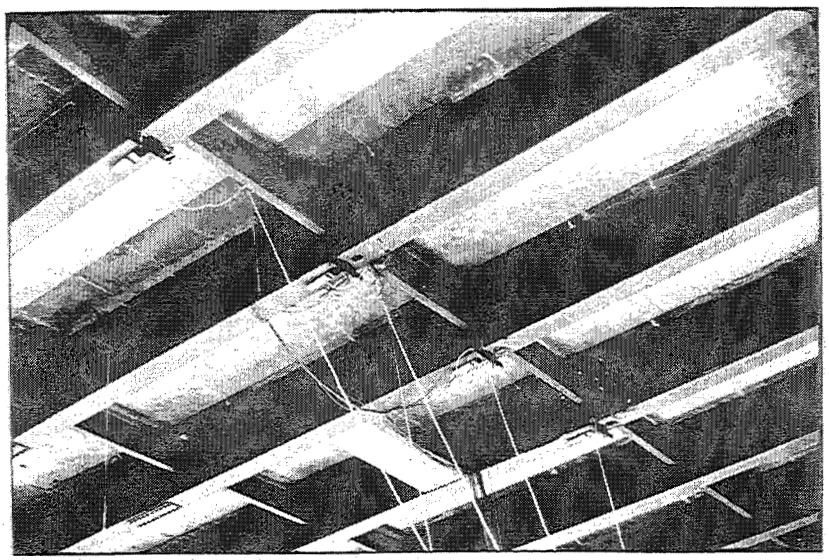

Figure 2.6. Deflectometers Mounted on the Bottom Flange of the Girders

pulling the wire down approximately 25 mm to maintain tension in the wire. As traffic crossed the bridge the girders deflected which resulted in deflection of the cantilever beam and a change in resistance across the full bridge on the deflectometers which could be converted into the deflection of the girders.

Strain gage patterns for the different connection types were selected so stress ranges at critical locations in the web gap could be measured. The distortion-induced vertical stress ranges in the girder web at the following locations were of interest: a) edge of the web to flange radius (this includes edge of web to flange weld for one plate girder bridge), b) top of the connection to girder web weld for welded connections, and c) top of the connection angle for bolted connections. Also, the horizontal stress ranges at the connection to girder web weld for welded connections were measured.

As an example Figure 2.7 shows the gaging pattern for a type A welded plate connection. Theoretically, measurements of the maximum distortion-induced stresses should be made at points A' and B' as shown in Figure 2.7. Placing strain gages at these discontinuities was not possible, so the stress ranges at points A' and B' were determined by extrapolation. Due to the small space in and around the web gap for type A connections it was not possible to align the gages in column C (see Figure 2.7) with the centerline of the plate connection. Stresses at the vertically oriented gages (C1 and C2) were used to extrapolate (linear) the stress at the edge of the web-flange radius (point A in Figure 2.7) and at the top of the weld (point B in Figure 2.7). The gages in column C, C1, and C2, were within 20 mm of the centerline welded plate connection, and the extrapolated stresses at points A and B (Figure 2.7) were assumed equal to the stresses at points A' and B'. By using the horizontally oriented

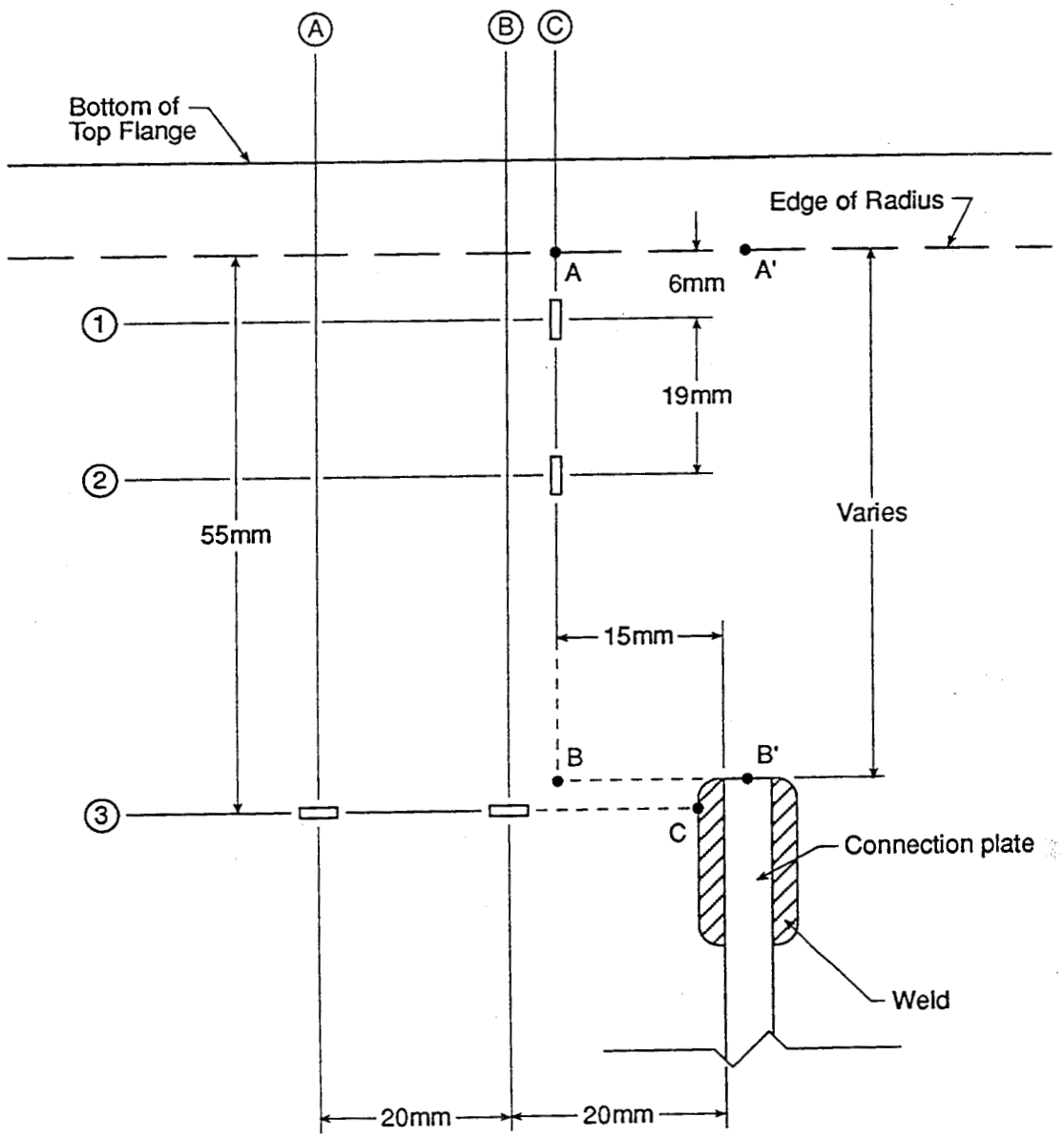

Critical Locations

Vertical stress extrapolations { A: Edge of radius; B: Top of connection to web weld

Horizontal stress extrapolations { C: Side of connection to web weld

Figure 2.7. Web Gap Gage Positions for Type A Welded Plate Connection

gages (A3 and B3) and linear extrapolation, the horizontal stress near the top of the connection weld (point C in Figure 2.7) was determined.

The type D bolted connection had a web gap larger than the type A connection and required a different gaging pattern as shown in Figure 2.8. Due to the width of the connection angle, four gages were spaced in a row (row 1) across the web gap so that the horizontal location of the maximum vertical stress range could be determined. Based on field test results column C was found to yield the highest stress ranges. Using the results for the vertically oriented gages in column C and linear extrapolation the stress ranges at the edge of web-flange radius (point A in Figure 2.8) and at the top of the connection angle (point B in Figure 2.8) were determined. The type F connection was instrumented in a similar fashion to determine horizontal and vertical stress ranges.

Since the type E connection had a very small web gap (Figure 2.9) a different strain gaging scheme was employed. The strain gages were placed on the girder web adjacent to the connection angle and web gap. Linear extrapolation was used to determine the stress ranges at point A in Figure 2.8. Due to the distance from the gages in column C to the web gap, these gages underestimated the level of stress in the web gap. The distribution of stress in the web gap of this type connection is discussed in a later section of this report.

The locations of the primary gages placed in the web gap at type G connections are similar to the locations for a type D connection and are shown in Figure 2.10. The strain measurements in the D column of gages were used to determine by extrapolation the stress ranges at the critical locations (A and B in Figure 2.10).

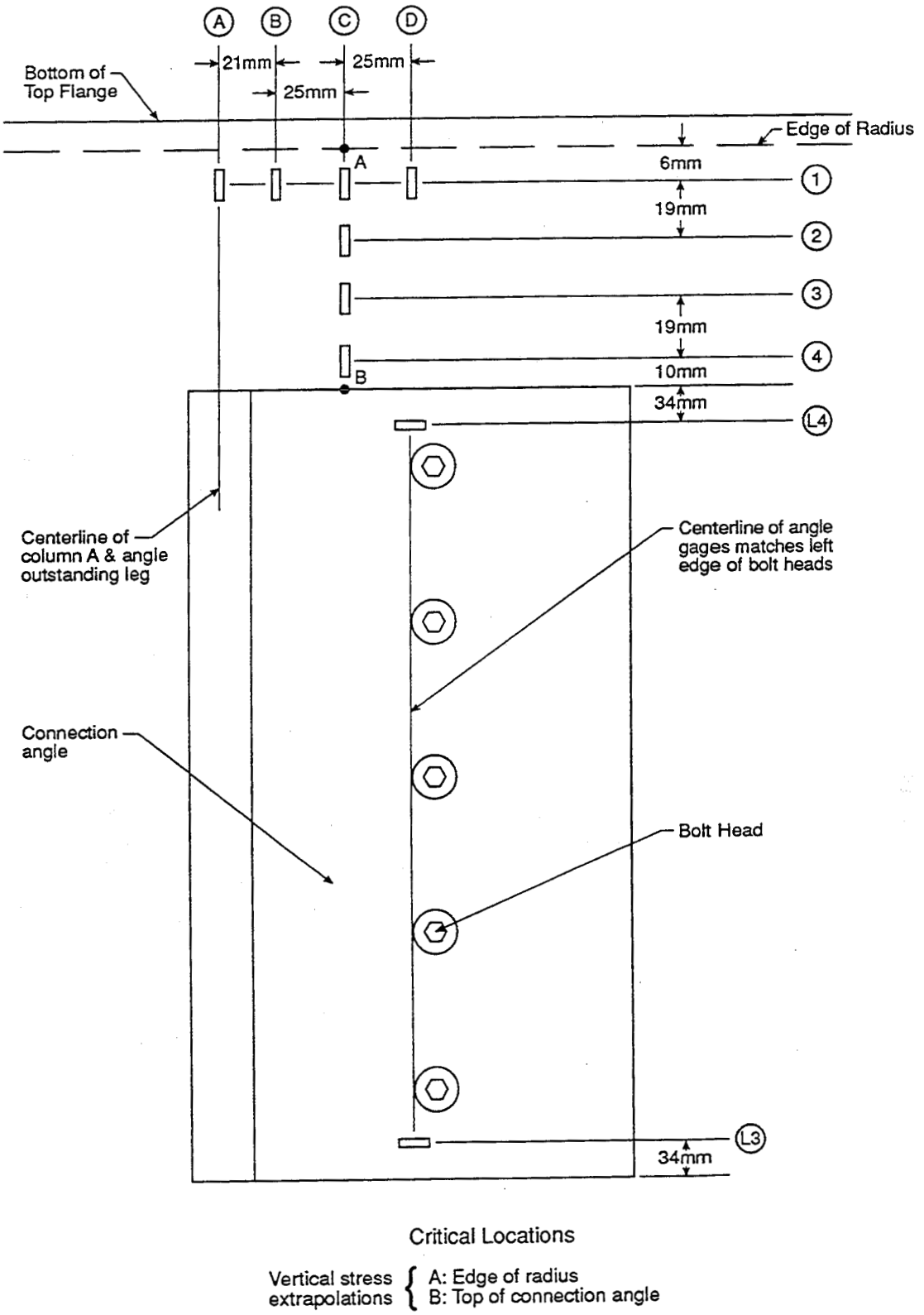

Figure 2.8. Web Gap Gage Positions for Type D Bolted Angle Connection

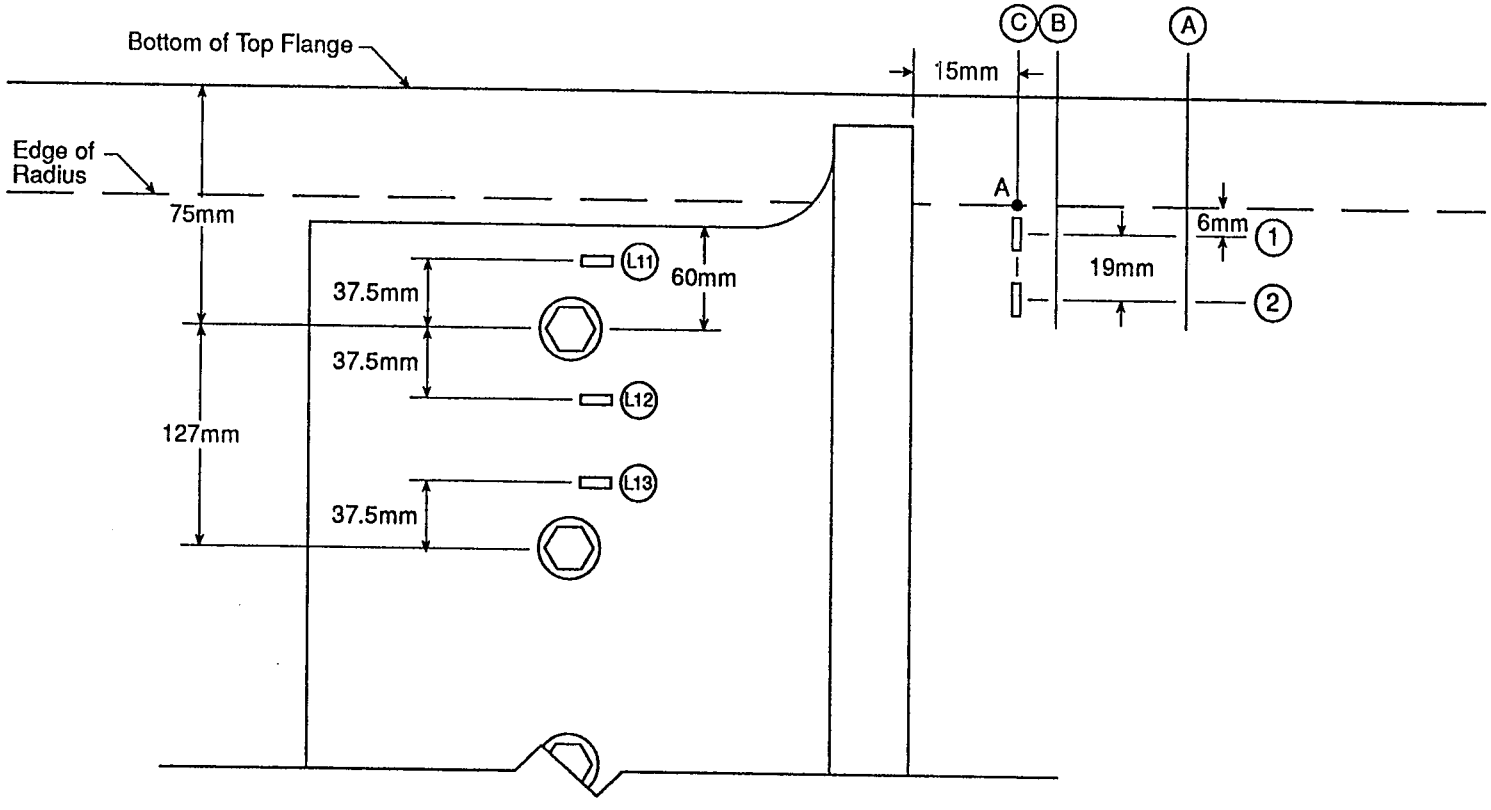

(Gages L14, L15, & L16 are symmetrically mounted on the bottom of the angle)

Critical Locations

Vertical stress extrapolation { A: Edge of radius

Figure 2.9. Web Gap Gage Positions for the Type E Bolted Angle Connection

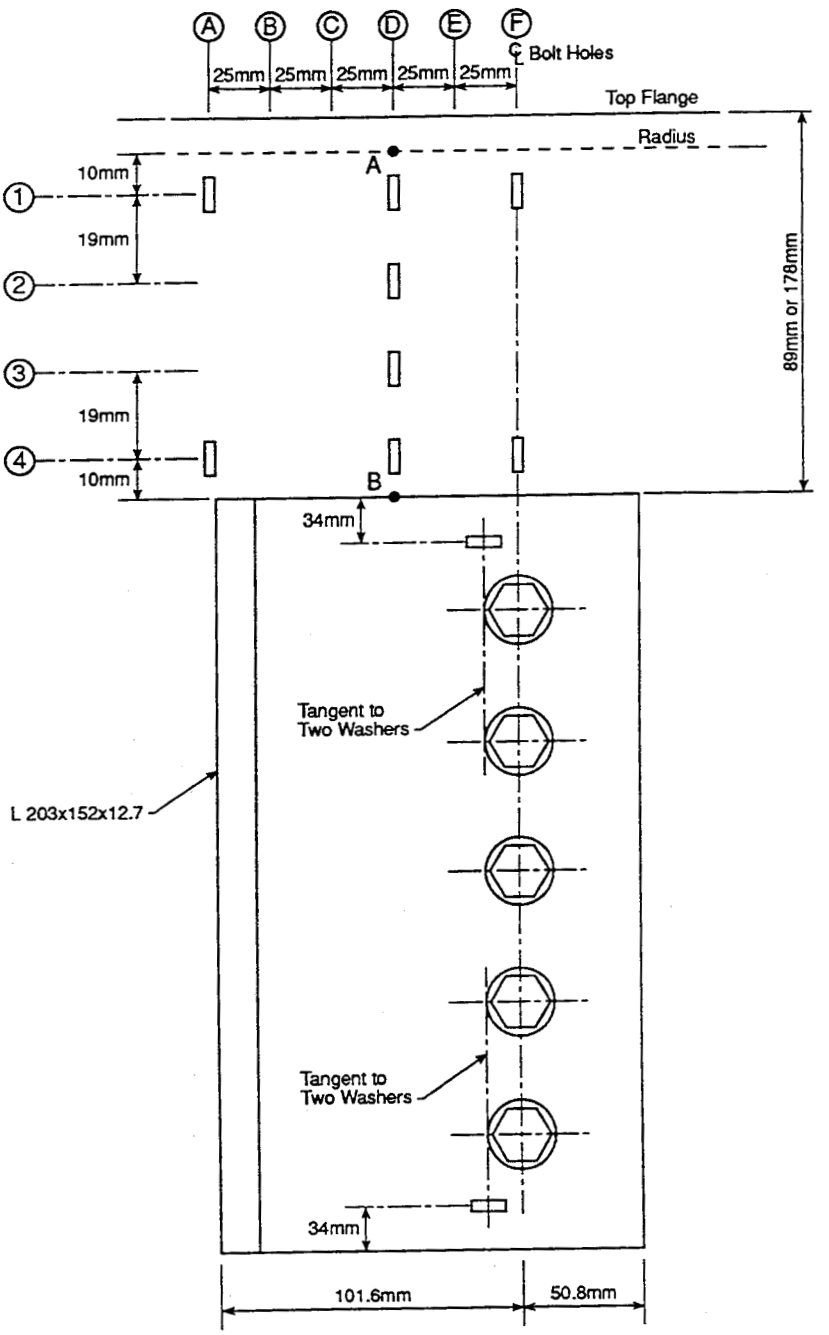

Critical Locations

Vertical stress extrapolations { A: Edge of radius
B: Top of connection angle

Figure 2.10. Typical Strain Gage Locations at Type G Connection

Many of the bolted replacement angles have developed fatigue cracks like the one shown in Figure 1.5. To investigate the cause of these cracks, the stress ranges in uncracked bolted angles were measured. From autopsies of cracked angles it was determined that the cracks in the angles initiated adjacent to the bottom bolt connecting the angle to the girder web as shown in Figures 1.7 and 1.8. Strain gages were mounted in the area near the bolt heads on the angle leg that was connected to the girder web. The location of the strain gages on the bolted connection angles are shown in Figures 2.8, 2.9, and 2.10. Due to space constraints strain gages could be placed no closer than about 25 mm from the point of expected crack initiation. Therefore, the measured stress ranges are lower than the actual stress range at the point of crack initiation.

Along with the web gaps, the diaphragms between the girders were instrumented with strain gages. Also, strain gages were mounted on the top and bottom flanges of the girder to measure girder in-plane bending stress.

All site preparation, instrumentation, and field testing at the eight test sites occurred during the summer months between early June and late September. On average each test site required a week of site preparation and instrumentation before field testing commenced. Generally, the site preparation and instrumentation occurred during the daylight hours between 7:00 a.m. and 5:00 p.m., Monday through Friday.

Data Acquisition System

All field test data were collected using a MEGADAC data acquisition system and 486-33 personal computer with compatible software (OPTIM 1994). For a typical test, 32 channels were used for recording strain gage data, 4 channels were used for

deflectometers, and 4 channels were used for LVDTs. All data recorded by the MEGADAC were automatically transferred to the hard drive of the personal computer. This data acquisition system allowed for automatically recording strain ranges caused by truck traffic within the traffic flow with an automatic trigger. Data recording was controlled with a function key for calibration truck crossings. All data were recorded for moving truck loading using a sampling rate of 400 samples/second/channel.

Calibration Tests

Calibration tests were performed at each test site to investigate the structural behavior of the connection details under known traffic loading. To insure that data was collected for heavy trucks, calibration truck weights slightly higher than the legal weight limit were used. The calibration tests were also used to investigate the effect of truck lane location on bridge behavior.

ALDOT provided two identical specialized calibration testing trucks which were designed and purchased for the purpose of load testing ALDOT's bridges. The axle weights and gross vehicle weight of these unique vehicles can be varied by maneuvering specially made load blocks to different positions on the flatbed, using an on-board crane. Each different load block combination was characterized by ALDOT and labeled with a unique name. The load placement utilized during all calibration testing was the LC-4 loading. The test truck dimensions and axle weights for this type loading are provided in Figure 2.11.

Generally, the calibration tests were started about 8:00 p.m. and sometimes lasted until about 2:00 a.m. The reason for testing at night was to avoid the higher volume of traffic present during daytime. Once the traffic had diminished to an

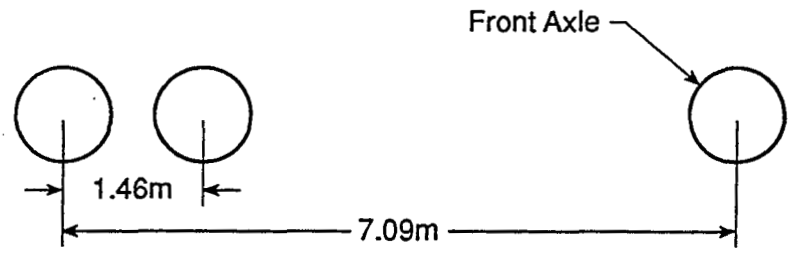

Axle Spacing

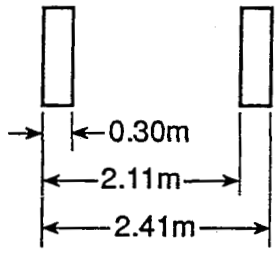

Front Axle

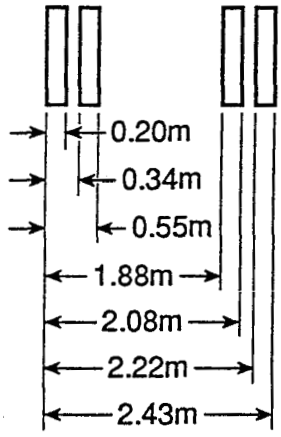

Rear Axle

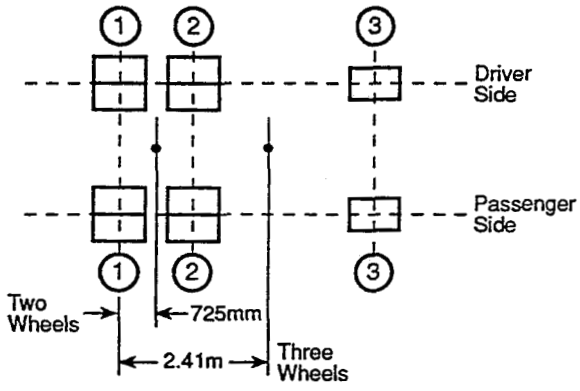

WHEEL LOADS

Total Wt (kN) 345.9	Wheel Set 3 (kN)	Wheel Set 2 (kN)	Wheel Set 1 (kN)
Driver	65.3	65.3	46.4
Passenger	62.5	61.4	45.1
Average	63.9	63.3	45.8

Wheel Loads

Figure 2.11. Calibration Load Truck Configuration and Measurements

acceptable level, the test was started. Both calibration trucks merged into traffic from entrance ramps several miles before the span being tested. As the trucks built up speed coming into traffic off the ramp, the drivers found a clear spot in the traffic. The trucks crossed the bridge in the correct lane at a designated speed with no other vehicles on the span being tested.

Data for two types of truck crossings were recorded at each location: single truck crossings and double truck crossings. For single truck crossings a single calibration truck crossed the bridge in the center of a lane. For the double truck crossings both calibration trucks crossed the bridge side-by-side in adjacent lanes. The speed of the trucks for both single and double truck crossings varied from 64 kph to 97 kph.

Traffic Tests

Although it was important to understand the structural behavior for trucks of known weight in specific traffic lanes, it was also important to understand the behavior for normal traffic loading. The stress ranges collected from normal traffic were used to calculate an equivalent constant amplitude stress range, or effective stress range, at critical points in the web gap and on the connection angles. Along with calculating effective stress ranges, histograms and several other statistical analysis techniques were used to analyze the data.

For the normal traffic tests the data acquisition system was programmed to automatically record data for heavy trucks. The data acquisition system continuously scanned a select gage, or series of gages, in the web gap region for strains that exceeded a prescribed limit which was set to capture only heavy truck crossings.

When the strain at a trigger gage exceeded the trigger magnitude, data were recorded. The data acquisition system recorded all data scans for approximately 2 seconds before the trigger and approximately 3 seconds after the trigger. The pre-trigger and post-trigger time lengths were chosen at each test site to insure that a complete record of the truck crossing was obtained.

Through past experience from similar bridge projects, it has been found that recording 250 truck crossings for use in effective stress range calculations produce reasonably accurate values (Stallings et al. 1993, Vol. I) when coupled with data from heavy calibration trucks. Statistical analysis of measurements of the magnitudes of the out-of-plane displacements and distortion-induced stresses at the diaphragm-girder connections and effective stress range calculations were done for 250 truck crossing events at each location.

During the traffic tests all equipment required, including work vehicles, were located under the bridge, out of view of the passing motorists on the interstate above. This was done to ensure that the speeds and lane positions followed normal traffic patterns.

Data Reduction

The data collected during all traffic and calibration tests was processed by the data acquisition system and then stored on the computer hard drive. Due to the large amount of hard disk space required to store the information, the data was transferred to data cartridges.

Strain ranges using the peak-to-peak method were determined for both the calibration and truck traffic data records. In the peak-to-peak method, a strain range is

defined as the absolute difference between the maximum and minimum strain values. Each truck crossing record was considered to create one strain range. Transform equations were written in the software test files to calculate the strain range. Stress ranges were then found by multiplying the strain ranges by the modulus of elasticity for steel of 200,000 MPa.

In addition to finding the strain ranges, the transforms were used to extrapolate strains from gage locations to areas of interest. Equations for the extrapolations were written to find the horizontal and vertical strain in the web at the critical locations (Figures 2.7, 2.8, 2.9, and 2.10). These, too, were converted to stress ranges using the modulus of elasticity of steel.

Effective Stress Range

One of the primary goals in reducing the variable amplitude data gathered from normal truck traffic was to determine the effective stress range (equivalent constant amplitude stress range) at critical points in the connection. The effective stress range can be calculated from variable amplitude stress range data by a number of different methods. The two most common methods used are the root-mean-square (RMS) and Miner's effective stress range, also called the root-mean-cubed method (RMC). Both of these methods can be represented by the following equation:

$$S_{re} = \left[\sum_{i=1}^{k} \frac{(n_i S_{ri}^{b})}{N} \right]^{\frac{1}{b}} \qquad (3)$$

where k is the number of different stress range magnitudes; i is the current stress range; n_i is the number of stress cycles at the ith stress range S_{ri}; and N is the total

number of cycles. For Miner's effective stress range, b, which is related to the slope of a log-log plot for constant amplitude fatigue life data, is given a value of 3. For the root-mean-square method, b is equal to 2.

Both the root-mean-square method and the Miner's method have shown good correlation with experimental data from previous reports (Fisher 1978, Yamada and Albrecht 1976, Fisher et al. 1989). Miner's effective stress range tends to give a larger result than the RMS method (Fisher et al. 1989), and is also more theoretically based (Yamada and Albrecht 1976). The root-mean-square method, however, has been found to show slightly better correlation to the test data but this results in a less conservative value (Fisher et al. 1989). Even though both methods have been widely used in research, Miner's effective stress range produces a more conservative estimate and is therefore more commonly used for bridge fatigue analysis. For this reason, all effective stress ranges were calculated using the Miner's effective stress range.

TEST RESULTS, BEHAVIOR AND ANALYSIS

There were several objectives of the field testing. The first was to measure the level of distortion-induced stresses and girder deflections that a typical multi-girder bridge undergoes. This information was used to design laboratory tests of bolted connections. The second objective was to measure fatigue stress ranges at previously uncracked connections, to compare the measured stress ranges with realistic fatigue limits, and to predict if further cracking is expected. The viability of continuing to use the hole drilling retrofit technique in Birmingham was examined as well.

In order to develop laboratory experiments that represent actual field conditions, the behavior at each test site was investigated. This was accomplished by examining the vertical girder deflections and in-plane bending stresses of the girder flanges as well as web gap stress ranges and angle stress ranges. A comparison of field and laboratory results is included in Chapter Three.

Methodology for Evaluating Field Measurements

Potential areas of crack initiation in the girder web are in the web gap immediately below the radius and at the web to connection interface. Stress ranges were measured at the gage locations and extrapolated to critical areas as illustrated in Figures 2.7, 2.8, 2.9, and 2.10. The critical area for crack initiation in the angles is immediately in front of the bottom bolt, and stress ranges at this location are assumed equal to the stress ranges measured at the strain gage locations shown in Figures 2.8, 2.9, and 2.10.

Fatigue crack initiation and propagation can occur for fatigue limit accedence rates as low as 0.1 percent even when the effective stress range (S_{re}) is less than the fatigue limit (Keating et al. 1987, and Fisher et al. 1983). Hence, an estimate of the maximum stress range due to truck traffic is required for drawing a conclusion regarding whether fatigue crack initiation will occur. In this project 250 random truck events were recorded at each connection for use in calculation of S_{re}. For estimating a maximum stress range due to truck traffic the same 250 events were used plus the calibration truck data. Including the calibration truck data ensures that some data from heavy single and side-by-side trucks is included. Because the length of time required to record the 250 random truck events was short (relative to the life of the bridge), one

stress range out of 250 represents a significant number of truck crossing events during the life of the bridge. When one stress range out of the 250 random truck crossing events, or the stress range from any calibration test, exceeded the fatigue limit for the connection under examination, then it was assumed that fatigue cracking will occur at some time in the future. If no recorded stress range exceeded the fatigue limit then it was assumed that cracking will not occur based on current traffic conditions. Based on the limited amount of truck traffic data recorded, common logic would suggest that a conclusion that cracking will occur carries more weight (and is statistically more significant) than a conclusion that cracking will not occur. Once a crack has initiated, an effective stress range (S_{re}) which is below the fatigue limit can propagate the crack. The higher the effective stress range, the faster the crack will initiate and grow, and the shorter the fatigue life.

Only predictions of whether or not fatigue cracking is expected to occur are given below. No attempts are made to estimate the remaining life of any connections. Due to the high volume of traffic on the bridges (7 to 23 million truck crossings to-date), if cracking is predicted to occur, it is reasonable to expect cracking within the remaining useful life of the bridge.

Fatigue Categories for Critical Locations in Web Gap

The smooth radius area at the web-to-flange transition in rolled-section girders is a location of mild stress concentration, and the AASHTO (1992) category A fatigue limit is assumed here to provide an upper bound for that location.

All of the girders investigated in Birmingham were rolled girders with the exception of the girders at test site 7 which were built-up plate girders. During

laboratory experiments conducted by Fisher et al. (1990) on built-up plate girders with welded attachments, cracks only developed when the distortion-induced stress range at the web-flange weld exceeded (15 ksi) 103 MPa. The stress range at the edge of the web-flange weld for the built-up plate girders is compared to a fatigue limit of 103 MPa in the following evaluations.

The web at the top of the connection plate weld at the type A, B and C welded connections is assumed to have an AASHTO category C fatigue limit of 69 MPa based on results reported by Fisher et al. (1990).

In the type D, E, F, and G bolted replacements, the area of the web near the top of the angle had a plate welded to the web before retrofit of the bolted connection. The connection plate was removed, and the weld was ground smooth before the bolted connection was installed. If the bolted connections were installed in new bridges, then the fatigue limit of the smooth web area at the top of the angle would be assumed equal to AASHTO category A. Due to the large number of load cycles that occurred before the original welded connections were removed and the possibility of remaining defects from the original welds, category A does not seem appropriate. Since the welded attachment and stress concentration has been removed, category C is not appropriate either. The AASHTO category B (with a fatigue limit of 110 MPa) is not specifically for this situation, but it is used here as a compromise for an estimate of the fatigue limit of the web at the top of a bolted angle.

Analysis of Web Gap Stress Range Results

Figures 2.12, 2.13, and 2.14 contain the reduced stress results from traffic truck crossings and calibration truck crossings plotted along with the pertinent fatigue limit.

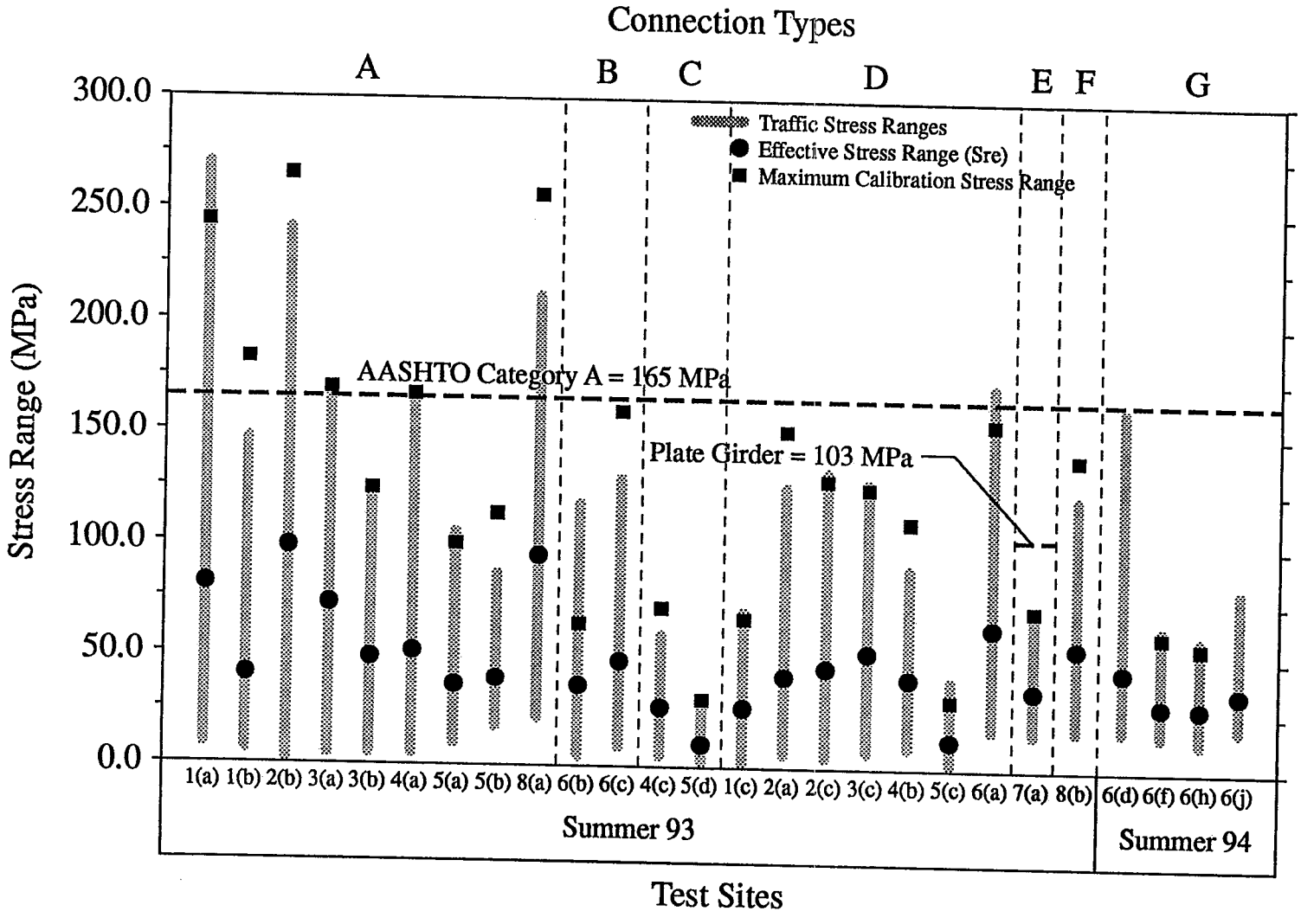

Figure 2.12. Web Stress Ranges at the Web-Flange Radius

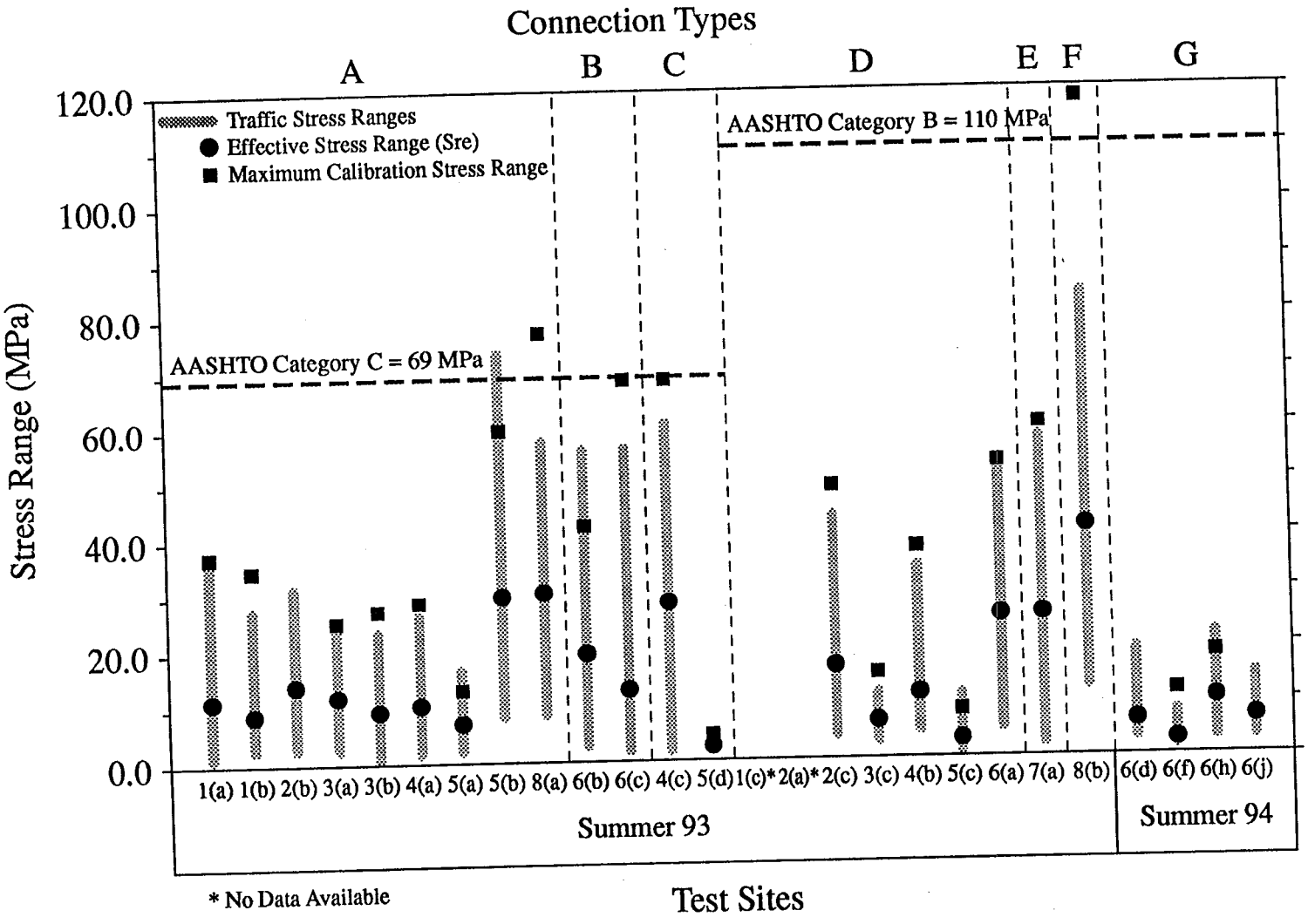

Figure 2.13. Web Stress Ranges at the Top of the Connection

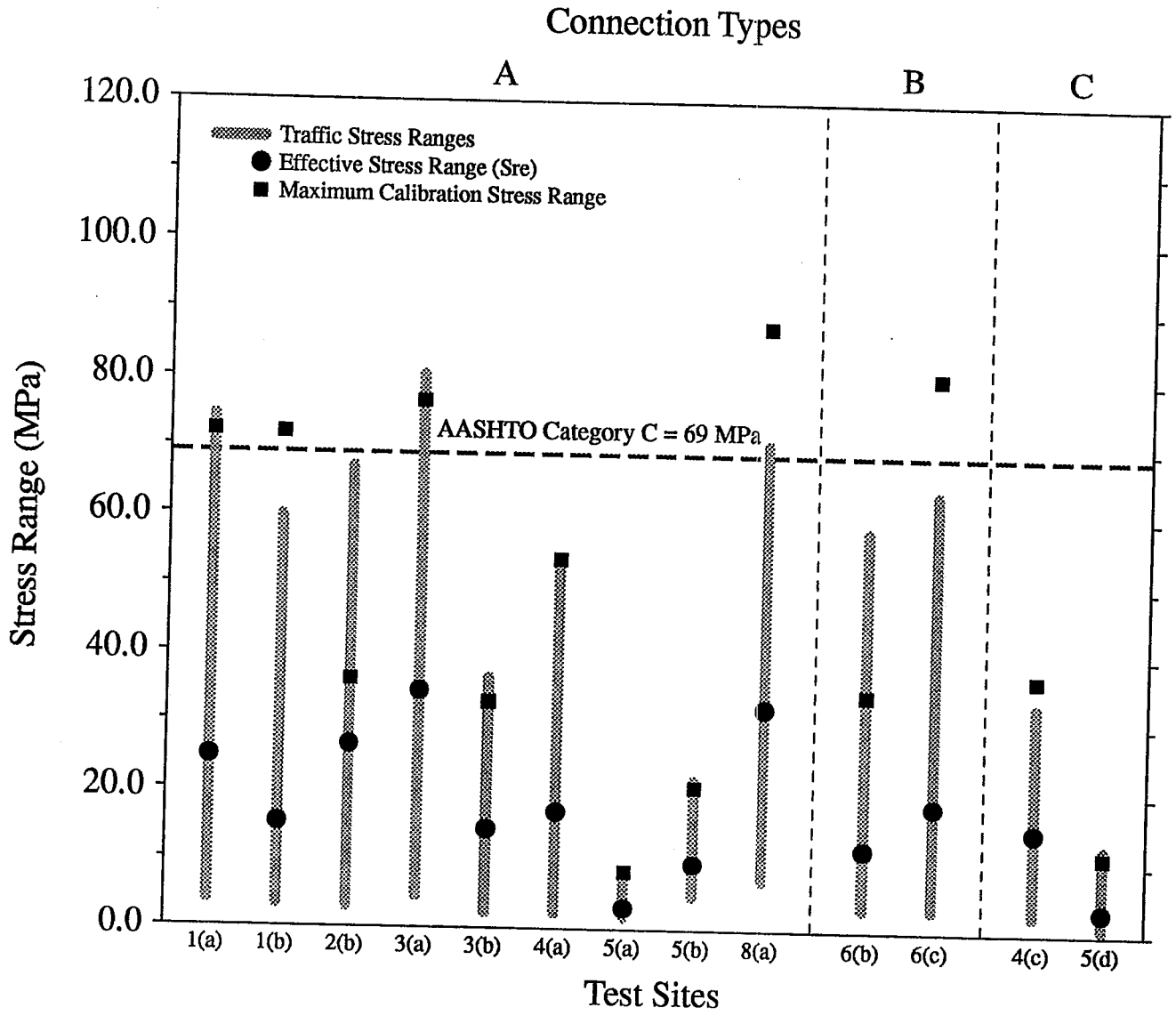

Figure 2.14. Web Gap Horizontal Stress Ranges

In each of these plots for several test sites there were significant differences between the largest stress range due to trucks in the traffic flow and the largest stress range caused calibration trucks. Generally, the largest stress range from a calibration test was greater than or equal to the largest stress range from a truck in the traffic flow. There are a couple of explanations for these differences. Data were recorded while the calibration trucks crossed the bridges in every available lane; however, due to the normal traffic flow, the heaviest traffic trucks may have naturally avoided the lane which would produce the largest stress ranges in a given connection. Also, the largest stress ranges sometimes resulted from side-by-side calibration truck crossings. This loading configuration may not have occurred from trucks in the traffic flow while data was being recorded.

For each of the type connections instrumented, out-of-plane displacement of the connection was measured as trucks crossed the span. Generally, the more flexible the web gap, the greater the out-of-plane movement. However, the flexibility of each web gap is determined by a combination of features such as the web gap length and the web thickness. The relationship between the stress range at the radius and out-of-plane displacement range for each of the connections was investigated by plotting these two ranges versus each other. In general, stress range and out-of-plane displacement were linearly related for the calibration and truck traffic crossings for each connection.

Type A Welded Plate Connection

For the type A connections the web gap area adjacent to the web-flange radius experienced large stress ranges. Six of the nine type A connections investigated had

at least one stress range from a traffic or calibration truck crossing which exceeded the fatigue limit of 165 MPa (category A, 24 ksi). In addition, for connections 1(a), 2(b), and 8(a), Figure 2.12 shows that some measured stress ranges were greater than the yield stress of the steel used in these bridges (250 MPa). The measured stress range due to truck crossings contained both tension and compression stresses. By examining the actual stress records for these individual truck crossings it was determined that the maximum stress measured was less than 250 MPa; therefore, the yield stress was not exceeded.

Another area of concern for the type A connection is at the top of the weld which connects the plate and the girder web. The stresses for this area were considerably less than those at the web-flange radius. Stress ranges above the fatigue limit of 69 MPa (category C) were measured at two connections (5(b) and 8(a)). The effective stress ranges (S_{re}) for this critical area varied at the nine connections from 7 MPa to 30 MPa.

The maximum and effective stress ranges for the horizontal stress at the connection plate to web weld were generally higher than the vertical stress ranges at the same location. The only exceptions to this were at test site 5, where the diaphragms were staggered. Excluding the connections at test site 5, the maximum stress range varied from 37 MPa to 89 MPa, which was approximately twice the vertical stress range magnitudes for the corresponding connections. Four of the connections had horizontal stress range magnitudes that were above the fatigue limit of 69 MPa (category C).

In summary, the field data corroborates a conclusion that distortion-induced stresses are the cause of the fatigue cracking in the girder webs in the bridges being considered. The field data indicate that distortion-induced web and weld cracking will occur at additional type A connections.

Type B Welded Plate Connection

Both the type B connections investigated were at test site 6, and the largest stress ranges were record at connection 6(c). For connection 6(b) the stress ranges for both truck traffic and calibration tests were below the assumed fatigue limits.

The maximum stress ranges at the web-flange radius for connection 6(c) from truck traffic and calibration truck crossings did not exceed the fatigue limit of 165 MPa (category A). The largest vertical stress range at the connection plate to web weld for connection 6 (c) was from a calibration truck test and was approximately equal to the category C fatigue limit. The largest stress range due to truck traffic for the horizontal stresses was 64 MPa which was slightly below the fatigue limit. The maximum horizontal stress range from a calibration test was 81 MPa and was larger than the category C limit of 69 MPa.

For the two type B connections the web immediately below the web-flange radius is not expected to crack. At connection 6(c) the horizontal and vertical stress ranges at the connection plate to web weld were sometimes larger than the category C fatigue limit (69 MPa); therefore, cracking is expected at the connection plate to web weld in one of the these two connections.

Type C Welded Angle Connection

The web-flange radius stress ranges for the two type C welded angle connections investigated were considerably lower than the category A fatigue limit (165 MPa). The maximum stress range values at the radius were 59 MPa and 28 MPa for these two connections. The welded angle connection at location 5(d) was part of a system of staggered diaphragms, which could explain the smaller level of stress in the web gap.

The stress ranges found at the connection to web weld were at or below the fatigue limit for category C of 69 MPa. For connection 4(c) the largest calibration test stress range was slightly less than the fatigue limit. The horizontal stress range results and web-flange radius stress range results for the type C welded angle connections investigated were well below the fatigue limit.

Overall, no cracking is expected in the area immediately below the radius at the two type C welded angle connections investigated. The horizontal and vertical stress ranges at the connection to web weld from traffic and calibration truck crossings were below the fatigue limits except for the largest calibration truck crossing at connection 4(c). This indicates that fatigue cracking is possible at one of the two type C connections.

Type D Bolted Angle Connection

Only one of the seven type D bolted angle connections investigated developed stress ranges at the edge of the web-flange radius that were above the fatigue limit of 165 MPa. At test site 6 a maximum stress range of 171 MPa was measured as a result of truck traffic. The magnitudes for the stress ranges at the edge of the radius at

test site 5 which had staggered diaphragms were considerably lower than those at the other test sites.

The relationship between stress range at the radius and web gap length was investigated for the type D, F, and G connections that were back-to-back bolted attachments. Table 2.4 shows the maximum and effective stress range results in descending order of web gap size for these five connections. The connection on girder three at test site 2 was not included in this trend because the bolted angle connection was back-to-back with a welded connection which had a smaller web gap. In addition, the connections at test site 5 where the diaphragms were staggered were not included. Generally, there was no discernable relationship between web gap size and stress range at the web-flange radius.

The stress range results at the top of the connection angle are not available due to data acquisition system channel limitations for two of the seven connections investigated. The magnitudes at the remaining 5 type D connections were lower than the fatigue limit (category B, 110 MPa). The highest stress range recorded at the top of the bolted connection angle was 54 MPa. The effective stress range values at the top of the connection angle ranged from 3 MPa (test site 5) to 25 MPa (test site 6).

Based on the assumed fatigue limit and the magnitudes of the results, cracks at the web-flange radius are only expected to form at one of the connections investigated. Cracking is not expected in the web near the top of the angle because the stresses recorded at all the connections were below the fatigue limit.

Table 2.4. Maximum and Effective Stress Ranges (Sre) at the Web-Flange Radius for the Type D Bolted Angle Connections

Location	Connection	Web Gap (mm)	Maximum (MPa)	Sre (MPa)
6*	G	178	159	45
6*	G	178	65 (62)	31
1	D	131	69.6 (65.6)	26.3
4	D	103	89.0 (109)	39.8
2	D	95	132 (128)	44.4
6*	G	89	64 (52)	32
6*	G	89	82	38
6	D	87	171 (154)	63.1
3	D	80	128 (124)	50.5
8*	F	35*	121 (139)*	54.9*

*Test site 6 connections tested during summer of 1994
( ) Maximum stress range recorded from calibration tests

Type E Bolted Angle Connection

One type E bolted angle connection was instrumented. The measured stress ranges at the web-flange radius and at the top of the connection are shown in Figures 2.12 and 2.13, respectively. The one instrumented type E connection was at test site 7 where welded built-up plate girders were used as the main load carrying members. Because this connection angle was tight-fit against the top flange, gages for measuring distortion-induced stresses in the web could not be placed in the web gap, but strain gages were placed adjacent to the web gap as shown in Figure 2.9. Stress ranges shown in Figures 2.12 and 2.13 are not extrapolated into the web gap area, and it is believed that stresses in the web gap are larger than those measured adjacent to it.

During the laboratory testing phase of this project connections with similar web gap and connection angle dimensions to the type E connection were instrumented with strain gages beside the web gap as done in the field and with strain gages in the web gap. This was done so that the stress range within the web gap for type E connections could be estimated. Two connections were instrumented during the laboratory tests: the first on a simply supported girder with back-to-back connection angles and a 15.4 mm thick web and the second on a continuously supported exterior girder with a 18.4 mm thick web. The first connection is a closer replicate of the connection instrumented in the field mainly because the type E connection in the field was on a girder with a web thickness of 12.7 mm. However, since neither laboratory connection matches the type E connection precisely, the results from both laboratory connections will be compared to the field results.

For the first connection an average 15% increase in stress ranges in the web gap at both critical locations were observed during the laboratory tests as compared to an average 223% for the second connection. The largest measured stress ranges in the field adjacent to the web gap were from calibration trucks and were 71 MPa and 60 MPa at the web-flange weld and top of connection angle, respectively. These measured stress ranges are 31% (32 MPa) and 45% (50 MPa) below the respective fatigue limits. If a 15% increase of measured stress ranges is assumed then cracks would not be expected to form in the web at the top of the connection angle or at the web-flange weld. If a 223% increase is assumed then cracks are expected to initiate at both locations in the web gap. Fatigue cracking is, therefore, a possibility at the type E connection instrumented in the field. If this type E connection had been on a

rolled girder instead of a plate girder, the potential for cracking would be somewhat lessened.

Type F Bolted Angle Connection

The one type F bolted connection investigated had stress ranges from truck traffic at the web-flange radius below the fatigue limit. However, one calibration test yielded a stress range at the web-flange radius over the category A fatigue limit of 165 MPa. Cracking is possible at the web-flange radius for the type F connection based on the calibration tests.

Type G Bolted Angle Connection

Four type G bolted angle connection web gaps were instrumented so that the stress ranges in the girder web at the edge of the radius and at the top of the connection could be measured. A web gap length (defined as L in Figure 2.2) of 178 mm was used at the connections referred to as 6 (d) and 6 (f) in Figures 2.12 and 2.13, and a web gap length of 89 mm was used at connections 6 (h) and 6 (j). The field test results do not show any significant differences between the stress ranges measured at these connections which can be attributed to the web gap length. None of the type G connections experienced stress ranges greater than the respective fatigue limits at the critical locations.

For the type G bolted connection at location 6 (a) the largest trucks from the traffic flow created stress ranges at the edge of the radius slightly less than the fatigue limit of 165 MPa. The largest stress range from truck traffic was 159 MPa with the second largest only slightly less than 159 MPa. The third smallest stress range was 83 MPa with a good distribution of stress ranges from 83 to the minimum stress range of

16 MPa. The two largest stress ranges are probably due to unusually heavy trucks crossing the bridge during the time data was being recorded. The third largest stress range of 83 MPa is more in line with the maximum stress ranges recorded at the three other type G connections.

Based on the magnitudes of recorded stress ranges at the four type G connections, cracking is not expected to occur in the web at the edge of the radius or at the top of the connection angle. The field test results do not show any significant differences between the two web gap lengths tested.

BEHAVIOR OF BOLTED CONNECTION ANGLES

Some of the angles which were used to replace the welded diaphragm-girder connections have cracked in the leg which attaches to the web. Although fatigue cracking has occurred in the type D connections only, there is some concern that other types of angle connections may experience similar cracking after sufficient load cycles. The cracks that have been found typically initiated underneath or immediately in front of the washer or bolt head at the bottom connection bolt and propagated through the thickness of the angle and lengthened along the angle (Figure 1.5). Due to the tightening of the bolts to the angle with an impact wrench the outside surface of the angle underneath the bolt head or washer is indented, which creates a stress concentration and a site for crack initiation in some cases (Figure 1.7). The stress ranges that cause crack initiation and growth are the result of traffic causing differential girder deflections which result in prying and pushing of the bottom of the angle.

The prying of the angle away from the girder web and pushing of the angle to close unintended gap (Figure 1.9) results in stress ranges with large tension and

compression stress components depending on which action occurs. Large stress ranges (above the fatigue limit) will cause a crack to form irregardless of the sign of the stress range. However, a tension component of the stress range is necessary for crack growth. Table 2.5 shows a comparison of effective stress ranges to effective tension stress ranges which were calculated by using the magnitude of the tension part of the full stress range for four of the type D connection angles and all of the type G connection angles. All of these connections have a significant tension component in the effective stress ranges which would cause crack growth after crack initiation.

Table 2.5. Effective Stress Ranges (Sre) and Tension Effective Stress Ranges (Sre(T)) for Type D and Type G Connection Angles

Type D		
Location	Sre (MPa)	Sre (T) (MPa)
1 (c)	76	18
2 (a)	63	28
2 (c)	68	5
3 (c)	134	30
Type G		
6 (d)	45	36
6 (e)	57	10
6 (f)	70	17
6 (g)	30	11
6 (h)	43	9
6 (i)	38	3
6 (j)	20	3
6 (k)	49	11

Previous to the research described in this report a fatigue limit for the fatigue cracking mechanism in the bolted connection had not been established. Laboratory testing aimed at determining the fatigue limit was conducted as part of this project and is discussed in Chapter Three. As a result of this testing a fatigue limit of 165 MPa was established for the connection angle stress range.

The following sections present the stress range data from the field tests for the four types of bolted connection angles. The field test data are summarized in Figure 2.15.

Type D Angle

The highest stress ranges were measured at the bottom gage locations on the type D angles; therefore, only the results for the bottom angle gages are shown in Figure 2.15. As shown in Figure 2.15, all but one of the seven type D angles developed stress ranges at or above the assumed fatigue limit (165 MPa) at the gage locations.

Stress ranges at two of the type D angles exceeded the yield strength of the steel (250 MPa). Many of the stress ranges recorded in the bottom gages on the angles had large stress reversals; therefore, even though a stress range exceeded 250 MPa that would not necessarily mean there was yielding of the angle at the gage location. Stress ranges higher than 250 MPa were measured at connections, 3(c) and 6(d) in Figure 2.15. At connection 3(c), four truck crossings resulted in stress ranges with a tension component that exceeded the yield limit of steel, and at connection 6(d) one truck crossing resulted in yielding of the angle. Although the measured strains

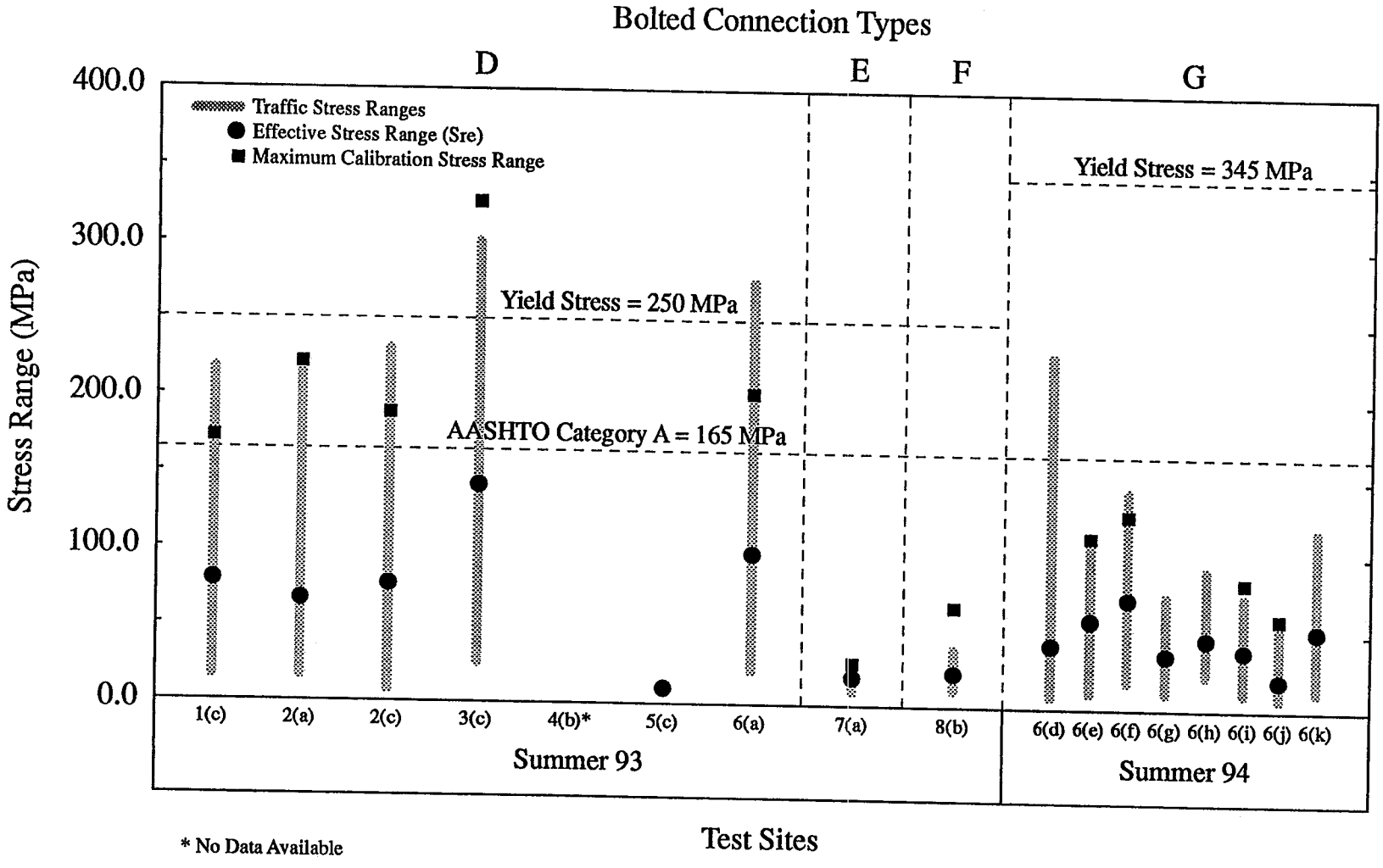

Figure 2.15. Angle Stress Ranges at Top or Bottom of Angles

exceeded the yield strain, fictitious stresses were calculated using Hooke's Law ($\sigma = E\epsilon$) and are shown in Figure 2.15.

The bottom gage location for the angles was approximately 25 mm below the point at which fatigue cracks initiate; therefore, the stress at the point of crack initiation is higher than measured at the gage. This indicates that even though only a few truck crossings caused yielding at the gage location on the bottom of the angle, more caused yielding of the angle in the area of crack initiation.

Overall, the stress ranges recorded in the type D connection angles were high and are expected to cause cracking. The higher the stress ranges at individual angles, the faster that cracks initiate and propagate. The results of the field inspections indicate that the service life of the angles is as short as one or two years. At test site 6 where fatigue cracking of a large number of type D angles has occurred, approximately seven million heavy trucks have crossed the bridges since type D angles were first installed in 1990.

Type E Angle

The angle investigated at a type E connection was instrumented with a series of gages extending from the top to the bottom of the angle of girder six at test site 7. The stress ranges recorded for the top gage mounted on the angle were found to be the largest and are shown in Figure 2.15.

This angle experienced low stress ranges that are well below the assumed fatigue limit of 165 MPa, and it is unlikely that cracking will occur in the angle. Angles of this types, based on the inspections previous to 1993, have not developed cracking due to fatigue. The stress magnitudes at the top of the connection are higher and

decreased going down the angle connection. This indicates that if stress ranges high enough to induce cracking were developed in this type angle, the crack would probably initiate near the top bolt head.

Type F Angle

The one type F connection angle examined during the summer of 1993 was at test site 8. Field inspections, as of 1993, have not found any fatigue cracking in angles of this type. Figure 2.15 shows the stress ranges for this connection at the top gage location. The overall magnitudes of the stress ranges in the angle were very low and should not result in fatigue cracking. The stresses at the gage locations in the angle are highest at the top, some what lower at the bottom, and lowest in the middle of the angle. This shows that if the stress ranges were significantly increased, cracks would possibly initiate at the top of the angle.

Type G Angle

The stress ranges recorded at the bottom gage on each of the eight type G connection angles are shown in Figure 2.15. At one of the eight type G angles, stress ranges from traffic trucks and/or calibration trucks exceeded the fatigue limit of 165 MPa. Fatigue cracking is expected to occur at this connection angle.

Effectiveness of the Hole Drilling Retrofit Technique

Because stresses in the web gap region were high enough to cause and have caused fatigue cracking, an economical and effective repair for web cracking is needed. As discussed earlier in this report, crack growth can be arrested under some conditions by drilling a hole at the crack tips (Fisher et al. 1990). Fisher et al. concluded that growth of distortion-induced web cracks can be stopped with drilled

holes provided the distortion-induced cyclic stress range is less than 105 MPa and the in-plane bending stress is less than 42 MPa.

At all test sites considered in this study, in-plane bending stress ranges were less than 42 MPa. Eight of the nine type A connections investigated had stress ranges above 105 MPa so that a repair of distortion-induced web cracks by drilling holes could be effective at only one of these connections. Both of the type B welded connections had stress ranges at the web-flange radius above the limit for the drilled hole retrofit technique. The type C welded angle connections had stress ranges less than the 105 MPa limit. For most of the original welded connections (types A, B, and C), the drilled hole retrofit will not be a permanent fix.

The drilled hole retrofit should provide a permanent repair for distortion-induced cracks along the web-flange radius for two of the seven type D bolted connections investigated. In addition, it is believed that cracks repaired in the web gap between the radius and top of the connection angle, where a welded connection has been removed, will not reinitiate. Crack reinitiation is not expected because this region is a low stress area after replacement of the welded connection with a bolted connection.

Distortion-induced cracks in the web at critical areas of the type E connections can be permanently retrofitted by drilling holes. A problem with this attachment is encountered in the location and discovery of the cracks which may be hindered by the tight-fit angle. The tight-fit angle makes visual inspection or dye penetration tests extremely difficult. In order to discover distortion-induced web cracks and drill holes at the crack tips, the angle may have to be removed. This would generally defeat the purpose of the connection and retrofit technique. The stress ranges at the edge of the

radius for the type F connection were too large for the hole drilling retrofit to be effective; however, the vertical stress ranges at the top of the bolted connection and the horizontal stress ranges in the web gap were small enough that hole drilling should stop further crack growth.

Discussion of the Bolted Connection Results

The purpose of using a bolted angle connection is to eliminate cracked welds in the original connection and to reduce the web gap stresses. By reducing the stresses, there is less likelihood of crack initiation or propagation in the web. The bolted angle connections for which field measurements were made generally had lower stresses in the web gap region than did the welded connections (Figures 2.12 and 2.13). The field test results indicate that use of the bolted connections does reduce the web gap stress ranges. Although some of the stress ranges in the web gap region are still above the fatigue limit and above the level required for hole drilling to be a permanent repair, use of a bolted connection will extend the life of the web at the diaphragm-girder connection.

Overall Comparison of the Bolted Web Gap and Angle Results

It would be desirable to use a bolted angle connection in the field that is not expected to crack and has web gap stresses below the fatigue limit; however, none of the four angle connections performed in this manner. Generally, web gap stresses were lowest in the type G connection, and the angle stresses were lowest in the type E or F angles which were longer and thicker than the type D or G angle. The potential for fatigue cracking in the girder web is considered here to be less desirable than for cracking of the angle. Therefore, based on the field testing results the type G

connection angle appears to be the best alternative when a welded or bolted connection must be replaced. The connection angle types were further investigated in an experimental testing program which is discussed in Chapter Three.

EFFECTS OF STAGGERED DIAPHRAGMS

At one test site (test site 5), the diaphragm-girder connections of a bridge with staggered diaphragms were examined. These connections consisted of two type A welded plate connections, one type C welded angle connection, and one type D bolted angle connection. The stress ranges at test site 5 shown in Figures 2.10, 2.11, 2.12, and 2.13 are considerably lower than the stress ranges at similar connections at test sites with straight lines of diaphragms. It appears that the web gap stresses may be lower in bridges with staggered diaphragms. However, additional investigation and testing should be done in order to examine the effectiveness of staggering diaphragms to reduce web gap stresses.

CONCLUSIONS

Determining the potential for cracking in the girder web at diaphragm-girder connections and in bolted connection angles was one objective of this report. Stress and displacement measurements were taken at eight bridge test sites in the Birmingham area. Cracking in the web and welds of the original welded stiffener connection and in the bolted replacement angles has been discovered in the past 5 years.

The field measurements verified that the stress ranges occurring at the connection plate to web welds and at the web-flange radius for the original welded connections (type A, B, and C connections) were large enough to cause fatigue

cracking. Hence, based on the field measurements at uncracked connections, distortion-induced fatigue cracking in the web at welded diaphragm-girder connections can be expected to occur at many of the remaining uncracked connections.

For bolted angle connections (type D, E, F, and G connections) the stress ranges in the web gap were lower than those for the welded connections (type A, B, and C connections) indicating that these replacement angles were successful in reducing the likelihood of web gap cracking. However, the stress ranges in the web gaps of the bolted angle connections were large enough at some connections to eventually result in cracking of the web. Generally, the type G connection angle had the lowest gap stresses as compared to the other bolted connection angles.

Numerous cracks have been discovered in the type D replacement angles (L152 x 152 x 9.52 (mm) by 0.482 m long) by bridge inspectors. Based on the measurements from seven type D connection angles, cracking of these angles is expected to continue to occur. Bridge inspectors have not discovered cracks in any of the type E (152 x 102 x 12.7 (mm) by 1.11 m long) or type F (152 x 102 x 15.9 (mm) by 0.66 m long) connection angles and the stress ranges measured in those types of connections were significantly lower than those measured in the type D angles. Neither of the type E or the type F angles instrumented had measured stress ranges that were large enough to result in cracking of these angles. The proposed new connection angle (type G) experienced stress ranges at one of eight locations large enough to cause cracking in the angle leg at the bottom bolt hole. Overall, the field tests results indicate the type G connection angle is best suited for use in connection replacement.

Another objective of this report was to evaluate the effectiveness of the hole drilling retrofit. Based the stress ranges measured in the web gaps of the six connection types, hole drilling will stop crack growth at some connections, but at most connections it will only temporarily arrest crack growth. No pattern was observed in the field test results that would allow easy identification of the connections where drilling holes will be a permanent repair.

CHAPTER THREE

LABORATORY INVESTIGATION OF BOLTED CONNECTIONS

INTRODUCTION

Some of the angles which were used to replace the welded diaphragm-girder connections have cracked in the leg which is attached to the girder web (Figure 1.5). Although fatigue cracking has occurred in the type D connections only, there is some concern that other types of angle connections may experience similar cracking after sufficient load cycles. The cracks that have been found typically initiated underneath or immediately in front of the washer or bolthead (Figures 1.7 and 1.8) at the bottom connection bolt and propagated through the thickness of the angle and lengthened along the angle. Due to the tightening of the bolts to the angle with an impact wrench the outside surface of the angle underneath the bolthead or washer was indented, and often at this location the cracks initiate and grow through the thickness of the angle and upwards and downwards. The stress range that causes crack initiation and growth is the result of traffic causing differential girder deflections which cause prying and pushing of the bottom of the angle away from and toward the girder web. Also, a contributing factor to crack initiation and growth is the gap between the angle and girder web which results from fit-up error, the installation procedure and/or yielding of the angle due to overloads. Figure 3.1 shows an overhead view of an angle to web connection with a gap. Also, the location where cracks have been found to initiate at the bottom bolt on the connection angle is labeled in Figure 3.1.

A laboratory testing program was conducted to further investigate the causes of fatigue cracking and to develop a longer lasting replacement angle with a longer

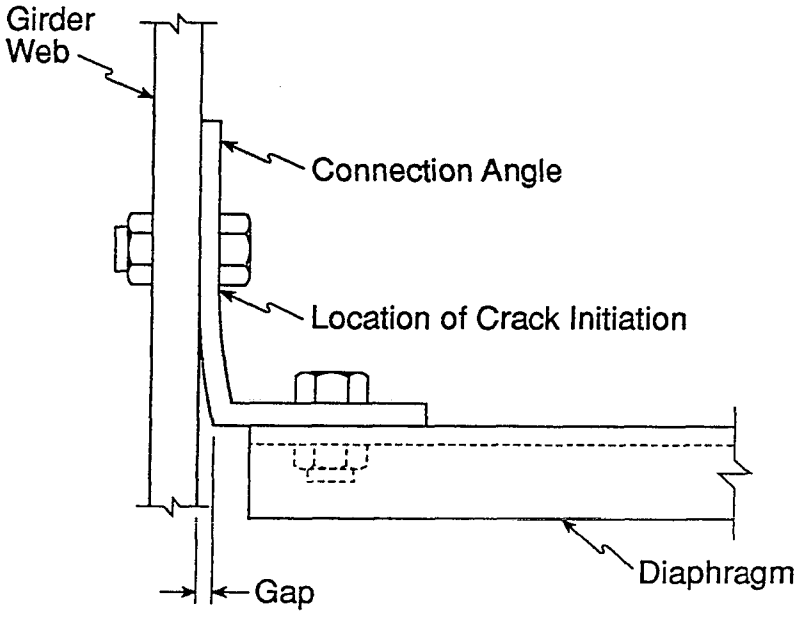

Figure 3.1. Gap Between Connection Angle and Girder Web

fatigue life that does not increase the likelihood of web gap cracking. In the Auburn University Structural Engineering Research Laboratory a model was constructed and tested which allowed simultaneous testing of 18 diaphragm-girder connections. The dimensions, member sizes, and support conditions for the connections in the model were similar to those in the bridges in Birmingham that have experienced fatigue cracking at the diaphragm-girder connections. Fatigue tests were performed using a closed loop servo-hydraulic testing system to apply and control the load and a high speed data acquisition system to record data.

Several different connection angle designs were included in the model during two fatigue tests to ten million cycles each. The model used in each test is referred to

here as a test set-up. The first test set-up contained multiple diaphragm-girder connections made with three connection angle designs which were identical or similar to angles used in the field over the past five years. In the second test set-up two connection angle designs were used. One was used in the first test set-up and the other was a connection angle design (type G) that is proposed for use in future connection replacements. For all four types of connection angles tested in the laboratory considerable field test data from calibration tests and truck traffic has been collected and was discussed in the previous chapter.

The objectives of this chapter are to discuss the laboratory test results for the four types of connection angles and to answer the following questions:

a) How does the presence of a gap between the connection angle and girder web affect the stress in the angle and girder web?

b) What is an appropriate fatigue limit for the area of the connection angles where fatigue cracks initiate?

c) Which of the four connection angle designs perform better (i.e. provide the lowest probability of angle cracking without increasing the potential for web gap cracking)?

d) What is an appropriate fatigue limit for the web at the edge of the girder radius?

TEST SPECIMEN AND TEST DESIGN

Connection Angle Sizes

Inspection of cracked connection angles has revealed that the point of crack initiation is at or near the bolthead on the outside of the angle leg bolted to the girder

web. One goal of the laboratory model was to recreate the area of potential crack initiation in the connection angles selected for testing. This was done by using connection angles bolted to the girder web with as close as possible to the actual size of connection angles, bolts, and bolt spacings that were used in the field.

Four angle sizes were selected for testing and were given the following designations (types):

1) L 152 x 152 x 9.5 (mm) by 0.483 m long (type D)

2) L 152 x 152 x 7.9 (mm) by 0.483 m long (type D*)

3) L 152 x 102 x 15.9 (mm) by 0.724 m long (type EF)

4) L 203 x 152 x 12.7 (mm) by 0.483 m long (type G)

Figure 3.2 shows details of the four angles and the web gap length used for each. Channel diaphragms were centered at mid-height of the angles and bolted to the out-standing angle leg.

The type D connection angle was selected for testing because it is the primary angle type used for repair in the Birmingham area and many of the type D angles have cracked in service. The type D* connection angle is identical to the type D angle except thinner which allowed for investigation of the effect of angle thickness on the stress ranges in connections containing type D and D* angles. The web gap (the distance between the connection angle and the girder flange) used for the type D and D* connections was chosen as 101.6 mm which is the approximate average web gap found in the type D connections in the field.

The type EF connection angle is a hybrid of the type E and type F angles described in Chapter Two. To date no cracking of type E or type F angles has been

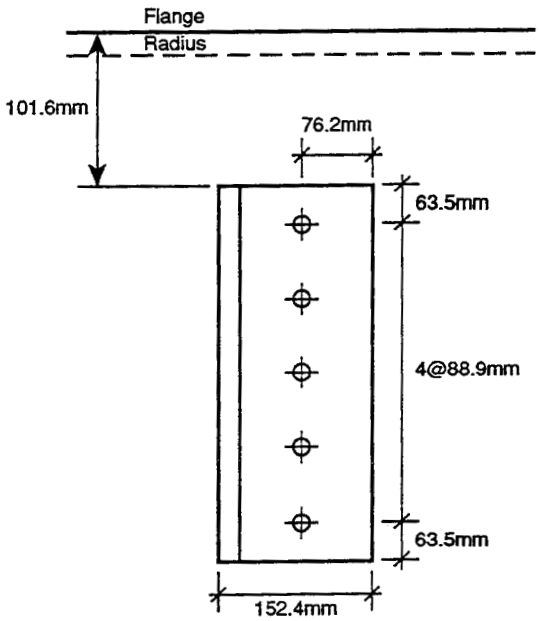

a) Type D

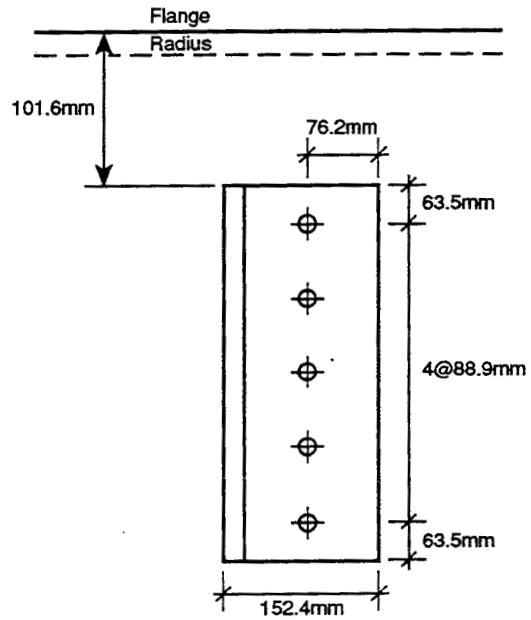

b) Type D*

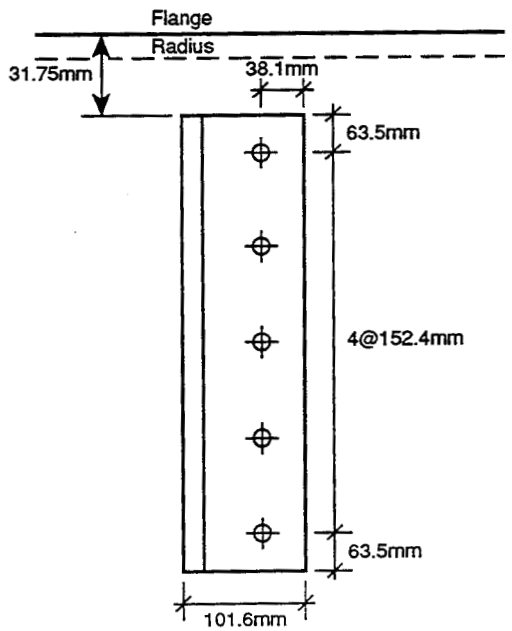

c) Type EF

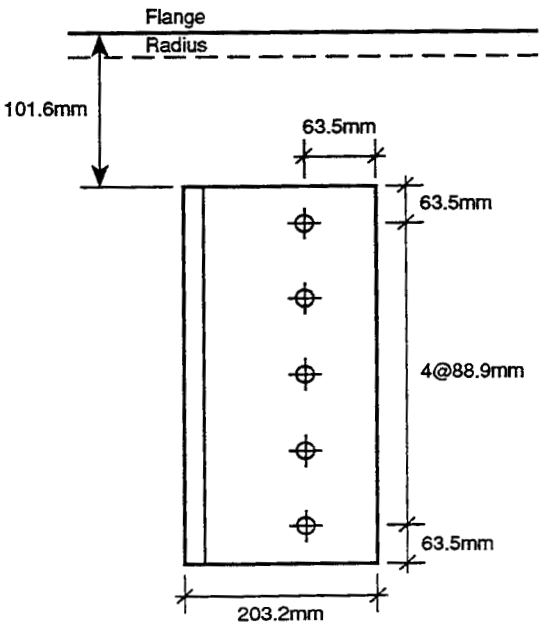

d) Type G

Figure 3.2. Connection Angle Details

discovered indicating that the type E and type F angles may not be as susceptible to fatigue cracking as the type D angle. There are two possible reasons for type E and F angles not cracking. The type E and F connection angles are thicker and significantly longer than the type D connection angle which may decrease the level of fatigue stress at the point of crack initiation in the type E and type F angles. Also, the type E and F connection angles have not been exposed to as many cycles of loading as the type D connection angles due to the lower traffic volume on the bridges containing the type E and F connection angles. The angle size and web gap length of the type EF connection were chosen to approximate the connections containing type E and type F angles.

The type G connection angle is a new angle design proposed for use in connection replacements. The type G connection angle is the same length as the type D but is thicker, is made with a higher yield strength steel, and has a longer leg attached to the girder web. The web gap for the type G connection angle was the same as the type D and D* connection angles. The type G angle was tested to give a direct comparison of the performance of the proposed angle to the angle (type D) most often used in the past to replace damaged diaphragm-girder connections.

Laboratory Model Description

The laboratory model was designed to recreate the differential girder deflections that result in bending of the connection angle which produces a stress range at the point of crack initiation. Figure 3.3 is a plan view and Figure 3.4 is a transverse cross-sectional view of the model. The laboratory model consisted of two inside girders simply supported at the ends and two outside girders continuously supported on

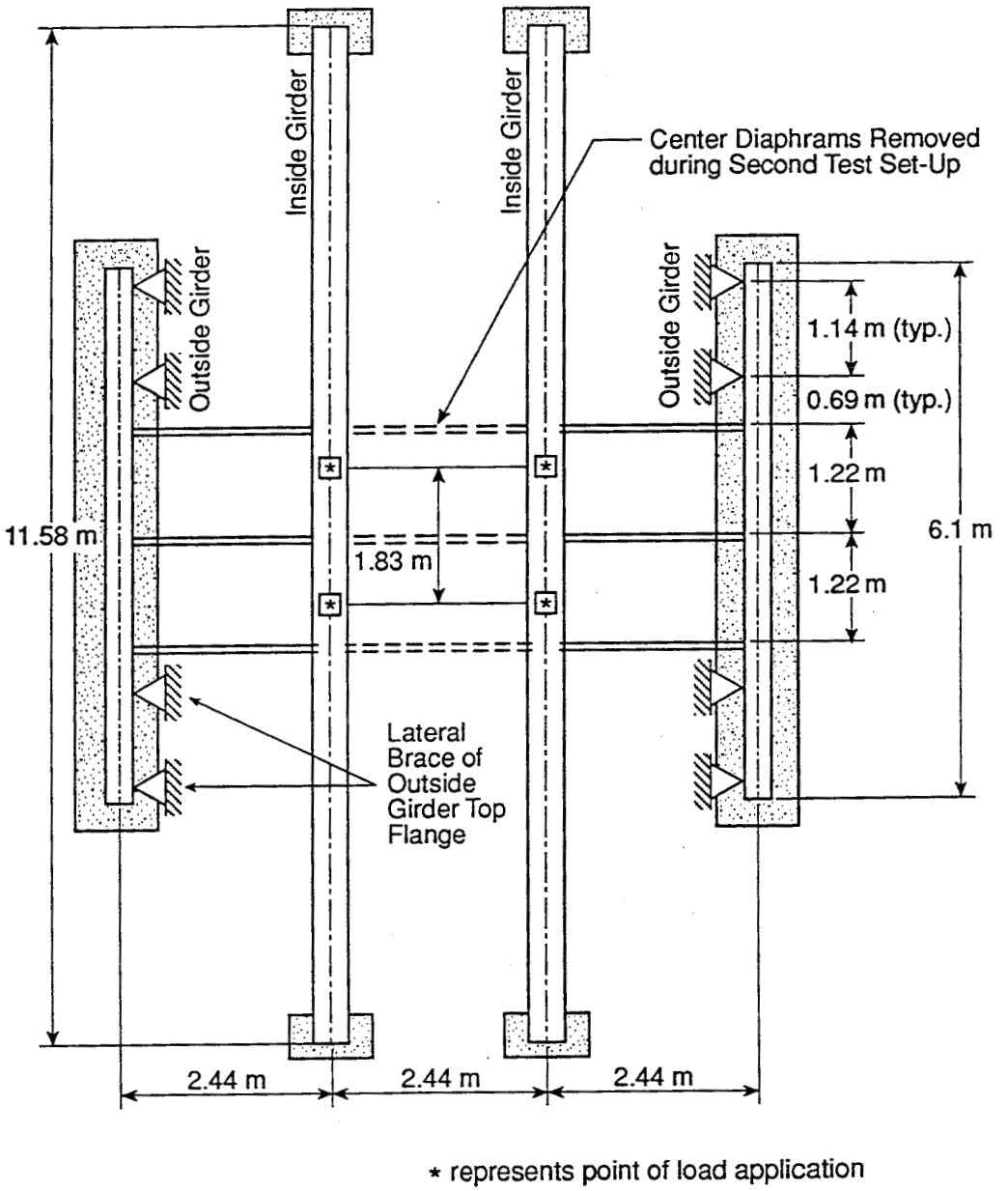

Figure 3.3. Plan View of Laboratory Model

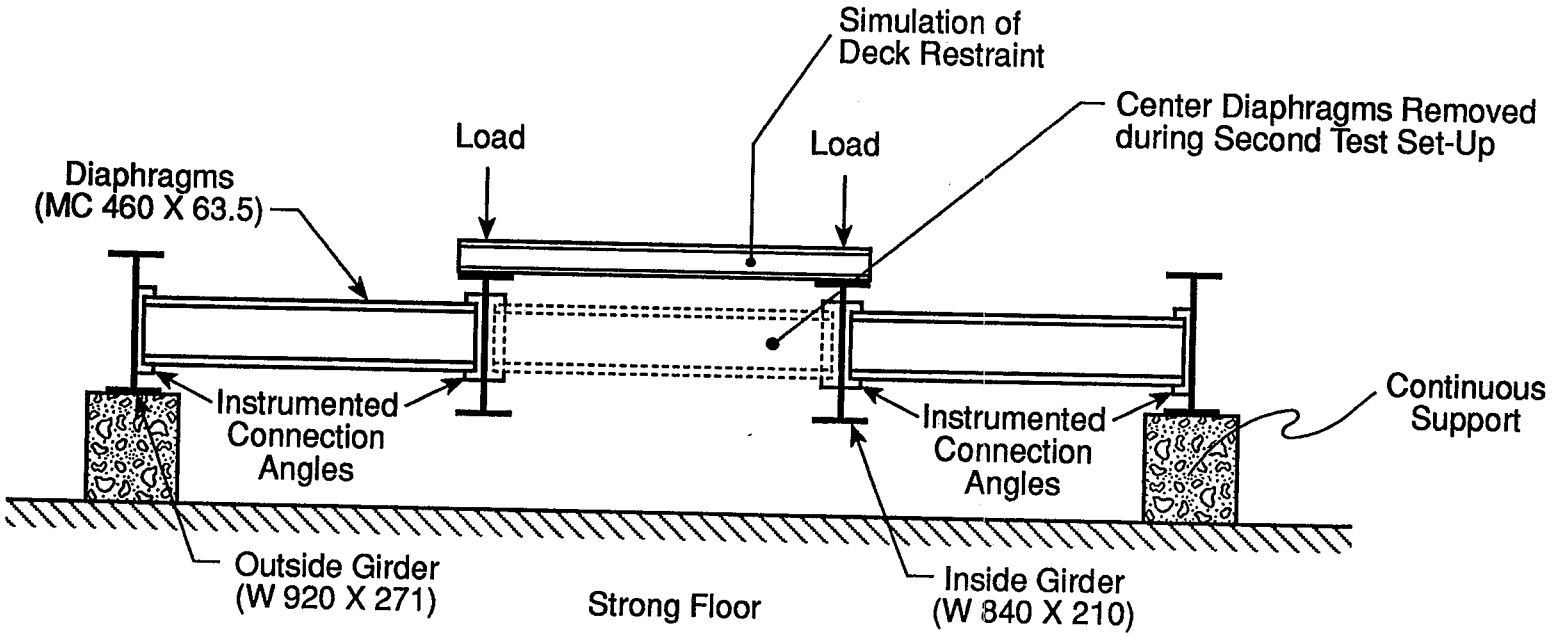

Figure 3.4. Transverse Cross Section through Laboratory Model

concrete piers.

Three rows of diaphragms connected the inside and outside girders providing 18 locations for diaphragm-girder connections. Wide flange sections connected the top flanges of the inside girders to simulate the restraint of a reinforced concrete bridge deck. The connections on the inside girder were conventionally oriented. The two outside girders are oriented upside down, that is the continuous support of the outside girder bottom flange represents the continuous top flange support of a concrete bridge deck, and the critical web gap is between the connection angle and the girder bottom flange. The top flange of the outside girders was braced against horizontal movement to further stiffen the outside girders. The four girders were spaced 2.44 m apart which is typical of transverse girder spacings in the field. In the first test set-up the three rows of diaphragms were continuous from outside girder to outside girder (Figure 3.3); however, for the second test set-up the center diaphragms were omitted.

The steel used in the Birmingham bridges had a yield stress of 250 MPa, therefore, steel with the same yield stress was used in the laboratory model (girders, diaphragms, and connection angles) except for the type G angle. The type G connection angle was made from steel with a yield stress of 345 MPa. All bolts used in the laboratory were A325 as were those used in the field.

The size of the girders was chosen to be representative of the web thicknesses in the Birmingham bridges. Two W 840 x 210 (web thickness = 15.4 mm) were used for the inside girders and two W 920 x 271 (web thickness = 18.4 mm) were used for the outside girders. All diaphragms in the field were MC 460 x 63.5 channel sections, and this channel was used in the laboratory model.

A total of 20 connection angles were tested during the fatigue tests of the two test set-ups. Table 3.1 contains the type, number, and location of each. In the first test set-up the three transverse lines of diaphragms each contained one type of connection angle. For the second test set-up only the connection angles on the inside girder were replaced with new type D and type G connection angles.

Table 3.1. Type, Location, and Number of Connection Angles Tested

Test Set-up	Girder Location	Connection Types	Number Tested
1	Inside	D D* EF	2 3[1] 3[1]
	Outside	D D* EF	2 2 2
2	Inside	D G	2 4
	Outside[2]	D D* EF	2 2 2

[1] designates one connection angle cracked before completion of fatigue test. This angle was replaced and fatigue test continued.
[2] angles on outside girder not changed for second test set-up.

Loading Method

A hydraulic loading system that consisted of a 284 lpm hydraulic power supply, two hydraulic service manifolds, four 356 kN capacity hydraulic actuators, and four digital controllers was used to provide the load and stroke necessary to test the laboratory model. A 1.5 MN capacity structural steel load frame was designed and

constructed to provide the applied load. The load frame was designed to have minimal deflection in order to maximize the efficiency of the hydraulic loading system. The load frame was post-tensioned to the reaction floor of the laboratory using high strength steel rods. A picture of the load frame and hydraulic loading system is shown in Figure 3.5.

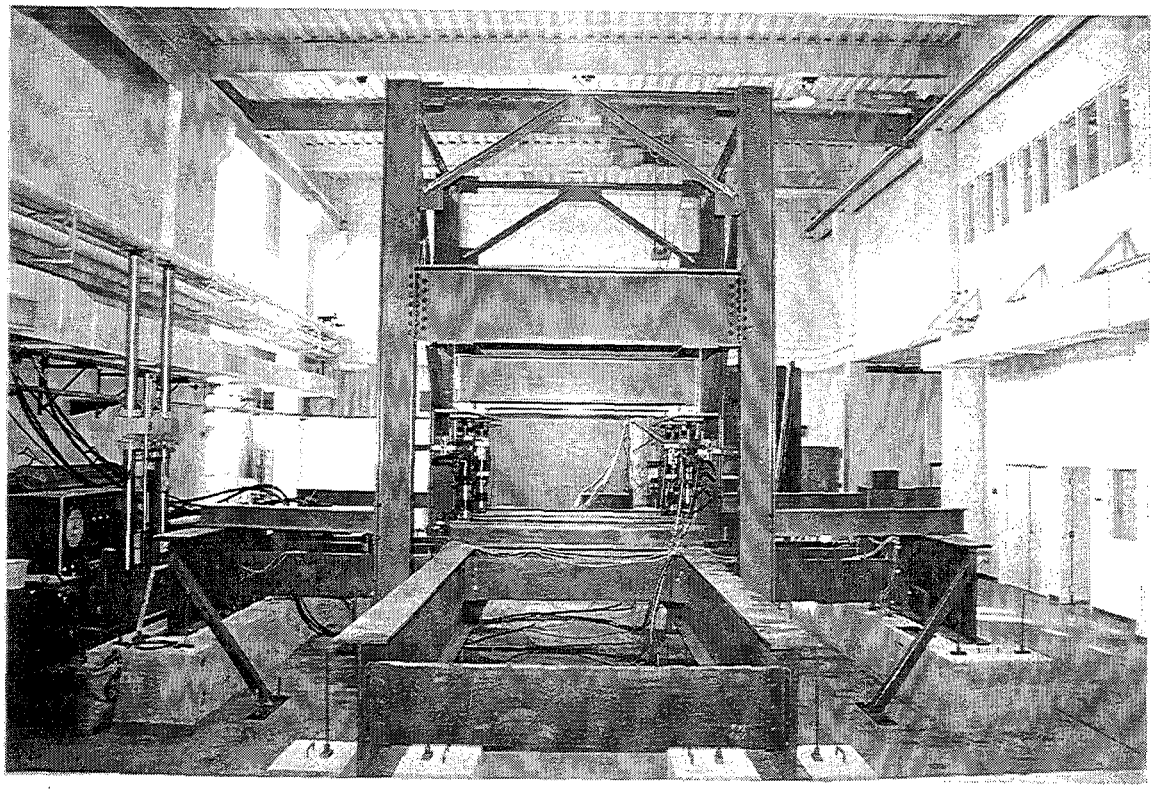

Figure 3.5. 1.5 MN Capacity Load Frame and Hydraulic Loading System

Two actuators were connected to each inside girder and the load frame, and four digital controllers were used to control the shape, frequency, and magnitude of the loading function for each. Each of the four actuators produced a sinusoidal loading of the same amplitude and phase yielding identical differential girder deflections between the two inside and outside girders.

The loading system was operated in displacement control mode to insure constant amplitude girder deflections. Displacement control was also used to prevent further damage to the model in the event that some part of the model failed. The loading system was operated at a frequency between 0.5 Hz and 2.1 Hz with the majority of the fatigue test being performed from 1.5 Hz to 2.1 Hz.

For the first test set-up the inside girders were initially deflected 5 mm down (at each actuator) then cycled 3.8 mm above and below that point to provide a 7.6 mm sine wave amplitude. The initial deflection and wave amplitude were increased for the second test set-up in order to increase the stress ranges in the connection angles. The initial deflection and sine wave amplitude for the second test set-up were 7.4 mm and 9.6 mm, respectively. The compression load in each actuator cycled between approximately 1 kN and 142 kN in the first test set-up and between 6 kN and 140 kN in the second test set-up.

Instrumentation

Load, displacement, and strain were measured during the laboratory tests. The load applied to each laboratory model was monitored with load cells attached in series to each actuator.

Vertical displacements were measured with linear variable differential transformer's (LVDT's). One LVDT was placed under each of the inside girders in the direct line of action of each of the four hydraulic actuators. LVDT's were used to measure the deflection during system start-up and, periodically during the tests. Constant monitoring of girder deflection was accomplished by LVDT's located inside the hydraulic actuators that provided a displacement signal to the digital controllers.

The amplitude measured by the internal LVDT's was slightly higher than that measured by the external LVDT's due to some deflection of the load frame. All measurements reported in this chapter as vertical girder deflections were from the external LVDTs.

Electrical resistance strain gages were used to measure the surface strains on the test specimen. All strain gages were temperature compensated foil gages encapsulated in polyamide with a nominal resistance of 350 ohms. The strain gages used in all locations had a 3.18 mm gage length except for on the diaphragms and on the girder flanges where 12.7 mm gages were used. Measured strains were converted to stress by multiplying the strain ranges by the modulus of elasticity of steel (200 GPa).

Critical locations for potential crack initiation within the web gap were in the web at the edge of the radius and at the top of the connection angle. Due to discontinuities in the girder web, strain gages could not be placed at the critical locations. Linear extrapolation of strains measured nearby was used to determine stresses at the critical locations. Due to the difference in the geometry of the web gaps for the type D and D* connections, the type EF connection, and the type G connection, three different strain gage patterns were used to instrument the web gaps at these type connection angles. Figures 3.6 and 3.7 show the strain gage patterns for the type D and D* connections and type G connections, respectively. The strain gage patterns used on the outside girders at type D and D* connections were upside down from the strain gage pattern in Figure 3.6.

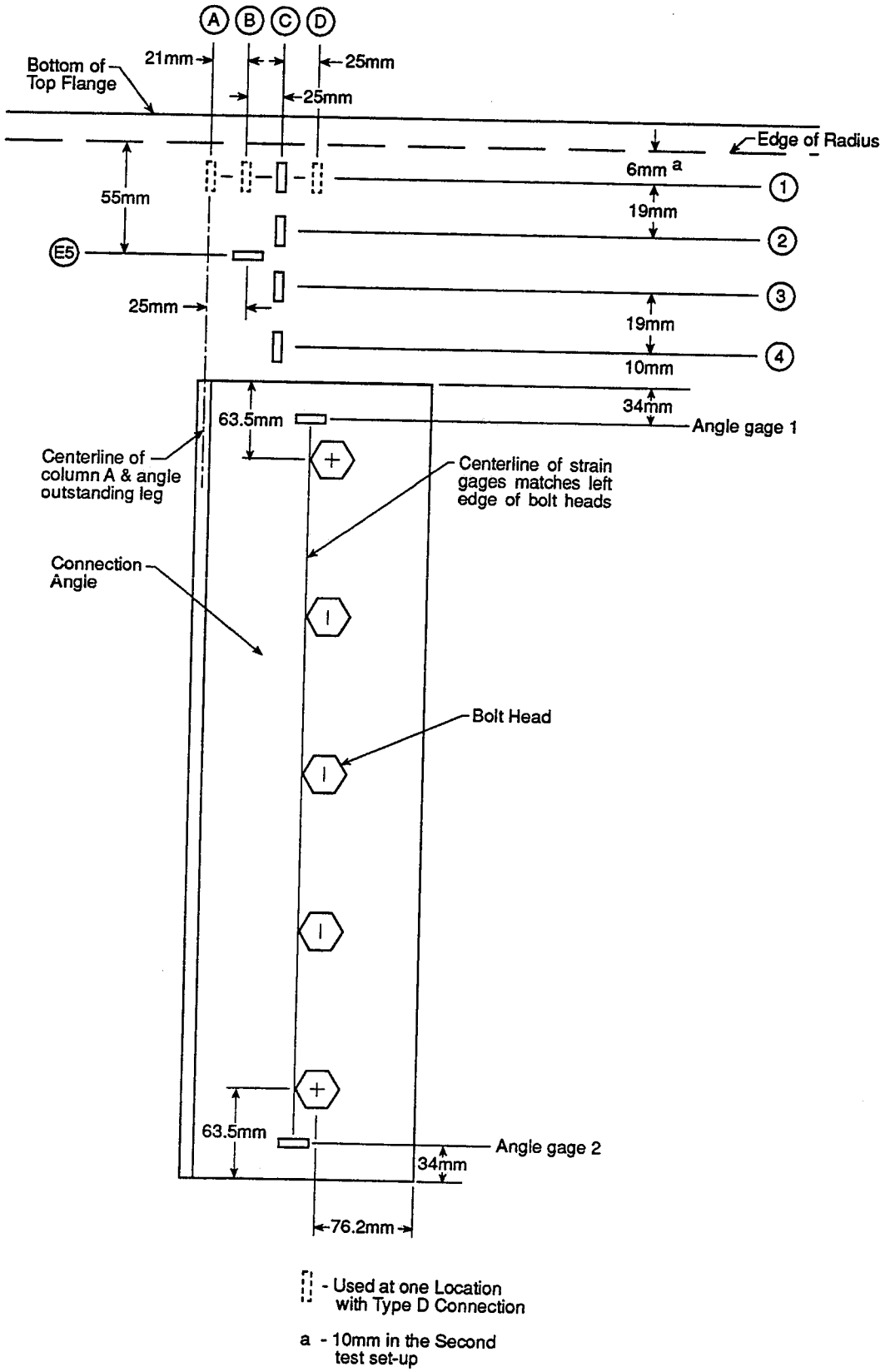

Figure 3.6. Gaging Patter for Type D and Type D* Connections on Inside Girders

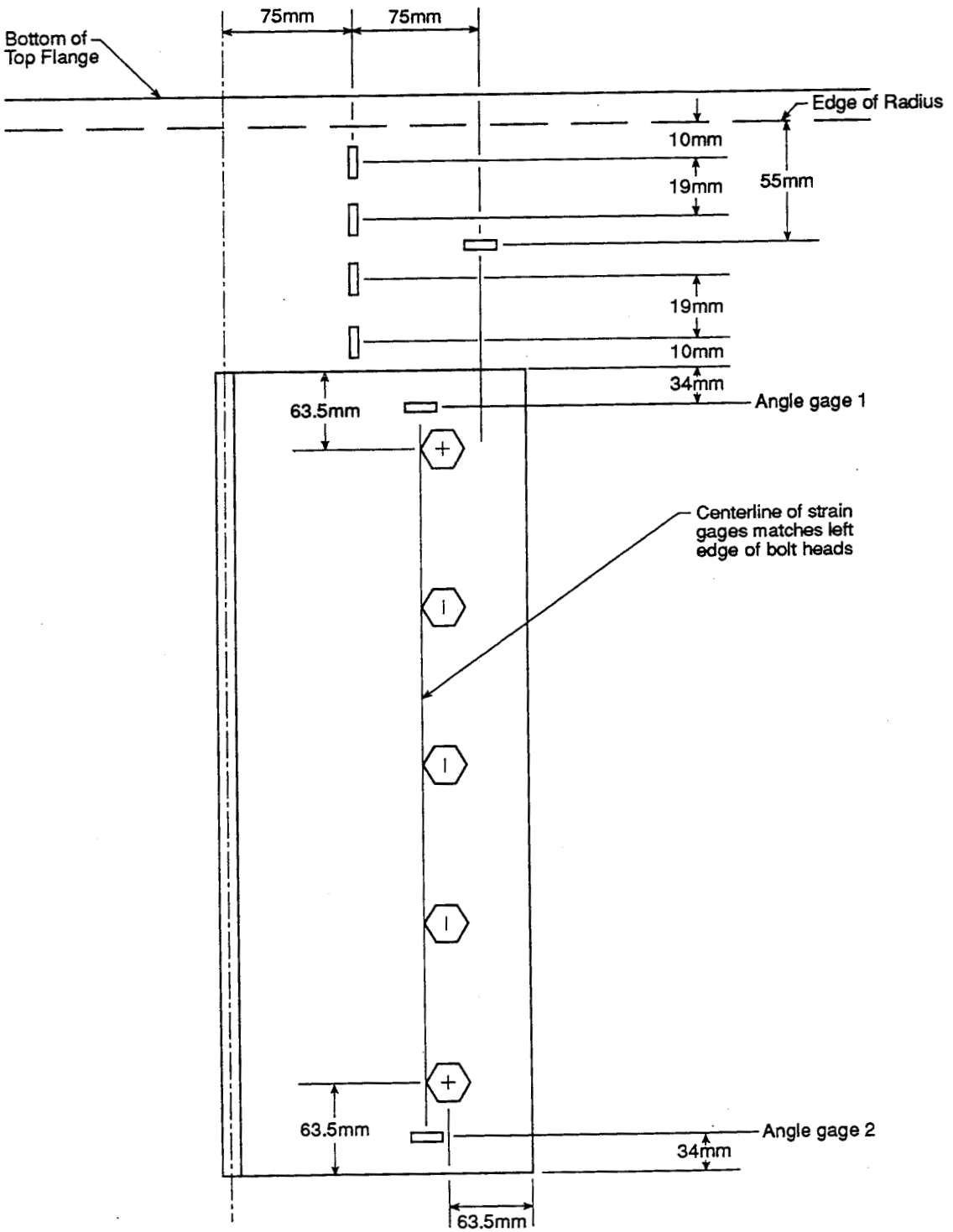

Figure 3.7. Gaging Pattern for Type G Connections on Inside Girders

The web gaps at type EF connections were too small to allow for a column of strain gages to be placed within the web gaps. The following three paragraphs describe two attempts to determine the relationship between stresses within the web gap and near the web gap for type EF connections.

The web gaps at type EF connections on the inside girders were small which prevented a column of strain gages from being placed within the web gap, and the stress ranges at the critical locations within the web gap could not be directly determined. Strain gages were applied to the girder webs adjacent to the web gaps on the inside girders as represented in Figure 3.8 by the open blocks. For one of the two type EF connections on the inside girders one row of gages was placed within the web gap and these gages are represented by solid blocks in Figure 3.8. Even though the stress ranges at critical locations within the web gap could not be extrapolated the

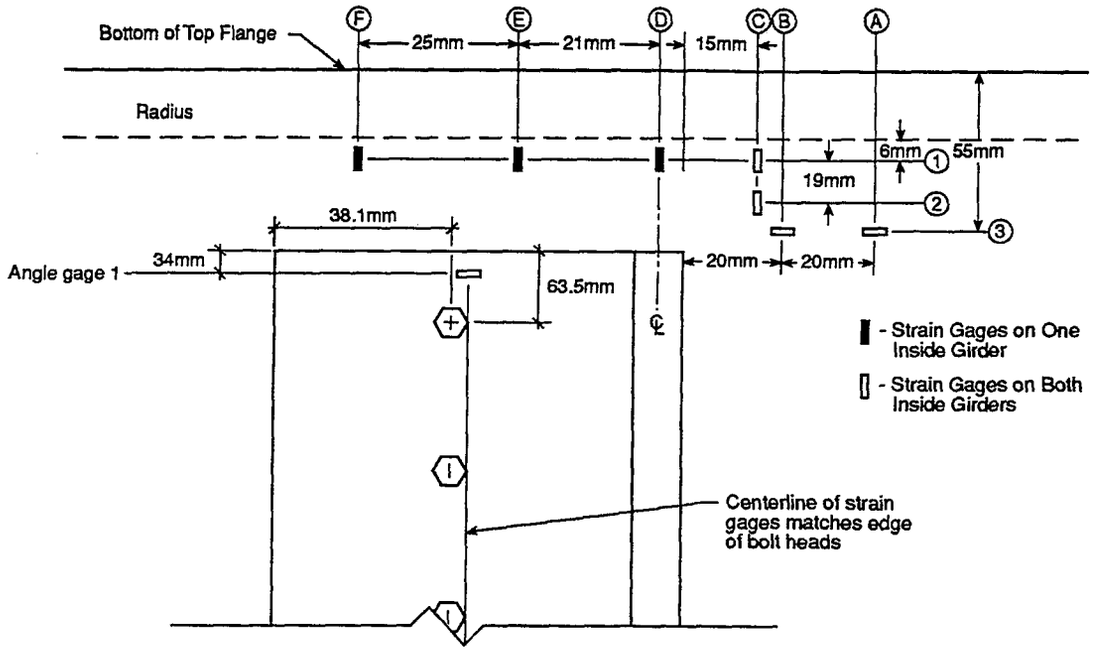

Figure 3.8. Gaging Pattern for Type EF Connections on Inside Girders

stress range at the gage location C1 was compared to that at gage locations D1, E1, and F1. A maximum stress range increase within the web gap at gage location E1 of 15% over that at gage location C1 was measured.

At the type EF connections on the outside girders a pattern of strain gages could be placed within the web gap on the side of the girder web without a connection angle. At the two type EF connections on the outside girders strain gages were placed adjacent to the web gap in an identical pattern to that used on the inside girders as shown in Figure 3.9. In addition, one outside girder had strain gages placed within the web gap (represented by the dashed blocks in Figure 3.9) that allowed extrapolation of the stress range to the edge of the radius within the web gap. The stress range at the edge of the radius within the web gap (point b in Figure 3.9) was compared to the stress range at the edge of the radius adjacent to the web gap (point c in Figure 3.9). The ratio of the stress at point b to point c during a cycle of load was calculated, and a 223% increase in stress range at the edge of the radius within the web gap was determined.

To completely evaluate the type EF connections as compared to the three other types of connection tested an estimate of the stress range within the web gap at the edge of the radius was needed. In the two previous paragraphs results from selected gages placed within the web gap on the inside and outside girders were presented. These results are inconclusive in evaluating web gap behavior based on the large difference in percent increase in stress range within the web gap at the edge of the radius as compared to that at the strain gages adjacent to the web gap. The relationship between stress range within the web gap and adjacent to the web gap is

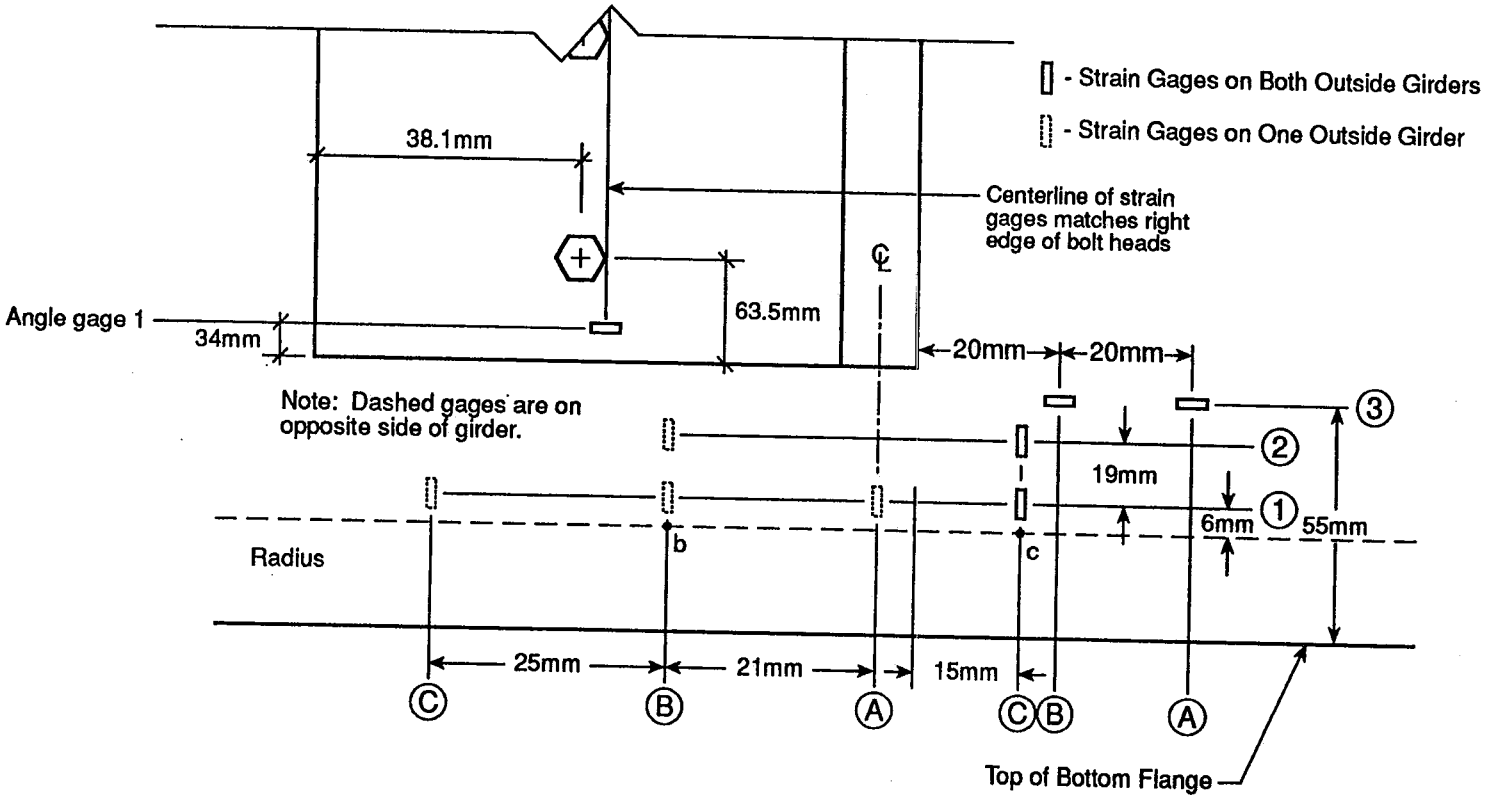

Figure 3.9. Gaging Pattern for Type EF Connections on Outside Girders

probably a function of the girder web thickness and the restraint condition of the girder flange closest to the web gap which were not the same for the inside and outside girders. Therefore, the stress ranges at the edge of the radius adjacent to the web gap for the type EF connections will be used as the lower bound of the stress range within the web gap at the edge of the radius.

Each connection angle was instrumented with two 3.18 mm strain gages measuring bending stress in the locations shown in Figures 3.6, 3.7, 3.8, and 3.9. Strain gages were installed on the leg of the angle attached to the girder web at both the end of the angle closest to the critical web gap and at the opposite end of the angle. These connection angle gage locations are referred to as gage locations one and two, respectively.

All gaging patterns used on connection angles and web gaps were identical to the gaging patterns used in field tests with the exception of the additional gages within the web gaps of the type EF connections.

The top and bottom flanges of the diaphragms were instrumented with four 12.7 mm strain gages. Strain gages (12.7 mm) were installed on the top and bottom flanges of the inside girders (in-plane gages) to measure the in-plane strain.

Data Acquisition

All laboratory test data was collected using a Megadac 3108AC dynamic data acquisition system (Technical Manual 1994) and 486-33 personal computer with compatible TCS 5.1 software (Technical Manual 1994). Recorded data were automatically transferred to the hard drive of a personal computer. A sampling rate of 400 samples per second per channel was used for the fatigue tests. A total of 24

channels were available for data acquisition. Sixteen of the channels were used for strain measurements, and 8 channels were used for load and displacement measurements. Each test set-up had in excess of 80 strain gages attached to the test specimen which required multiple test files for each fatigue test. Data was recorded periodically for each strain gage throughout each ten million cycle fatigue test.

Load and vertical girder deflection at each actuator were monitored periodically during each test. In addition, the four digital controllers provided a digital readout of load cell and internal LVDT data with limited storage capability.

ANALYSIS AND DISCUSSION OF RESULTS

Bolted Angle Behavior

The primary factor contributing to crack initiation and growth in connection angles in the field is unintentional gaps between the angle and girder web due to bolt-up technique, angle legs that are not at right angles to each other or yielding of the angle due to overloads.

In the field, differential girder deflections result from trucks crossing a bridge, and, since the girders are connected with diaphragms and connection angles, load is transferred transversely through the diaphragms. Large variable amplitude stress ranges were measured in the connection angles in the field. Gaps between the connection angles and girder webs (as shown in Figure 3.1) have been observed at many connections in the field. As the girders deflect due to truck traffic the gap at the bottom of the connection angles close or open depending on the direction of relative girder deflection. Closing of the gap creates tensile stress at the surface of the angle in front of the bottom which causes fatigue crack initiation. The larger the initial gap

size, the larger the tensile stress (range) which increases the likelihood of fatigue cracking.

Gaps as shown in Figure 3.1 were also present in the connections tested in the laboratory. In the laboratory model, downward deflection of the inside girders caused the gaps at the top of the angles on the inside girders and at the bottoms of the angles on the outside girders to close. Hence, those are the locations where fatigue cracking was likely and where cracking was observed. These critical locations are close to strain gage location one on the angles.

In the laboratory model the stress ranges at gage location one on the connection angles were generally higher than the opposite end of the angle. Feeler gage measurements and LVDT readings were made at two connections in test set-up two to illustrate the effect of gap size on angle stress ranges. Figure 3.10 shows the location of LVDT and feeler gage measurements with respect to the connection angle. The LVDT was mounted to measure the relative displacement between the outstanding leg of the angle and the point shown in Figure 3.10. Measurements were made as the gap closed during loading at the feeler gage points manually and the deflection of the LVDT was recorded continuously as the gap closed. The LVDT measured displacement of the gap as close as physically possible to the top feeler gage measurement point. These measurements were made at two connections on the inside girder in the second test set-up: one with a type D connection angle and the other with a type G connection angle. In addition vertical deflection of the girders and strains in the connection angles were continuously recorded. Figures 3.11 and 3.12 show the results of these measurements.

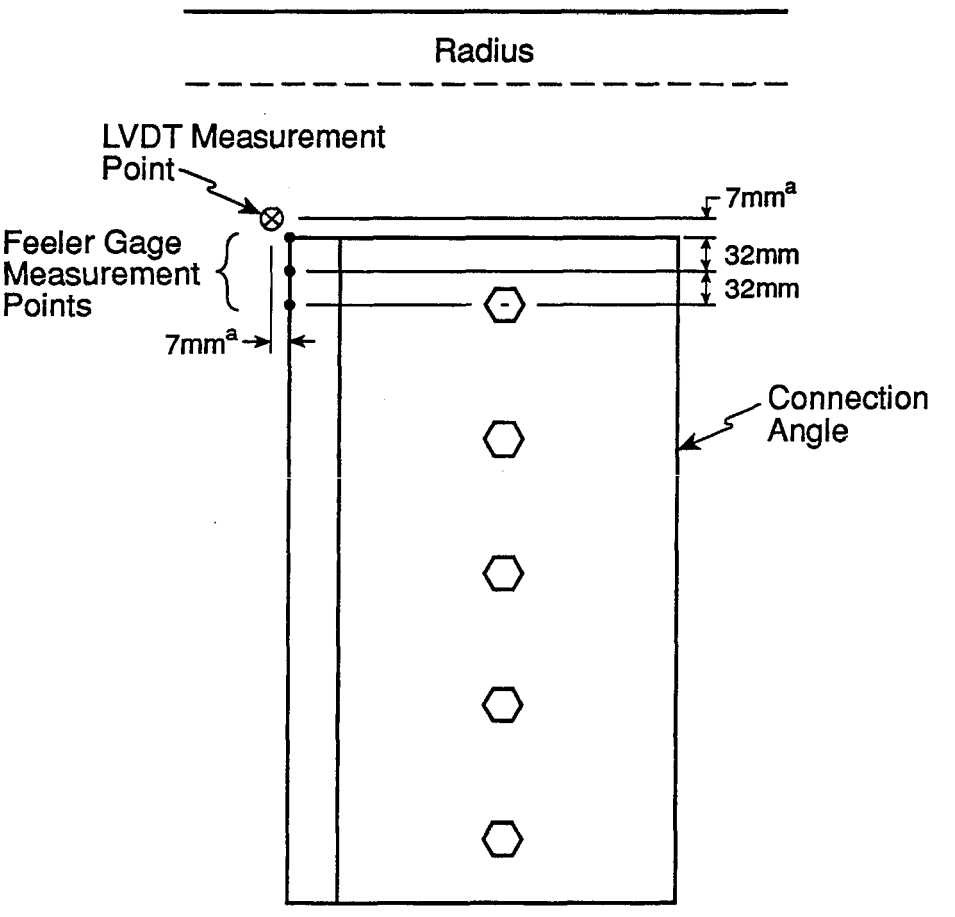

a - approximate dimension

Figure 3.10. LVDT and Feeler Gage Measurement Points

In Figure 3.11 a) and b) the stress in the top gage on the type D and G connection angles, respectively, is plotted versus girder deflection for one cycle of the fatigue test loading. The cycle was stopped intermittently to allow for the feeler gage measurements to be taken. Super-imposed on the plots are the feeler gage measurements taken as the girders deflect down and the gaps close. The feeler gage measurements given are at the three locations shown in Figure 3.10. For the type D connection angle the gap between the connection angle and the girder web closed at a girder deflection between 4 mm and 6.4 mm as shown by the zero feeler gage measurements beyond a girder deflection of 4 mm. This generally coincides with the point at which the stress range in the connection angle reaches a plateau. Hence, the stress range in the connection angle is a direct result of bending of the connection angle until the gap between the connection angle and the girder web closes.

For the type G connection angle the gap is larger than the gap at the type D angle and did not close during the load cycle. This can be seen from the feeler gage measurements that do not reach zero and the fact that the stress at the connection angle strain gage did not level off. Hence, the measured stress range in the type G connection angle results from the full cycle of relative girder deflection and the stress range in the type D angle results from only part of the relative girder deflection. This shows that minimizing the initial gap width so that the gap fully closes does place a limit on the magnitude of the stress range in the angle.

Figure 3.12 shows a comparison of the feeler gage measurements with the LVDT readings. LVDT readings were made due to the possible inaccuracies inherent in feeler gage measurements. The LVDT data illustrates the same trends as the feeler

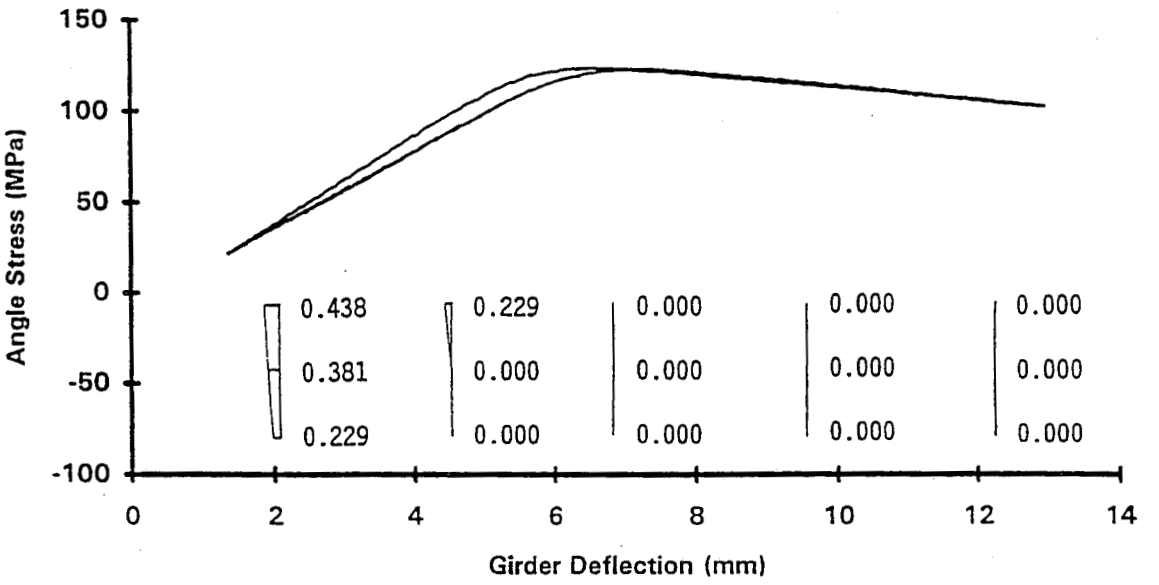

a) Type D Connection Angle

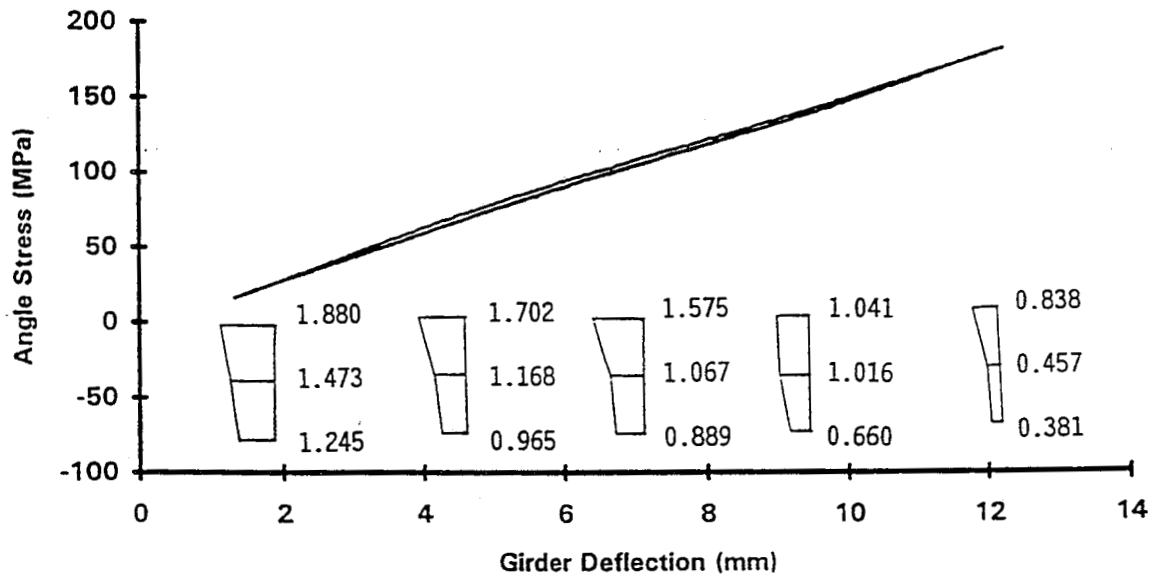

b) Type G Connection Angle

Figure 3.11. Angle Stress and Feeler Gage Measurements vs. Girder Deflection

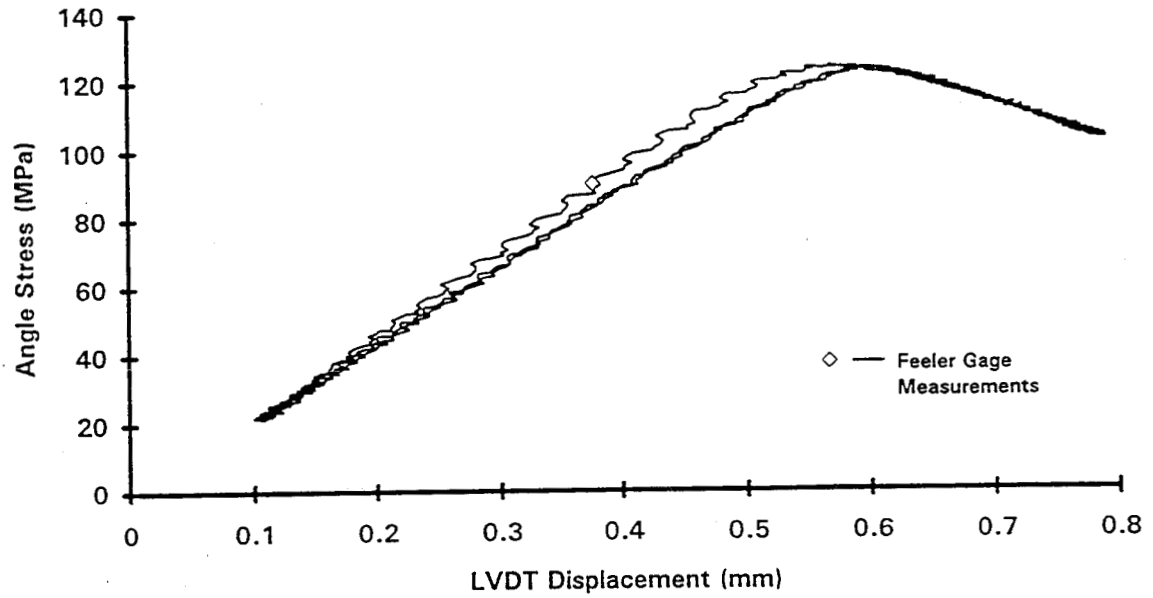

a) Type D Connection Angle

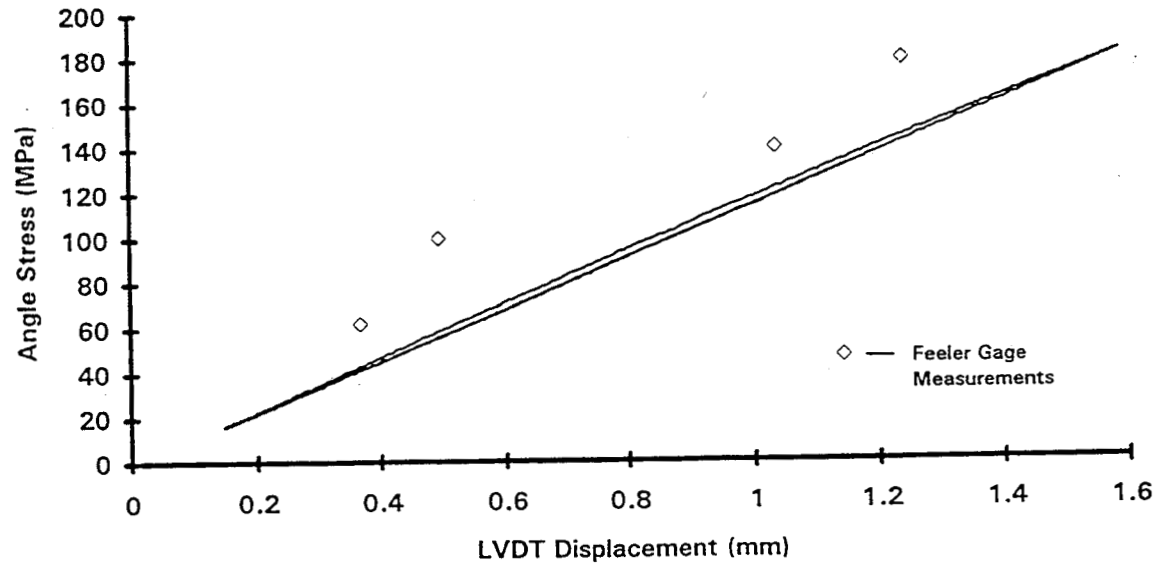

b) Type G Connection Angle

Figure 3.12. Angle Stress and Feeler Gage Measurements vs. LVDT Measurements

gage measurements and verify the accuracy of the feeler gage readings.

Fatigue Test Results

The effective stress ranges applied in the fatigue tests at the strain gage locations on the connection angles are given in Tables 3.2 and 3.3. The effective stress ranges in Tables 3.2 and 3.3 (and in Tables 3.4 and 3.5 presented later) are Miner's effective stress ranges. Even though every effort was made to maintain a constant stress range at each gage during the tests this was not possible. During testing the stress range in each gage drifted slightly due to seating of the specimen and load frame. Also, there were several planned and unplanned interruptions of each fatigue test. It was not possible to re-start the tests at exactly the same stress ranges in each of the strain gages.

At least two tests of each connection type were performed; however, the effective stress ranges varied substantially in the tests. The pushing of the angle to close the gap results in the stress range in the angle, and different stress ranges result from the variability of the size of the gaps.

Another factor contributing to the variability of effective stress ranges in the angles was the different behavior of connection angles bolted to the inside girders as compared to those bolted to the outside girders. Typically, for the connection angles bolted to the inside girder, gage one measured a tensile stress range where as gage 2 measured a smaller tensile stress range or a compressive stress range. An example of this can be seen from the first entry in Table 3.2. For the first connection angle shown in Table 3.2 (a type D* connection angle) gage one has a stress range of 164 MPa in tension and gage 2 has a stress range of 51 MPa in compression. The

Table 3.2. Angle Effective Stress Ranges and Duration of Tests for First Test Set-Up

Angle Type	Angle[1] Location	Gage Location	Sre (MPa)	Cycles[2] (1,000,000)
D*	I	1[4]	164	10.3
		2[5]	-51	
	I[3]	1	226	0.3
		2	-68	
	I	1	36	5.8
		2	-82	
	0	1	-21	10.3
		2	-46	
	0	1	-57	10.3
		2	-23	
D	I	1	116	10.3
		2	-103	
	I	1	49	10.3
		2	-110	
	0	1	-10	10.3
		2	-12	
	0	1	-49	10.3
		2	-61	
EF	I[3]	1	175	1.8
		2	-83	
	I	1	209	5.8
		2	-78	
	I	1	90	10.3
		2	-73	
	0	1	122	10.3
		2	-35	
	0	1	143	10.3
		2	-65	

[1] and 0 denotes inside or outside girders
[2] number of cycles shown are number of cycles to crack initiation (for cracked connection angles) or to termination of test for other connection angles
[3] connection where a fatigue crack initiated
[4] angle gage at end of angle adjacent to web gap
[5] angle gage at end of angle away from web gap

Table 3.3. Angle Effective Stress Ranges and Duration of Tests for Second Test Set-Up

Angle Type	Angle[1] Location	Gage Location	Sre (MPa)	Cycles[2] (1,000,000)
D	I[3]	1[4]	269	1.2
		2[5]	-16	
	I	1	215	10.2
		2	-112	
	0	1	43	10.2
		2	-39	
	0	1	115	10.2
		2	-15	
EF	0	1	91	10.2
		2	-81	
	0	1	111	10.2
		2	-105	
G	I	1	146	10.2
		2	-14	
	I	1	139	10.2
		2	-56	
	I	1	35	10.2
		2	-18	
	I	1	126	10.2
		2	-60	
D*	0	1	74	10.2
		2	-41	
	0	1	92	10.2
		2	-14	

[1] and 0 denotes inside or outside girders
[2] number of cycles shown are number of cycles to crack initiation (for cracked connection angles) or to termination of test for other connection angles
[3] connection where a fatigue crack initiated
[4] angle gage at end of angle adjacent to web gap
[5] angle gage at end of angle away from web gap

behavior of the connection angles bolted to the outside girders was less consistent. Tensile stress ranges were measured at some of the gage one locations on the connection angles and compressive stress ranges were measured at others. This is

seen most readily in the results for connection angles on the outside girder during the first test set-up (Table 3.2). For the type D* and D connection angles the strain gages at the gage one location were in compression during the fatigue tests as compared to the similar gages on the type EF connection angle which were in tension.

Tables 3.4 and 3.5 contain the effective stress ranges in the web gaps for all the connections tested. The effective stress ranges at two critical locations in the web gap

Table 3.4. Web Gap Effective Stress Ranges for First Test Set-Up (for 10.3 million cycles)

Angle Type	Angle[1] Location	Extrapolation Location	Sre (MPa)
D*	I	FG[2]	+93
		CN[3]	+17
	I	FG	+68
		CN	+ 9
	0	FG	+64
		CN	-80
	0	FG	+63
		CN	-83
D	I	FG	+112
		CN	-58
	I	FG	+83
		CN	-25
	0	FG	+97
		CN	-90
	0	FG	+74
		CN	-81
EF[4]	I	FG	+ 92
	I	FG	+138
	0	FG	+48
	0	FG	+84

[1] and 0 denotes inside or outside girders
[2] FG extrapolated effective stress range in girder web at edge of radius
[3] CN extrapolated effective stress range in girder web at top of connection angle
[4] stress ranges shown for type EF connection are outside the web gap

Table 3.5. Web Gap Effective Stress Ranges for Second Test Set-Up (for 10.2 million cycles)

Angle Type	Angle[1] Location	Extrapolation Location	Sre (MPa)
D	I	FG[2]	160
		CN[3]	-50
	I	FG	197
		CN	-67
	0	FG	47
		CN	-81
	0	FG	38
		CN	-73
EF[4]	0	FG	89
	0	FG	60
G	I	FG	94
		CN	-32
	I	FG	115
		CN	-32
	I	FG	99
		CN	-24
	I	FG	100
		CN	-45
D*	0	FG	23
		CN	-14
	0	FG	33
		CN	-69

[1] and 0 denotes inside or outside girders
[2] FG extrapolated effective stress range in girder web at edge of radius
[3] CN extrapolated effective stress range in girder web at top of connection angle
[4] stress ranges shown for type EF connection are outside the web gap

were determined by extrapolation from stresses at gage locations. The effective stress range in the girder web at the edge of the radius was one of the critical locations and is labeled with "FG" in the tables. The other critical location is in the girder web at the top of the connection angle and is labeled with "CN" in the tables. The effective stress ranges at the top of the connection angle for type EF connections are not available

due to the gaging pattern used.

Typically the effective stress ranges measured at the edge of the radius were larger than the effective stress ranges measured at the top of the connection, therefore, only the effective stress ranges at the edge of the radius are used in later discussions comparing the relative performance of connection types. The effective stress ranges in the web gap did vary from connection to connection but not as much as for the effective stress ranges in the connection angles. The reasons stated previously for the variation in the connection angle stress ranges contributed to the variation in web gap effective stress ranges.

Comparison of Performance of Connection Angle Types

To evaluate the expected performance of the four connection angle types tested in the laboratory model, the gage distance as defined in Figure 3.13 of each type of angle was evaluated. Wilson (1940) developed an equation for a lower limit for gage to insure flexibility of connection angles. The equation is:

$$g = (Lt\backslash 8)^{1/2} \qquad \text{(Eq. 3.1)}$$

where:

g = gage
L = length of stringer
t = thickness of angle

This equation was developed for riveted connection angles in railroad bridges and is based on fatigue tests of connection angles, review of cracked field connections, and mathematical analyses. The equation was developed to eliminate fatigue cracking in the outstanding legs of angle connections at stringer to floorbeam connections. Hence, the fatigue crack type is different than at diaphragm-girder connections. Also,

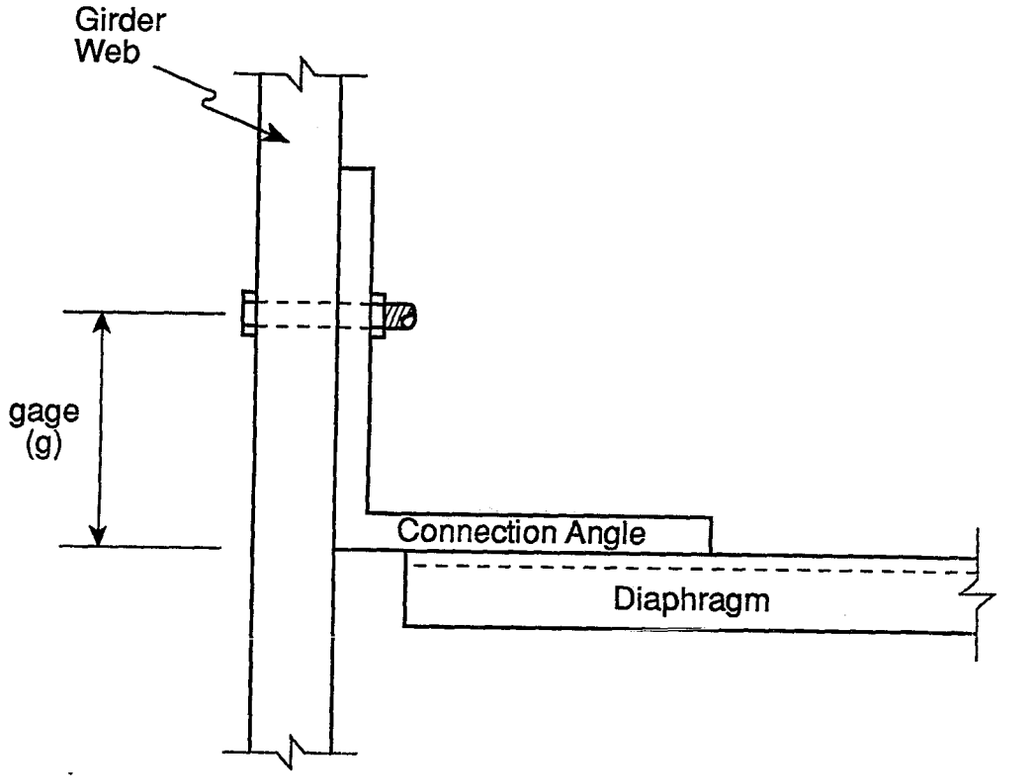

Figure 3.13. Gage of Connection Angles

the stringer length (L) and the empirical constant 8 in the denominator of the equation are related to stringer end rotations common for railroad bridges. The portion of equation 3-1 that is an indicator of the relative performance of connection angles at diaphragm-girder connections is the ratio g^2/t.

Table 3.6 shows the provided gage and thickness of the four connection angles tested in the laboratory model. Also, included in the table is the ratio g^2/t calculated for each connection type. The connection types are listed in increasing order of the g^2/t ratio. The larger the ratio g^2/t the more flexible the diaphragm-girder connection, and hence, the less likely the connection is to crack. The data in the table indicates that the type G connection angle should perform better than the other three connection angles tested.

Table 3.6. Comparison of (g^2/t) Ratios for Test Specimens

Angle Type	Provided Gage (mm)	Thickness (mm)	g^2/t	Number of Angles that Cracked[1]
EF	64	15.7	258	1 of 3
D	76	9.5	608	1 of 6
D*	76	7.9	731	1 of 3
G	137	12.7	1478	0 of 4

[1] for connection angles on inside girder only

Flexibility of Bolted Angle Connections

The flexibility of each connection angle tested was calculated to provide a relative measure of the susceptibility to cracking of each angle. The flexibility of a connection angle is defined here as the change in stress in the angle per unit of vertical inside girder deflection. The vertical inside girder deflection is equivalent to differential deflection since the outside girders do not deflect. For the gage one locations on the connection angles the flexibility of the connection angle was the average slope of the plot of angle stress versus girder deflection while the gap between the connection angle and girder web was open. At the gage two locations the connection angle was being pried away from the girder web during the fatigue tests and the gap did not close. Therefore, for the gage two locations the flexibility is the average slope of the total angle stress versus girder deflection plot.

Figure 3.14 shows the stress at the top (gage one) and bottom (gage two) gages on a connection angle on an inside girder plotted versus vertical girder deflection for one of the type G connection angles. A gap was present between the top of this

connection angle and the girder web, and the flexibility at the top of this connection angle was calculated from the straight line portion of the plot. The average slope of the plot of angle stress versus girder deflection is used as the flexibility at the bottom gage location. Shown on the plots are the calculated flexibilities for the top and bottom of the connection angle.

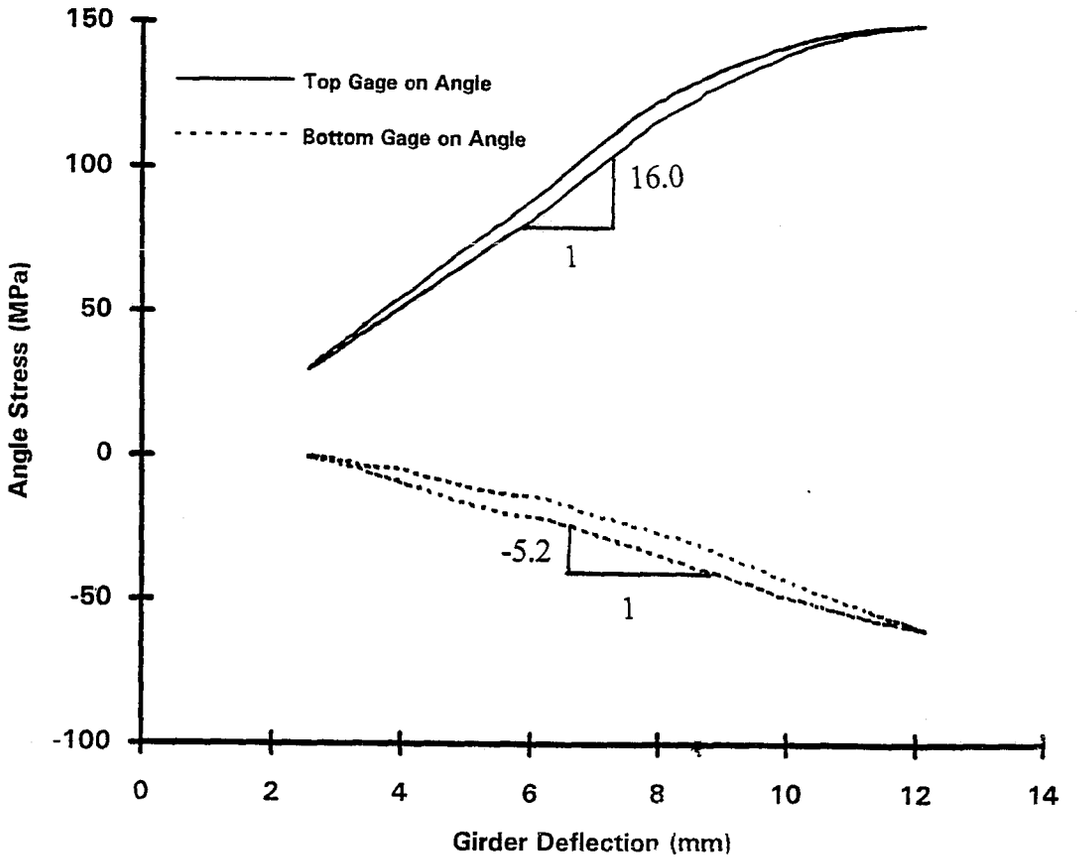

Figure 3.14. Angle Stress vs. Girder Deflection for a Type G Connection Angle

The flexibility of each connection angle on the inside girders was similarly calculated, and these results are presented in Table 3.7. Flexibilities of angles on the outside girders exhibited some inconsistencies and were not included in Table 3.7. The flexibilities for each connection angle type are summarized in Table 3.8. In Table

Table 3.7. Flexibilities of Connection Angles on the Inside Girders

Angle Type	Ratios (MPa/mm)	
	Top of Angle	Bottom of Angle
D*	35.5 9.0 42.4	- 8.7 -10.7 -20.5
D	16.7 35.9 26.5 29.1 28.2 25.9	-14.6 -13.3 -10.4 -11.8 -13.1 - 9.1
EF	14.9 22.5 28.3	- 9.4 -10.9 -10.4
G	13.9 16.0 17.0 15.2	-5.4 -5.2 -4.7 -4.1

Table 3.8. Flexibilities of Connection Angles on the Inside Girders

Angle Type	Average Ratios (MPa/mm)	
	Top of Angle	Bottom of Angle
D*	29.0	-13.3
D	27.1	-12.1
EF	21.9	-10.2
G	15.5	- 4.9

3.8 the angle types are arranged in decreasing order of flexibility magnitudes. For a given level of differential girder deflection, the angles with the largest flexibilities experience the largest stress ranges. Hence, the angle type G has the lowest flexibility and is the one that is least likely to crack due to fatigue when used in the field. This conclusion is based on the following assumptions: a) each connection angle type has the same fatigue limit, b) each connection angle type has the same size gap, and c) the differential girder deflections that occur in the field are independent of the angle type. The validity of the first assumption will be illustrated with test results later in this chapter. The second assumption is difficult to justify quantitatively, but laboratory and field observations suggest that the angle type does not significantly affect the gap size at the time of installation. However, field test data do show that yielding of the type D angles due to overloads occur which increases the gap size. Field test results presented in Chapters Five and Six show the validity of the third assumption.

The order of angle types in Tables 3.6 and 3.8 is of interest. Table 3.6 lists angle types in order of increasing g^2/t ratio, and Table 3.8 lists angle types in order of increasing flexibility. In both tables the angles are listed in decreasing order of likelihood of cracking. The results shown in the two tables agree that the type G angle is least likely to have fatigue cracking, however, the order of the other three angle types is different in the two tables.

Fatigue Performance of Connection Angles

As part of the Interim Report, Stallings et al. (1995), that presented the results from the field tests conducted during the summer of 1993, an assumed fatigue limit for the connection angles was discussed. Pending the results of the laboratory testing it

was assumed that the fatigue limit for the connection angles was 110 MPa (equal to AASHTO Category B). One goal of the laboratory testing was to establish a fatigue limit for connection angles.

A total of twenty connection angles were tested in the laboratory. Of these 5 were type D*, 6 were type D, 5 were type EF, and 4 were type G. Fatigue cracking occurred in three of the connection angles tested: one type D*, one type D, and one type EF. Each of the angles that cracked was on an inside girder and the crack initiated under or near the bolt head at the top of the connection angle. Figure 3.15 shows a photograph of a typical fatigue crack. The crack initiation site and crack growth in the laboratory tests was consistent with failed angles in the field.

Effective stress ranges from the laboratory tests at the strain gage location on each connection angle are given in Tables 3.2 and 3.3. Also, shown are the number of cycles each connection angle was subjected to before a crack initiated or until the test was terminated. Plots of effective stress range versus number of cycles to crack initiation or to termination of a test were made on log-log paper and are given in Figures 3.16 and 3.17. This data is shown on two figures to allow for easier interpretation of the results.

With the exception of one type EF connection angle all connection angles with a stress range higher than 165 MPa (AASHTO category A) cracked. Also, fatigue cracking did not occur in any angle with a stress range below 165 MPa. A fatigue limit of 165 MPa is concluded to be appropriate for the connection angles.

The type G connection angle is being proposed as a new connection angle for retrofits in the field. The four type G connection angles tested in the laboratory were

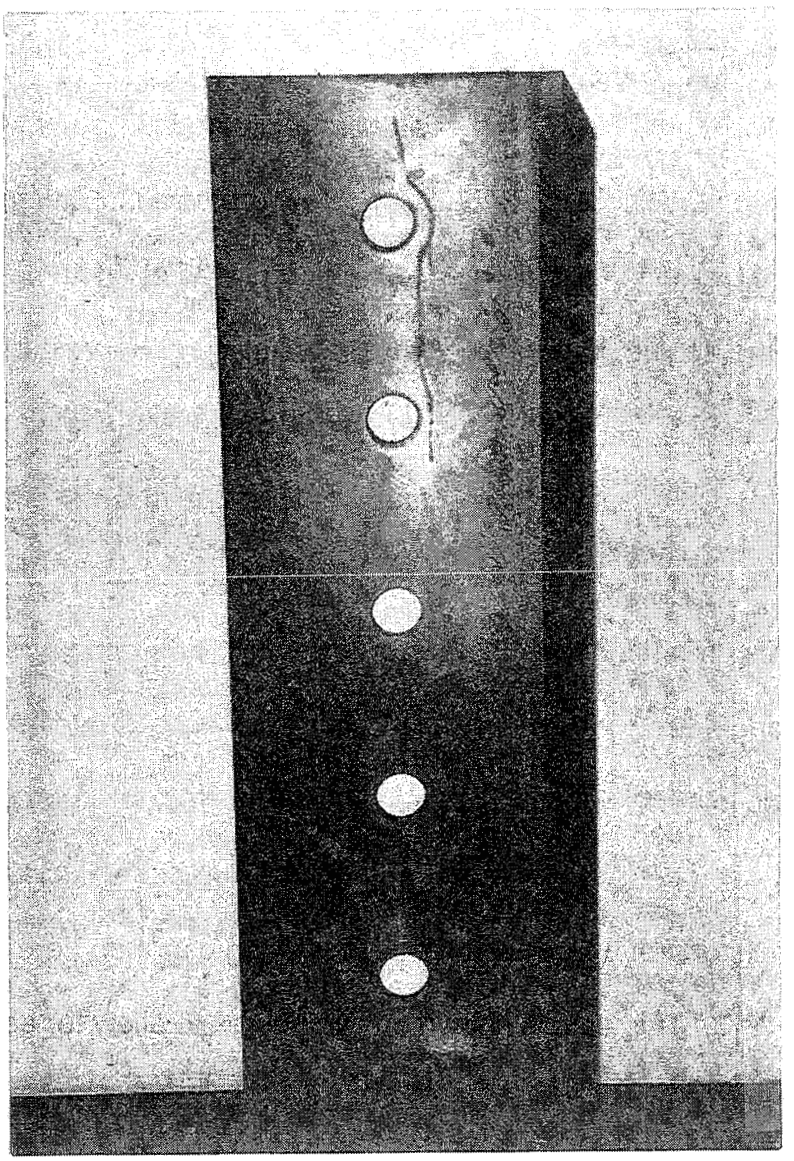

Figure 3.15. Fatigue Crack in Type D Connection Angle

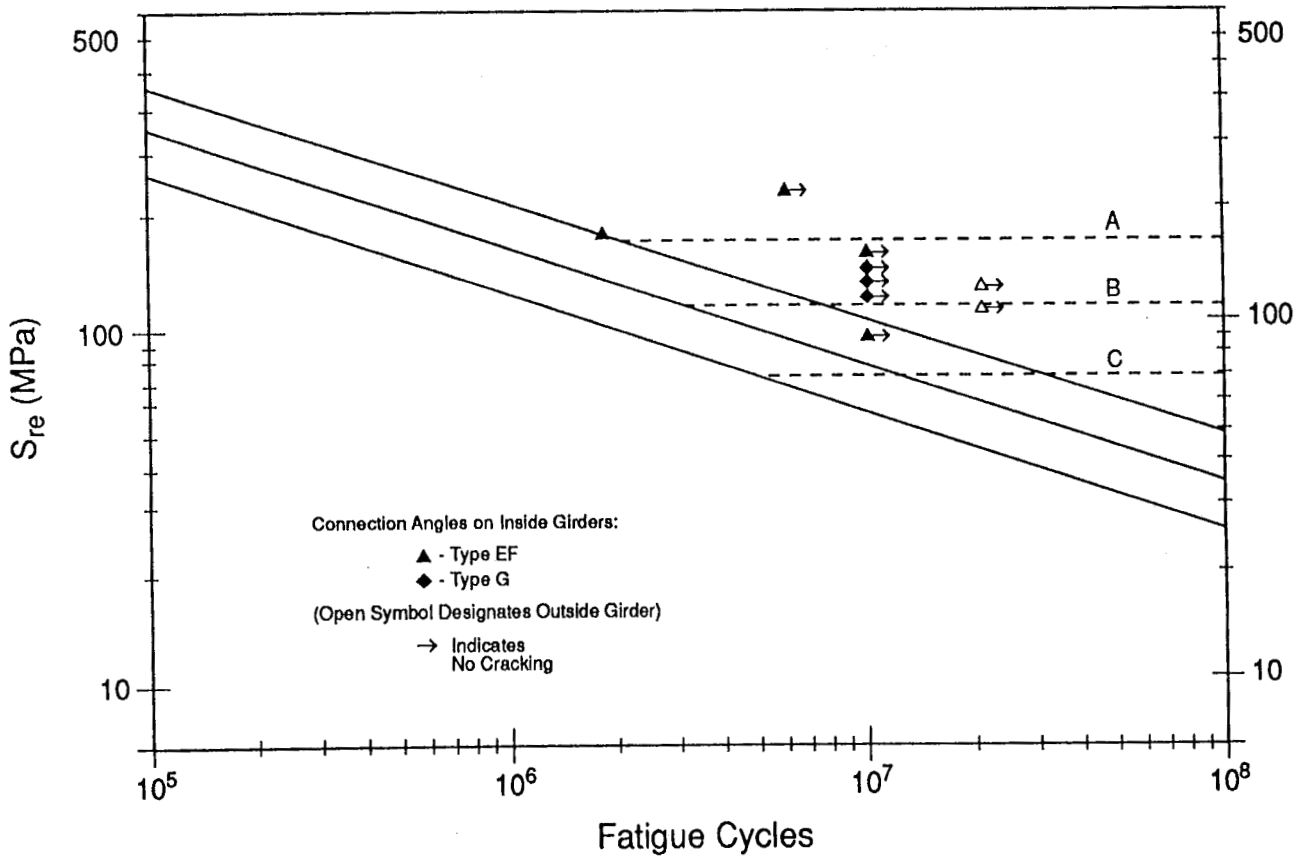

Figure 3.16. Effective Tension Stress Ranges in Type EF and G Angles with AASHTO Fatigue Categories

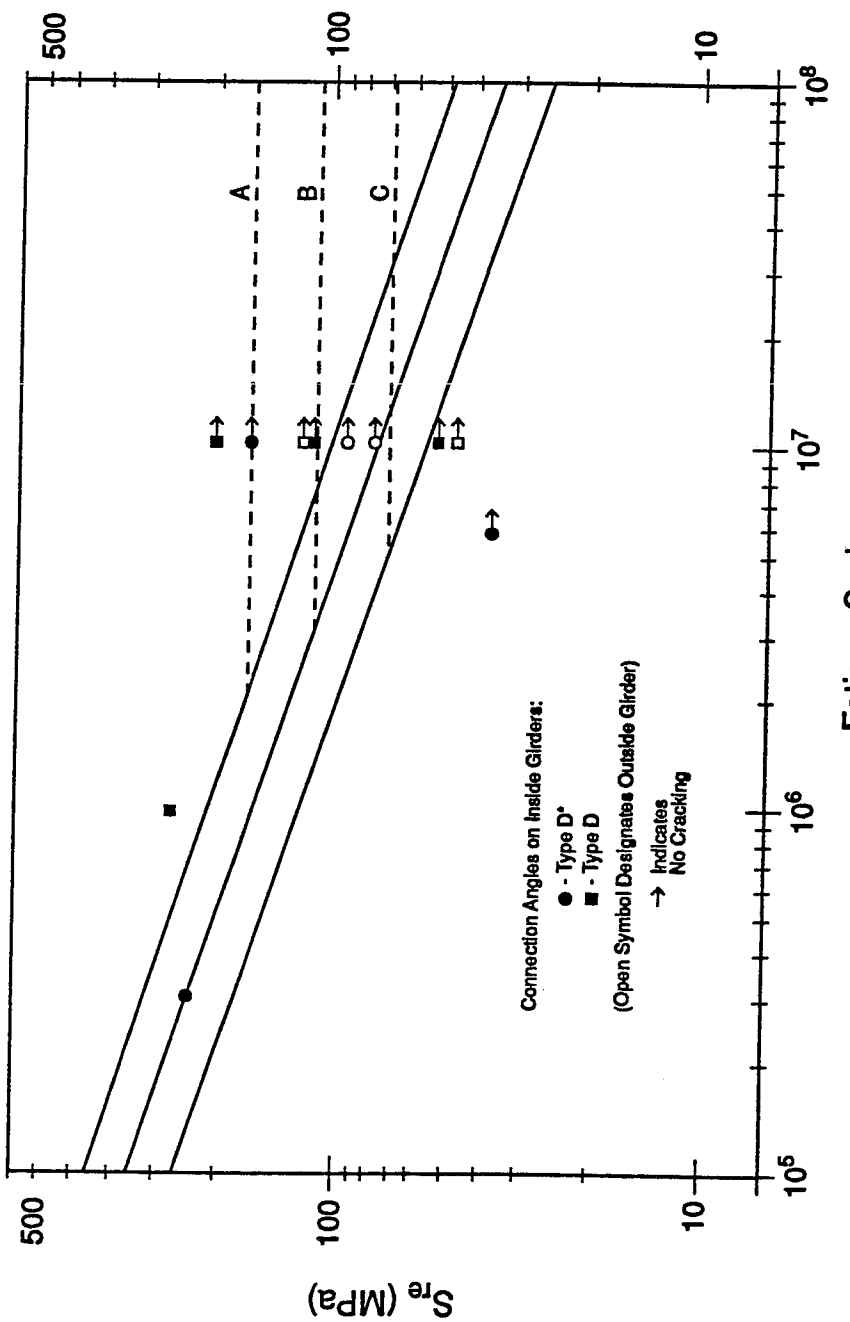

Figure 3.17. Effective Stress Ranges in Type D* and D Connection Angles with AASHTO Fatigue Categories

subjected to effective stress ranges between 126 and 146 MPa at the top gage and none cracked. It is important to note that the type G connection angles survived in excess of 10,000,000 cycles of load at stress ranges just slightly less than 165 MPa.

Web Gap Behavior

A plot of stress at the top gage on a connection angle and stress in the girder web at the edge of the radius in the web gap versus girder deflection measured during a load cycle is shown in Figure 3.18. The plots are for a type D connection on an inside girder. Feeler gage measurements verify the presence of a gap between the

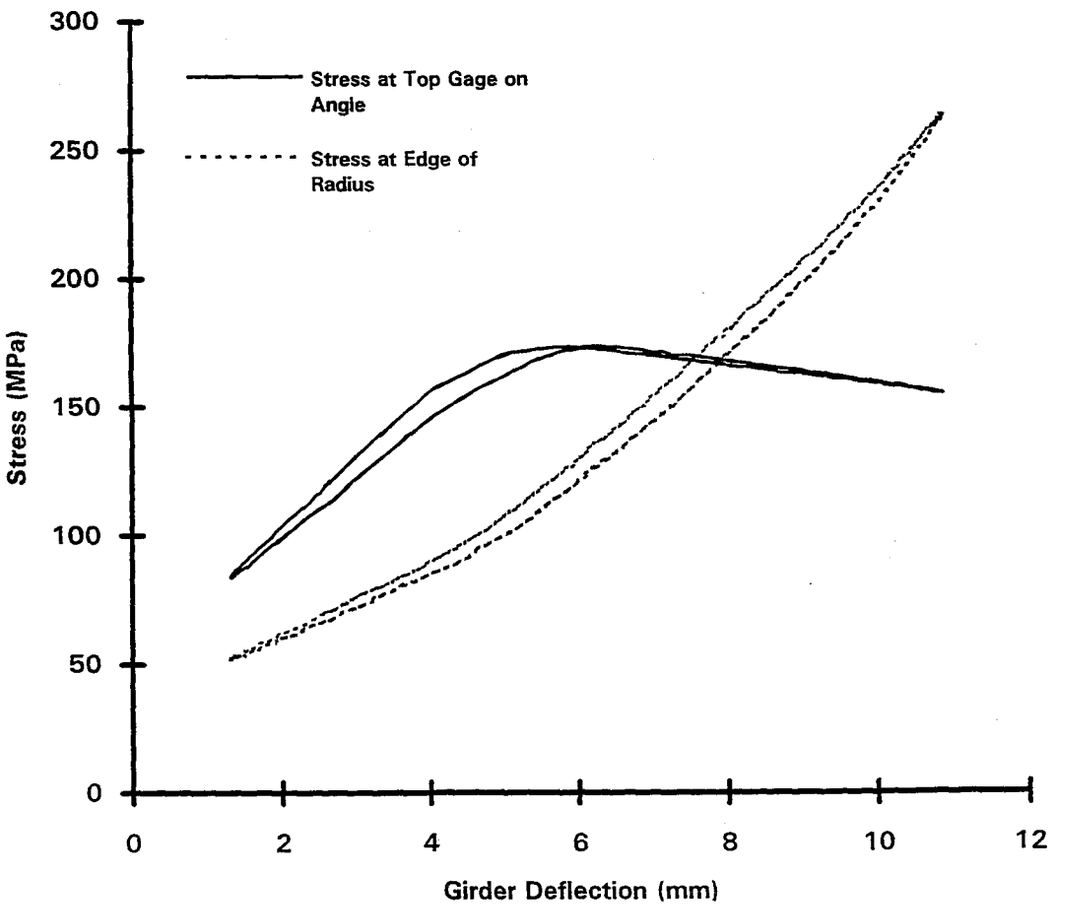

Figure 3.18. Angle Stress and Web Stress at Edge of Radius at a Type D Connection Angle

connection angle and girder web at the connection. The feeler gage measurements show that the gap closed at a vertical girder deflection of about 5.1 mm which corresponds to the point in Figure 3.18 where both plots change slope. As the gap at the top of the connection angle closed the rate of increase in stress in the angle decreases dramatically and stops. However, at the edge of the radius the rate of increase of stress in the web increases after the gap closes. This behavior is typical of that seen at many connections with the exception that at some connections there was no discernable change in the rate of increase of stress at the edge of the radius. The effect of the presence of a gap between the connection angle and girder web on the stress range in the web gap during a load cycle was not as pronounced as was seen for connection angle stress ranges. In general, the closing of the gap between the connection angle and girder web had a small or no effect on the slope of the web stress at the edge of the radius versus deflection plot.

Effect of Connection Angle Type on Web Gap Flexibility

A relative measure of the susceptibility of web gaps to fatigue cracking was developed by determining the flexibility of each web gap. The flexibility of a web gap was defined as the change in distortion-induced web stress at the edge of the radius divided by the total girder deflection. In Figure 3.18 the flexibility of the web gap is defined as the average slope of the plot of stress at the edge of the radius versus girder deflection for one load cycle and in this case is 22.2 MPa/mm. The average slope in the load cycle was used because of the small effect the closing of the gap between the connection angle and the girder web had on the stress at the edge of the radius.

Table 3.9 contains the flexibilities of the web gaps on the inside girders grouped by connection angle type. The flexibilities of the web gaps adjacent to type EF connection angles are not included in the results presented in Table 3.9. As discussed earlier in this chapter the primary gages for determining the stress within the web gap at the edge of the radius at type EF connection angles were placed outside to the web gap (Figures 3.8 and 3.9).

Table 3.9. Ratios of Web Gap Stress to Girder Deflection for Type D*, D, and G Connection Angles on Inside Girders

Angle Type	Ratio (MPa/mm)	Average Ratio (MPa/mm)
D*	7.5 10.7 12.6	10.3
D	11.1 14.9 17.2 22.2 17.1 21.8	17.4
G	10.7 10.0 11.7 12.2	11.2

The lower the web gap flexibility, the more desirable the connection. When used in the field, the connections with the smallest flexibilities are likely to experience smaller stress ranges due to truck traffic and are less likely to crack due to fatigue. The web gaps at type D* and type G angles had the smallest average web gap

flexibilities and are less susceptible to web cracking than web gaps adjacent to type D connection angles.

Fatigue Performance of Web Gaps

During the laboratory tests each test setup was subjected to over ten million load cycles. The effective stress ranges in the web at the edge of the radius are given in Tables 3.4 and 3.5. All but one of the effective stress ranges were below 165 MPa (AASHTO fatigue limit for Category A). Plots of effective stress range versus number of cycles are given in Figures 3.19 and 3.20. This data is shown in two plots to facilitate interpretation of the results.

Figures 3.19 and 3.20 show that AASHTO category A is a good lower bound for the fatigue limit at the edge of the radius in web gaps. Five web gaps were tested at stress ranges above the 110 MPa fatigue limit of AASHTO Category B, and one web gap was tested above the 165 MPa fatigue limit of Category A. Because no cracking occurred in any of the tests a fatigue limit cannot be established with great certainty, but a value as high as 165 MPa appears reasonable. The fatigue limit for distortion-induced stress ranges in the webs of rolled girders at the web-flange radius is concluded to be 165 MPa.

CONCLUSIONS

Fatigue tests of diaphragm-girder connections were performed in the Auburn University Structural Engineering Research Laboratory. Four connection angle types were used in the laboratory tests. Three of the connection angle types (types D, D*, and EF) were identical or similar to those used in the field for repair of damaged diaphragm-girder connections. The other (type G) was a new connection angle design

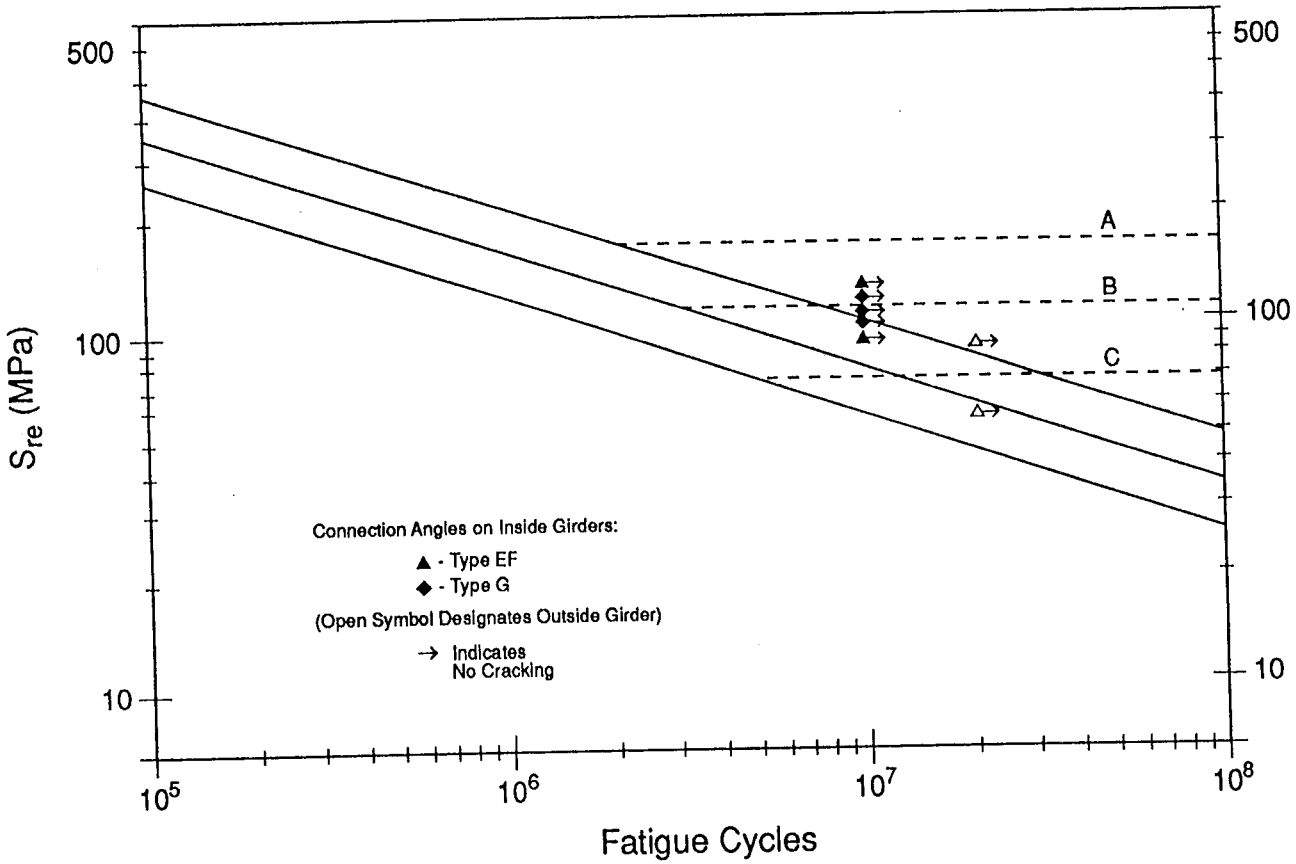

Figure 3.19. Effective Stress Ranges in Web at Edge of Radius for Connections with Type EF and G Angles with AASHTO Fatigue Categories

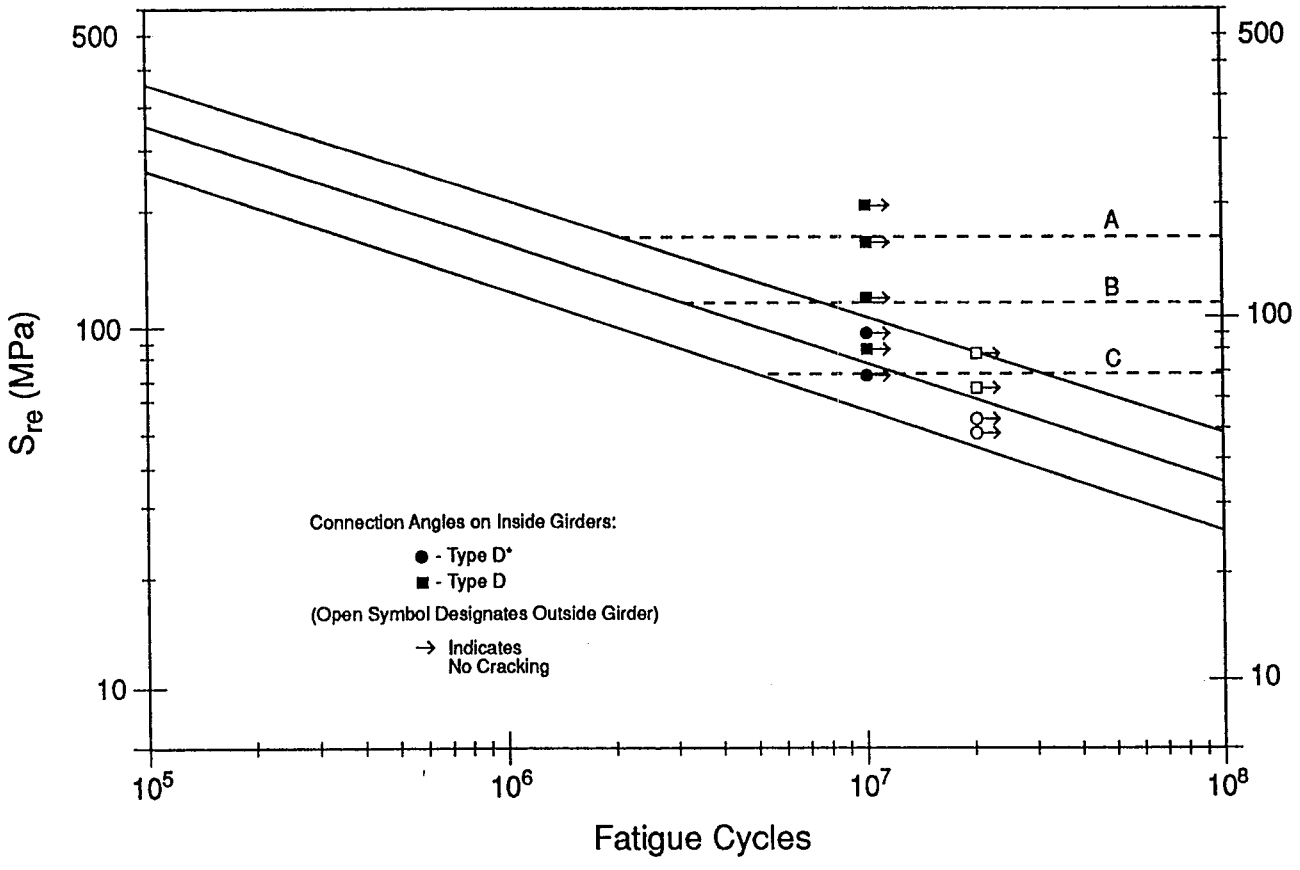

Figure 3.20. Effective Stress Ranges in Web at Edge of Radius for Connections with Type D* and D Angles with AASHTO Fatigue Categories

proposed for use in future repairs. The primary focus of this investigation was the relative performance of the different connection angle types and web gaps.

The gap between the connection angle leg bolted to the girder web and the girder web has a significant effect on the stress range in the connection angle. The stress range which causes fatigue cracking results when the gap is pushed closed. During load cycles of the fatigue tests the stress in the connection angles increased while the gap was open and stopped once the gap closed. However, the stress in the girder web at the edge of the radius was not significantly effected by the presence of the gap.

The relative performance of the connection angle types was compared by determining the flexibility of each connection angle. The flexibility of a connection angle was defined as the ratio of stress range in the connection angle while the gap is open divided by the differential girder deflection range. The lower the flexibility the less likely a connection angle is to crack. For the four types of connection angles tested the type G had the lowest average flexibility and was concluded to be the least likely to crack when used in the field.

Fatigue performance of the various connection angle types was concluded to depend primarily on the stress range near the end bolt on the leg of the angle bolted to the girder web. The potential for fatigue cracking was independent of the angle type for a given applied stress range. A fatigue limit of 165 MPa was established for the connection angle stress range.

Behavior of the web gaps adjacent to the connection angles was compared using the flexibility of the web gaps. The flexibility of the web gap was defined as the

ratio of the distortion-induced stress range in the web at the edge of the radius divided by the range of differential girder deflection. The lower the flexibility of a web gap the less likely that cracking will occur at the edge of the radius. Web gaps adjacent to the type G connection angle had the lowest average flexibility.

A fatigue limit of 165 MPa was estimated for distortion-induced stress ranges in the girder web at the web-flange radius for rolled section girders.

CHAPTER FOUR

STRUCTURAL EVALUATIONS

INTRODUCTION

Current AASHTO *Specifications* (1992), Article 10.20.1, require transverse diaphragms to be placed in multi-girder steel bridges at a maximum spacing of 7.62 m (25 ft) between lines of diaphragms. A theoretical explanation for the required maximum spacing is not available. The requirement is probably a rule-of-thumb and dates back to 1949. Between 1931 and 1949, diaphragms were required at a maximum spacing of 6.10 m (20 ft). The new AASHTO *LRFD Specifications* (1994) do not have a strict requirement for diaphragms but allow the designer to use diaphragms as needed. In this chapter the structural necessity for diaphragms in existing bridges is investigated for the purpose of identifying typical structural types where diaphragms may be removed to reduce maintenance costs. Only the interior lines of diaphragms are considered for removal. Diaphragms at the supports are required for resistance to horizontal transverse loads. However, because there is no relative vertical deflection between girders at the supports, diaphragms there do not experience the fatigue cracking common at the interior diaphragms, and there is no motivation to remove diaphragms at supports.

As part of this research, a structural evaluation was performed on four interstate bridges with designs typical to the Birmingham, Alabama area. The bridges analyzed were a 24.5 m right simple span, a 15.5 m skewed simple span, a 3-span continuous, and a 5-span continuous. These four bridges were chosen from eight field test locations and are referred to in Table 1.1 as Test Sites 3, 8, 6 and 2, respectively. In

addition, a fifth bridge was analyzed as part of the structural evaluations. This bridge is also a 3-span continuous structure but carries only two lanes of traffic. The fifth bridge is located in Tuscaloosa County, Alabama and is typical of two-lane steel girder bridges located throughout Alabama.

The structural evaluations performed on the bridges consisted of four aspects: 1) a structural analysis, 2) a lateral-torsional buckling (LTB) analysis, 3) a wind load analysis, and 4) a rating analysis. The bridges were evaluated using the existing conditions and possible future conditions. The continuous spans were originally designed and built as non-composite sections. A possible condition investigated was composite action in the positive moment regions of the continuous spans which can be created in a future deck replacement.

The structural analysis was performed to determine the maximum moments at critical locations in accordance with AASHTO *Standard Specifications for Highway Bridges* (1992). The bridges were analyzed using a continuous beam analysis program capable of modeling moving loads, *Bridge* by Wang (1991), and a frame analysis program, *Frame1O* by Stallings (1991). Both computer programs utilize the direct stiffness method of analysis.

The LTB analysis was performed to determine the capacity of the girders in the continuous span bridges after removal of some or all of the interior diaphragms. First, the existing non-composite continuous span bridges were analyzed assuming all interior diaphragms were removed. Complete diaphragm removal was found not feasible for the non-composite bridges, and the bridges were reevaluated assuming that only the first line of diaphragms from the interior bents remained. Next, the

bridges were analyzed assuming composite action, a possible future condition, and accounting for the additional LTB capacity resulting from torsional bracing provided by the concrete deck.

The simple span bridges were designed and built as composite sections. A LTB analysis was not performed for the simple span bridges since the compression flange is continuously braced by the deck slab which prevents lateral-torsional buckling of the girders.

A potential problem is the increase in girder stresses resulting from removing diaphragms. The rating analysis was performed to address this issue. The desired result of the rating analysis is for the girders to have excess live load capacity so that an increase of 10% to 15% in the maximum girder stress will be acceptable. One clear way to prove this is for the Inventory Rating Factors to be at least 1.10 to 1.15. Inventory Ratings, instead of Operating Ratings, are used here because of the extremely high traffic volume on the Interstate Highways.

Wind load analyses were performed using basic engineering principles with guidance from the AISC *Highway Structures Design Handbook* (1986) and the AASHTO *LRFD Bridge Design Specifications* (1994). First attempts at the wind load analyses were reported by Davis (1995) where the method of AASHTO (1992) was applied. However, this method is based on the assumption of load sharing through the diaphragms which is not rational for bridges with complete diaphragm removal.

THEORETICAL BACKGROUND: LATERAL-TORSIONAL BUCKLING

A primary objective of this research is to determine whether diaphragms are required in typical continuous span steel girder bridges to prevent lateral torsional

buckling (LTB) in the negative moment regions near the supports. To meet this objective, the results of previous investigations of the LTB capacity of beams performed at The University of Texas at Austin are utilized extensively. The key theoretical points are summarized below and example calculations are provided in Appendix A and B.

For girders which do not meet the criteria set forth by AASHTO for width to thickness ratios and lateral bracing required for reaching the plastic moment capacity, AASHTO Equation 10-102c defines the lateral-torsional buckling moment capacity as:

$$M_r = 91X10^6\ C_b \left(\frac{I_{yc}}{L_b}\right) \left[0.772\frac{J}{I_{yc}} + 9.87\left(\frac{d}{L_b}\right)^2\right]^{1/2} \leq M_y \qquad (4\text{-}1)$$

where C_b is the moment gradient modifier; I_{yc} is the moment of inertia of the compression flange about an axis in the plane of the web; L_b is the unbraced length of the compression flange; J is the torsional constant of the girder; and d is the depth of the girder.

Most commonly the unbraced length L_b in Equation 4-1 is interpreted to be the distance between diaphragm lines. For this interpretation, the LTB moment capacity, M_r, from Equation 4-1 does not account for any additional capacity provided by lateral or torsional braces between the ends of the segment. In the bridges studied for this report, lateral bracing is provided by the continuous bracing of the top flange by the slab. In the case of composite bridges, additional torsional bracing is provided by the slab through the connection contributed by the shear studs.

Yura (1984) studied various loading situations in order to develop improved moment gradient factors, C_b, for cases involving LTB. The specific results pertinent to this report are for beams braced at the ends and with the top flange continuously braced. The loading is assumed downward and applied at the top flange. If the moment at neither end of the segment produces a compressive stress on the bottom flange, there is no buckling in the segment. If the moment at either or both ends produce a compressive stress on the bottom flange, the moment gradient factor is given as:

$$C_b = 3.0 - \frac{2}{3}\left(\frac{M_1}{M_0}\right) + \frac{8}{3}\frac{M_{CL}}{(M_0 + M_1)} \qquad (4\text{-}2)$$

where M_0 is the end moment that produces the largest compressive stress on the bottom flange; M_1 is the other end moment; and M_{CL} is the moment at the centerline of the segment. Positive values should be substituted into Equation 4-2 for M_o and M_1 when these moments produce compressive stress in the bottom flange. A positive value should be substituted for M_{CL} when this moment produces tensile stress in the bottom flange. For the quantity (M_0+M_1) in the Equation 4-2, M_1 should be taken as zero when the term M_1 is negative. In other words, the term (M_0+M_1) must be between M_0 and $2M_0$. It should also be noted that there is no upper bound for C_b.

The moment gradient factor given by Equation 4-2 may be used in Equation 4-1 to calculate the LTB capacity for comparison with the end moment M_o that produces the largest compressive stress on the bottom flange. The maximum moment must be used to check yielding of the section. Equation 4-2 is used extensively throughout this

report in calculating the LTB capacities of the girders in the bridges studied. Examples of its use are given in Appendix A and B.

The LTB capacity of beams is explained thoroughly in a paper by Yura (1992). The topic of most interest for this report is the buckling strength of torsionally braced beams. Yura expanded the exact buckling strength equation, given by Taylor and Ojalvo (1973), for the critical moment of a doubly-symmetric beam under uniform moment with continuous torsional bracing. The exact equation is given as:

$$M_{cr} = (M_C^2 + \beta_T EI_{eff})^{1/2} \tag{4-3}$$

where M_C is the buckling capacity of the unbraced beam (considered here to be given by Equation 4-1 with $C_b = 1$), and β_T is the attached torsional brace stiffness. Yura showed that an equivalent continuous torsional brace stiffness can be calculated by summing all the discrete brace stiffness (such as those provided by diaphragms) and then dividing by the beam length. The result is the development of a buckling strength equation for discrete torsional bracing such as provided by diaphragms or for continuous torsional bracing such as provided by a composite deck slab. The modified equation is given as follows:

$$M_{cr} = \left(C_{bu}^2 M_c^2 + \frac{C_{bb}^2 \beta_T EI_{eff}}{C_T} \right)^{1/2} \leq M_y \tag{4-4}$$

where C_{bu} and C_{bb} are the two limiting C_b factors corresponding to an unbraced beam

(very weak braces) and an effectively braced beam (buckling between braces), respectively.

The previously discussed moment gradient factor, C_b, accounts for the non-uniform moment along the length of the beam. In determining the moment gradient factors for the use in Equation 4-4 for this report, C_{bu} was calculated using Equation 4-2 and C_{bb} was conservatively assumed as 1.0. C_T is a top flange loading modification factor; C_T = 1.2 for top flange loading, and C_T = 1.0 for centroidal loading. Also, for singly symmetric sections the effective moment of inertia can be approximated as:

$$I_{eff} = I_{yc} + \left(\frac{t}{c}\right) I_{yt} \tag{4-5}$$

where I_{yc} and I_{yt} are the lateral moment of inertia of the compression flange and tension flange, respectively; and c and t are the distances from the neutral axis to the centroid of the compression and tension flanges, respectively. For doubly symmetric sections, the distances from the centroid, c and t, are equal and the effective moment of inertia is the sum of the moments of inertia for the top and bottom flanges.

For use in design, a further modification of Equation 4-4 was recommended by Yura (1994). Yura recommended that a factor of safety of 2.0 be used in calculating the additional moment capacity resulting from torsional bracing. The complete equation, which is used in calculating the LTB capacities for composite continuous beams for this project, is given as follows:

$$M_{cr} = \left(C_{bu}^2 M_o^2 + \frac{C_{bb}^2 \beta_T EI_{eff}}{2C_T} \right)^{1/2} \leq M_y \tag{4-6}$$

Regardless of the calculated elastic LTB capacity of the beam, the maximum negative moment strength of the beam is limited by M_y, the yield moment. Equation 4-6 is not used here to calculate moment capacities or ratings for non-composite bridges because no torsional bracing is provided by the slab. For non-composite continuous span bridges Equation 4-1 and 4-2 were used.

In Equation 4-6, β_T represents the effective torsional brace stiffness and can be calculated using the following equation:

$$\frac{1}{\beta_T} = \frac{1}{\beta_b} + \frac{1}{\beta_{sec}} + \frac{1}{\beta_g} \tag{4-7}$$

where β_b is the stiffness of the attached torsional brace; β_{sec} is the girder web stiffness; and β_g is the girder system stiffness. The general use of Equation 4-7 is discussed in detail by Yura (1992). The discussion of Equation 4-7 in this report is limited to an explanation of how it is used in this chapter in the structural evaluations for composite bridges.

The torsional brace stiffness provided by a diaphragm on one side of a girder can be calculated from:

$$\beta_b = \frac{6EI_b}{S} \tag{4-8}$$

where E is the modulus of elasticity; S is the girder spacing; and I_b is the moment of inertia of the diaphragm. For an interior girder braced by two diaphragms, the torsional stiffness is twice the value of Equation 4-8. In the case of a composite bridge with no diaphragms, the attached brace stiffness is provided continuously by the slab. For the

calculation of β_b, the moment of inertia, I_b, is the moment of inertia of the slab per unit width perpendicular to the girder.

The effectiveness of a torsional brace is reduced if distortion of the web occurs during buckling. The web stiffness can be approximated for cases where the diaphragm is attached to a full length transverse stiffener that is not attached to the girder flanges by the use of the following equation:

$$\beta_{sec} = \frac{3.3E}{h}\left[\frac{(N + 1.5h)t_w^3}{12} + \frac{t_s b_s^3}{12}\right] \qquad (4\text{-}9)$$

where h is the depth of the web; t_w is the web thickness; t_s is the stiffener thickness; b_s is the width of the stiffener; and N is the contact length along the girder of the torsional brace. The term (N+1.5h) in the brackets represents the effective web width along the girder at the attachment point of the torsional brace. For continuous bracing provided by a composite slab, an effective width of 1.0 should be used in place of (N+1.5h). The second term in the brackets accounts for the stiffness provided by the transverse stiffener. For the composite bridges with no diaphragms, the contribution of the transverse stiffeners remaining after diaphragm removal is neglected for conservatism, and the second term in the brackets is omitted.

When a torsional brace is attached to a girder web by a partial length stiffener, the calculation of β_{sec} must be modified. This is accomplished by separating β_{sec} into three components.

$$\frac{1}{\beta_{sec}} = \frac{1}{\beta_c} + \frac{1}{\beta_s} + \frac{1}{\beta_t} \qquad (4\text{-}10)$$

where

$$\beta_c,\beta_s,\beta_t = \frac{3.3E}{h_i}\left(\frac{h}{h_i}\right)^2\left[\frac{(N + 1.5h_i)t_w^3}{12} + \frac{t_s b_s^3}{12}\right] \tag{4-11}$$

where $h_i = h_c$, h_s, and h_t, and the definitions of h_c, h_s, and h_t are illustrated in Figure 4.1.

The girder system stiffness for Equation 4-7 is defined as the contribution provided by the in-plane girder flexibility. For a two-girder system the stiffness is given as:

$$\beta_g = \frac{12S^2EI_x}{L^3} \tag{4-12}$$

where S is the girder spacing; I_x is the moment of inertia for the girder about the strong axis; and L is the span length. For a multi-girder system, the factor 12 should be replaced by the term $24(n_g^2-1) / n_g$, where n_g is the number of girders.

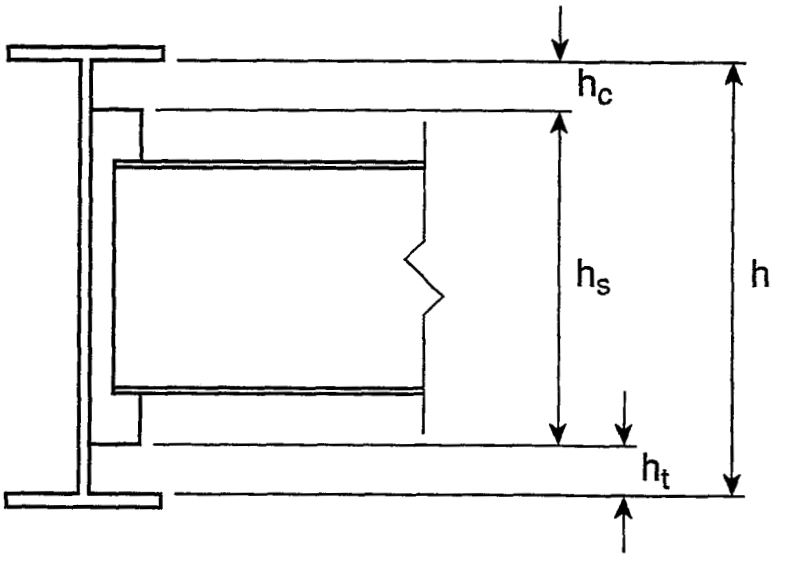

Figure 4.1. Definition of Terms for Equation 4-11

Equation 4-6, developed by Yura, accounts for all the aspects of lateral and torsional bracing that contribute to the LTB capacity of beams. The additional LTB capacity calculated by using Equation 4-6, instead of AASHTO Equation 10-102c, can be significant when evaluating the feasibility of diaphragm removal.

For non-composite bridges, where complete diaphragm removal is not feasible, the remaining diaphragm locations are assumed to be braced points. In order to constitute a braced point, the diaphragms must provide the stiffness and strength sufficient to force buckling between the diaphragms. Yura (1992) provides a means of calculating the strength and stiffness that must be provided by a diaphragm to produce a fully braced point. The equations used for this check are presented below. An example of this calculation is provided in Appendix A. The effective stiffness required to produce a fully braced point is given as:

$$\beta_T = \frac{2.4LM_f^2}{nEI_{eff}C_{bb}^2} \tag{4-13}$$

where M_f is the maximum factored beam moment; n is the number of torsional braces along the span; and L is the span length. The bracing strength (moment capacity of the brace) required to produce a fully braced point is given as:

$$M_{br} = \frac{0.04LM_f^2}{nEI_{eff}C_{bb}^2} \tag{4-14}$$

LATERAL-TORSIONAL BUCKLING ANALYSES

The goal of the LTB analyses was to determine the moment capacity of the continuous girders in the negative moment regions with some or all of the interior diaphragms removed. Since the top flanges of the continuous girders considered here are continuously braced against lateral movement by embedment in the concrete deck, LTB can only result from negative bending moments near the ends of the continuous spans. Hence, only the load case (HS20-44 lane or truck) which produced the maximum negative moment at the end of the unbraced segment, or at the bent, was used to determine the required moment resistance, $M_{REQ'D}$, for an Inventory Rating factor of one.

The actual (provided) moment resistance of the beam is dependent on the moment gradient factor, C_b, which is dependent on the applied loading moment diagram. Because of the dependence of C_b on the applied loading, various load placements were checked to ensure that the moment capacity did not drop below the required capacity for a loading not commonly considered critical. For all of the continuous span bridges considered here, the smallest C_b values for interior spans were found for loading cases with a lane loading (including two concentrated loads) positioned to produce the maximum negative moments at the piers. For exterior spans, the smallest C_b may result when the exterior span is not loaded, but this was not found to be a controlling case for any bridge considered here because the required moment capacity was relatively low for this type loading. C_b values for composite bridges were calculated by assuming all dead load to act on the non-composite section and all live load to act on the composite section.

Under the current AASHTO *Specifications* (1992) the moment capacity of a beam is limited to the yield moment, M_y, unless adequate resistance to local buckling and sufficient bracing to prevent LTB is provided so that a plastic hinge with large inelastic rotation capacity can form. This is unlike the current AISC *Load and Resistance Factor Design Specifications* (1994) which allows intermediate values between the yield moment and plastic moment capacities to be used. In this report, the negative moment capacity was limited to the yield moment of the steel section in all cases where the calculated LTB capacity was greater than the yield moment. The resistance to local buckling and LTB of the original designs of the bridges considered here was adequate for use of the plastic moment capacity, M_p. Hence, for cases involving partial removal of the diaphragms, limiting the calculated moment capacity to the yield moment is conservative. For the cases of complete diaphragm removal for non-composite spans and possible future composite spans, the moment capacity was limited to the yield moment because the ability of bridge girders to develop plastic hinges with large inelastic rotation capacity without diaphragms is not yet well established.

In the LTB analysis, the diaphragm locations were assumed to be points braced against twist. The assumption that the diaphragm with a bolted diaphragm-girder connection actually produced a braced point was also checked for one of the 3-span bridges. In order to constitute full bracing against twist, the diaphragms must provide adequate stiffness to force buckling between the diaphragms. An example of this calculation is shown in Appendix A. The calculation indicates that if the proposed new bolted diaphragm connection (described in Chapter Three) is 25% as stiff as the

original welded connection, the diaphragm will produce full torsional bracing. Although the true stiffness provided by bolted diaphragm-girder connection is not known, it appears reasonable to assume full bracing is provided.

Results of the LTB Analyses

The results of the LTB analysis for a 5-span continuous non-composite bridge at the railroad viaduct on I-65 (Test Site 2) are shown in Table 4.1. The span lengths and girder sizes for the bridge are shown in Figure 4.2. The transverse girder spacing is 2.44 m, and the deck thickness is 165 mm.

Table 4.1 is based on complete diaphragm removal. The LTB capacities, M_r, and C_b values were calculated from Equations 4-1 and 4-2, respectively. The yield moments, M_y, were calculated for the steel cross section alone. Included in Table 4.1 are values of the applied factored negative bending moment at the supports, $M_{REQ'D}$, required for an Inventory Rating factor of 1.0 for HS20-44 loading by the load factor method. The results indicate the LTB capacity of the first interior spans is not

Table 4.1. LTB Analysis Results for the Non-Composite 5-Span Continuous Bridge with No Interior Diaphragms

Span(s)	C_b	M_r (kN-m)	M_y (kN-m)	$M_{REQ'D}$ (kN-m)
Exterior	4.63	3270	2530	2340
Interior at 2nd Int. Support	3.35	1790	2200	1990
Center	3.74	2000	2200	1990

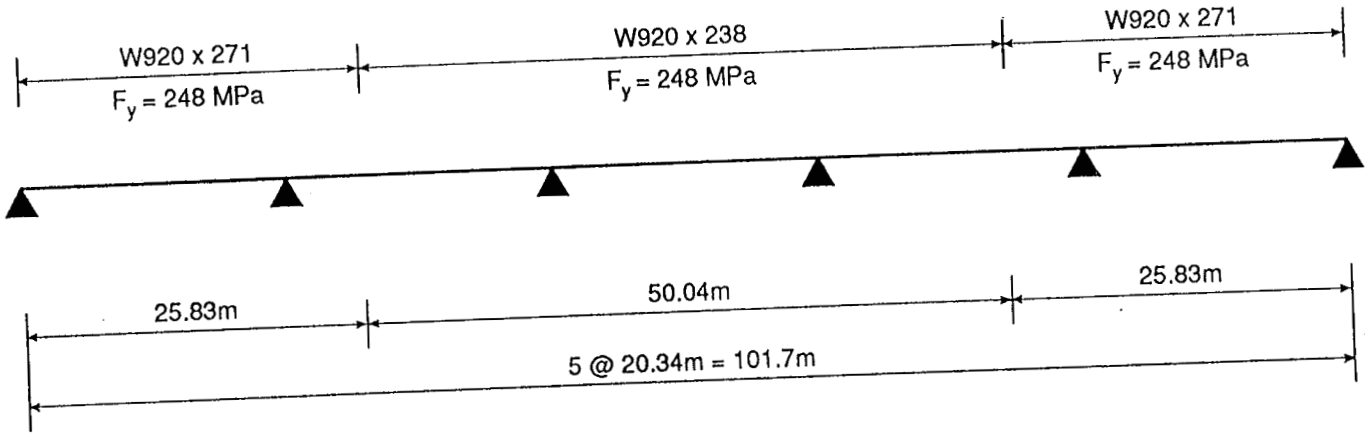

Figure 4.2. Girder Details for the 5-Span Continuous Bridge

adequate to allow complete removal of the diaphragms. The capacity of the center span is greater than the moment requirement but is not large enough for the girder to yield before buckling.

The LTB capacity shown in Table 4.1 for the interior spans is conservative. The spans were analyzed assuming the entire span was a W920 x 238 girder. As shown in Figure 4.2, the W920 x 271 girder in the exterior spans continues over the bents into the interior spans. The additional capacity provided by considering the W920 x 271 girder in part the interior spans was estimated using a weighted average of cross section properties as suggested by Trahair (1993). The capacity estimated by the more rigorous calculation did not allow for complete removal and was not listed in Table 4.1 as the LTB capacity.

A LTB analysis was performed for partial removal of the diaphragms assuming the first line of diaphragms from each interior bent remains in-place. The LTB capacities for this condition are sufficient so that yielding controls the negative moment capacities. This proposal eliminates 7 of the 15 original lines of interior diaphragms, leaving 8 lines of interior diaphragms to be maintained. (The 6 lines of diaphragms at the bents must remain.)

LTB analysis results for the 5-span bridge assuming composite girders with no interior diaphragms are shown in Table 4.2. The critical moment capacities, M_{cr}, from Equation 4-6, were calculated assuming shear studs placed continuously in the positive moment regions and discontinued at the field splices. This assumption results in a smaller calculated increase in moment capacity than would result for a span which is composite end to end. The C_b values and required capacities were calculated

assuming all dead load acts on the steel section and all live load acts on the composite girder. An interesting result of the composite action is a reduction in required moment capacity at the supports relative to the non-composite case (Table 4.1).

Table 4.2. LTB Analysis Results for a Composite 5-Span Continuous Bridge with No Interior Diaphragms

Span(s)	C_b	M_r (kN-m)	M_{cr} (kN-m)	M_y (kN-m)	$M_{REQ'D}$ (kN-m)
Exterior	5.06	3570	4140	2530	2000
Interior at 2nd Int. Support	3.45	1850	2470	2200	1690
Center	3.98	2130	2690	2200	1690

Table 4.2 shows that complete removal of the interior diaphragms is possible since the critical moments are larger than the required capacities and the yield moments for all five spans. With the torsional bracing provided by the addition of the shear studs, the increased LTB capacity of the interior and center spans ensures that the girders will yield prior to buckling.

LTB analysis results for the 3-span continuous non-composite bridge at the CBD Interchange on I-59/20 (Test Site 6) are shown in Table 4.3. The span lengths and girder details for the bridge are shown in Figure 4.3. The transverse girder spacing is 2.13 m, and the deck thickness is 165 mm.

Table 4.3. LTB Analysis Results for the Non-Composite 3-Span Continuous Bridge at the CBD Interchange with No Interior Diaphragms

Span(s)	C_b	M_r (kN-m)	M_y (kN-m)	$M_{REQ'D}$ (kN-m)
Exterior	3.76	2090	4350	3770
Center	3.56	3160	4350	3770

The LTB capacity shown in Table 4.3 for each span is less than the required capacity and is not sufficient to allow complete removal of the diaphragms. An analysis was performed assuming all interior diaphragms are removed except the first line on each side of each interior support. Hence, 4 of the original 8 lines of interior diaphragms are removed. The results indicate that the girders can reach the yield moment without LTB for this partial removal scheme. The yield moments are significantly above the required capacities.

Similar to the 5-span continuous bridge, the girders in the exterior spans of the 3-span bridge are a combination of two sizes, as shown in Figure 4.3. The section properties of the smaller cross section were used to calculate the capacities shown in Table 4.3. Estimates of the moment capacities were made using a weighted average of the properties for the two girder sizes. The results did not change the conclusion that complete diaphragm removal is not possible.

LTB analysis results for an assumed future composite bridge at the CBD Interchange are shown in Table 4.4. The LTB capacity for the exterior spans is not adequate when the section properties of the smaller cross section (W920 x 253) are

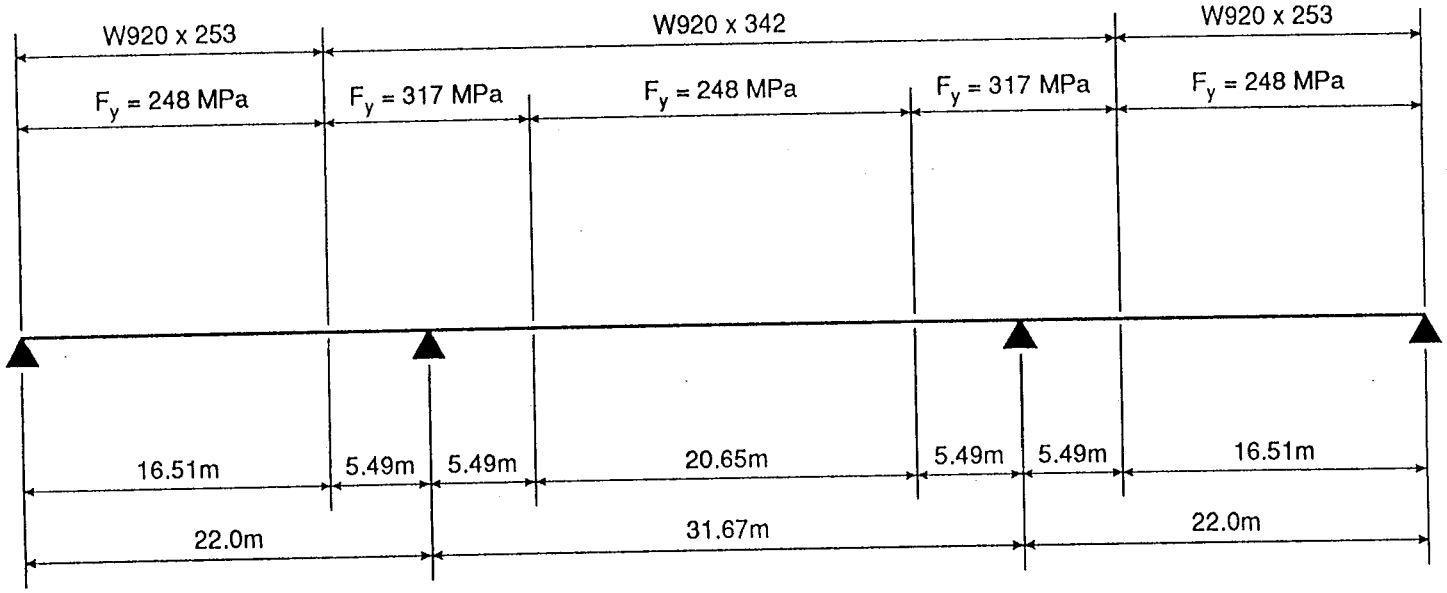

Figure 4.3. Girder Details for the 3-Span Continuous Bridge at the CBD Interchange

used for the entire span. Section properties were recalculated using the weighted average approach suggested by Trahair (1993). By using the averaged cross section properties (I_{yc}, J, d, t_w, and I_{eff}), the LTB capacity exceeds the required capacity but is not large enough to prevent buckling prior to yielding. This means that complete removal of the diaphragms is technically possible, but is less desirable than for cases where yielding will control the moment capacity.

Table 4.4. LTB Analysis Results for a Composite 3-Span Continuous Bridge at the CBD Interchange with No Interior Diaphragms

Span(s)	C_b	M_r (kN-m)	M_{cr} (kN-m)	M_y (kN-m)	$M_{REQ'D}$ (kN-m)
(a) Capacities Using Smallest Cross Section in Span					
Exterior	4.04	2250	2910	4350	3320
Center	4.01	3560	5150	4350	3320
(b) Capacities Using Weighted Average of Cross Section Properties					
Exterior	4.04	3090	3880	4350	3320

The LTB analysis results for the non-composite 3-span continuous bridge in Tuscaloosa County are shown in Table 4.5. The span lengths and girder details are shown in Figure 4.4. The bridge has a 152 mm thick deck and a 2.44 m girder spacing. The section properties for this bridge require a different analysis approach than the previous bridges. This bridge has W920 x 223 girders in all three spans with cover plates at the interior bents and at midspan of the center span. The weighted

Table 4.5. LTB Analysis Results for the Non-Composite 3-Span Continuous Bridge in Tuscaloosa County with No Interior Diaphragms

Span(s)	C_b	M_r (kN-m)	M_y (kN-m)	$M_{REQ'D}$ (kN-m)
(a) Complete Diaphragm Removal				
Exterior	5.58	3160	2960	2590
Center	3.77	1570	2960	2590

average approach is used here to account for the cover plates in the calculation of the cross sectional properties.

The exterior spans have adequate LTB capacity so that all of the interior diaphragms can be removed as shown in Table 4.5. However, the interior span has only approximately half of the LTB capacity required for removal of all the interior diaphragms. Hence, it is necessary to maintain the first line of diaphragms inside the supports for bracing of the interior spans. The LTB capacities of all three spans exceed the yield moment if the first line of diaphragms on each side of the interior bents remain in-place. This partial removal scheme eliminates four of the original eight lines of interior diaphragms.

In Table 4.6, LTB analysis results for the 3-span continuous bridge with composite girders shows that providing shear studs to create torsional bracing does not allow complete removal of the interior diaphragms. The LTB capacity for the center span is about four percent below the required capacity.

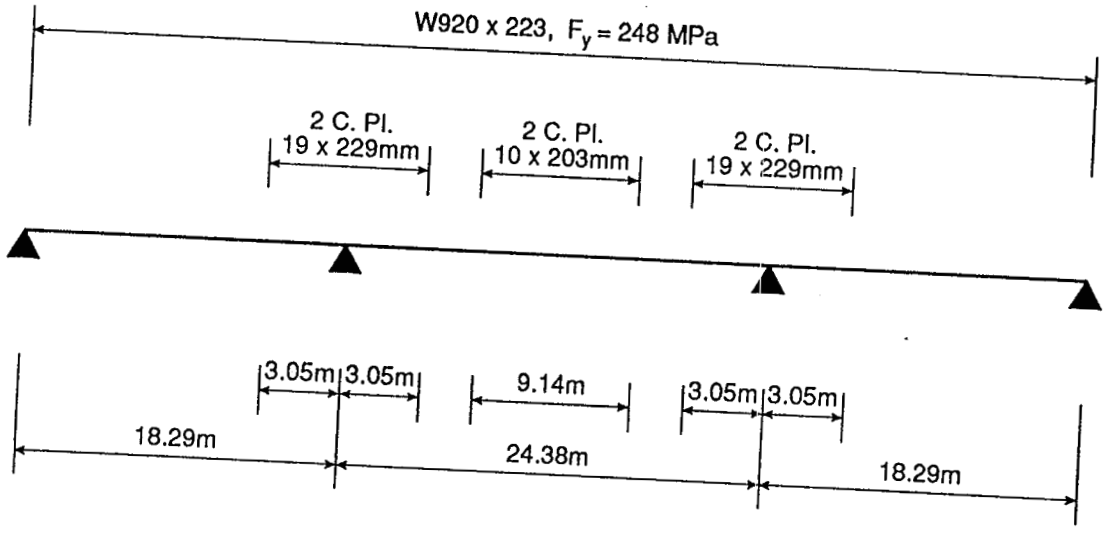

Figure 4.4. Girder Details for the 3-Span Continuous Bridge in Tuscaloosa County

Table 4.6. LTB Analysis Results for the Composite 3-Span Continuous Bridge in Tuscaloosa County with No Interior Diaphragms

Span(s)	C_b	M_r (kN-m)	M_{cr} (kN-m)	M_y (kN-m)	$M_{REQ'D}$ (kN-m)
Exterior	4.13	2350	2800	2960	2280
Center	3.63	1520	2190	2960	2280

The three continuous span bridges analyzed here represent a sample of the various bridge configurations in use. The analyses point out the feasibility of removing approximately half of the interior lines of diaphragms from existing continuous span bridges. The addition of shear studs during a future deck replacement in some cases will eliminate the need for the remaining lines of interior diaphragms.

RATING ANALYSES

Calculations for the bridge ratings followed the Load Factor Method of the AASHTO *Manual for Maintenance Inspection of Bridges* (1983). The Inventory Rating factors reported here are for HS20-44 loading. Removal of some or all lines of diaphragms has no effect on the rating factors for the existing simple span bridges and for the positive moment regions of the existing continuous spans. The rating analysis of these bridges followed the same procedures as the original design.

For the 15.5 m skewed simple span bridge, the skew is small, so the bridge was analyzed using the AASHTO (1992) wheel load distribution factors. Investigation of bridges with severe skew was beyond the scope of this study.

The moment capacity in positive moment regions for the non-composite continuous span bridges was taken as the plastic moment capacity. The top flanges of the girders were continuously braced by embedment in the slab, and local buckling of the flange or web was found not to control. All negative moment capacities were taken as the smaller of the yield moment or the LTB capacity determined in the previous section. Where only partial diaphragm removal is proposed, the negative moment capacity at the supports could be taken as the plastic moment capacity which would increase the ratings reported here. The plastic moment capacity was not used simply for conservatism.

For continuous bridges assumed to be composite, the positive moment capacities were calculated as the ultimate moment of the composite section by AASHTO (1992) Article 10.50.1. Negative moment capacities were limited to the yield moment or the LTB capacity. Use of the plastic moment capacity of the steel section was not assumed appropriate at supports of a bridge with no interior diaphragms.

Tables 4.7 through 4.14 summarize the results of the rating analyses. Listed are the moment capacity, M_u, factored dead load moment, 1.3D, and factored live load moment plus impact, 2.17 (LL+1), for each critical location. The factored dead load moments for all the composite bridges were calculated assuming all dead load acts on the non-composite steel section.

Rating factors for all the simple spans and non-composite continuous spans show excess live load capacity since the rating factors exceed one. The smallest rating factor calculated for these bridges was 1.11. The composite 5-span bridge and 3-span bridge at the CBD Interchange also exhibit excess capacity. Hence, increases

Table 4.7. Rating Analysis Results for the Non-Composite 5-Span Continuous Bridge after Partial Diaphragm Removal

Critical Location	Cross Section	M_u (kN-m)	1.3D (kN-m)	2.17 (LL+I) (kN-m)	Inventory RF
2nd Int. Bnt.	W920 x 238	2200	587	1400	1.15
1st Int. Bnt.	W920 x 271	2530	792	1550	1.12
Cntr. Span[1]	W920 x 238	2540	343	1560	1.41
Ext. Span[1]	W920 x 271	2920	576	1970	1.19

[1] Positive moment ratings

Table 4.8. Rating Analysis Results for a Composite 5-Span Continuous Bridge with No Interior Diaphragms

Critical Location	Cross Section	M_u (kN-m)	1.3D (kN-m)	2.17 (LL+I) (kN-m)	Inventory RF
2nd Int. Bnt.	W920 x 238	2200	587	1100	1.47
1st Int. Bnt.	W920 x 271	2530	792	1210	1.44
Cntr. Span[1]	W920 x 238	4070	343	1760	2.12
Ext. Span[1]	W920 x 271	5280	576	2100	2.24

[1] Positive moment ratings

Table 4.9. Rating Analysis Results for the Non-Composite 3-Span Continuous Bridge at the CBD Interchange after Partial Diaphragm Removal

Critical Location	Cross Section	M_u (kN-m)	1.3D (kN-m)	2.17 (LL+I) (kN-m)	Inventory RF
Int. Bent	W920 x 342	4350	1520	2250	1.26
Ext. Span[1]	W920 x 253	2720	545	1960	1.11
Cntr. Span[1]	W920 x 342	3830	930	2510	1.16

[1] Positive moment ratings

Table 4.10. Rating Analysis Results for the Composite 3-Span Continuous Bridge at the CBD Interchange with No Interior Diaphragms

Critical Location	Cross Section	M_u (kN-m)	1.3D (kN-m)	2.17 (LL+I) (kN-m)	Inventory RF
Int. Bent	W920 x 342	3880	1520	1800	1.31
Ext. Span[1]	W920 x 253	4500	545	2120	1.87
Cntr. Span[1]	W920 x 342	6450	930	2780	1.99

[1] Positive moment ratings

Table 4.11. Rating Analysis Results for the Non-Composite 3-Span Continuous Bridge in Tuscaloosa County after Partial Diaphragm Removal

Critical Location	Cross Section	M_u (kN-m)	1.3D (kN-m)	2.17 (LL+I) (kN-m)	Inventory RF
Int. Bent	W920 x 223[2]	2960	890	1700	1.22
Ext. Span[1]	W920 x 223	2360	370	1660	1.20
Cntr. Span[1]	W920 x 223[3]	2800	445	1870	1.26

[1] Positive moment ratings at midspan
[2] Cross section has 2 - 19 mm x 229 mm cover plates.
[3] Cross section has 2 - 10 mm x 203 mm cover plates.

Table 4.12. Rating Analysis Results for the Composite 3-Span Continuous Bridge in Tuscaloosa County with No Interior Diaphragms

Critical Location	Cross Section	M_u (kN-m)	1.3D (kN-m)	2.17 (LL+I) (kN-m)	Inventory RF
Int. Bent	W920 x 223[2]	2190	890	1393	0.93
Ext. Span[1]	W920 x 223	3850	370	1770	1.97
Cntr. Span[1]	W920 x 223[3]	5030	445	2060	2.23

[1] Positive moment ratings at midspan
[2] Cross section has 2 - 19 mm x 229 mm cover plates.
[3] Cross section has 2 - 10 mm x 203 mm cover plates.

Table 4.13. Rating Analysis Results for the 24.5 m Composite Simple Span Bridge at 2nd Avenue South with No Interior Diaphragms

Cross Section	M_u (kN-m)	1.3D (kN-m)	2.17 (LL+I) (kN-m)	Inventory RF
W920 x 488	7761	1576	3125	1.98
W920 x 289[1]	7360	1576	3125	1.85

[1] Cross section has a 32 mm x 267 mm cover plate.

Table 4.14. Rating Analysis Results for the 15.5 m Composite Simple Span Bridge at Red Oak Road with No Interior Diaphragms

Cross Section	M_u (kN-m)	1.3D (kN-m)	2.17 (LL+I) (kN-m)	Inventory RF
W840 x 176	2900	536	1570	1.51

in girder stresses resulting from diaphragm removal will not significantly effect those bridges. However, the 3-span continuous bridge in Tuscaloosa County has a rating factor less than one for the assumed composite condition which results from insufficient LTB capacity with all diaphragms removed. Complete diaphragm removal is not feasible for this bridge even when torsional bracing is provided by a composite deck.

WIND LOAD ANALYSIS

A potential problem with the partial or complete removal of the diaphragms is the increased stress on the bottom flanges of the exterior girders due to wind loads. Diaphragm lines serve as supports for the exterior girders in resisting wind load and distribute the horizontal force to the interior girders. Analyses were performed to

investigate potential problems associated with the wind loads that may result from removing interior diaphragms.

Wind load analyses were performed using basic engineering principles with guidance from the AISC *Highway Structures Design Handbook* (1986) and the AASHTO *LRFD Bridge Design Specifications* (1994). A first attempt was reported by Davis (1995) where the method of AASHTO (1992) was applied. However, this method is based on the assumption of load sharing through the diaphragms which is not rational for bridges with complete diaphragm removal. The wind load analyses reported here are based on the assumption that all wind loading on the bottom half of the exterior girder is transmitted to the braced points by flexure in the bottom flange. The supports and remaining diaphragm locations are considered as braced points. The maximum lateral flange moment in the exterior girder is taken as

$$M_w = \frac{1}{10} WL_b^2 \tag{4-15}$$

for bridges with partial diaphragm removal, and

$$M_w = \frac{1}{8} WL_b^2 \tag{4-16}$$

for bridges with complete diaphragm removal where W is the wind force per unit length on the bottom flange, and L_b is the diaphragm spacing. These moments are consistent with the intent of AASHTO (1994).

For continuous span bridges with all interior diaphragms removed the moment from Equation 4-16 is assumed to occur at the points of both maximum tension and compression live load stress in the bottom flange. Wind load stresses were only investigated at the point of maximum tension live load stress for partial removal cases since the conditions near the girder supports are not significantly changed from the original design. Wind load stresses near midspan were investigated for simple span bridges using Equation 4-16.

Bottom flange stresses due to wind load, dead load and live load were factored and added for Group II and Group III combinations as outlined in the AISC *Handbook* (1986). Combined stresses were calculated as follows:

$$\text{GROUP II}: \quad F = 1.3\,(F_{DL} + F_W) \tag{4-17}$$

$$\text{GROUP III}: \quad F = 1.3\,(F_{DL} + F_{LL+I} + 0.3F_W) \tag{4-18}$$

where F_{DL} is the dead load stress; F_W is the wind load stress; and F_{LL+I}, is the stress due to live load plus impact. The limit on the combined stress was taken as the smaller of the yield stress or the stress corresponding to LTB.

Results from the analyses are summarized in Tables 4.15 through 4.22. Tables are provided for the continuous span bridges for both the existing non-composite condition and the assumed composite condition. Results for the non-composite bridges are based on "partial diaphragm removal" as discussed in the previous section. All interior diaphragms were assumed to be removed for the composite bridges, and all dead load was assumed to act on the steel girder alone.

Results of the analyses show that wind loading will not restrict complete removal of diaphragms from the composite simple span bridges nor partial diaphragm removal

Table 4.15. Wind Load Analysis Results for the Non-Composite 5-Span Continuous Bridge after Partial Diaphragm Removal

Critical Location	F_{DL} (MPa)	F_{LL+I} (MPa)	F_w (MPa)	Group II (MPa)	Group III (MPa)	F_y (MPa)
Ext. Span	43	81	53	125	182	248
Int. Span	21	73	26	61	132	248
Cntr. Span	30	74	24	70	145	248

Table 4.16. Wind Load Analysis Results for a Composite 5-Span Continuous Bridge with No Interior Diaphragms

Critical Location	F_{DL} (MPa)	F_{LL+I} (MPa)	F_W (MPa)	Group II (MPa)	Group III (MPa)	F_y (MPa)
Ext. Span	43	65	120	212	187	248
1st Int. Bent	60	50	120	234	190	248
Int. Span	21	61	141	211	162	248
2nd Int. Bent	51	52	141	250	189	248
Cntr. Span	30	62	141	222	175	248

Table 4.17. Wind Load Analysis Results for the Non-Composite 3-Span Continuous Bridge at the CBD Interchange after Partial Diaphragm Removal

Critical Location	F_{DL} (MPa)	F_{LL+I} (MPa)	F_W (MPa)	Group II (MPa)	Group III (MPa)	F_y (MPa)
Ext. Span	44	89	54	127	194	248
Cntr. Span	52	78	42	122	185	248

Table 4.18. Wind Load Analysis Results for a Composite 3-Span Continuous Bridge at the CBD Interchange with No Interior Diaphragms

Critical Location	F_{DL} (MPa)	F_{LL+I} (MPa)	F_W (MPa)	Group II (MPa)	Group III (MPa)	F_y (MPa)
Ext. Span	44	66	152	256	203	248
Int. Bent	86	57	152	310	245	283[1]
Cntr. Span	52	64	146	257	208	248

[1] Limiting stress based on LTB (F_y = 317 MPa at Bent)

Table 4.19. Wind Load Analysis Results for the Non-Composite 3-Span Continuous Bridge in Tuscaloosa County after Partial Diaphragm Removal

Critical Location	F_{DL} (MPa)	F_{LL+I} (MPa)	F_W (MPa)	Group II (MPa)	Group III (MPa)	F_y (MPa)
Ext. Span	35	84	69	135	182	248
Cntr. Span	35	81	89	161	195	248

Table 4.20. Wind Load Analysis Results for a Composite 3-Span Continuous Bridge in Tuscaloosa County with No Interior Diaphragms

Critical Location	F_{DL} (MPa)	F_{LL+I} (MPa)	F_W (MPa)	Group II (MPa)	Group III (MPa)	F_y (MPa)
Ext. Span	35	68	124	207	182	248
Int. Bent	58	49	165	290	203	183[1]
Cntr. Span	35	75	197	302	220	248

[1] Limiting stress based on LTB (F_y = 248 MPa)

Table 4.21. Wind Load Analysis Results for the 24.5 m Composite Simple Span Bridge at 2nd Avenue South with No Interior Diaphragms

Girder	F_{DL} (MPa)	F_{LL+I} (MPa)	F_W (MPa)	Group II (MPa)	Group III (MPa)	F_y (MPa)
New[1]	61	54	59	156	173	248
Old[2]	74	61	99	225	214	248

[1] New Girder - W920 x 488
[2] Old Girder - W920 x 289 with 32 mm x 267 mm cover plate

Table 4.22. Wind Load Analysis Results for the 15.5 m Composite Simple Span Bridge at Red Oak Road with No Interior Diaphragms

F_{DL} (MPa)	F_{LL+I} (MPa)	F_W (MPa)	Group II (MPa)	Group III (MPa)	F_y (Mpa)
70	83	121	248	246	248

from the existing non-composite continuous spans. However, the combined stresses are very high for the 15.5 m simple span. This points out the need for a wind load analysis before diaphragms are removed from any bridge.

For the assumed future condition of composite girders for the continuous spans, wind loading does prevent complete diaphragm removal from both of the 3-span bridges since the combined stresses exceed the yield strength (or the limit based on LTB). The Group II combined stress at the second interior bent of the 5-span bridge is sightly above the limit (250 MPa versus 248 MPa limit), but this is not a significant overstress.

TEMPORARY BRACING REQUIREMENTS

Preceding discussions indicate that partial or complete removal of the diaphragms is possible within the limits discussed. A negative consequence appears

during any future deck slab replacement. With the diaphragms completely or partially removed from the existing bridges, the stability of the girders during reconstruction of the slab will be inadequate in many cases. To alleviate this problem one of two general options are possible. The first solution would be to require shoring to reduce the moments on the steel girders. The second solution would be to require temporary bracing for the girders. Either option could be used to ensure the stability of the girders during the construction of the new slab.

CONCLUSIONS

Structural evaluations were performed to assess the feasibility of removing the interior diaphragms from typical multi-girder steel bridges. Primary considerations were the effects that diaphragm removal has on the resistance to wind loading, resistance to lateral torsional buckling (LTB) of continuous spans, and on the Inventory Ratings. The possible future condition of making the continuous span bridges composite was also investigated.

Inventory Ratings for the two simple span bridges investigated are 1.5 or larger. Wind load stresses do not exceed the limiting value for either bridge. Calculated ratings for this type bridge are not affected by the presence or absence of diaphragms. Diaphragms are not needed for these spans to prevent LTB since the top flanges of the composite simple span girders are continuously supported by the deck slab. The removal of all interior lines of diaphragms from these and other composite simple spans appears feasible based on the results of the structural evaluations. The results do indicate that a structural evaluation including a wind load analysis should be performed before diaphragms are removed from any existing bridge.

Diaphragms adjacent to each interior support are necessary for bracing against LTB in the non-composite continuous span bridges. For all bridges investigated, removal of all interior diaphragms except the first line on each side of the interior supports (referred to as partial diaphragm removal) is possible without changing the Inventory Rating of the bridge. Wind load stresses do not restrict partial diaphragm removal for these three bridges. Removing all interior diaphragms except one line on each side of the interior supports will eliminate approximately half of the existing diaphragm lines.

During a future deck replacement, composite action can be created between the girders and the deck slab by installing shear studs onto the top flanges of the continuous span girders. This produces torsional bracing by the slab which increases the LTB capacity of the girders. Of the three continuous span bridges investigated assuming composite girders, complete diaphragm removal is only feasible at the 5-span bridge. The 3-span bridge at the CBD Interchange has insufficient resistance to wind loading with all interior diaphragms removed. The 3-span bridge in Tuscaloosa County has insufficient resistance to LTB and wind loading with all diaphragms removed.

Calculations reported by Davis (1995) indicate that the existing girders can support an extra inch of normal weight concrete deck without a significant reduction in Inventory Rating if composite action is created by adding shear studs and shored construction is used.

CHAPTER FIVE

EFFECTS OF REMOVING DIAPHRAGMS FROM A 24.5 METER COMPOSITE SIMPLE SPAN

INTRODUCTION

A 24.5 m composite simple span along I-65 over 2nd Avenue South was the first test site chosen for a field evaluation of the effects diaphragms have on the lateral distribution of traffic loads. Four series of tests were performed on the bridge. Two series of tests were performed with trucks of known weight and axle configuration; one series with diaphragms in-place and one series with all interior diaphragms removed. Tests were also performed before and after the diaphragms were removed in which data were recorded for trucks in the normal traffic stream. Descriptions of these tests and test results are in this chapter.

BRIDGE DESCRIPTION

The simple span bridge carries 5 traffic lanes of northbound I-65 traffic. The bridge span consists of 9 rolled steel wide flange girders spaced at 2.44 m transversely. A numbering system for the girders, diaphragms, and traffic lanes is shown in Figure 5.1. Seven of the girders (Girders 1 through 7) are W920 X 289 rolled sections with 33 mm X 267 mm X 15.8 m cover plates welded to the bottom flange. These seven girders are part of the original bridge construction and are located on the east side of the span. The two girders located on the west side of the span (Girders 8 and 9) are W920 X 488 rolled sections and were added when I-65 was widened over the railroad viaduct between 2nd Avenue South and 1st Avenue North. All of the

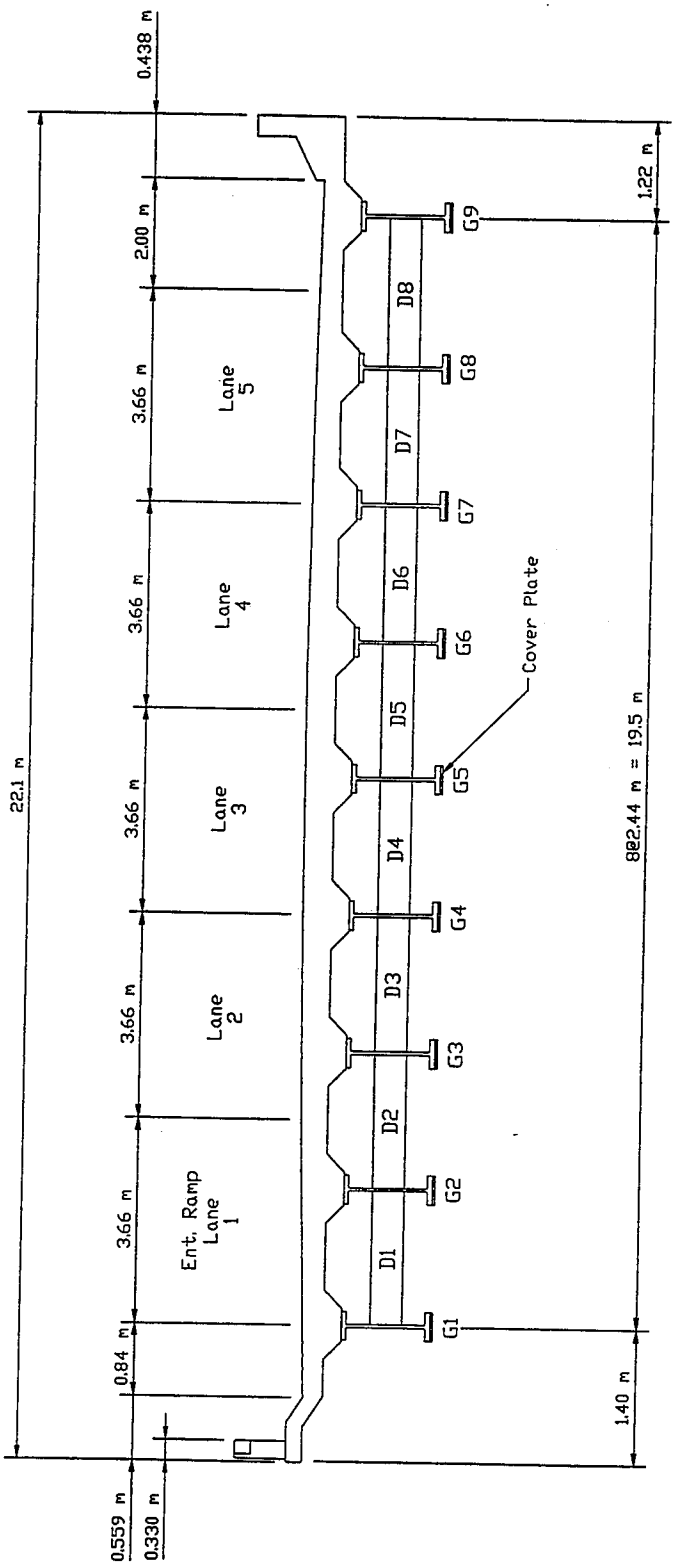

Figure 5.1. Cross Section of the 24.5 m Simple Span (Looking into Traffic)

girders have shear studs to provide composite action with the 165 mm thick concrete deck.

The girders were connected by three lines of interior diaphragms and one line at each support. All diaphragms were rolled steel sections MC460 X 63.5 and oriented perpendicular to the girders. The diaphragms were spaced at 6.18 m on centers as shown in the plan view of the simple span in Figure 5.2. Originally the diaphragm-girder connections consisted of a 101 mm X 9.5 mm X 762 mm connection plate welded to the web and to each end of the channel diaphragms. Due to fatigue cracking at the connections and the bridge widening, about half of the diaphragm girder connections were bolted connections using an angle L 152 X 152 X 9.5 mm by 483 mm long. The tops of the channel diaphragms were approximately 130 mm below the underside of the concrete deck.

INSTRUMENTATION AND DATA ACQUISITION

To evaluate the effects of removing the interior diaphragms from the bridge, girder bending strains and deflections were measured before and after the diaphragms were removed. Instrumentation included electrical resistance strain gages for measuring surface strains and deflectometers for measuring vertical displacements. Instrumentation focused on measuring bending strains and deflections of the girders at midspan.

The strain gages were self temperature compensating foil gages with polyamide encapsulation and preattached lead wires. All gages had a nominal resistance of 350 ohms and a gage length of 9.55 mm. After each gage was mounted, the preattached lead wires were soldered to light gage stranded wire which was connected to a

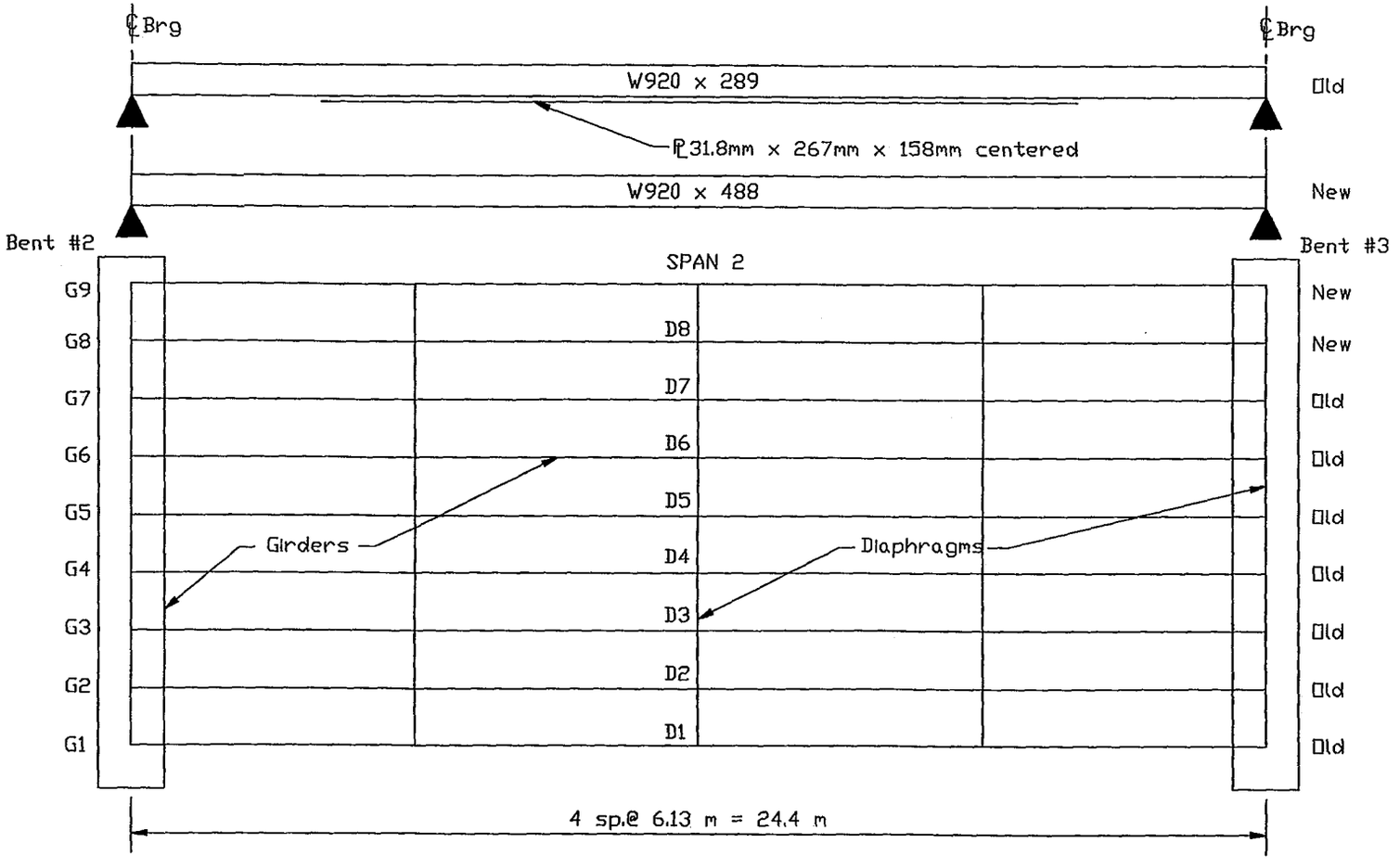

Figure 5.2. Plan View and Girder Details for the 24.5 m Simple Span

terminal block. Electrical tape was placed underneath and on top of the soldered connections to prevent electrical grounding of the wires to the girder. The gage was then covered with a waterproof neoprene pad with an adhesive back.

The strain gages were connected to the data acquisition system using a three-wire quarter bridge connection. Shielded cable was used to reduce the electronic noise recorded with the data. The shielded cables were attached to the terminal blocks at the gages and neatly and strategically routed along the girders with C-clamps to reduce any electronic noise that might be produced by vibration of the cables at the terminal block. The cables were then routed directly to the data acquisition van where they were connected to the data acquisition system through screw terminal blocks (STBs). To avoid errors in the measurements, the same strain gages and cables were used in the tests before and after the diaphragms were removed.

Strain gages were mounted on the top and bottom flange of the girders at midspan as shown in Figure 5.3. The bottom flange gages were used for making the principle measurements concerning the removal of the diaphragms. Top flange gages were used to verify composite action of the girders and deck. As expected for composite girders, the measured top flange strains were very small, and the girders were concluded to be acting compositely with the deck as designed. A limited number of bottom flange gages were mounted near the supports for an indication of the presence of horizontal restraint at the bearings. Top and bottom flange gages were installed on the diaphragms near each end in the line of diaphragms at midspan of the bridge. The purpose of these gages was to measure strains from which the shear, moment, and thrust at the ends of the diaphragms could be calculated. However, the

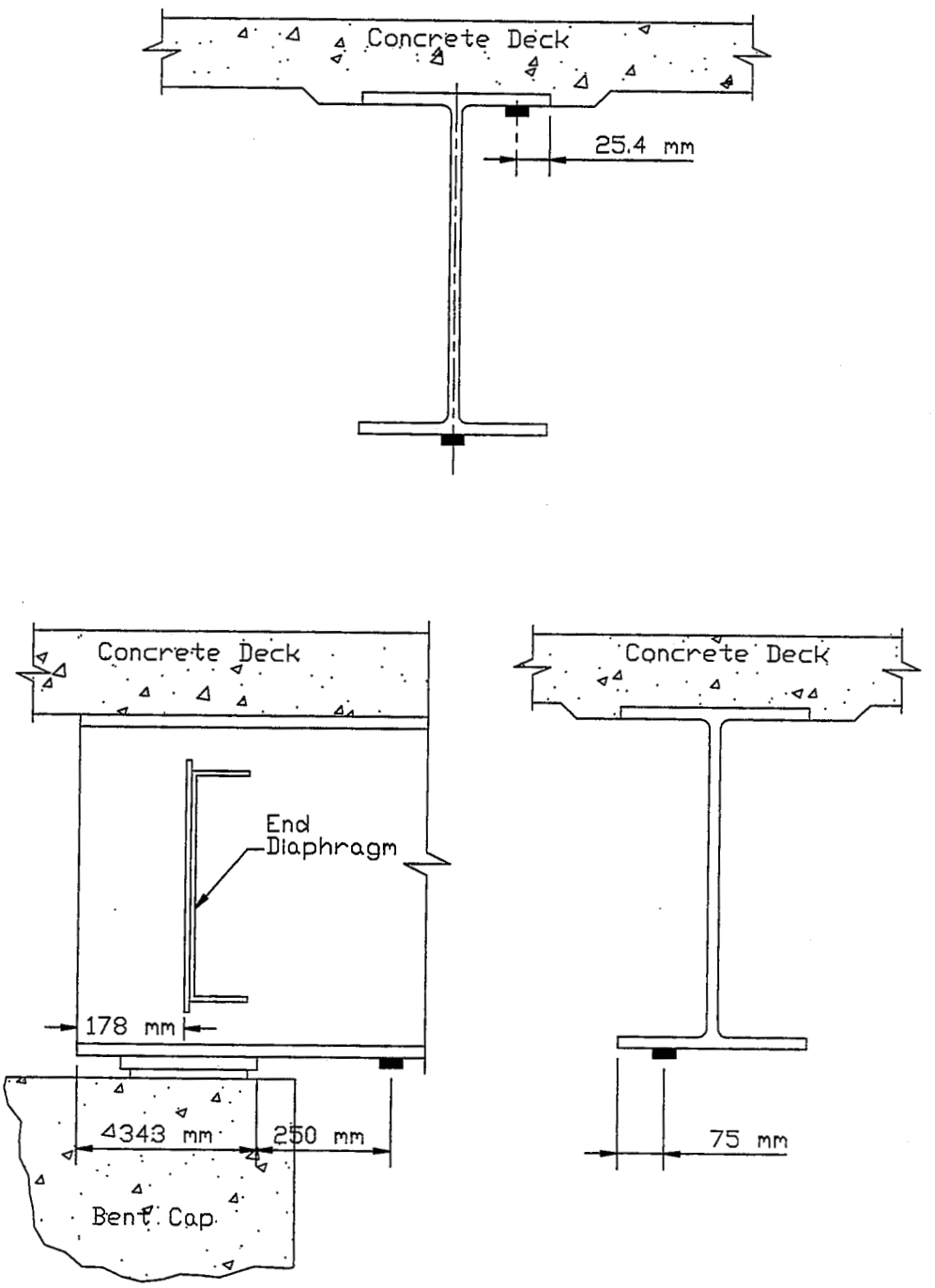

Figure 5.3. Strain Gage Locations on Girders

magnitudes of the measured diaphragm strains were typically so small as to be unreliable for the intended purpose.

Vertical deflections of the girders were measured with demountable deflectometers which were essentially calibrated cantilever beams. Each deflectometer consisted of an aluminum alloy bar instrumented with a full bridge of strain gages. Deflectometers were mounted at midspan of each girder using C-clamps to firmly secure them against the bottom flange. The free end of the deflectometer was equipped with a small ring for attaching a light gage wire. A plumb bob was used to center a weight directly beneath the small ring. A light gage steel wire was then attached to the weight. The end of the deflectometer at the small ring was predeflected to approximately 32 mm and then the light gage wire was attached. As traffic crossed the span, some of the predeflection was relieved which created a measurable signal from the calibrated full bridge of strain gages on the deflectometer. A four-wire shielded cable was used to connect the deflectometers to the data acquisition system. To avoid errors in the measurements, the same deflectometers were placed beneath each girder using the same cables for tests performed before and after the diaphragms were removed.

Deflectometers were mounted at midspan as close as possible to the midspan strain gages. Because the data acquisition system was limited to 8 channels for deflectometer measurements, girder deflections were measured at girders 2 through 9. Girder 1 was located under an exit ramp where there was relatively little traffic.

A MEGADAC 3108AC dynamic data acquisition system (Technical Manual 1994) manufactured by OPTIM Electronics Corporation was used to collect all of the field test

data. This system is a high speed measurement system capable of recording 25,000 samples per second. The field tests measurements reported here were made using a sampling rate of 400 samples per second per channel.

The data acquisition system was driven by a 486 -25 MHZ personal computer. The personal computer was equipped with TCS 5.1 (OPTIM 1994) which is a software package also created by OPTIM Electronics Corporation that is compatible with the MEGADAC 3108AC. The personal computer and software allowed immediate inspection of the raw strain and deflection data. The data acquisition system was linked with the personal computer via an IEEE-488 communications card. This connection allowed direct communication between the MEGADAC 3108AC and the personal computer and enabled recorded data to be immediately stored onto the hard drive of the personal computer. When all tests were completed for the day, the recorded data was backed up from the hard drive of the computer to 250 megabyte mini data tapes. All electrical equipment used for instrumentation and collection of data was powered by a portable generator.

The data acquisition system and personal computer displayed a tendency to malfunction in the hot humid conditions typical of the field test sites. A cool, arid atmosphere was provided to protect the personal computer and the data acquisition system from exposure by placing a small, window unit type air conditioner in the rear door of a van. A specially cut piece of plywood was placed around the air conditioner to allow access for the lead wires and to insulate the van from heat gain or loss. This provided the appropriate working environment for the electronic equipment.

DESCRIPTION OF FIELD TESTS

Field measurements were taken before and after all interior diaphragms were removed with loadings from trucks of known weight and axle configuration and from trucks in the normal daily traffic stream. Field measurements taken for loading by trucks of known weight and axle configuration will be referred to as "test truck" data or "calibration truck" data. Field measurements taken for loading by trucks in the normal daily traffic stream will be referred to as "normal traffic" data or "truck traffic" data. Due to the high volume of traffic on the interstates, traffic was not stopped for any tests and all data was taken for trucks travelling at normal traffic speeds.

Calibration Tests

The calibration tests were performed using two identical load testing trucks provided and owned by the Alabama Department of Transportation Bridge Rating and Load Testing Section. Both test trucks had 3 axles which were characteristic of short heavy trucks. Figure 2.11 displays a schematic of the test truck axle configuration and axle weights. The front axle had a weight of 91 kN and the total weight of the two rear axles was 255 kN. The total weight of each truck was slightly higher than the legal load limit for this axle configuration.

Calibration tests were conducted late at night, typically between 11 p.m. and 2 a.m. During this time period the normal traffic volume was low enough so that data could be recorded with only test trucks on the bridge.

During the tests, radio communication was used to exchange information regarding the test details. Communication was maintained between a spotter, who had a clear view of the bridge and traffic, the test truck drivers, and the data acquisition

system operator. The spotter, instructed the data acquisition operator to start and stop recording data. During recording of data, radio silence was observed to eliminate the possibility of the data acquisition system recording electronic noise emitted from the radios.

Before the calibration tests were performed, the data acquisition system was balanced to establish zero live load strains and deflections. Balance data were taken over a short period of time during which there was minimal or no vehicular activity on the bridge. Additional data sets were taken throughout the series of calibration tests so that shifts due to temperature changes could be accounted for.

A full series of calibration tests included 2 single truck crossings in each of the 5 traffic lanes and side-by-side truck crossings in lanes 2 and 3, 3 and 4, and 4 and 5. Table 5.1 illustrates a typical calibration test sequence. Once the data for a truck crossing had been recorded, comments about the particular truck crossing were also recorded on paper. These comments consisted of the test truck number, lane, velocity, and a rating. The rating pertained to other vehicular activity on the span at the time the test truck crossed. The definitions of the rating are shown in Table 5.2. Data from any truck crossing rated as "Bad" was not used, and the truck crossing was repeated.

Normal Traffic Tests

The goal of taking normal traffic data was to measure girder deflections and strains from loadings with trucks of different weights and axle configurations in specified lanes. Normal traffic data was recorded before and after all the interior diaphragms were removed.

Table 5.1. Calibration Test Sequence for Diaphragms Removed at the 24.5 m Simple Span

Data Set	Truck No.	Lane No.	Comments	Rating
001			Balance	
002	1	1	35 mph	Very Good
003	2	1	31 mph	Excellent
004	1	2	54 mph	Very Good
005	2	2	55 mph	Excellent
006	1	3	55 mph (truck on span at start in lane 1)	Good
007	2	3	55 mph	Excellent
008	1	4	55 mph	Excellent
009	2	4	52 mph	Very Good
010	1	5	55 mph	Good
011	2	5	55 mph	Excellent
012	1	3	55 mph	Excellent
013	2	3	57 mph	Excellent
014	½	2/3	55 mph (truck 1 lane 2 truck 2 lane 3)	Excellent
015	½	3/4	55 mph (truck 1 lane 3 truck 2 lane 4)	Excellent
016	½	4/5	55 mph (truck 1 lane 4 truck 2 lane 5)	Excellent

Table 5.2. System for Rating Test Data

Rating	Definition
Excellent	No vehicles on the span
Very Good	1 or 2 small vehicles on the span
Good	More than 2 vehicles on the span
Bad	Large vehicle on the span

The procedure for taking normal traffic data was essentially the same as the calibration tests. A spotter instructed the data acquisition system operator when to start and stop recording data, commented on which lane the truck was in as it crossed, and made other comments regarding the quality of the recorded data.

Typically, about 100 to 150 truck crossings were recorded in these tests. A data set was labeled "Bad" and disregarded if the truck changed lanes or if another heavy vehicle or more than two cars were on the span with the heavy truck. Because of very high traffic volume on the interstates, it was necessary to collect data at off-peak times so that single truck crossings could be recorded. The goal was to collect a minimum of 25 truck crossings in each traffic lane. Due to the normal traffic patterns, it was impossible to record a sufficient number of truck crossings in certain lanes in the limited time available. Due to this, the results presented below for the normal traffic tests are for truck crossings in lanes 3 and 4 only.

CALIBRATION TESTS RESULTS

The maximum bottom flange stresses from the calibration tests are shown in Table 5.3 for cases with diaphragms in-place (In) and with the diaphragms removed

(Out). For single lane loadings the average of two tests are shown, and the value shown for side-by-side truck crossings are from one test. For each particular lane crossing, one girder was observed to be the most heavily loaded girder (girder with largest measured strains) for all truck crossings in that particular lane. The data for the most heavily loaded girder are shown in bold type in Table 5.3.

Overall, removing the diaphragms caused an increase of 6 to 15% in the average measured maximum bottom flange stresses for the most heavily loaded girder. For single truck crossings, the largest increase of 15% in average measured bottom flange girder stress occurred at girder 8 for a truck in lane 5. The largest increase in measured girder stress for side-by-side truck crossings was 10% and occurred at girder 4 for trucks side-by-side in lanes 2 and 3.

Maximum girder deflection plots shown in Figures 5.4 through 5.6 provide another general illustration of how the bridge responded to removal of the diaphragms. The results in these figures are for the calibration truck loading so that the results for diaphragms in-place can be directly compared to the results with the diaphragms removed. Figures 5.4 and 5.5 provide plots of the average maximum midspan girder deflection from two tests for each of the 5 traffic lanes. Figure 5.6 shows the maximum midspan girder deflections for the side-by-side truck crossings. As can be seen from the plots, the most heavily loaded girders experienced an increase in average girder deflection as a result of diaphragm removal. In many cases, the girders farther away from the lane load experienced a decrease in average girder deflection. These observations indicate a change in load distribution and that the diaphragms do enhance the lateral distribution of truck loads to some degree.

Table 5.3. Measured Maximum Bottom Flange Stresses (MPa) from Calibration Truck Loading

Loading/ Dia. Status	Girder Number								
	1	2	3	4	5	6	7	8	9
Lane1/In	25	**29**	17	7	2	1	1	1	1
Lane1/Out	24	**32**	17	5	1	1	1	1	1
Lane2/In	7	17	**31**	26	11	5	3	2	1
Lane2/Out	6	18	**33**	26	9	3	2	1	2
Lane3/In	2	3	8	21	**27**	16	7	4	1
Lane3/Out	2	2	7	22	**30**	15	6	3	1
Lane4/In	2	1	2	6	13	**24**	21	11	3
Lane4/Out	2	1	2	5	11	**27**	24	11	2
Lane5/In	1	1	1	1	3	8	15	**20**	16
Lane5/Out	1	1	1	1	3	9	19	**23**	17
Lanes2+3/In	9	21	38	**42**	33	18	8	3	2
Lanes2+3/Out	7	20	40	**46**	34	18	7	3	2
Lanes3+4/In	2	3	10	27	38	**37**	27	13	3
Lanes3+4/Out	1	3	10	25	38	**40**	27	12	2
Lanes4+5/In	3	1	2	6	14	31	**36**	29	21
Lanes4+5/Out	2	1	2	5	15	35	**39**	30	18

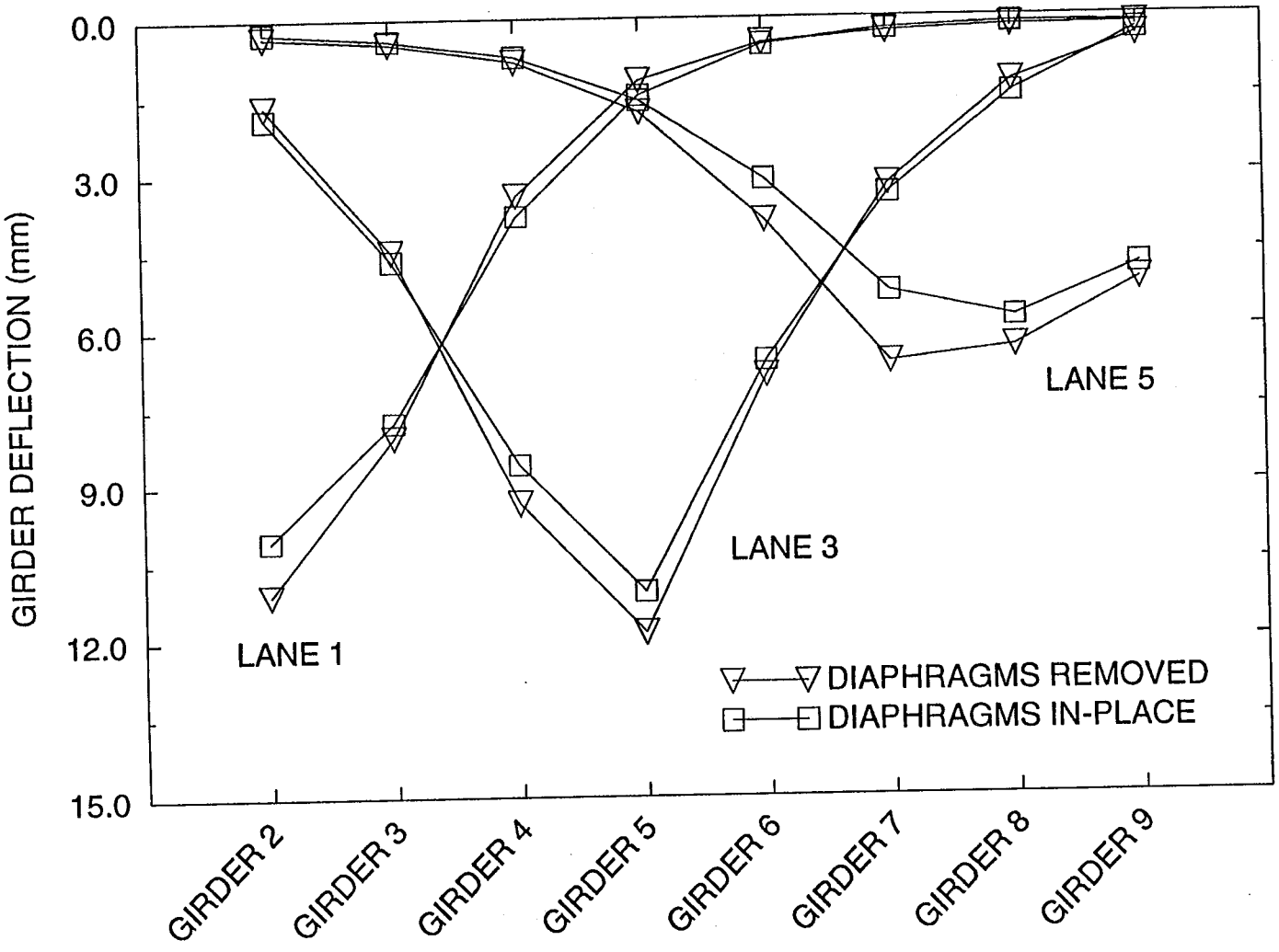

Figure 5.4. Average Maximum Midspan Girder Deflections for One Calibration Truck

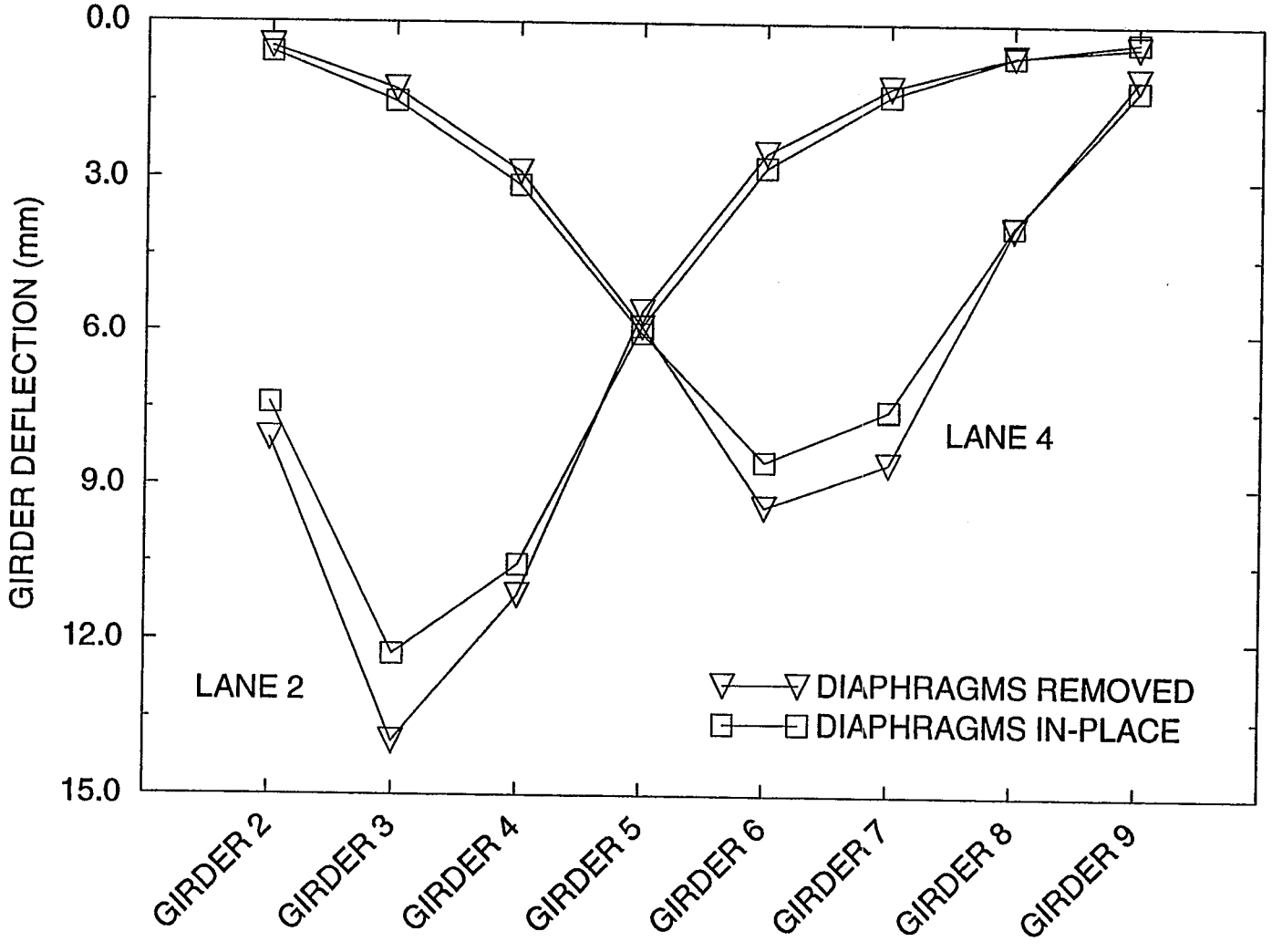

Figure 5.5. Average Maximum Midspan Girder Deflections for One Calibration Truck

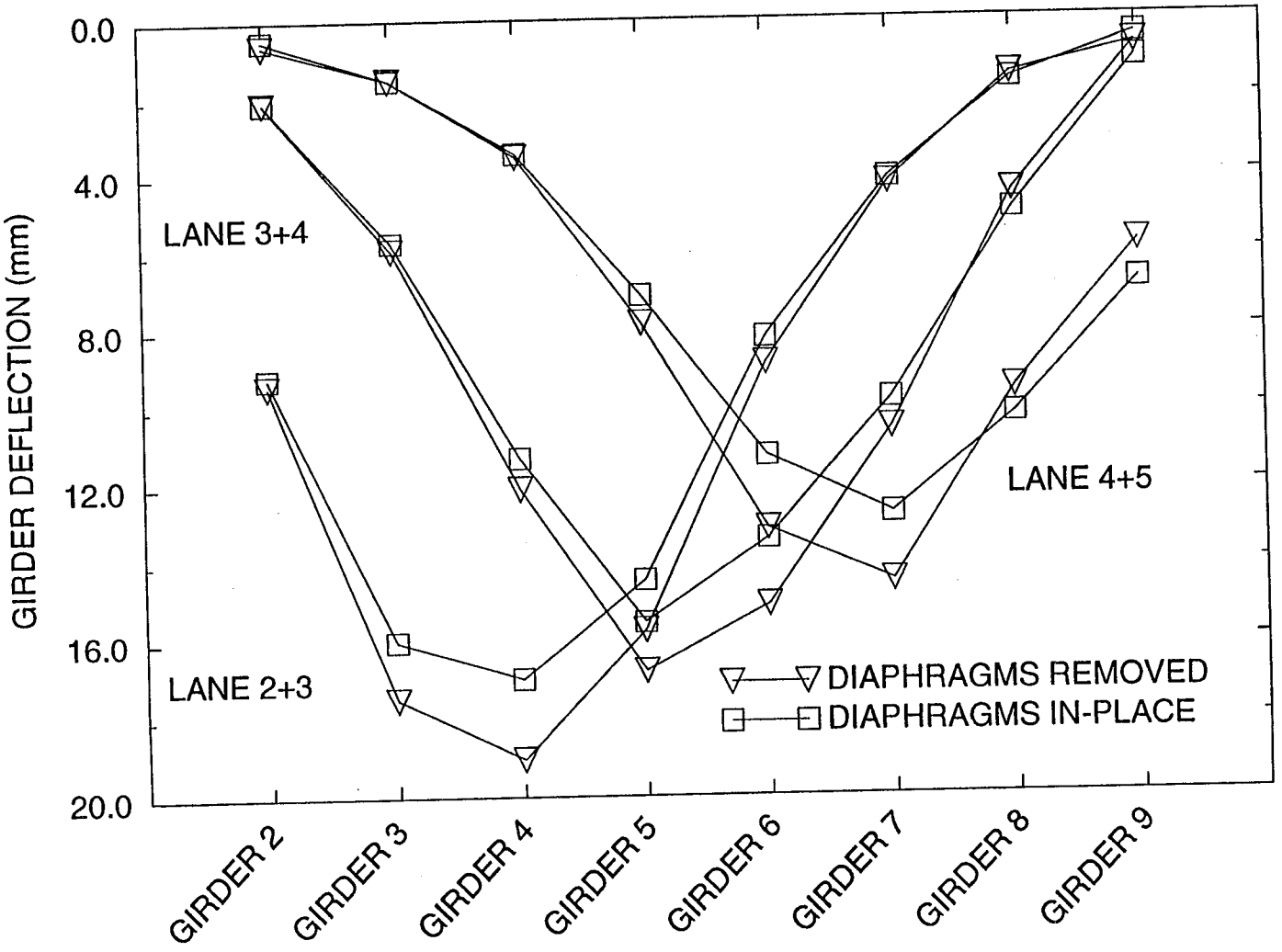

Figure 5.6. Maximum Midspan Girder Deflections for Side-by-Side Calibration Trucks

The maximum measured girder deflections from calibration tests are tabulated in Table 5.4. The values for single truck loadings are the average from two tests, and the values for side-by-side trucks are from one test. The values for the most heavily loaded girder are shown in bold type in the table. The girder deflections at the most heavily loaded girder increased as a result of removing the diaphragms from 6 to 14%. These increases in girder deflection compare well with the 6 to 15% increase in maximum measured girder stresses.

Comparisons with Calculated Stresses

Girder stresses were calculated to compare the measured stresses with the calculated stresses using AASHTO's (1992) simplified analysis method. AASHTO Impact and Wheel Load Distribution factors were applied to the midspan bending moment calculated for one wheel line of test truck loading to determine the maximum bending moment for each girder. The bottom flange stresses were then calculated by using the properties of the composite cross section determined by using an effective width of the concrete deck (with $f'_c = 28$ MPa) as specified by AASHTO.

For comparisons of the measured stresses to the calculated stresses, superposition of the average maximum measured bottom flange stresses had to be used to simulate the crossing of side-by-side trucks in all five traffic lanes. The superpositions are shown in Table 5.5 for diaphragms removed and diaphragms in-place. One superposition is obtained by adding together the single truck test results for each of the five lanes. The other superposition is obtained by adding the single truck results for lane 1 and side-by-side truck results for lanes 2 and 3, and lanes 4 and 5. Superposition of the live load yields a useful comparison with the AASHTO

Table 5.4. Measured Maximum Girder Deflections (mm) from Calibration Truck Loading

Loading/ Dia. Status	Girder Number							
	2	3	4	5	6	7	8	9
Lane1/In	**10.1**	7.8	3.8	1.5	.5	.2	.1	.1
Lane1/Out	**11.1**	8.0	3.4	1.2	.5	.3	.2	.2
Lane2/In	7.4	**12.3**	10.5	5.9	2.8	1.4	.6	.3
Lane2/Out	8.1	**13.9**	11.1	5.6	2.5	1.2	.6	.4
Lane3/In	1.9	4.6	8.6	**11.1**	6.6	3.4	1.4	.3
Lane3/Out	1.7	4.5	9.3	**11.8**	6.9	3.2	1.2	.4
Lane4/In	.6	1.5	3.1	6.0	**8.5**	7.5	3.9	1.2
Lane4/Out	.5	1.3	2.9	5.9	**9.4**	8.6	3.9	1.0
Lane5/In	.2	.4	.7	1.6	3.1	**5.3**	5.8	4.8
Lane5/Out	.3	.4	.8	1.8	3.9	**6.6**	6.4	5.1
Lanes2+3/In	9.2	16.0	**17.0**	14.4	8.2	4.1	1.6	.5
Lanes2+3/Out	9.41	17.5	**19.0**	15.7	8.8	4.2	1.4	.7
Lanes3+4/In	2.1	5.7	11.3	**15.5**	13.4	9.8	4.9	1.1
Lanes3+4/Out	2.1	5.9	12.1	**16.8**	15.1	10.5	4.5	.7
Lanes4+5/In	.5	1.5	3.4	7.1	11.3	**12.7**	10.2	6.8
Lanes4+5/Out	.6	1.5	3.5	7.8	13.1	**14.5**	9.5	5.8

Table 5.5. Calculated Stresses (MPa) and Superpositions of Measured Maximum Bottom Flange Stress (MPa) from Calibration Truck Loading

Loading/ Dia. Status	Girder Number								
	1	2	3	4	5	6	7	8	9
Calculated	68	74	74	74	74	74	74	67	61
1,2,3,4,5/In	37	51	59	61	56	54	47	38	22
1,2,3,4,5/Out	35	54	60	59	54	55	52	39	23
1,2+3,4+5/In	37	51	57	55	49	50	45	33	24
1,2+3,4+5/Out	33	53	59	56	50	54	47	34	21

measured stresses but results in some error. Error is created because the mass of the entire system (consisting of the trucks plus the structure) for true side-by-side loadings would be greater than the mass of the system for which field measurements were taken. The superposition results provide a useful approximate means of comparison with the calculated stresses, but due to uncertainty regarding the magnitude of the error introduced, it is probably not appropriate to use the superposition results to calculate percentage increases in girder stresses resulting from the removal of the diaphragms.

The results in Table 5.5 indicate that the measured stresses are somewhat lower than the calculated stresses. Hence, the conservatism commonly observed in comparisons of measured and calculated bridge girder stresses is not significantly changed by removing the diaphragms.

NORMAL TRAFFIC TESTS RESULTS

Normal traffic tests were used to study how the bridge responded to longer trucks of various weights after diaphragm removal. Because the weights and axle configurations of the trucks in normal traffic are not known, direct comparisons between before and after diaphragm removal cannot be used. Comparisons are made here by calculating estimates of the percentage of the applied load resisted by each girder. These percentages are referred to as load fractions. In the following discussion, four different methods of calculating load fractions are described and compared.

A load fraction is a dimensionless strain ratio that is defined as the maximum strain in one girder in the span divided by the sum of the maximum strains in all the girders in the same span for a particular truck event. For comparison, load fractions were also calculated as the maximum vertical girder deflection of a particular girder divided by the sum of the maximum vertical deflections of all the girders. The two methods of calculating load fractions described above will be referred to as "max strains" load fractions and "max deflections" load fractions.

Previous research by Bakht and Moses (1988) has shown, that in calculating the percentage of the load carried by a girder as a live load crosses a bridge, the actual percentage varies as the live load moves across the span. For simple spans under static loading, the percentage has been shown to remain essentially constant for the trucks located in the central portion of the span. To investigate this for dynamic truck data, a special data analysis routine was used to calculate the load fractions for each girder as a function of time from the raw strain data. A plot of the load fraction for

girder 5 over time is shown in Figure 5.7. As can be seen from the figure, the load fraction for the girder varies greatly except while the test truck is on the bridge (usually about .5 seconds before and after the point of peak strain) because the load fraction is calculated for electronic noise. While the truck is on the bridge the load fraction is reasonably constant.

Another data analysis routine was developed to calculate the mean of the load fraction values over the constant interval shown between points 1 and 2 shown in Figure 5.7. This averaged value was taken as a load fraction and will be referred to as "time strains" load fractions.

Performing continuous load fraction calculations for raw deflection data produced similar results. Load fractions calculated from the continuous deflection data are referred to as "time deflections" load fractions. Time strains and time deflections load fractions were calculated for all normal traffic data from which max strains and max deflections load fractions were calculated.

Since all the test data resulted from dynamic load testing, some special characteristics of the data had to be accounted for in calculating the load fractions. As heavy trucks crossed the bridge span, all the girders did not simply deflect downward in unison to resist the applied load. At the instant in time when the truck was at midspan, it was not uncommon for some of the girders to be deflecting upwards instead of downwards. These particular girders tended to show very little response to the load and primarily vibrated up and down with bottom flange strains in tension and compression between 5 and -5 microstrains. Girders that exhibited this type behavior each time a truck crossed in a particular lane were referred to as nonparticipating

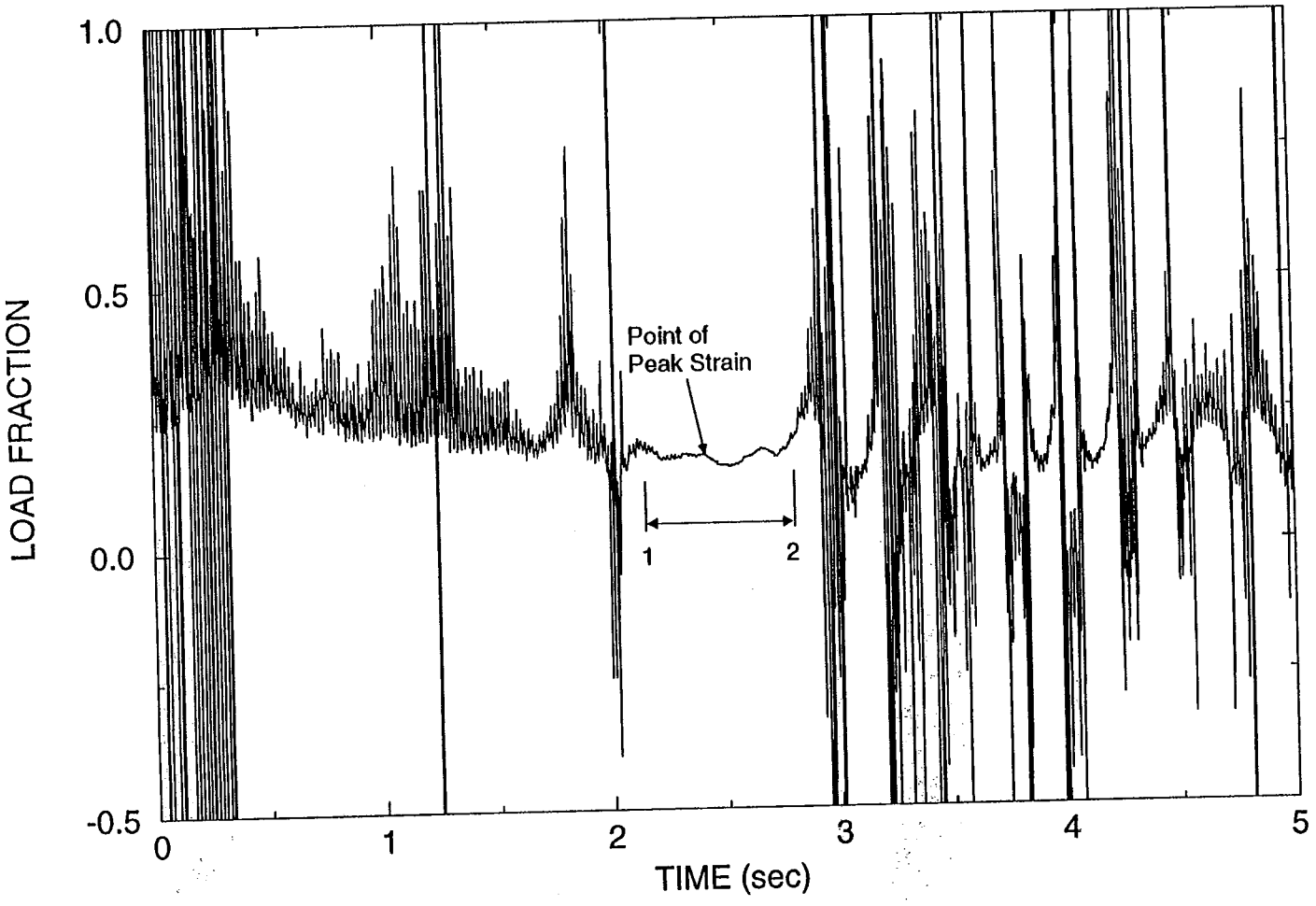

Figure 5.7. Continuous Load Fraction for Girder 5 with Calibration Truck in Lane 3

girders. The remaining girders were called the participating girders because those girders appeared to act together in resisting the applied loading. All load fractions reported here were calculated by considering only the strains, or deflections, for the participating girders. For example, load fractions for max strains were calculated as the maximum strain in a participating girder divided by the sum of the maximum strains in all the participating girders. Table 5.6 lists the participating girders used to calculate load fractions for normal traffic loading in lane 3 and 4. Lane 3 and 4 were the only traffic lanes for which a significant amount of normal traffic data was recorded both before and after the diaphragms were removed.

Table 5.6. Participating Girders for the 24.5 m Simple Span

Lane 3	Lane 4
Girder 2	Girder 4
Girder 3	Girder 5
Girder 4	Girder 6
Girder 5	Girder 7
Girder 6	Girder 8
Girder 7	Girder 9
Girder 8	

Averages and standard deviations of the load fractions calculated for each participating girder for truck traffic in lanes 3 and 4 are shown in Tables 5.7 through 5.10. As can be seen from the tables, trucks in lane 3 produced the largest load

fractions in girder 5, and trucks in lane 4 produced the largest load fractions in girder 6. These observations correspond to earlier observations from Tables 5.3 regarding which girders were the most heavily loaded. Base on the results for the most heavily loaded girders, the 4 methods for calculating load fractions basically produce the same results. The differences between methods ranges less than 0.04 which roughly corresponds to 4% of the applied single truck load. It can be observed that the load

Table 5.7. Load Fractions from Normal Traffic Data Calculated from Maximum Measured Bottom Flange Strains

Loading Dia. Status		Girder Number								
		1	2	3	4	5	6	7	8	9
Lane 3 Dia. In	Ave. of 23	-	.049	.110	.249	**.292**	.168	.086	.047	-
	Std. Dev.	-	.011	.015	.017	.022	.016	.010	.011	-
Lane 3 Dia. Out	Ave. of 32	-	.032	.098	.261	**.342**	.168	.065	.033	-
	Std. Dev.	-	.010	.023	.017	.027	.014	.010	.009	-
Lane 4 Dia. In	Ave. of 30	-	-	-	.081	.173	**.310**	.256	.141	.042
	Std. Dev.	-	-	-	.015	.021	.024	.021	.014	.013
Lane 4 Dia. Out	Ave. of 36	-	-	-	.063	.164	**.336**	.272	.129	.035
	Std. Dev.	-	-	-	.015	.018	.024	.022	.016	.018

- Nonparticipating girder

Table 5.8. Load Fractions from Normal Traffic Data Calculated from Maximum Measured Girder Deflections

Loading Dia. Status		Girder Number								
		1	2	3	4	5	6	7	8	9
Lane 3 Dia. In	Ave. of 23	-	.059	.133	.237	**.281**	.164	.087	.039	-
	Std. Dev.	-	.011	.012	.014	.015	.013	.011	.009	-
Lane 3 Dia. Out	Ave. of 32	-	.049	.122	.248	**.308**	.169	.076	.032	-
	Std. Dev.	-	.020	.012	.014	.013	.012	.010	.007	-
Lane 4 Dia. In	Ave. of 30	-	-	-	.108	.193	**.288**	.243	.126	.041
	Std. Dev.	-	-	-	.016	.027	.016	.017	.013	.010
Lane 4 Dia. Out	Ave. of 36	-	-	-	.092	.197	**.303**	.257	.121	.030
	Std. Dev.	-	-	-	.013	.014	.010	.012	.009	.012

- Nonparticipating girder

Table 5.9. Load Fractions from Normal Traffic Data Calculated Using Time Strains Method

Loading Dia. Status		Girder Number								
		1	2	3	4	5	6	7	8	9
Lane 3 Dia. In	Ave. of 23	-	.041	.114	.269	**.301**	.178	.071	.022	-
	Std. Dev.	-	.015	.016	.023	.016	.018	.012	.008	-
Lane 3 Dia. Out	Ave. of 32	-	.017	.091	.283	**.351**	.177	.054	.020	-
	Std. Dev.	-	.013	.014	.020	.026	.015	.015	.010	-
Lane 4 Dia. In	Ave. of 30	-	-	-	.072	.187	**.311**	.257	.140	.029
	Std. Dev.	-	-	-	.017	.022	.015	.016	.017	.013
Lane 4 Dia. Out	Ave. of 36	-	-	-	.048	.170	**.344**	.279	.137	.166
	Std. Dev.	-	-	-	.014	.019	.015	.018	.014	.016

- Nonparticipating girder

Table 5.10. Load Fractions from Normal Traffic Data Calculated Using Time Deflections Method

Loading Dia. Status		Girder Number								
		1	2	3	4	5	6	7	8	9
Lane 3 Dia. In	Ave. of 23	-	.052	.130	.251	**.295**	.164	.077	.029	-
	Std. Dev.	-	.012	.014	.017	.016	.014	.011	.011	-
Lane 3 Dia. Out	Ave. of 32	-	.037	.116	.260	**.325**	.165	.067	.023	-
	Std. Dev.	-	.012	.013	.017	.018	.017	.014	.007	-
Lane 4 Dia. In	Ave. of 30	-	-	-	.100	.190	**.300**	.252	.124	.031
	Std. Dev.	-	-	-	.016	.021	.013	.016	.013	.013
Lane 4 Dia. Out	Ave. of 36	-	-	-	.081	.194	**.311**	.267	.120	.023
	Std. Dev.	-	-	-	.012	.016	.009	.014	.010	.010

- Nonparticipating girder

fractions calculated for the most heavily loaded girder from the deflection data are somewhat lower than the load fractions calculated for the same girder using the strain data. The load fractions calculated for the girders farther away from the loaded lane also are in good agreement for the four methods with only a few cases having differences greater than 0.04. The load fractions for girders far away from the loaded

lane also tend to somewhat higher when deflection data is used rather than strain data.

The load fractions for the most heavily loaded girders (shown in bold type in the tables) increased as a result of removing the diaphragms. The percent increases in load fractions resulting from removing the diaphragms ranged from 8 to 17% when bottom flange strain data was used and ranged from 4 to 10% based on the deflection data. These values compare well with the 6 to 15% increases in maximum bottom flange stress observed in the calibration tests.

Plots were developed to determine if truck size or type had a significant effect on the fractions. Load fractions were plotted against a truck size parameter. The truck size parameter is a nondimensional strain ratio (ϵ/ϵ_{TT}) defined as the maximum strain recorded in the designated girder divided by the maximum strain recorded in the designated girder for a calibration truck loading. The strain ratio is a measure of the weight of the truck in normal traffic relative to the calibration truck weight and scales the results relative to the calibration truck results. Plots for the most heavily loaded girders for trucks in lane 3 and lane 4 are shown in Figures 5.8 through 5.15. Plots are shown for load fractions calculated from each of the 4 described methods. The figures point out that the load fractions were not significantly affected by truck size with or without diaphragms since the data essentially fall along a horizontal line. This was observed in additional plots of load fractions for each of the girders for trucks in lanes 3 and 4.

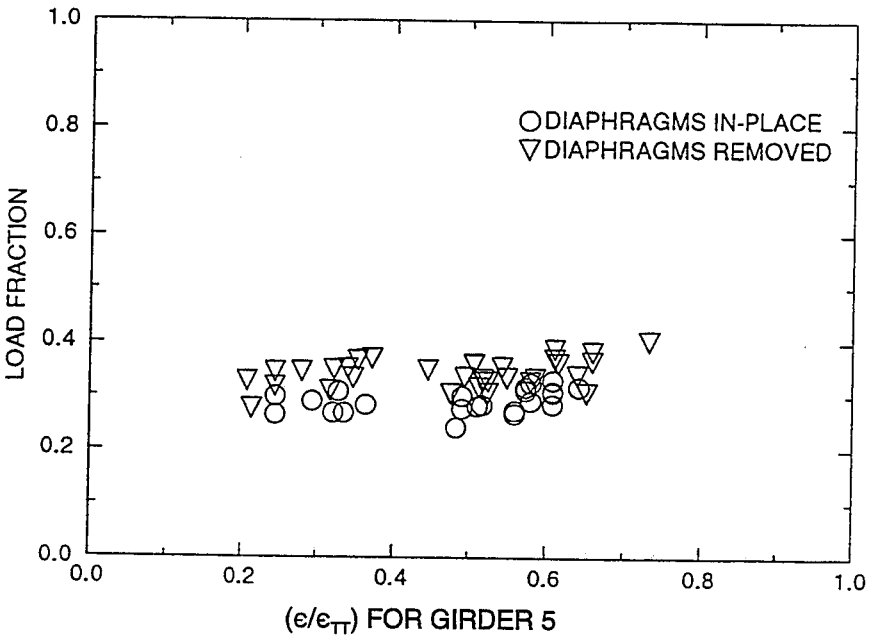

Figure 5.8. Max Strains Load Fractions for Girder 5 with Truck Traffic in Lane 3

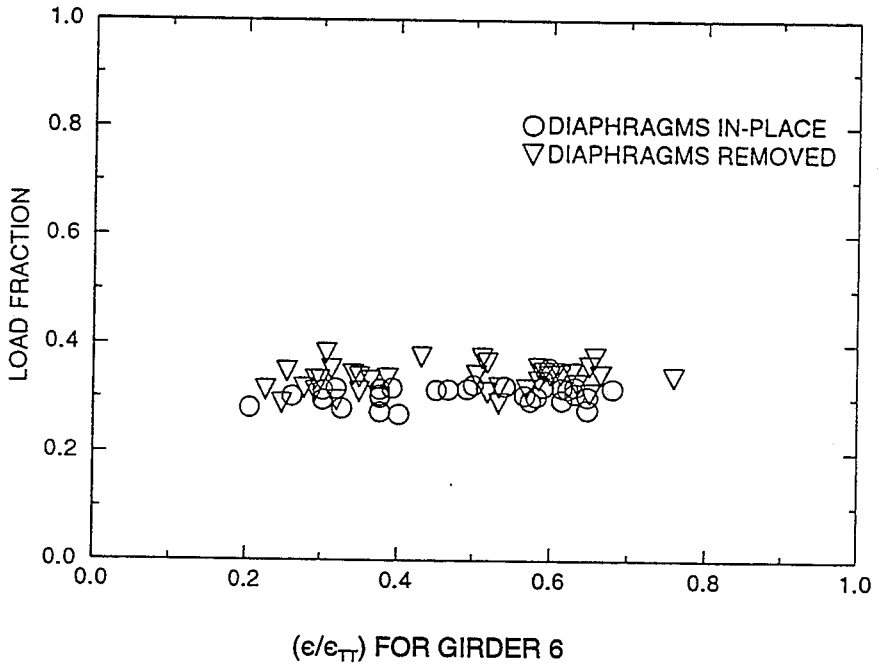

Figure 5.9. Max Strains Load Fractions for Girder 6 with Truck Traffic in Lane 4

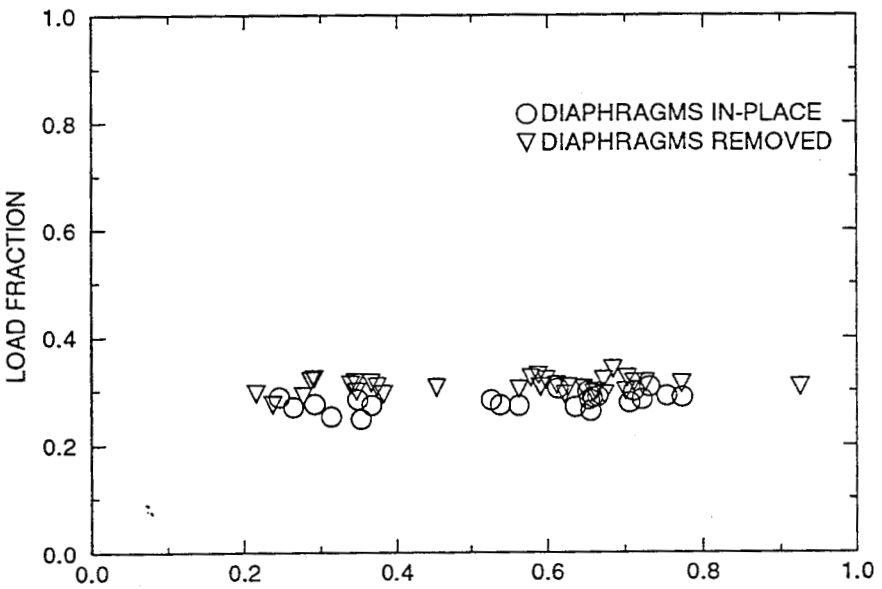

Figure 5.10. Max Deflections Load Fractions for Girder 5 with Truck Traffic in Lane 3

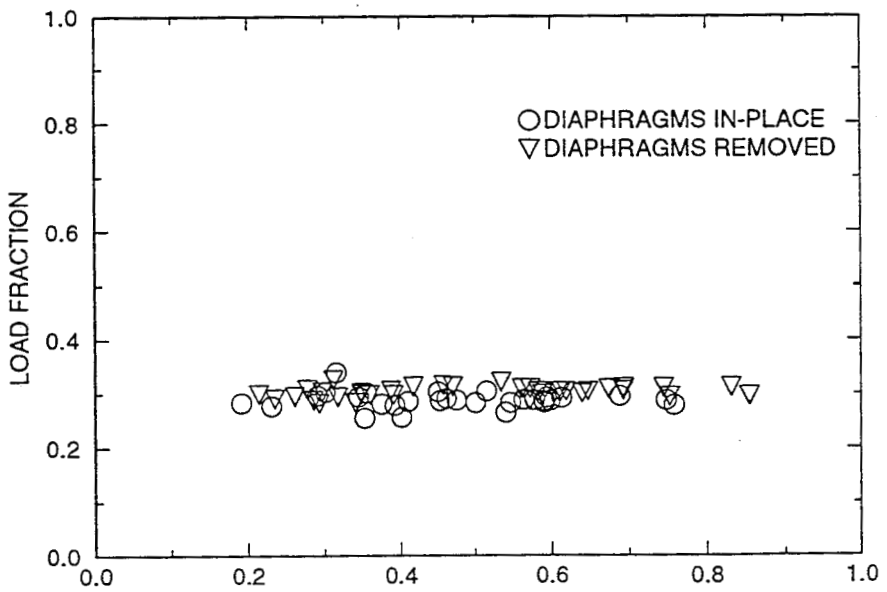

Figure 5.11. Max Deflections Load Fractions for

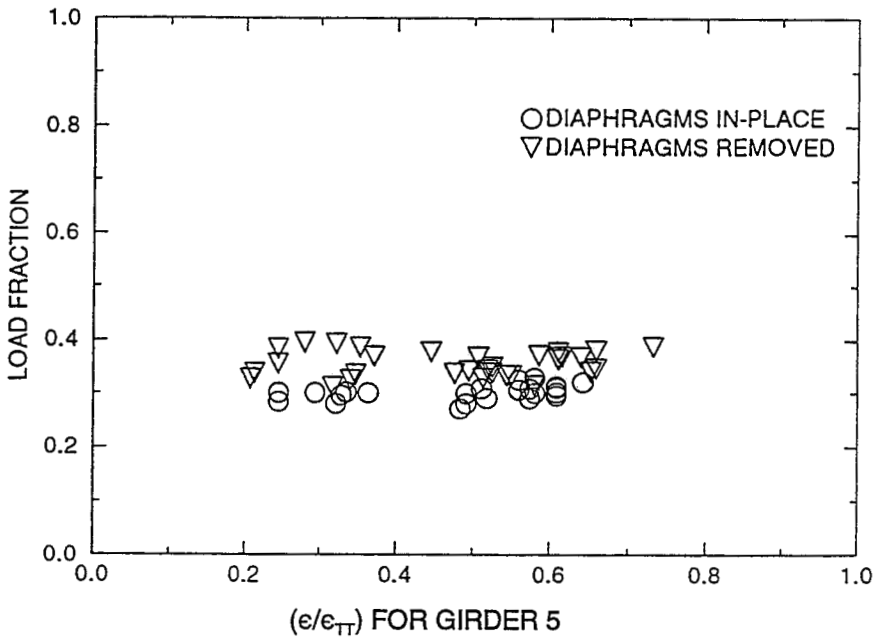

Figure 5.12. Time Strains Load Fractions for Girder 5 with Truck Traffic in Lane 3

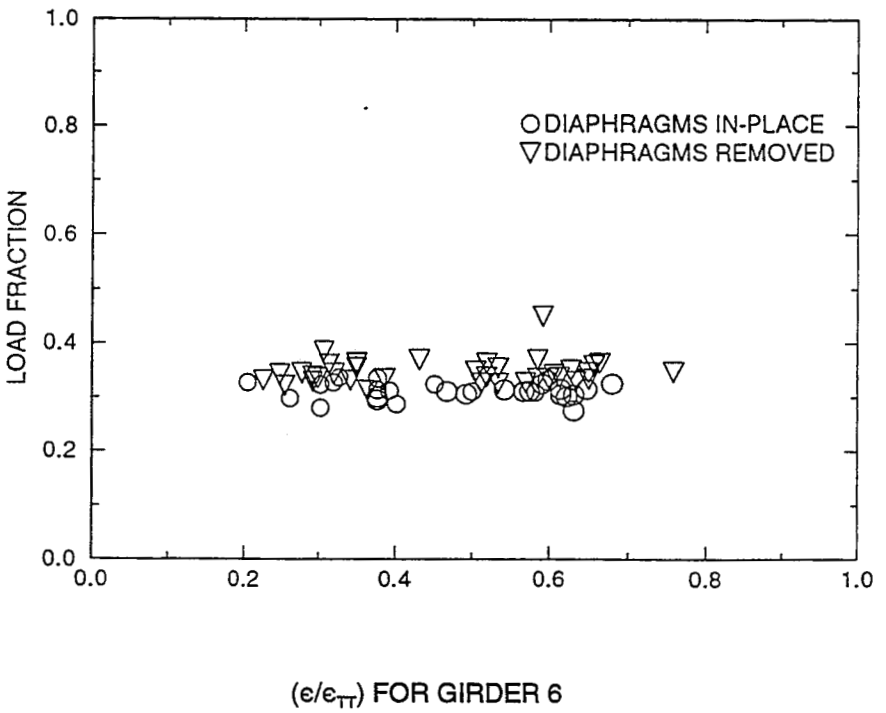

Figure 5.13. Time Strains Load Fractions for Girder 6 with Truck Traffic in Lane 4

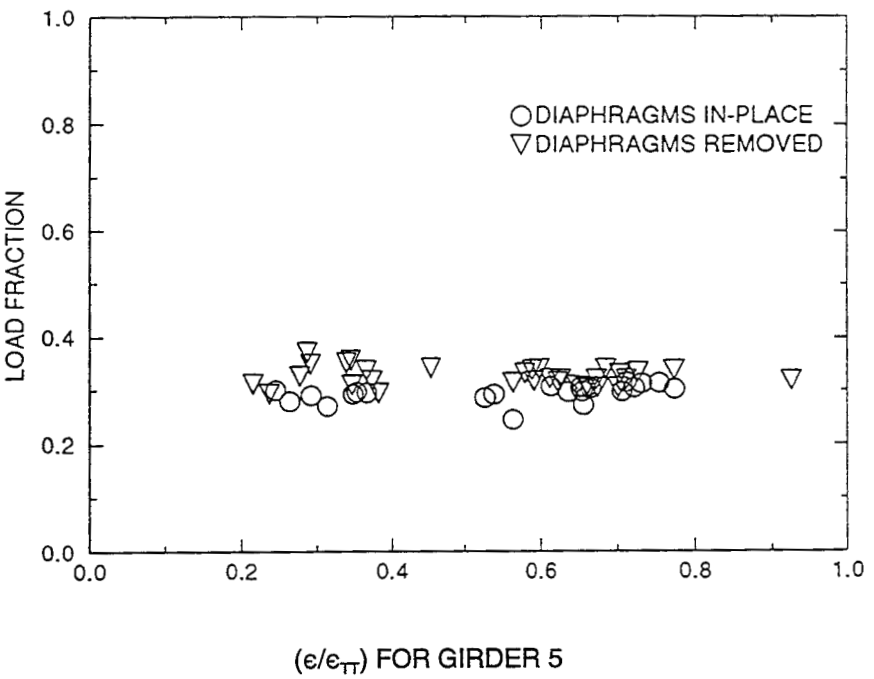

Figure 5.14. Time Deflections Load Fractions for Girder 5 with Truck Traffic in Lane 3

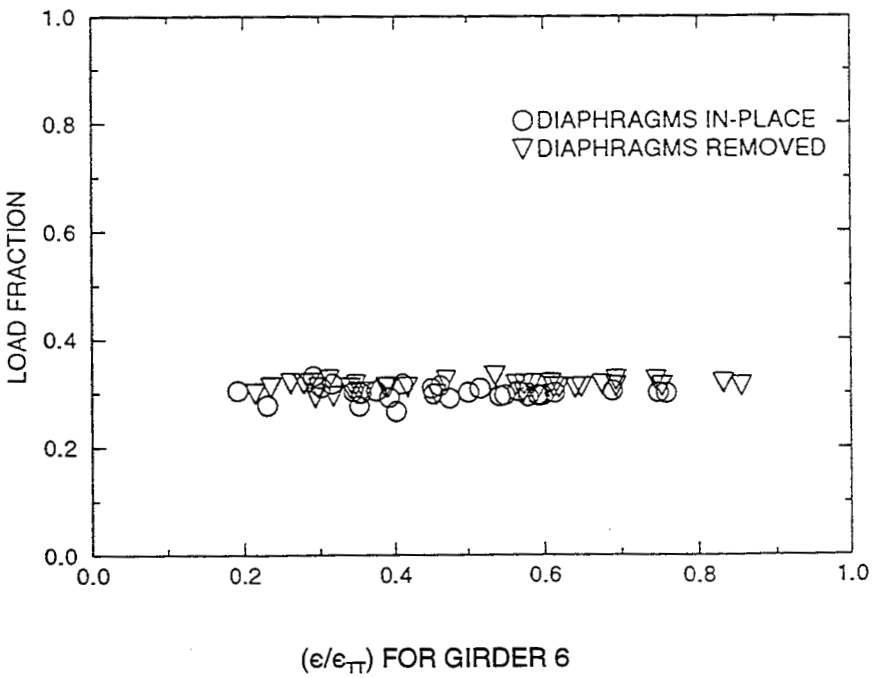

Figure 5.15. Time Deflections Load Fractions for Girder 6 with Truck Traffic in Lane 4

AASHTO WHEEL LOAD DISTRIBUTION FACTORS AND CALCULATED WHEEL LOAD DISTRIBUTION FACTORS

The simplified analysis method presented by AASHTO (1992) requires that the moment determined from one wheel line of truck loading be multiplied by an Impact and Wheel Load Distribution factor to determine the bending moment in a girder. The impact factor accounts for dynamic loading and the wheel load distribution factor accounts for the transverse distribution of load for a fully loaded bridge.

According to AASHTO, the wheel load distribution factors for the simple span bridge reported here are calculated as S/5.5 for interior girders and S/(4.0 + 0.25S) for exterior girders, where S is the girder spacing in feet. The AASHTO wheel load distribution factors for the individual girders of the 24.5 m simple span bridge are shown in Table 5.11.

Table 5.11. AASHTO Wheel Load Distribution Factors and Wheel Load Distribution Factors Calculated Using Superposition of Measured Maximum Bottom Flange Strains for Calibration Truck Loading

Loading/ Dia./Status	Girder Number								
	1	2	3	4	5	6	7	8	9
AASHTO	1.33	1.45	1.45	1.45	1.45	1.45	1.45	1.45	1.33
1,2,3,4,5/In	0.86	1.15	**1.31**	**1.32**	1.27	1.21	1.10	1.10	0.70
1,2,3,4,5/Out	0.81	1.26	**1.32**	1.24	1.24	1.27	1.21	1.03	0.62
1,2+3,4+5/In	0.88	1.19	**1.34**	1.27	1.18	1.27	1.18	0.99	0.72
1,2+3,4+5/Out	0.76	1.29	**1.36**	1.28	1.20	1.34	1.21	0.96	0.60

To calculate distribution factors from test truck loading that are comparable to AASHTO's, superposition of the test truck loads in all five traffic lanes must be used. A distribution factor for full loading is obtained by adding load fractions for trucks in each traffic lane. This sum would represent the percentage of a single truck resisted by a particular girder. A wheel load distribution factor, comparable to AASHTO, is then obtained by multiplying the sum by 2.

Table 5.11 displays wheel load distribution factors calculated by superposition of the calibration truck test results for diaphragms in-place and diaphragms removed. One set of distribution factors was obtained from using single truck loadings in each of the five traffic lanes, and the other was obtained from a single truck loading in lane 1 and side-by-side truck loadings in lanes 2 and 3, and lanes 4 and 5. The largest calculated wheel load distribution factors are shown in bold type in the table. Girder 3 is observed to have the largest calculated wheel load distribution factors from calibration truck loading. The tabulated results indicate that there is no significant difference in calculating the distribution factors from either of the two superpositions of lane combinations. Also, the distribution factors for the most heavily loaded girder are seen to be only modestly affected by the removal of the diaphragms.

Superpositioning of the calibration truck loads provides a useful means to calculate wheel load distribution factors but some error results from using superposition of the dynamic test results as discussed earlier in this chapter. The AASHTO wheel load distribution factors presumably account for the worst possible transverse positioning of trucks for each girder. During the calibration tests, the test truck drivers were instructed to drive in the center of traffic lanes as best possible.

Within these limitations, the wheel load distribution factors obtained from superposition of the test results are concluded to be somewhat less than the AASHTO wheel load distribution factors for cases with and without diaphragms. Hence, the conservatism often considered to be a part of the AASHTO wheel load distribution factors is not eliminated by removing the diaphragms.

CONCLUSIONS

Field tests were performed to evaluate the effects of removing channel diaphragms from a simple span multi-girder steel bridge. Girder stresses and deflection were measured at midspan for loading by trucks of known weight and by trucks in the normal daily traffic stream.

Results from the tests with trucks of known weight and axle configuration indicated that removing the interior diaphragms resulted in a 6 to 15% increase in maximum bottom flange stresses, and a 6 to 14% increase in maximum girder deflections for the most heavily loaded girder. Results from the normal traffic data indicated that the most heavily loaded girder carried up to 17% more of a single truck load after all interior diaphragms were removed. The normal traffic results also showed that load fractions calculated using strain or deflection data produce similar results and that there is no significant difference in calculating a load fraction using maximum recorded values or by using continuous records of strain or deflection.

Girder stresses and wheel load distribution factors were calculated according to AASHTO (1992) specifications and were compared to stresses and wheel load distribution factors calculated from calibration tests. The results showed that the conservatism of the AASHTO methods is not eliminated by removing the diaphragms.

CHAPTER SIX

EFFECTS OF REMOVING DIAPHRAGMS FROM A 76 METER 3-SPAN CONTINUOUS BRIDGE

INTRODUCTION

A 3-span continuous bridge on I-20/59 between 18th and 19th Streets South in downtown Birmingham was chosen for a second field evaluation of the effects diaphragms have on the lateral distribution of traffic loads. A total of six series of tests were performed on this bridge to identify the role diaphragms play in distributing truck loads. Series of tests were performed both with trucks of known weight and with trucks in normal traffic for cases with the original diaphragms in-place, with no diaphragms, and with the minimum number of rows of diaphragms required for full lateral bracing of the girders.

BRIDGE DESCRIPTION

The bridge carries four lanes of westbound traffic of the I-20/59 interchange in the central business district (CBD) of downtown Birmingham, Alabama. The superstructure consists of eight steel wide flange girders supporting a 165 mm thick reinforced concrete deck. Three different wide flange sections, W920 X 289, W920 X 342 and W920 X 365, were spliced together as shown in Figure 6.1 to make up each girder. Figure 6.2 shows a cross-sectional view of the bridge and a numbering system for the girders and the traffic lanes. Shear studs were not provided on any of the girders. Due to this, the girders were not considered to be composite with the concrete deck.

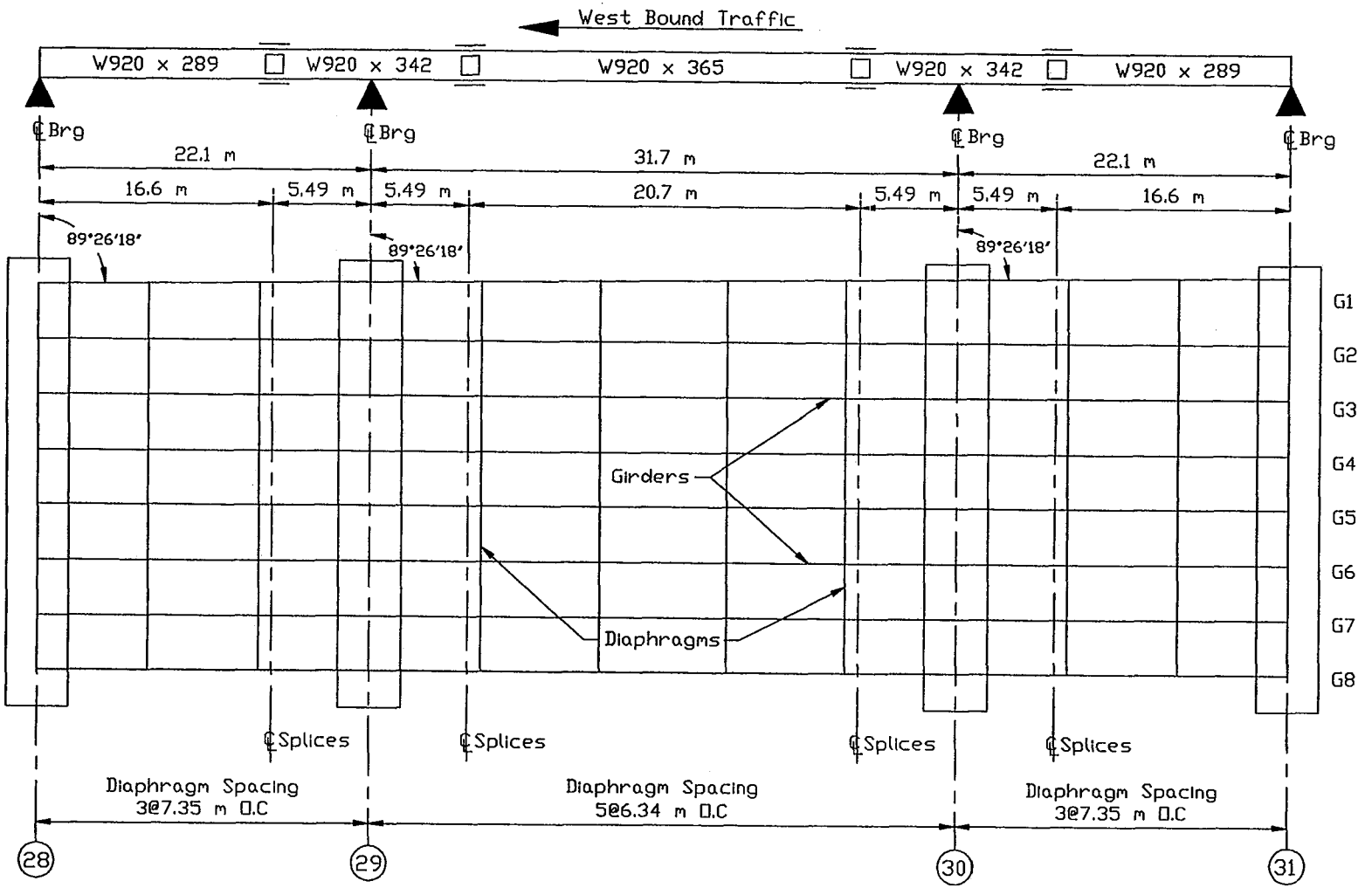

Figure 6.1. Plan View and Girder Details for the 76 m 3-Span Continuous Bridge with Original Diaphragms In-Place

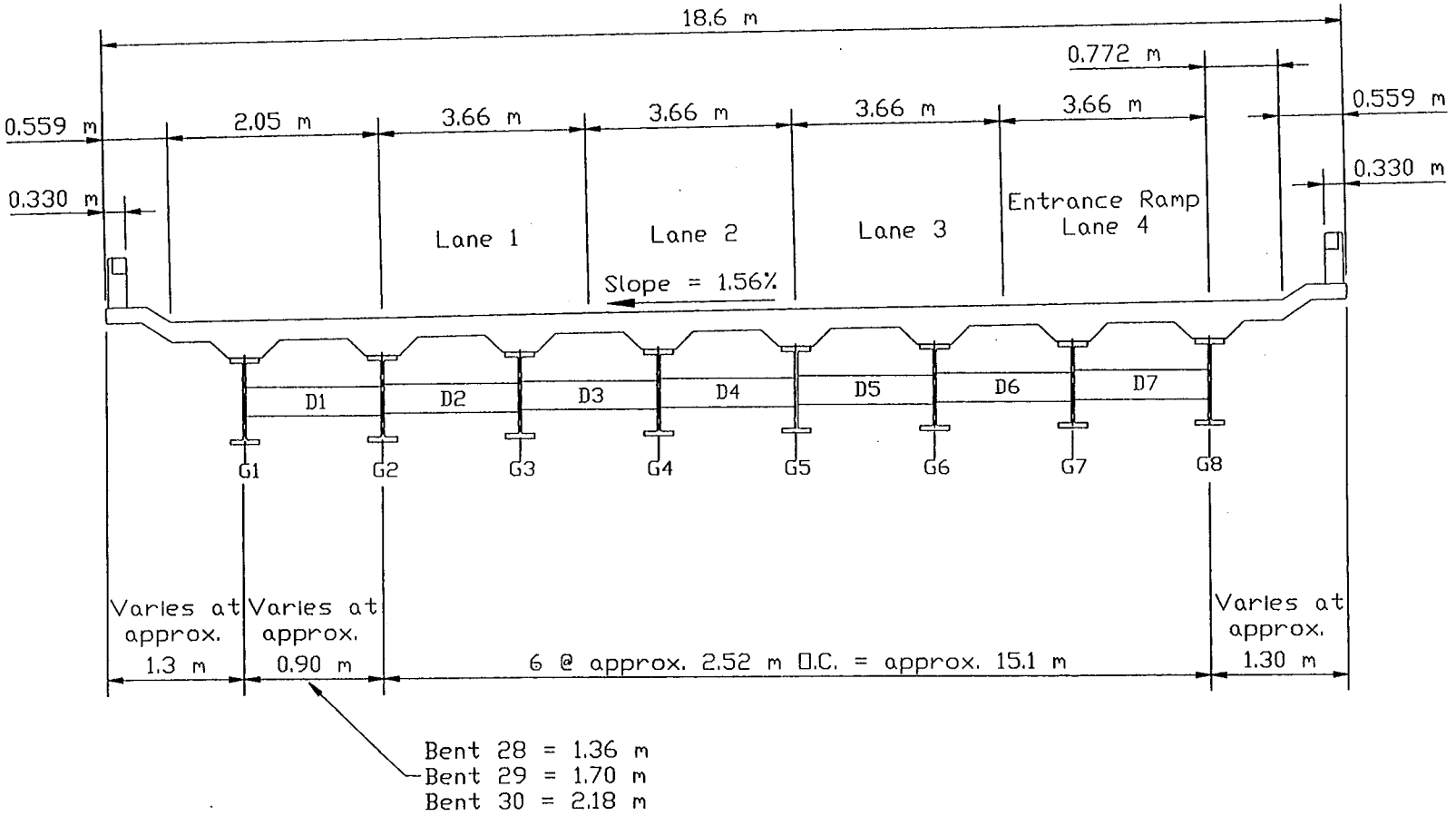

Figure 6.2. Cross Section of the 76 m 3 Span Continuous Bridge (Looking into Traffic)

The 3 spans which are referred to as span 28, span 29, and span 30 on ALDOT drawings were 22, 32 and 22 m in length respectively. The exterior girder on the north side of the bridge is slightly skewed as shown in Figure 6.1. The other seven girders are parallel and are spaced 2.5 m transversely.

At the beginning of the field tests, the 22 m spans (span 28 and 30) had 2 lines of interior diaphragms oriented perpendicular to the girders and spaced at 7.35 m along the roadway. The 32 m span (span 29) had 4 lines of interior diaphragms spaced at 6.34 m and oriented perpendicular to the girders. All diaphragms were rolled steel sections MC460 X 63.5. Figure 6.1 shows a plan view of the 3-span bridge system before field tests began. Originally the diaphragm-girder connection consisted of steel plates welded to the girder webs and to each end of the diaphragms. As a result of fatigue problems at certain diaphragm-girder connections, approximately 50% of the diaphragm girder connections had been replaced by a bolted angle connection.

Structural evaluations reported in Chapter Four indicate that some interior diaphragms are needed to maintain the original inventory rating capacity of the bridge. After tests were conducted with the original diaphragms in-place and with all interior diaphragms removed, a total of four lines of interior diaphragms were added back to the bridge system. Two lines were added to the 32 m span and 1 line to each of the 22 m spans. The 4 lines of diaphragms were placed at 6.86 m from each of the interior supports as shown by the plan view in Figure 6.3.

All the new diaphragm-girder connections were made using type G angles (Figure 2.2) bolted to the girder webs and to each end of the channel diaphragms. Two lines of diaphragms were connected to the girder webs with the angle bolted to

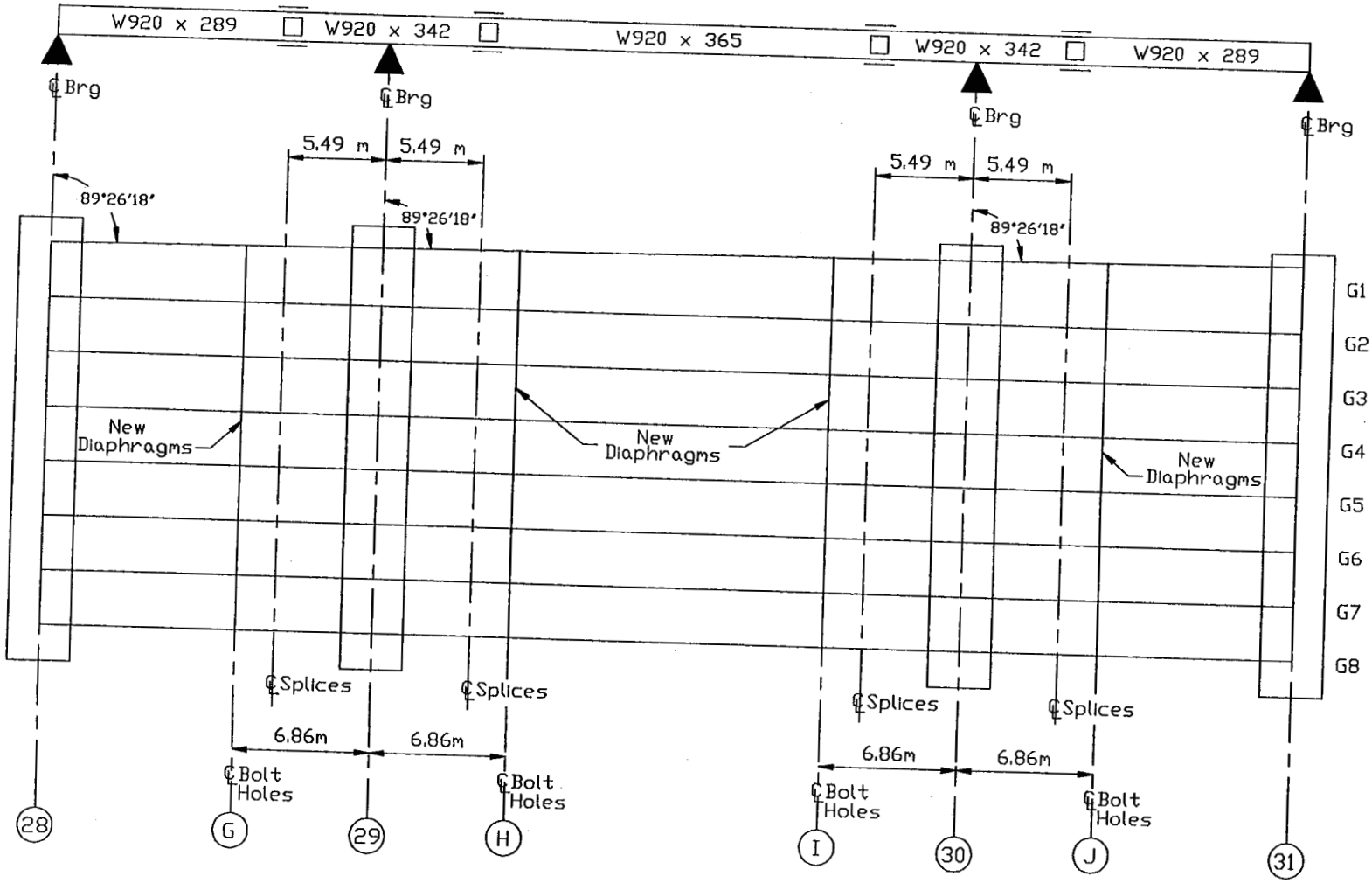

Figure 6.3. Plan View of the 76 m 3 Span-Continuous Bridge with New Diaphragms In-Place

to the girder webs with a distance of 178 mm between the top of the angle and the bottom of the top flange (178 mm web gap). At the two other lines of diaphragms the angle was connected to the girder web with a distance of 89 mm between the top of the angle and the bottom of the top flange (89 mm web gap). Figure 6.3, showing the plan view of the bridge with the new diaphragms, also indicates the locations of the two web gap sizes. The lines of diaphragms labeled "I" and "J" have 89 mm web gaps, and the lines of diaphragms labeled "G" and "H" have 178 mm web gaps. The new diaphragms were made of the same size rolled steel channel as the original diaphragms.

INSTRUMENTATION AND DATA ACQUISITION

Instrumentation included electrical resistance strain gages for measuring surface strains and deflectometers for measuring the vertical deflection of the girders. The procedures for mounting strain gages and deflectometers and for collection of the data as described in Chapter Five were also used for the 3-span bridge discussed here.

Strain gages were mounted on the bottom flange of all the girders at midspan of spans 28 and 29. Top flange gages were mounted as shown in Figure 6.4 on girders 5, 6, 7 and 8 at midspan in spans 28 and 29. Strain gages were also mounted 457 mm from the support on all the girders in span 28 as shown in Figure 6.4. Deflectometers were placed at midspan of span 29 to measure the vertical deflection of the girders.

Top and bottom flange gages were mounted on the diaphragms near each end of each diaphragm in the line of diaphragms at the west side of span 29. The purpose for these gages was to measure strains from which the shear, moment and thrust at

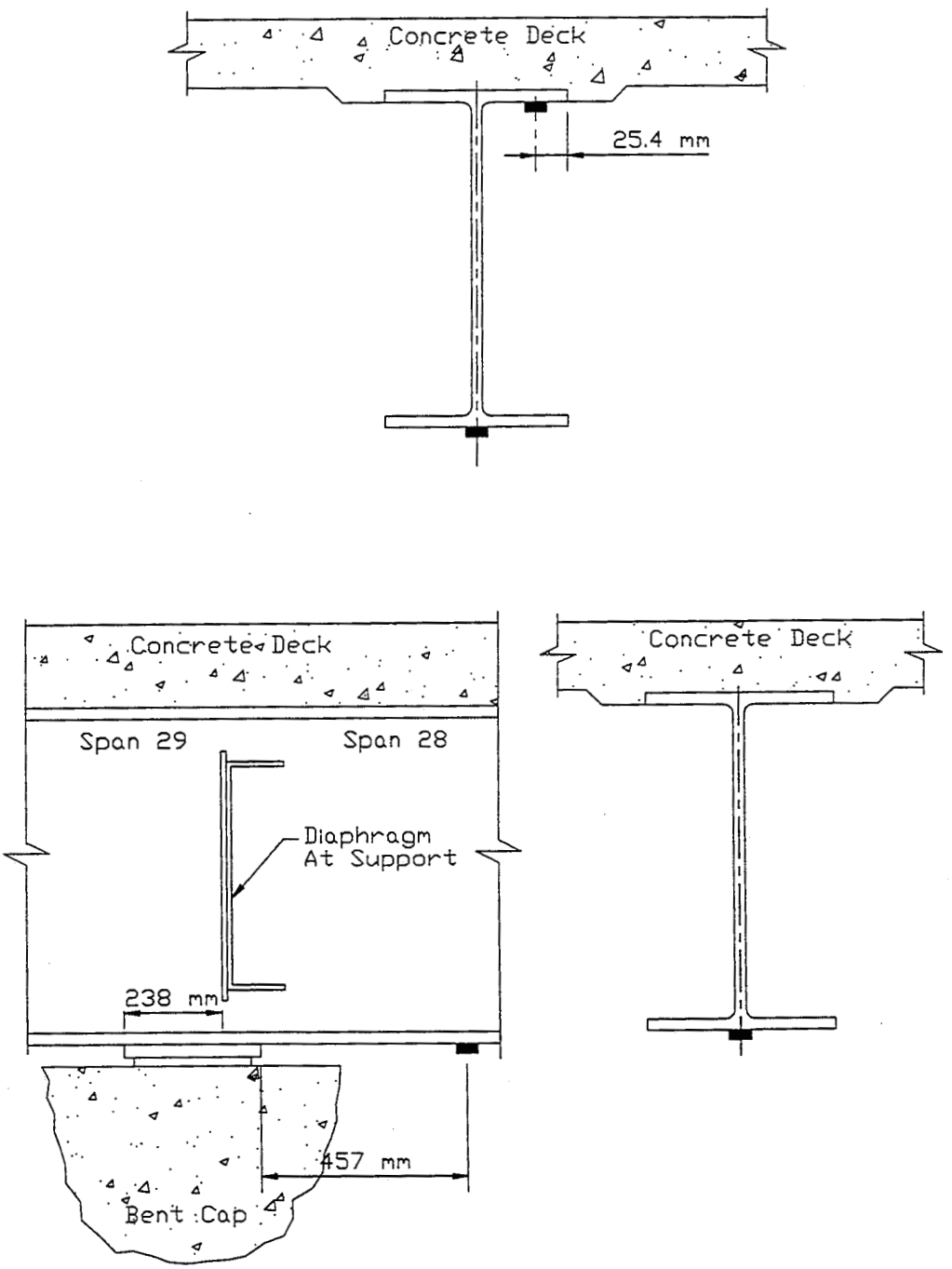

Figure 6.4. Strain Gage Locations on Girders

the ends of the diaphragms could be calculated. However, the measured strains in the diaphragms were so small that they were unreliable for that intended purpose.

DESCRIPTION OF FIELD TESTS

Six series of tests were conducted on the bridge to investigate the lateral distribution of live loads. Field measurements were taken for loadings by the calibration trucks with the original diaphragms in-place, with all interior diaphragms removed, and with the new diaphragms in-place. Field measurements were also taken for all the above mentioned cases for loading by trucks in the normal traffic stream. Due to the high volume of traffic on the interstates, traffic was not stopped for any tests and all data was taken for trucks travelling at normal traffic speeds.

The calibration tests were performed using the two identical load testing trucks described in Chapter Two. The calibration tests included 2 single truck crossings in each of the 4 traffic lanes and side-by-side truck crossings in lanes 1 and 2, and 2 and 3.

Data for trucks in normal traffic were recorded to measure girder strains and deflections from loadings with trucks of different weights and axle configurations. The goal was to collect a minimum of 25 truck crossings in each traffic lane. Due to the normal traffic patterns, it was impossible to record a sufficient number of truck crossings in certain lanes in the limited time available. Due to this, the results presented from these tests are from truck crossings in lanes 1 and 2 only.

CALIBRATION TESTS RESULTS

Measurements of the following five parameters were made for evaluating the effects diaphragms have on the distribution of truck loads: (1) bottom flange girder

stresses at midspan of span 28, (2) bottom flange girder stresses at midspan of span 29, (3) bottom flange girder stresses at the Bent 28 support due to the test truck in span 29, (4) bottom flange girder stresses at the Bent 29 support due to the test truck in span 28, and (5) vertical girder deflections at midspan of span 29. The maximum recorded bottom flange stresses for all three diaphragm scenarios are listed in Tables 6.1 through 6.4. In these tables the diaphragm status "In" represents all original diaphragms in-place, "Out" represents all interior diaphragms removed, and "Min" represents having one line of diaphragms on each side of each interior support. The single lane loading values are the average of 2 tests, and the multiple lane loadings are from one test. The values in bold indicate the most heavily loaded girder for each test.

The measured bottom flange stresses for the most heavily loaded girder at midspan of span 28 (Table 6.1) exhibited a slight increase of 0 to 10% as a result of removing the diaphragms. The largest increase was observed for a truck in lane 1. As shown in Table 6.1, removing all the diaphragms resulted in a decrease in measured bottom flange stress for a test truck in lane 3. The measured stresses for single truck crossings with minimum needed diaphragms in the span generally show no significant difference from those when all diaphragms were removed. The stresses from side-by-side crossings indicate very little difference between cases with the original diaphragms in-place and with minimum required number of diaphragms.

A smaller increase in measured bottom flange stress in the most heavily loaded girder as result of diaphragm removal is noted in span 29 as shown in Table 6.2. The largest increase resulting from complete diaphragm removal was 6% at girder 4 for a

Table 6.1. Measured Maximum Bottom Flange Stresses (MPa) at Midspan of Span 28 (22 m) from Calibration Truck Loading

Loading/ Dia. Status	Girder Number							
	1	2	3	4	5	6	7	8
Lane1/In	13	26	**29**	13	5	2	2	3
Lane1/Out	10	28	**32**	14	5	2	1	2
Lane1/Min	9	27	**33**	15	4	2	2	2
Lane2/In	1	5	17	**34**	24	8	3	2
Lane2/Out	2	5	18	**35**	25	8	2	2
Lane2/Min	1	6	18	**35**	23	7	2	2
Lane3/In	1	1	4	12	**32**	30	13	3
Lane3/Out	2	2	2	10	**30**	30	14	2
Lane3/Min	1	2	3	11	**31**	30	14	1
Lane4/In	2	1	1	2	6	16	**33**	24
Lane4/Out	2	1	1	2	4	16	**34**	28
Lane4/Min	2	1	1	2	4	16	**33**	25
Lanes1&2/In	13	34	**46**	46	28	10	3	2
Lanes1&2/Out	10	34	**49**	48	29	9	2	1
Lanes1&2/Min	11	33	**46**	47	31	11	2	2
Lanes2&3/In	2	7	23	43	**49**	37	16	2
Lanes2&3/Out	1	7	25	46	**53**	36	16	2
Lanes2&3/Min	1	6	22	43	**48**	39	19	2

Table 6.2. Measured Maximum Bottom Flange Stresses (MPa) at Midspan of Span 29 (32 m) from Calibration Truck Loading

Loading/ Dia. Status	Girder Number							
	1	2	3	4	5	6	7	8
Lane1/In	15	31	**31**	13	6	3	1	2
Lane1/Out	12	30	**30**	12	4	2	1	1
Lane1/Min	10	29	**31**	13	5	2	2	2
Lane2/In	2	7	23	**34**	21	8	2	2
Lane2/Out	1	7	23	**36**	23	8	2	1
Lane2/Min	1	7	23	**37**	22	7	2	1
Lane3/In	1	2	7	15	**34**	27	10	2
Lane3/Out	1	1	4	13	**33**	28	10	1
Lane3/Min	1	2	5	13	**34**	29	11	1
Lane4/In	1	1	1	3	8	18	**29**	18
Lane4/Out	2	1	1	2	6	17	**31**	20
Lane4/Min	2	1	1	2	6	17	**29**	20
Lanes1&2/In	13	35	**47**	44	26	9	2	1
Lanes1&2/Out	10	34	**49**	46	27	10	2	1
Lanes1&2/Min	10	34	**48**	46	29	10	3	1
Lanes2&3/In	2	8	29	46	**50**	34	12	1
Lanes2&3/Out	1	9	32	48	**51**	33	11	1
Lanes2&3/Min	1	7	28	46	**50**	38	14	2

truck in lane 2. For two of the four traffic lanes (lane 1 and lane 3) decreases in maximum measured bottom flange stresses in the most heavily loaded girder were observed for the single calibration truck loadings. Overall, there was very little

difference between stresses measured for the cases of having the minimum needed diaphragms, having the original diaphragms, or not having diaphragms.

Removing all interior diaphragms resulted in an increase between 0 and 15% of measured bottom flange stresses in the most heavily loaded girder at the instrumented support (Bent 29) for the calibration truck in span 28. A 0 to 13% increase was observed for the test truck being in span 29. The measured stresses were generally the same for no diaphragms and with the minimum needed diaphragms.

As illustrated by Tables 6.3 and 6.4 the largest bottom flange stresses at the instrumented support were recorded in the most heavily loaded girder when the test truck was in span 28. These results do not correspond with expected results based on a static analysis of the bridge as a continuous beam. Based on a classical static analysis, a truck in the 32 m center span (span 29) should produce a larger strain at the support than the same load on the 22 m end span (span 28). This difference between the measured and expected behavior is believed to result primarily from friction at the supports.

An illustration of how friction affects the theoretical beam moments is shown in Figure 6.5. When either of the two spans are subjected to loading, the girder has an inclination to deflect as shown in the figure. For a loading on span 29, a frictional force acting toward the center of span 29 is developed at Bents 29 and 30 to resist the rotation of the girder. A loading on span 28 produces a frictional force at Bents 29 and 28 acting toward the center of span 28. Since the frictional force is below the neutral axis of the beam, this force produces a moment in the girder, and the frictional force can be replaced by a statically equivalent force-couple system as shown in the figures.

Table 6.3. Measured Maximum Bottom Flange Stresses (MPa) at the Interior Support (Bent 29) from Calibration Truck Loading in Span 28 (22 m)

Loading/ Dia. Status	Girder Number							
	1	2	3	4	5	6	7	8
Lane1/In	5	15	**20**	8	2	2	2	2
Lane1/Out	1	15	**21**	7	1	1	1	1
Lane1/Min	2	15	**23**	8	1	1	1	1
Lane2/In	1	1	9	**23**	14	2	1	1
Lane2/Out	1	1	9	**25**	16	2	1	2
Lane2/Min	2	1	9	**25**	15	1	1	2
Lane3/In	2	1	1	4	**22**	19	6	1
Lane3/Out	1	1	2	3	**22**	19	5	1
Lane3/Min	1	1	2	3	**21**	23	5	2
Lane4/In	1	1	1	1	2	10	**20**	8
Lane4/Out	1	1	1	1	1	9	**23**	9
Lane4/Min	2	1	1	1	1	8	**22**	8
Lanes1&2/In	2	15	31	**30**	15	1	1	1
Lanes1&2/Out	1	14	31	**32**	15	2	2	1
Lanes1&2/Min	1	15	29	**30**	17	1	1	2
Lanes2&3/In	2	1	10	27	**33**	19	5	1
Lanes2&3/Out	2	1	11	28	**36**	20	4	2
Lanes2&3/Min	2	1	9	25	**31**	22	7	2

Table 6.4. Measured Maximum Bottom Flange Stresses (MPa) at the Interior Support (Bent 29) from Calibration Truck Loading in Span 29 (32 m)

Loading/ Dia. Status	Girder Number							
	1	2	3	4	5	6	7	8
Lane1/In	10	15	**15**	9	4	2	1	1
Lane1/Out	9	15	**15**	7	3	1	1	1
Lane1/Min	7	14	**16**	8	3	1	1	1
Lane2/In	1	6	13	**15**	11	6	2	1
Lane2/Out	1	6	13	**17**	12	5	2	1
Lane2/Min	1	5	13	**17**	12	5	2	1
Lane3/In	1	2	4	9	14	**14**	8	2
Lane3/Out	1	1	3	9	15	**15**	8	1
Lane3/Min	1	1	3	9	14	**16**	8	1
Lane4/In	1	1	1	2	5	10	**16**	10
Lane4/Out	1	1	1	1	4	10	**18**	12
Lane4/Min	1	1	1	1	4	9	**18**	12
Lanes1&2/In	10	20	**26**	21	14	7	3	1
Lanes1&2/Out	8	19	**28**	21	13	6	2	1
Lanes1&2/Min	8	18	**26**	22	15	8	3	2
Lanes2&3/In	1	7	16	22	**23**	18	10	2
Lanes2&3/Out	1	8	18	23	**25**	18	9	1
Lanes2&3/Min	1	6	16	22	**24**	19	11	2

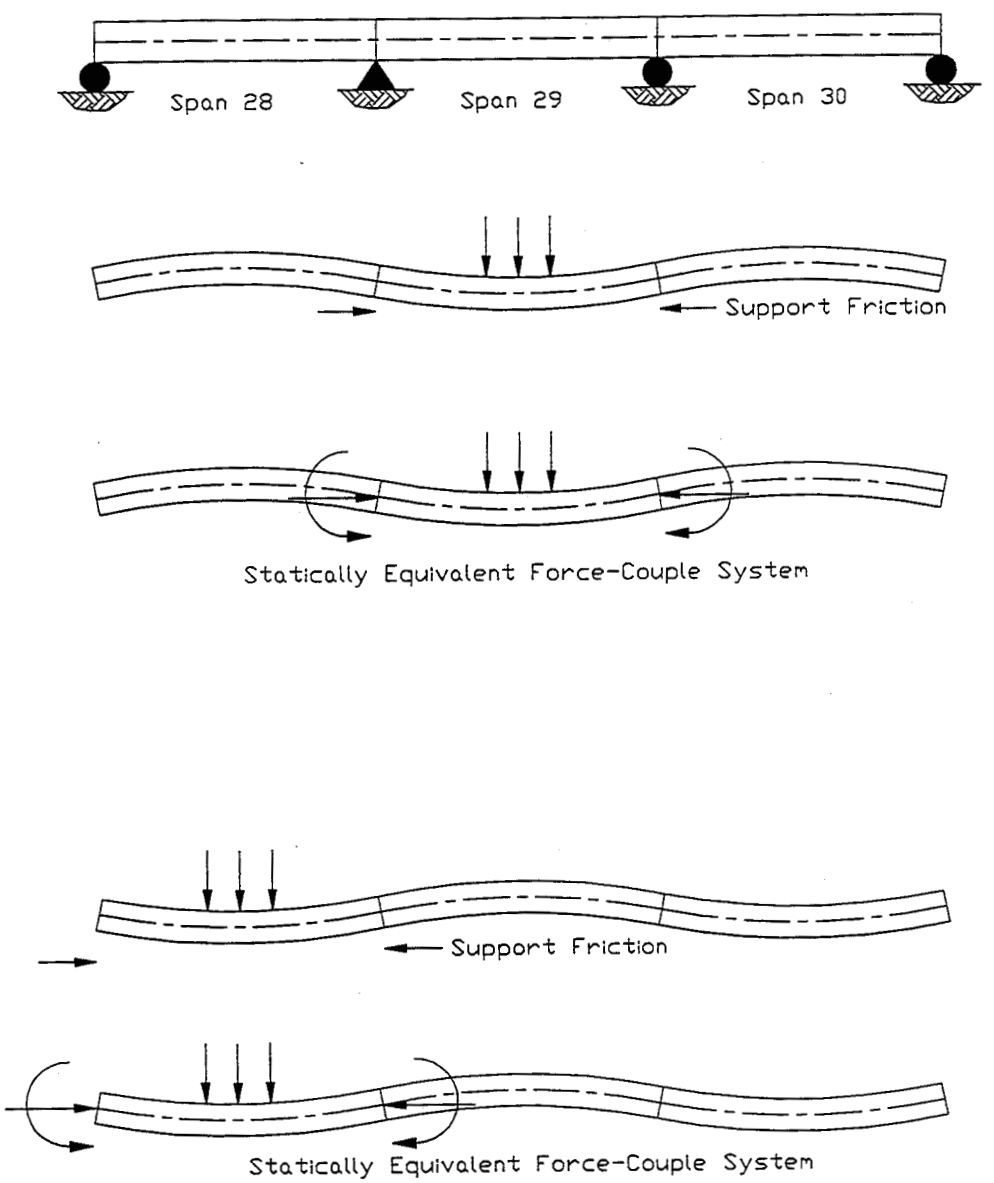

Figure 6.5. Illustration of Support Friction Effects on Theoretical Beam Moments

When a truck is on span 29, the additional moment created by friction at the support reduces the moment at the end of span 28 (strain gage positions, Figure 6.4). Conversely, when a truck is on span 28, the additional moment created by friction at the support causes the support to behave more like a fixed support which increases the moment at the end of span 28. This behavior is concluded to be the reason the measured stresses for a truck on span 28 were larger than measured stresses for a truck on span 29.

The overall behavior span 29 at midspan of with the original diaphragms, without diaphragms, and with minimum needed diaphragms can be seen in the plots of midspan girder deflection shown in Figures 6.6 through 6.11 and listed in Table 6.5. Figures 6.6 through 6.9 provide plots of average maximum midspan girder deflections recorded from 2 tests per traffic lane with a single test truck. Figure 6.10 and 6.11 show plots of maximum midspan girder deflections due to a single side-by-side test truck crossing. These plots generally indicate that girder deflections increased somewhat at the most heavily loaded girder as a result of removing all the diaphragms. The girder deflections with the minimum needed diaphragms were sometimes larger and sometimes smaller than the girder deflections measured with the original diaphragms in-place and with all diaphragms removed. As can be seen in most of the plots, girders away from the most heavily loaded girder display a slight decrease in deflection as a result of removing some or all the diaphragms.

The noted increases in bottom flange stresses and girder deflections indicate that diaphragms do play a role in the lateral distribution of traffic loads for this particular bridge. Generally, the increases were small, less than 15% for single truck loadings

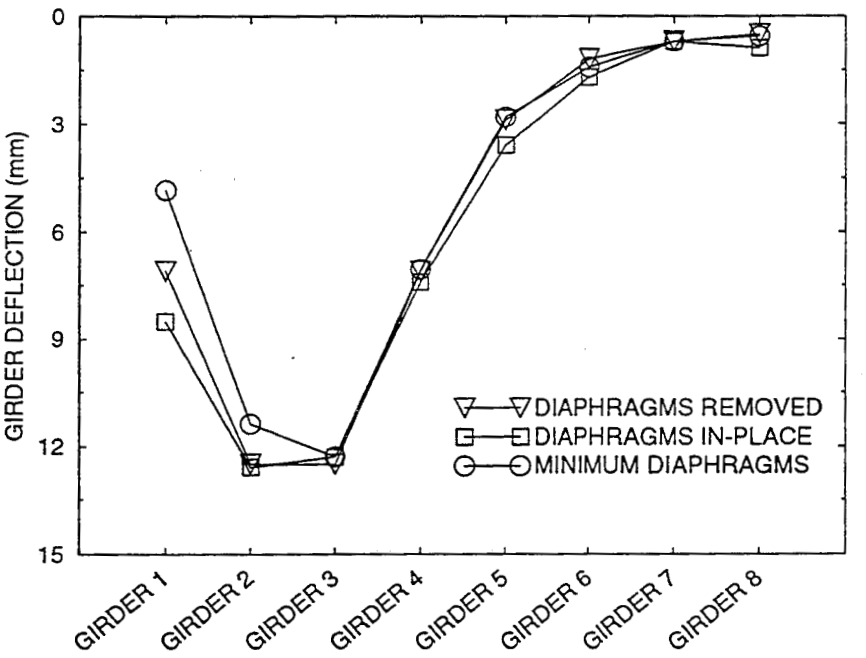

Figure 6.6. Average Maximum Measured Girder Deflections for a Calibration Truck Loading in Lane 1

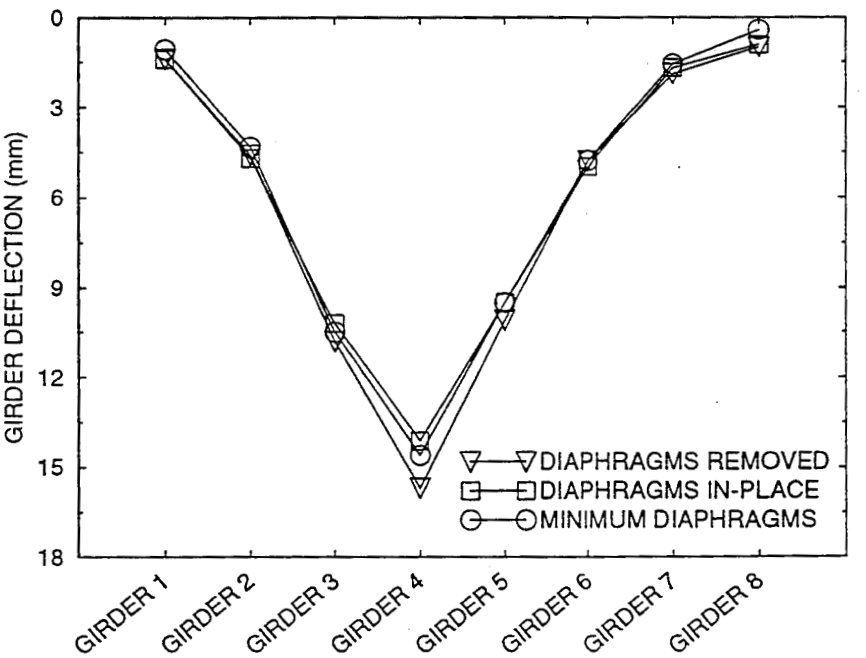

Figure 6.7. Average Maximum Measured Girder Deflections for a Calibration Truck Loading in Lane 2

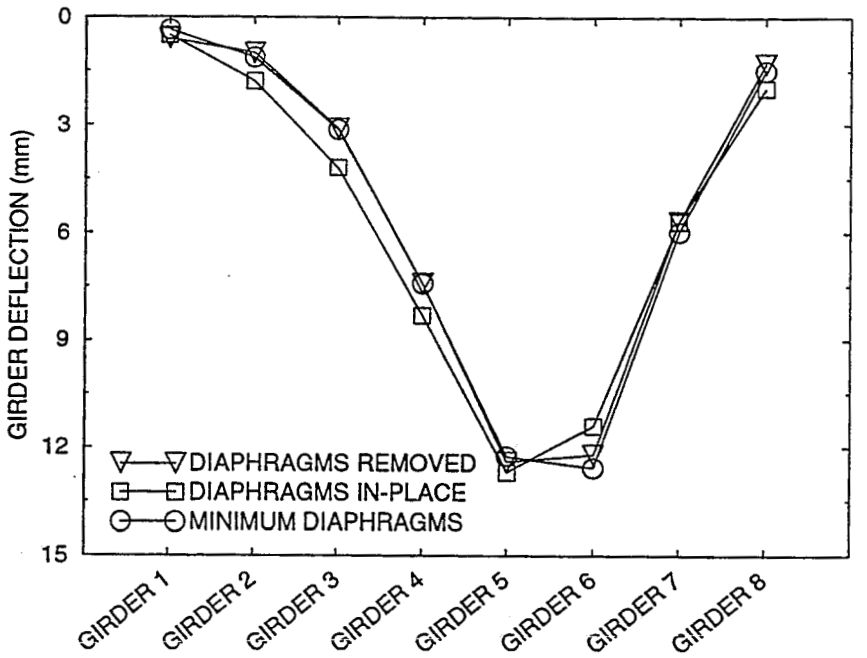

Figure 6.8. Average Maximum Measured Girder Deflections for a Calibration Truck Loading in Lane 3

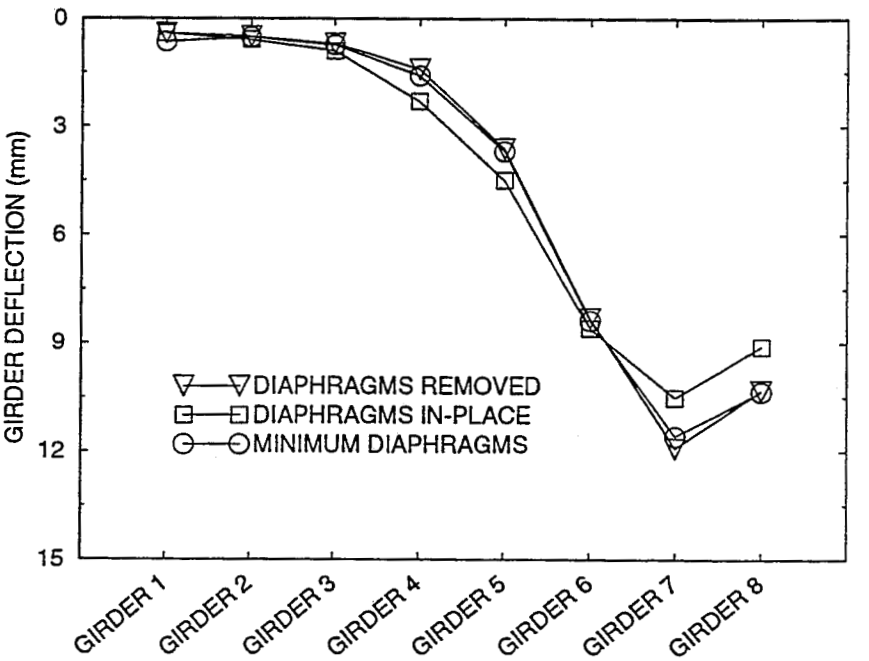

Figure 6.9. Average Maximum Measured Girder Deflections for a Calibration Truck Loading in Lane 4

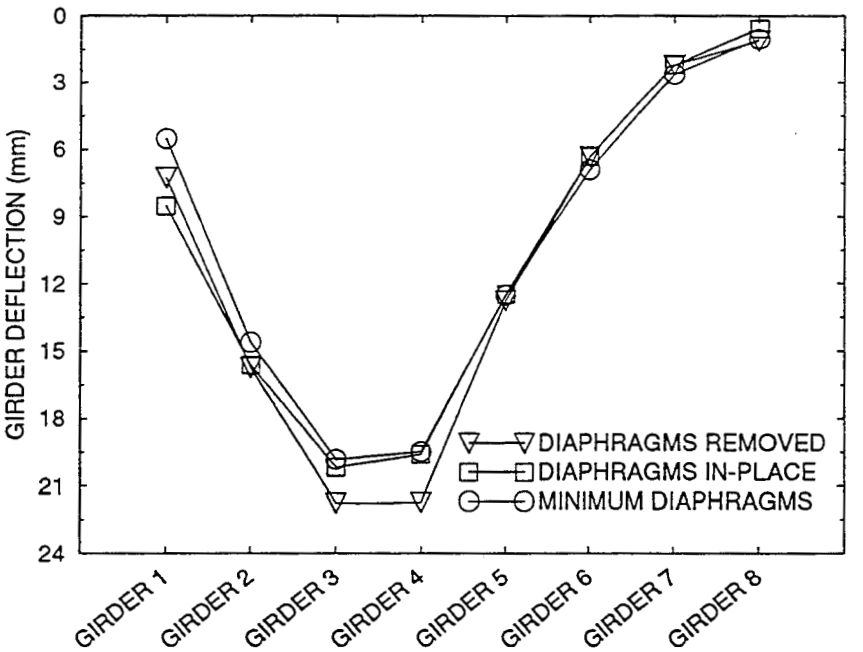

Figure 6.10. Maximum Measured Girder Deflections for Side-by-Side Calibration Truck Loading in Lanes 1 and 2

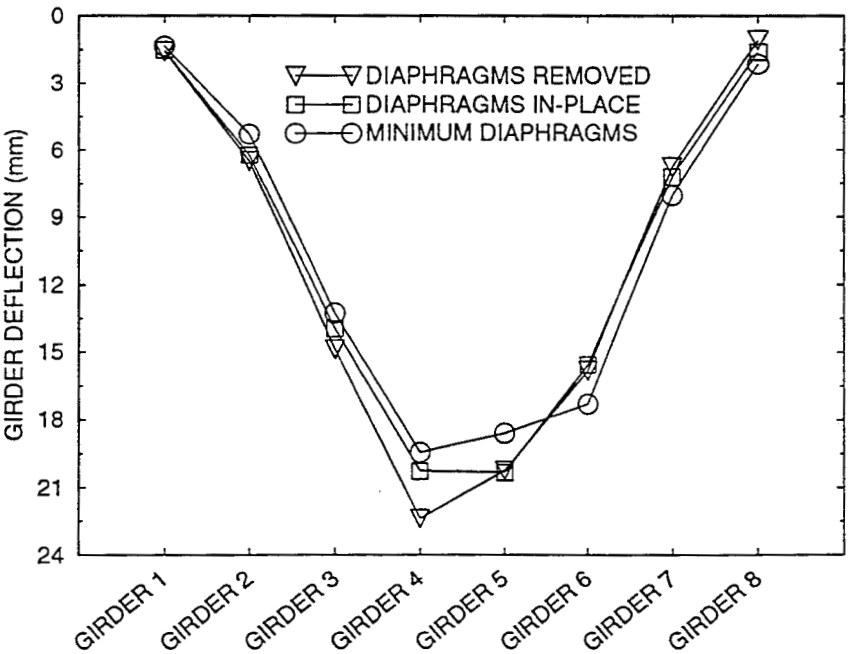

Figure 6.11. Maximum Measured Girder Deflections for Side-by-Side Calibration Truck Loading in Lanes 2 and 3

Table 6.5. Measured Maximum Girder Deflections (mm) at Midspan of of Span 29 (32 m) from Calibration Truck Loading

Loading/ Dis. Status	Girder Number							
	1	2	3	4	5	6	7	8
Lane1/In	8.5	**12.6**	**12.3**	7.4	3.6	1.7	.7	.9
Lane1/Out	7.1	**12.5**	**12.5**	7.1	2.9	1.2	.7	.5
Lane1/Min	4.9	**11.4**	**12.3**	7.1	2.8	1.4	.7	.6
Lane2/In	1.4	4.7	10.2	**14.1**	9.5	5.0	1.7	.9
Lane2/Out	1.4	4.6	10.8	**15.7**	10.1	4.8	1.9	1.0
Lane2/Min	1.1	4.3	10.5	**14.6**	9.5	4.8	1.6	.4
Lane3/IN	.5	1.8	4.2	8.3	**12.7**	**11.4**	5.7	2.0
Lane3/Out	.6	1.0	3.1	7.4	**12.4**	**12.2**	5.7	1.3
Lane3/Min	.4	1.1	3.1	7.4	**12.3**	**12.6**	6.0	1.5
Lane4/In	.4	.6	.9	2.3	4.5	8.6	**10.5**	9.1
Lane4/Out	.4	.5	.7	1.4	3.6	8.3	**11.9**	10.3
Lane4/Min	.6	.5	.7	1.6	3.7	8.4	**11.6**	10.3
Lanes1&2/In	8.5	15.6	**20.2**	**19.6**	12.5	6.3	2.2	.6
Lanes1&2/Out	7.2	15.7	**21.8**	**21.7**	12.8	6.3	2.2	1.1
Lanes1&2/Min	5.5	14.6	**19.8**	**19.5**	12.5	6.9	2.6	1.0
Lanes2&3/In	1.5	6.2	14.0	**20.3**	20.3	15.5	7.2	1.6
Lanes2&3/Out	1.6	6.5	14.9	**22.3**	20.2	15.8	6.8	1.1
Lanes2&3/Min	1.4	5.3	13.3	**19.4**	18.6	17.3	8.1	2.2

and less than 9% for side-by-side truck loadings, which indicate that diaphragms have only a small effect on the transverse distribution of truck loads.

COMPARISON WITH CALCULATED STRESSES

Bottom flange stresses were calculated for the test truck loadings based on AASHTO (1992) provisions for simplified analysis. Maximum midspan bending moments and maximum support bending moments were calculated for one wheel line of the test truck loading by using a structural analysis computer program. Girder bending moments were calculated by applying AASHTO Impact and Wheel Load Distribution factors to those bending moments. The bottom flange stresses were then calculated using the noncomposite girder cross section properties. The resulting calculated midspan bottom flange stresses for span 28, span 29, and at the support (Bent 29) are displayed in Tables 6.6 through 6.9.

To make a comparison between measured stresses and the calculated stresses, superposition of the live load must be used. Superposition of the maximum measured bottom flange stresses from the calibration tests were used to simulate the effects of side-by-side test trucks in all traffic lanes. Two superpositions are shown in Tables 6.6 through 6.9 for diaphragms in-place, diaphragms removed, and minimum needed diaphragms. One superposition was obtained by adding average single truck test results from each traffic lane, and one is from adding side-by-side results from lanes 1 and 2 with single truck results for lanes 3 and 4. Although the superposition provides a useful comparison with the calculated stresses, the superposition of dynamic test data results in some error as discussed in the previous chapter.

Based on the results in Tables 6.6 through 6.9 the superpositions of the measured stresses are seen to be considerably lower than the calculated stresses. The stresses at midspan of span 28 and 29 in the most highly stressed girders are less

Table 6.6. Calculated Stresses (MPa) and Superpositions of Measured Maximum Bottom Flange Stresses (MPa) at Midspan of Span 28 (22 m) from Calibration Truck Loading

Lane Loading Dia. Status	Girder Number							
	1	2	3	4	5	6	7	8
Calculated	65	106	106	106	106	106	106	96
1,2,3,4/In	17	33	51	61	**67**	56	51	32
1,2,3,4/Out	16	36	53	61	**64**	56	51	34
1,2,3,4/Min	13	36	55	63	**65**	55	51	30
1+2,3,4/In	16	36	51	60	**66**	56	49	29
1+2,3,4/Out	14	37	52	60	**63**	55	50	31
1+2,3,4/Min	14	36	50	60	**66**	57	49	28

Table 6.7. Calculated Stresses (MPa) and Superpositions of Measured Maximum Bottom Flange Stresses (MPa) at Midspan of Span 29 (22 m) from Calibration Truck Loading

Lane Loading Dia. Status	Girder Number							
	1	2	3	4	5	6	7	8
Calculated	81	107	107	107	107	107	107	97
1,2,3,4/In	19	41	62	65	**69**	56	42	24
1,2,3,4/Out	16	39	58	63	**66**	55	44	23
1,2,3,4/Min	14	39	60	65	**67**	55	44	24
1+2,3,4/In	15	38	55	62	**68**	54	41	21
1+2,3,4/Out	13	36	54	61	**66**	55	43	22
1+2,3,4/Min	13	37	54	61	**69**	56	43	22

Table 6.8. Calculated Stresses (MPa) and Superpositions of Measured Maximum Bottom Flange Stresses (MPa) at the Interior Support (Bent 29) from Calibration Truck Loading in Span 28 (22 m)

Lane Loading Dia. Status	Girder Number							
	1	2	3	4	5	6	7	8
Calculated	31	46	46	46	46	46	46	42
1,2,3,4/In	9	18	31	36	**40**	33	29	12
1,2,3,4/Out	4	18	33	36	**40**	31	30	13
1,2,3,4/Min	7	18	35	37	**38**	33	29	13
1+2,3,4/In	5	17	33	35	**39**	30	27	10
1+2,3,4/Out	3	16	34	36	**38**	30	30	11
1+2,3,4/Min	4	17	32	34	**39**	32	28	12

Table 6.9. Calculated Stresses (MPa) and Superpositions of Measured Maximum Bottom Flange Stresses (MPa) at the Interior Support (Bent 29) from Calibration Truck Loading in Span 29 (32 m)

Lane Loading Dia. Status	Girder Number							
	1	2	3	4	5	6	7	8
Calculated	49	72	72	72	72	72	72	66
1,2,3,4/In	13	24	33	**35**	34	32	27	14
1,2,3,4/Out	12	23	32	**34**	34	31	29	15
1,2,3,4/Min	10	21	33	**35**	33	31	29	15
1+2,3,4/In	12	23	31	32	**33**	31	27	13
1+2,3,4/Out	10	21	32	31	**32**	31	28	14
1+2,3,4/Min	10	20	30	32	**33**	33	29	15

than 65% of the calculated values. The stresses at the support due to negative moments in the most highly stressed girders are up to 86% of the calculated values for a trucks in span 28 and less than 56% of the calculated values for trucks in span 29. This significant difference in support stresses from the two loading conditions is believed to result from friction at the support which was described earlier in this chapter. There are no significant differences between the superposition results for the cases with the original diaphragms, no diaphragms, and with the minimum required number of diaphragms.

NORMAL TRAFFIC TESTS RESULTS

To study on how the bridge reacts to longer trucks of various weights, data was recorded for trucks in the normal traffic stream. The method of using load fractions for participating girders, which was described in Chapter Five, is used below to evaluate the role diaphragms play in lateral distribution of traffic loads due to normal traffic loading. Load fractions based on the maximum recorded strains and the maximum recorded deflections are used. Due to the normal traffic patterns it was only possible to acquire a sufficient number of truck crossings for lanes 1 and 2 for normal traffic loading. Table 6.10 shows the participating girders identified for those two traffic lanes.

Plots of load fraction versus a truck size parameter were generated to determine if truck size affected the load fractions obtained from the truck traffic data. These plots are shown in Figures 6.12 through 6.26 for the most heavily loaded girders. For a truck in lane 2, girder 4 was the most heavily loaded girder for all data recorded. For a truck in lane 1, girder 2 and girder 3 were equally likely to be the most heavily loaded

Table 6.10. Participating Girders for the 76 m 3 Span Continuous Bridge

Lane 1	Lane 2
Girder 1	Girder 2
Girder 2	Girder 3
Girder 3	Girder 4
Girder 4	Girder 5
Girder 5	Girder 6

girder. Neither girder was dominant in having the largest strain or deflection values. The reason for this is illustrated by the cross-sectional sketch of the bridge in Figure 6.3. As can be seen from the sketch, a truck in lane 1 could produce maximum values in girder 2 or 3 depending on the position of the truck inside the traffic lane. For this reason, load fraction plots were generated for girder 2, 3, and 4 for midspan gages in span 28 (Figures 6.12, 6.16 and 6.20), midspan gages in span 29 (Figures 6.13, 6.17 and 6.21), and support gages at Bent 29 (Figures 6.14, 6.15, 6.18, 6.19, 6.22 and 6.23). Load fraction plots were also generated based on midspan deflections of span 29 (Figures 6.24, 6.25, and 6.26). The horizontal axis in the plots is a nondimensional strain ratio (ϵ/ϵ_{TT}) defined as the maximum strain recorded at the girder for the normal traffic tests divided by the average maximum strain recorded at the girder for a calibration truck test. This ratio is a measure of the weight of the truck in normal traffic relative to the calibration truck weight.

These figures show that the load fractions were not significantly affected by the weight of the truck since all the data tends to fall on a horizontal line. The load

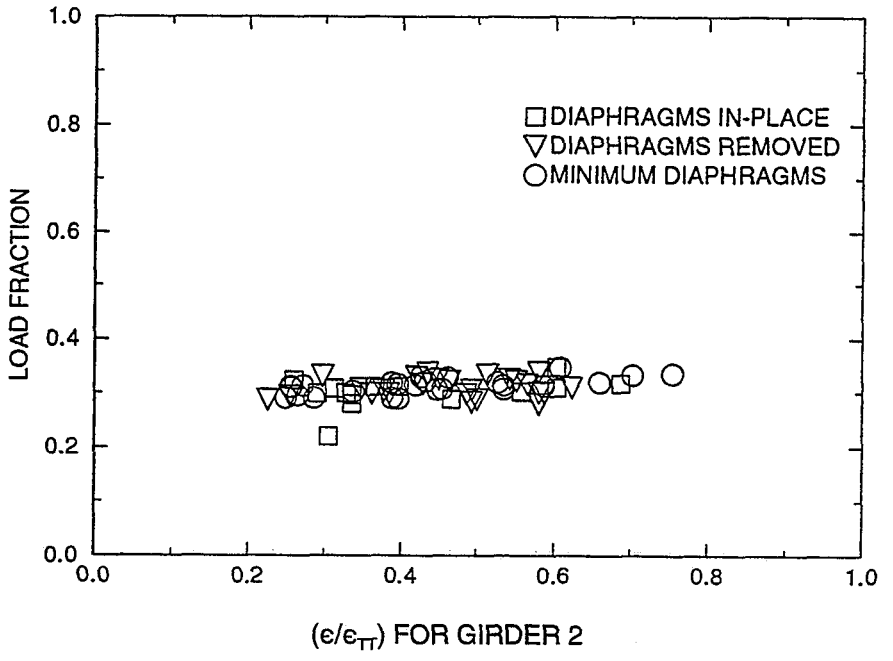

Figure 6.12. Load Fractions from Maximum Measured Bottom Flange Strains at Midspan of Span 28 for Truck Traffic in Lane 1

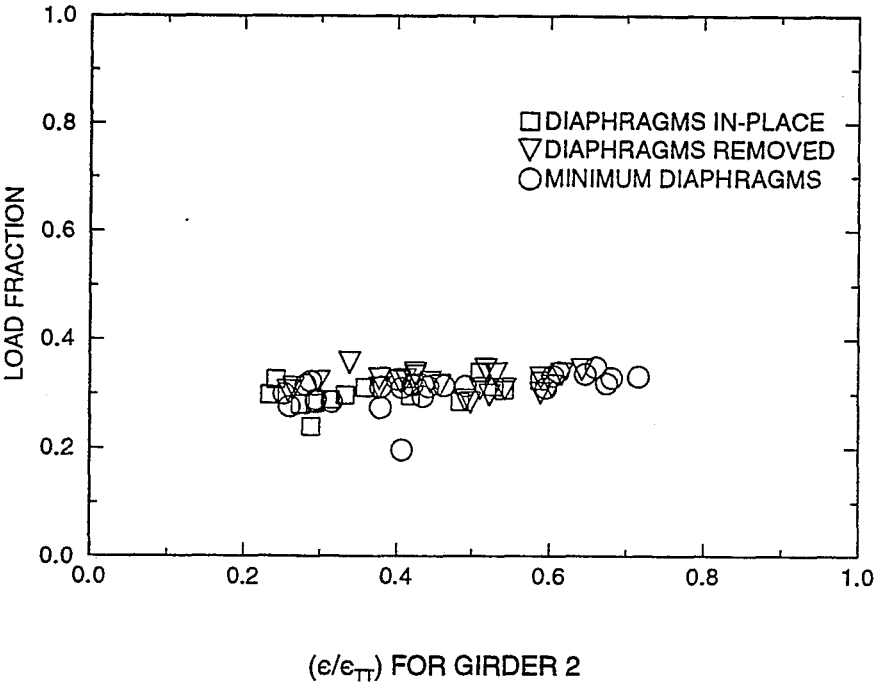

Figure 6.13. Load Fractions from Maximum Measured Bottom Flange Strains at Midspan of Span 29 for Truck Traffic in Lane 1

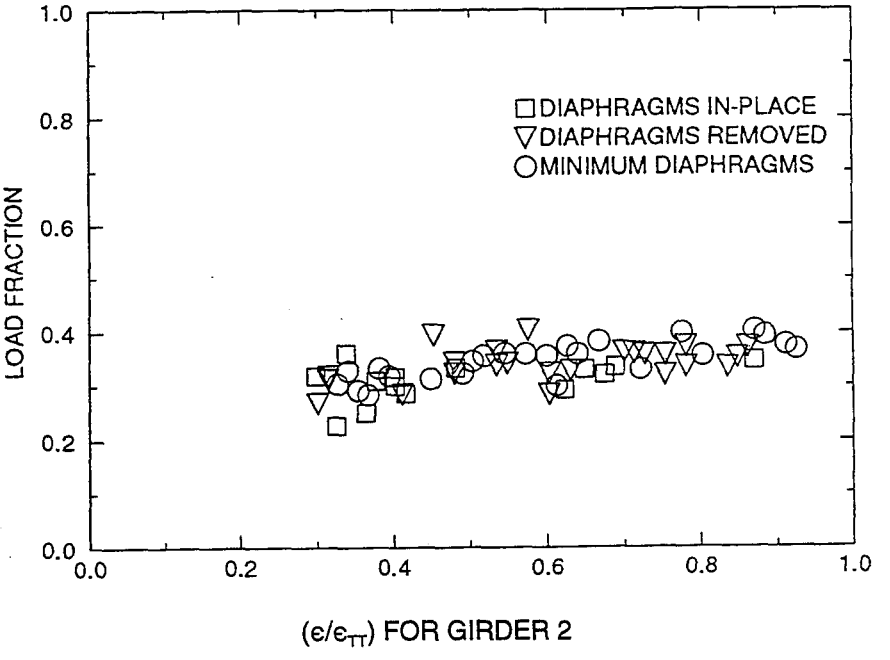

Figure 6.14. Load Fractions from Maximum Measured Bottom Flange Strains at the Interior Support (Bent 29) for Truck Traffic in Lane 1 (Truck on Span 28)

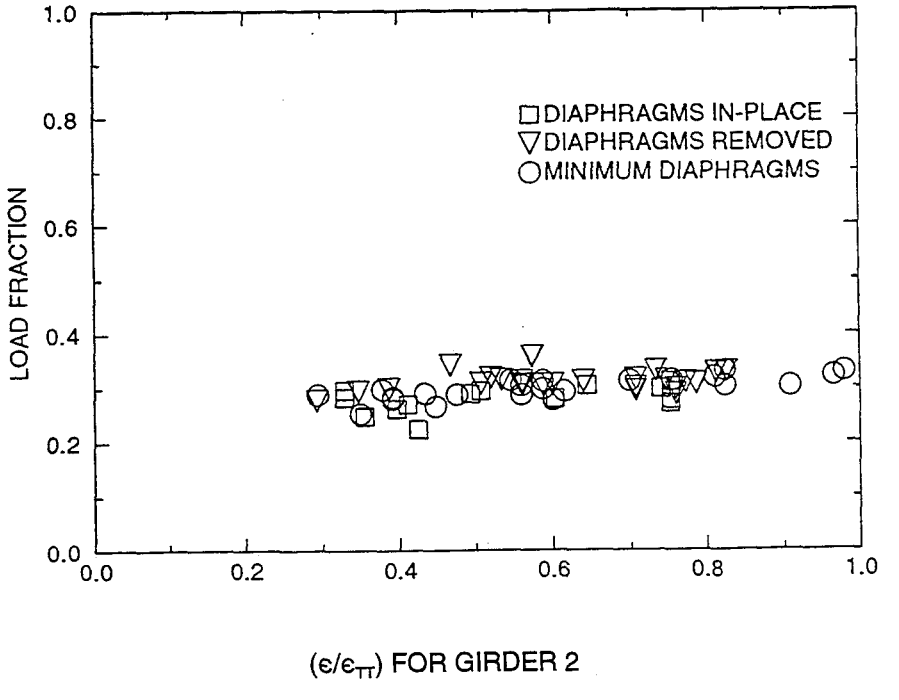

Figure 6.15. Load Fractions from Maximum Measured Bottom Flange Strains at the Interior Support (Bent 29) for Truck Traffic in Lane 1 (Truck on Span 29)

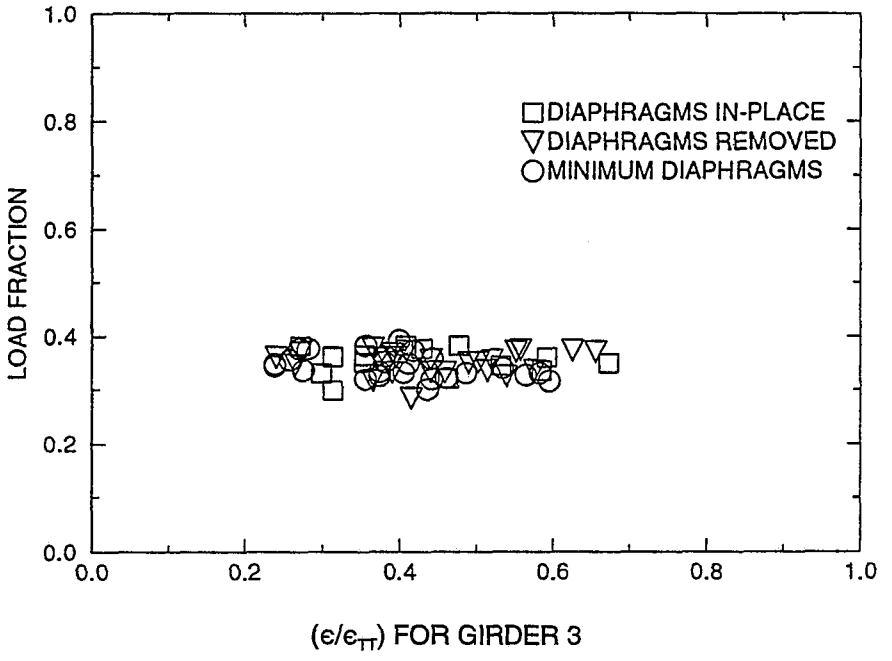

Figure 6.16. Load Fractions from Maximum Measured Bottom Flange Strains at Midspan of Span 28 for Truck Traffic in Lane 1

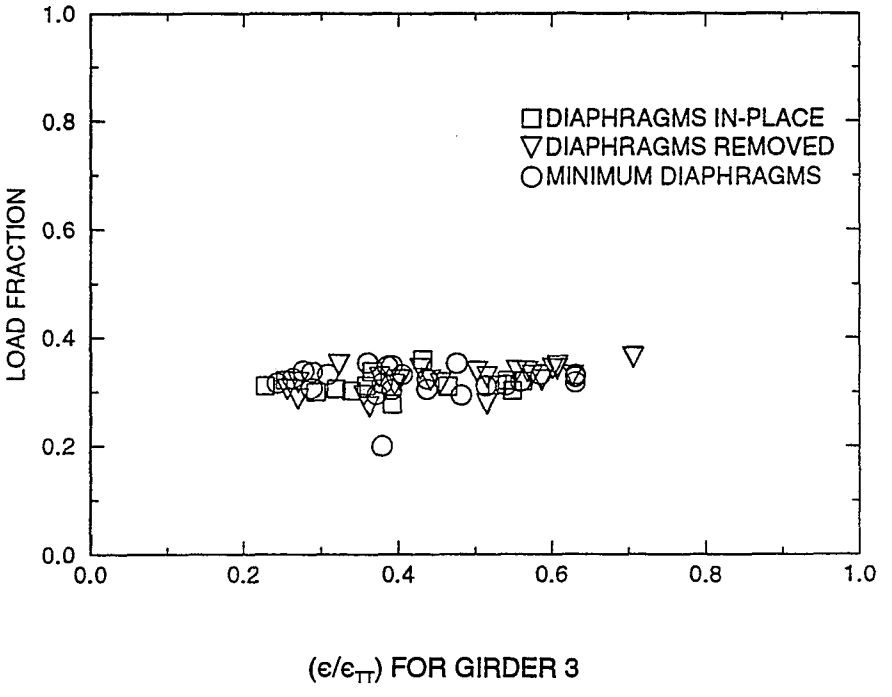

Figure 6.17. Load Fractions from Maximum Measured Bottom Flange Strains at Midspan of Span 29 for Truck Traffic in Lane 1

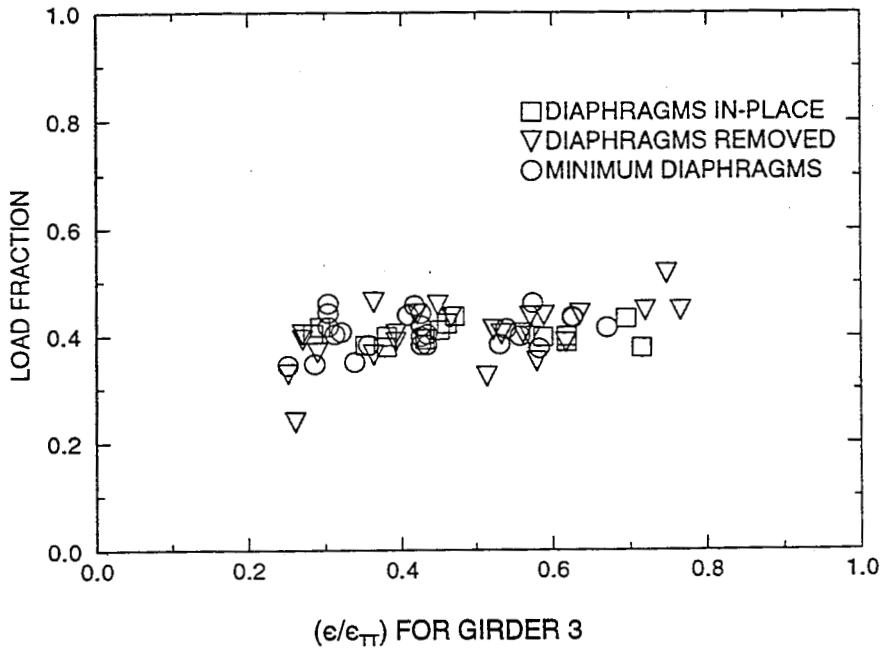

Figure 6.18. Load Fractions from Maximum Measured Bottom Flange Strains at Interior Support (Bent 29) for Truck Traffic in Lane 1 (Truck on Span 28)

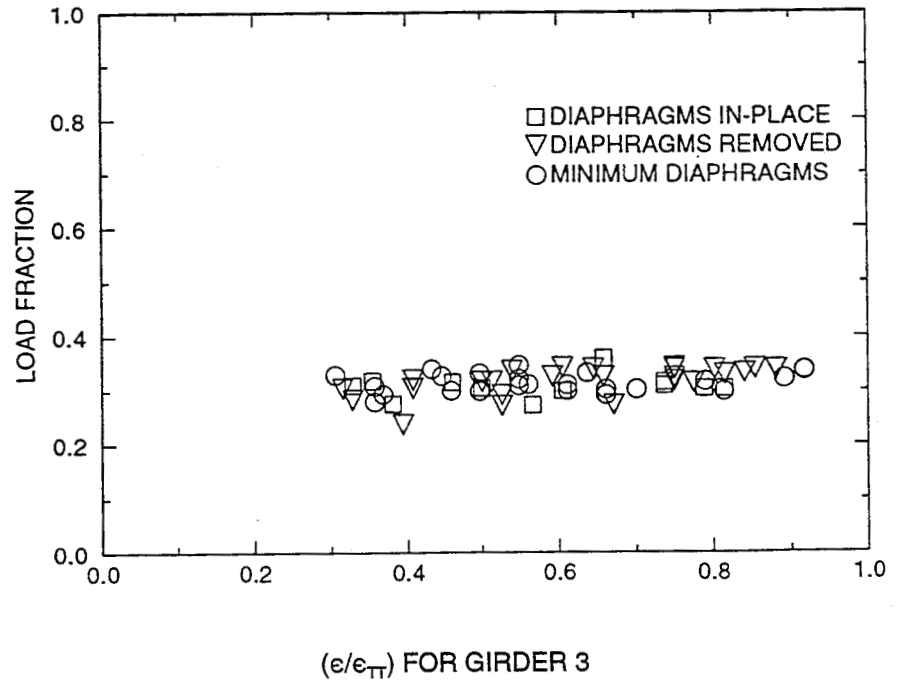

Figure 6.19. Load Fractions from Maximum Measured Bottom Flange Strains at Interior Support (Bent 29) for Truck Traffic in Lane 1 (Truck on Span 29)

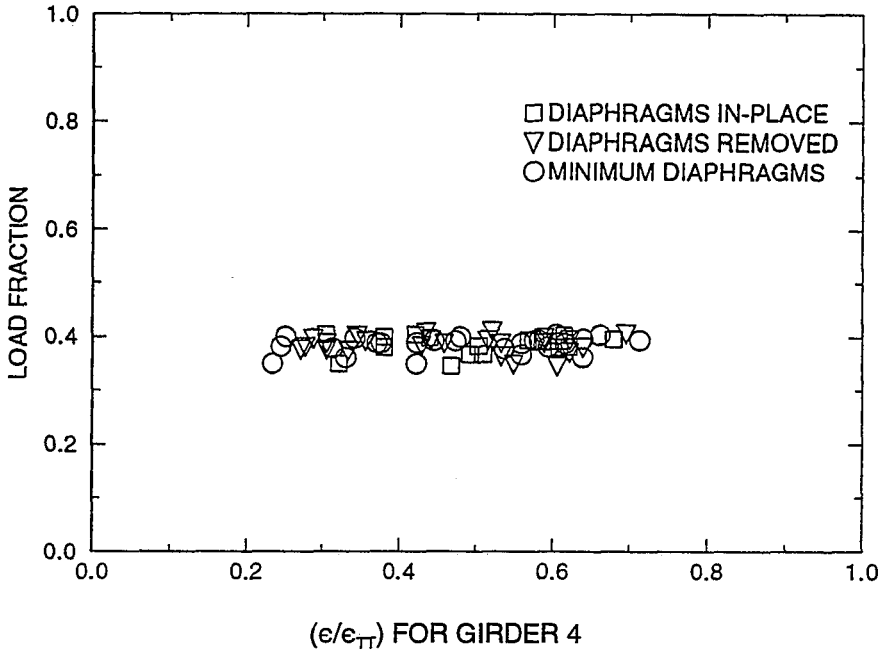

Figure 6.20. Load Fractions from Maximum Measured Bottom Flange Strains at Midspan of Span 28 for Truck Traffic in Lane 2

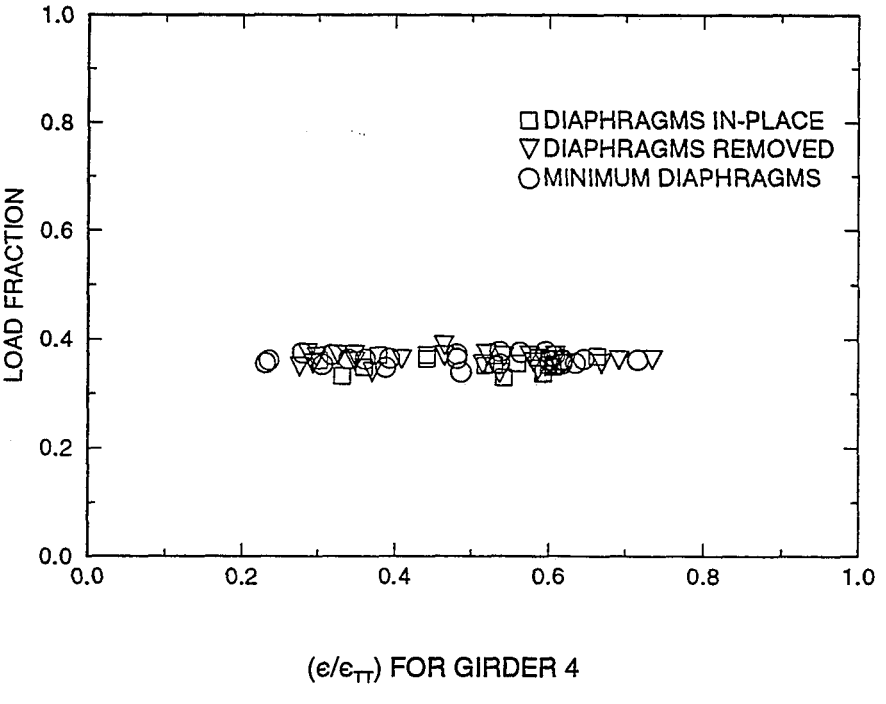

Figure 6.21. Load Fractions from Maximum Measured Bottom Flange Strains at Midspan of Span 29 for Truck Traffic in Lane 2

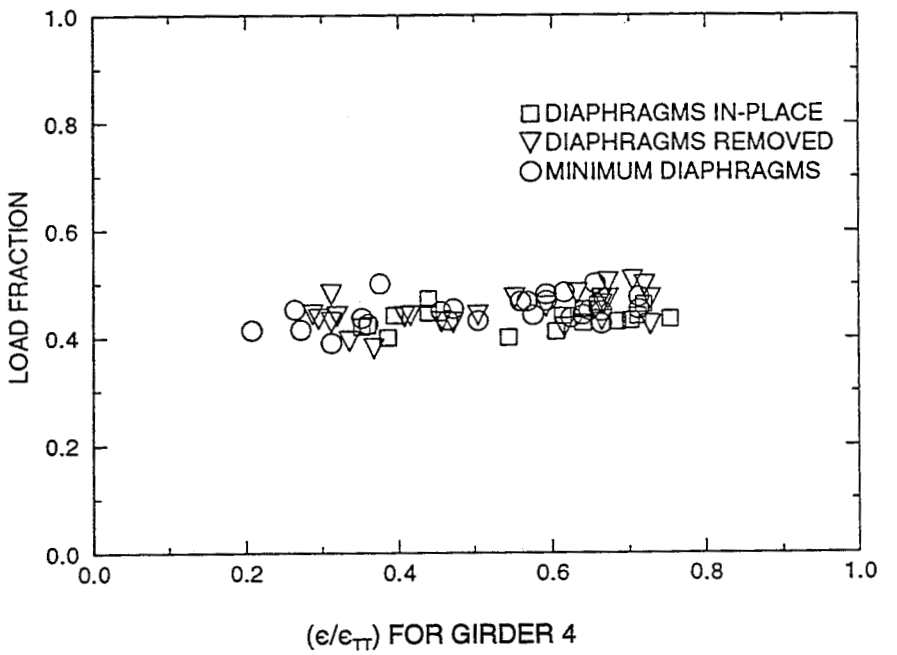

Figure 6.22. Load Fractions from Maximum Measured Bottom Flange Strains at Interior Support (Bent 29) for Truck Traffic in Lane 2 (Truck on Span 28)

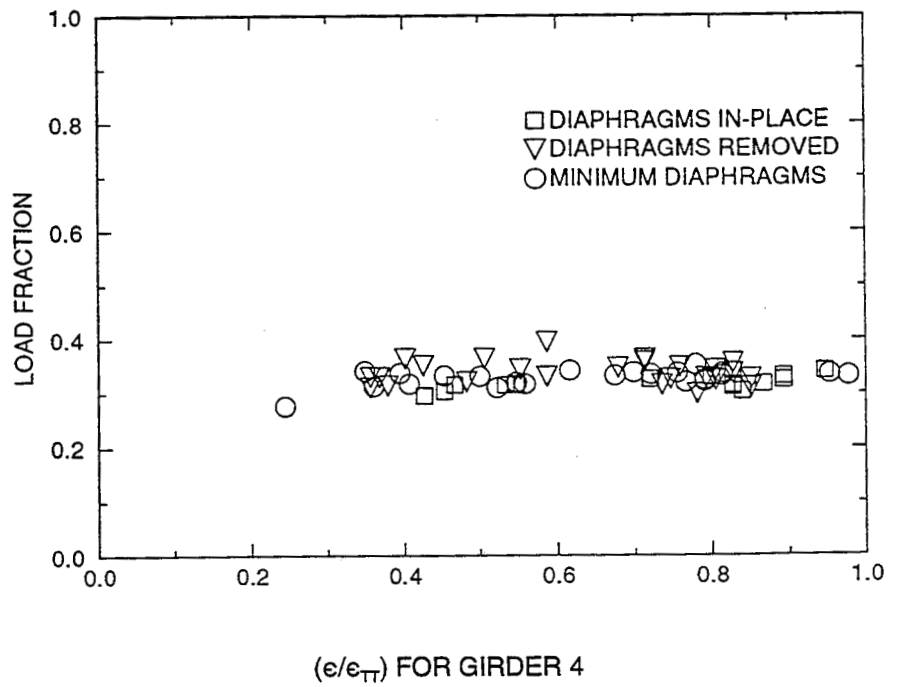

Figure 6.23. Load Fractions from Maximum Measured Bottom Flange Strains at Interior Support (Bent 29) for Truck Traffic in Lane 2 (Truck on Span 29)

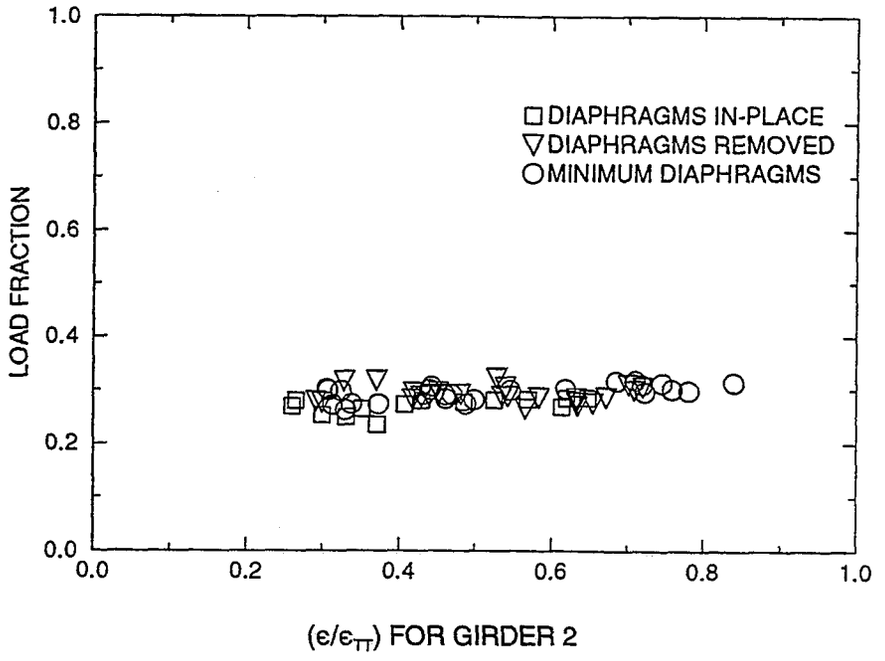

Figure 6.24. Load Fractions from Maximum Measured Deflections at Midspan of Span 29 for Truck Traffic in Lane 1

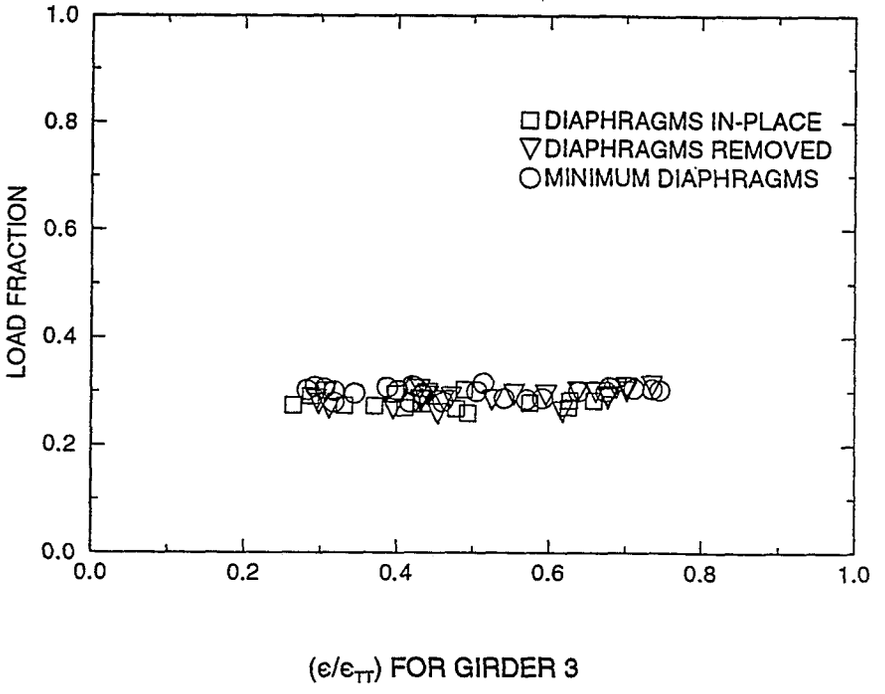

Figure 6.25. Load Fractions from Maximum Measured Deflections at Midspan of Span 29 for Truck Traffic in Lane 1

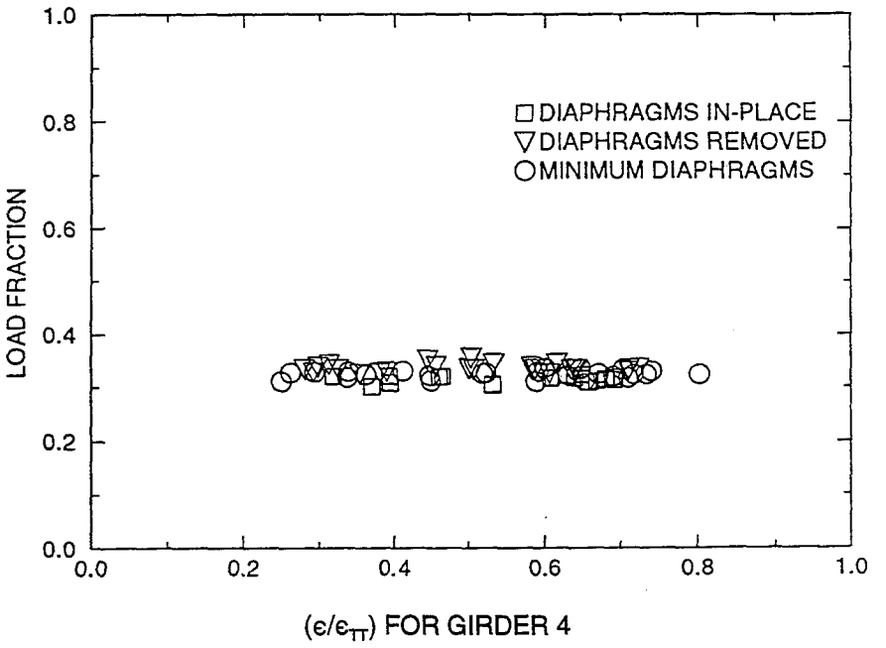

Figure 6.26. Load Fractions from Maximum Measured Deflections at Midspan of Span 29 for Truck Traffic in Lane 2

fractions in Figures 6.20 through 6.23 also appear somewhat more uniform than those in Figures 6.12 through 6.19. This is primarily due to girder 4 being the most heavily loaded girder for all truck events. By viewing the plots it can also be observed that the load fractions are well mixed for the cases of diaphragms in-place, diaphragms removed, and minimum diaphragms needed. Hence, based on these plots, differences in load distribution behavior for the three cases can not be readily identified.

The load fractions for the support at Bent 29 for a truck in span 28 tend to have a little more scatter and to be somewhat higher than the midspan load fractions. This is thought to be primarily the result of friction at the interior support.

Averages and standard deviations of the load fractions for the normal traffic data are given in Tables 5.11 through 5.15. The load fractions were not significantly

Table 6.11. Load Fractions from Normal Traffic Data Calculated from Maximum Measured Bottom Flange Strains at Midspan of Span 28 (22 m)

Loading/ Dia. Status		Girder Number							
		1	2	3	4	5	6	7	8
Lane1/ In	Ave. of 14	.118	.301	**.353**	.170	.058	-	-	-
	Std. Dev.	.018	.029	.025	.024	.014	-	-	-
Lane1/ Out	Ave. of 25	.114	.310	**.351**	.163	.062	-	-	-
	Std. Dev.	.025	.018	.022	.017	.013	-	-	-
Lane1/ Min	Ave. of 25	.116	.313	**.344**	.164	.062	-	-	-
	Std. Dev.	.027	.015	.023	.016	.019	-	-	-
Lane2/ In	Ave. of 17	-	.067	.207	**.384**	.250	.092	-	-
	Std. Dev.	-	.016	.013	.018	.017	.015	-	-
Lane2/ Out	Ave. of 25	-	.059	.211	**.384**	.256	.090	-	-
	Std. Dev.	-	.016	.018	.016	.024	.015	-	-
Lane2/ Min	Ave. of 25	-	.070	.211	**.384**	.247	.087	-	-
	Std. Dev.	-	.010	.021	.016	.026	.018	-	-

- Nonparticipating girder

Table 6.12. Load Fractions from Normal Traffic Data Calculated from Maximum Measured Bottom Flange Strains at Midspan of Span 29 (32 m)

Loading/ Dia. Status		Girder Number							
		1	2	3	4	5	6	7	8
Lane1/ In	Ave. of 14	.150	.299	**.313**	.156	.081	-	-	-
	Std. Dev.	.021	.025	.019	.020	.018	-	-	-
Lane1/ Out	Ave. of 25	.146	.320	**.323**	.146	.065	-	-	-
	Std. Dev.	.025	.018	.022	.017	.017	-	-	-
Lane1/ Min	Ave. of 25	.140	.308	**.319**	.151	.069	-	-	-
	Std. Dev.	.019	.030	.030	.022	.019	-	-	-
Lane2/ In	Ave. of 17	-	.092	.238	**.355**	.221	.094	-	-
	Std. Dev.	-	.010	.010	.013	.012	.011	-	-
Lane2/ Out	Ave. of 25	-	.090	.238	**.361**	.223	.088	-	-
	Std. Dev.	-	.012	.019	.012	.018	.013	-	-
Lane/2 Min	Ave. of 25	-	.087	.247	**.363**	.217	.086	-	-
	Std. Dev.	-	.010	.019	.009	.017	.010	-	-

- Nonparticipating girder

Table 6.13. Load Fractions From Normal Traffic Data Calculated from Maximum Measured Bottom Flange Strains at Support (Bent 29) from Loading in Span 28

Loading/ Dia. Status		Girder Number							
		1	2	3	4	5	6	7	8
Lane1/ In	Ave. of 14	.108	.309	**.403**	.123	.057	-	-	-
	Std. Dev.	.024	.036	.019	.025	.023	-	-	-
Lane1/ Out	Ave. of 25	.098	.342	**.404**	.106	.051	-	-	-
	Std. Dev.	.062	.034	.056	.035	.017	-	-	-
Lane1/ Min	Ave. of 25	.076	.346	**.408**	.115	.054	-	-	-
	Std. Dev.	.019	.033	.034	.023	.028	-	-	-
Lane2/ In	Ave. of 17	-	.055	.202	**.435**	.248	.061	-	-
	Std. Dev.	-	.017	.020	.020	.026	.023	-	-
Lane2/ Out	Ave. of 25	-	.038	.191	**.450**	.266	.055	-	-
	Std. Dev.	-	.025	.034	.032	.040	.021	-	-
Lane2/ Min	Ave. of 25	-	.038	.202	**.450**	.258	.052	-	-
	Std. Dev.	-	.014	.034	.027	.035	.022	-	-

- Nonparticipating girder

CHAPTER SEVEN

ANALYTICAL EVALUATION OF REMOVING DIAPHRAGMS

INTRODUCTION

To ascertain the effect of diaphragm removal upon a wider variety of bridge types than could feasibly be field tested, a comprehensive, three-dimensional, finite element method (FEM) analysis was conducted. Static and dynamic FEM analyses were performed for straight girder and skewed simple spans, wide (eight girders) continuous span bridges, and narrow (five girders) continuous span bridges. Both composite and non-composite bridges were analyzed. A total of nine different simple span bridges and four different continuous bridges were analyzed. The static and dynamic truck loading conditions simulated the ALDOT load test trucks as described in Chapters Four and Five of this report.

FINITE ELEMENTS MODELS

To verify the accuracy of the FEM models, a series of comparisons were made with analytical results and corresponding field test data reported in Chapter Five. The bridge chosen for this comparison is a simple span, the second in a 28 span viaduct, which carries the five northbound lanes of Interstate 65 over Second Avenue South in downtown Birmingham. The bridge, referred to in this Chapter as bridge A1, spans 24.8 m, and is supported by nine girders spaced at 2.44 m with three lines of interior diaphragms. The original bridge consisted of four lanes on seven girders and was constructed in 1966, with a fifth lane added on the left shoulder in 1987. The seven original girders are W920 x 289 (W36 x 194) rolled sections with a coverplate on the tension flange at the middle section of the span. The two newer girders are W920 x

342 (W36 x 230) sections without coverplates. All of the diaphragms are MC460 x 63.5 (MC18 x 42.7) channel sections, and the slab is 165 mm thick.

An isometric view of the three dimensional FEM model is presented in Figure 7.1. A typical transverse cross section of the model is presented in Figure 7.2. The FEM mesh of the bridge consists of 60 element segments along the length of the span, with eight element segments in the slab between each girder (see Figure 7.1). The full model with diaphragms includes 4260 shell elements in the slab, 2160 shell elements in the girder flanges, 80 beam and 160 truss elements in the diaphragms and diaphragm connections, 4680 plate elements in the girder webs, and over 10200 nodes with more than 53000 active degrees of freedom.

In the actual bridge, the deck slab had experienced cracking virtually everywhere. In order to model the cracked state of the slab, the elastic modulus of the slab elements was altered to produce an effective stiffness for the slab. This proved to be more amenable than altering the thickness of the shell elements. The slab cracks propagating transverse to the girders were assumed to close during primary flexure of the bridge, while the slab cracks parallel to the girders open during girder flexure and differential deflection of the girders. Hence, an orthotopic material model was defined for the deck slab elements. The elastic modulus in the longitudinal (Y) direction of the model was defined using the American Concrete Institute (ACI, 1989) standard of $57\sqrt{f'c}$, where f'c is the compressive strength of the concrete. For the transverse (X) direction, the elastic modulus was calculated as the ACI elastic modulus modified by the ratio of the cracked moment of inertia versus the gross moment of inertia of a unit

affected by removing the diaphragms or having the minimum needed diaphragms. For cases where there was an increase in load fraction, removal of all diaphragms and use of minimum diaphragms produced an increase over having diaphragms in place of 3% or less at midspan and 6% or less at the interior support. The largest noted increase in load fractions of 6% for the most heavily loaded girder, occurred at the support (Bent 29) due to a truck loading in span 29. The differences in load fractions calculated from strain values vary less than 0.02 for the most heavily loaded girder which roughly corresponds to 2% of the applied single truck load. The differences in load fractions calculated from strain or deflection values for a truck in span 29 range less than 0.04 for the most heavily loaded girder which corresponds to 4% of the applied single truck load.

CONCLUSIONS

The field tests reported here were used to evaluate the effects channel diaphragms have on transverse load distribution in a 3-span continuous multi-girder steel bridge. Results were reported from tests with the original diaphragms in-place, with all interior diaphragms removed, and with the minimum number of lines of diaphragms required for full lateral bracing of the girders.

Measurements of maximum bottom flange stresses from loadings by trucks of known weight and axle configuration indicated an increase between 0 and 10% at midspan of the 22 m end span and an increases between 0 and 6% at midspan of the 32 m center span as a result of complete or partial removal of diaphragms. The most heavily loaded girders over the support (Bent 29) showed an increase between 0 and 15% in maximum measured bottom flange stresses as a result of complete or partial

diaphragm removal. Generally, there was very little difference in measured stresses near midspan or at the support for cases with the original diaphragms in-place, all diaphragms removed, and having the minimum required number of diaphragm lines. The normal traffic results indicated that the load fractions were not significantly affected by removing diaphragms or having the minimum required diaphragms. The averages of the load fractions calculated from truck traffic indicated an increase in load fractions of 3% or less for positive midspan moments and 6% or less for negative support moments. These increases correspond to less than 2% of a single truck load. The results for all tests show that diaphragms have only small effect on the transverse distribution of truck loads.

Table 6.14. Load Fractions from Normal Traffic Data Calculated from Maximum Measured Bottom Flange Strains at Support (Bent 29) from Loading in Span 29

Loading/ Dia. Status		Girder Number							
		1	2	3	4	5	6	7	8
Lane1/ In	Ave. of 14	.166	.279	**.308**	.163	.083	-	-	-
	Std. Dev.	.024	.024	.020	.025	.019	-	-	-
Lane1/ Out	Ave. of 25	.169	.311	**.316**	.143	.060	-	-	-
	Std. Dev.	.039	.017	.027	.025	.021	-	-	-
Lane1/ Min	Ave. of 25	.156	.299	**.314**	.156	.075	-	-	-
	Std. Dev.	.023	.020	.018	.020	.024	-	-	-
Lane2/ In	Ave. of 17	-	.107	.247	**.320**	.221	.106	-	-
	Std. Dev.	-	.009	.012	.013	.012	.016	-	-
Lane2/ Out	Ave. of 25	-	.097	.244	**.338**	.226	.095	-	-
	Std. Dev.	-	.013	.019	.022	.019	.014	-	-
Lane2/ Min	Ave. of 25	-	.104	.253	**.328**	.219	.095	-	-
	Std. Dev.	-	.010	.018	.015	.017	.016	-	-

- Nonparticipating girder

Table 6.15. Load Fractions from Normal Traffic Data Calculated from Maximum Measured Girder Deflections at Midspan of Span 29

Loading/ Dia. Status		Girder Number							
		1	2	3	4	5	6	7	8
Lane1/ In	Ave. of 14	.181	.270	**.278**	.178	.093	-	-	-
	Std. Dev.	.020	.015	.012	.017	.014	-	-	-
Lane1/ Out	Ave. of 25	.178	.292	**.288**	.169	.073	-	-	-
	Std. Dev.	.022	.015	.014	.017	.014	-	-	-
Lane1/ Min	Ave. of 25	.150	.295	**.298**	.175	.081	-	-	-
	Std. Dev.	.012	.015	.010	.013	.012	-	-	-
Lane2/ In	Ave. of 17	-	.117	.236	**.315**	.215	.116	-	-
	Std. Dev.	-	.006	.008	.006	.008	.010	-	-
Lane2/ Out	Ave. of 25	-	.108	.240	**.336**	.212	.105	-	-
	Std. Dev.	-	.009	.013	.008	.012	.013	-	-
Lane2/ Min	Ave. of 25	-	.112	.246	**.324**	.208	.109	-	-
	Std. Dev.	-	.010	.012	.007	.011	.011	-	-

- Nonparticipating girder

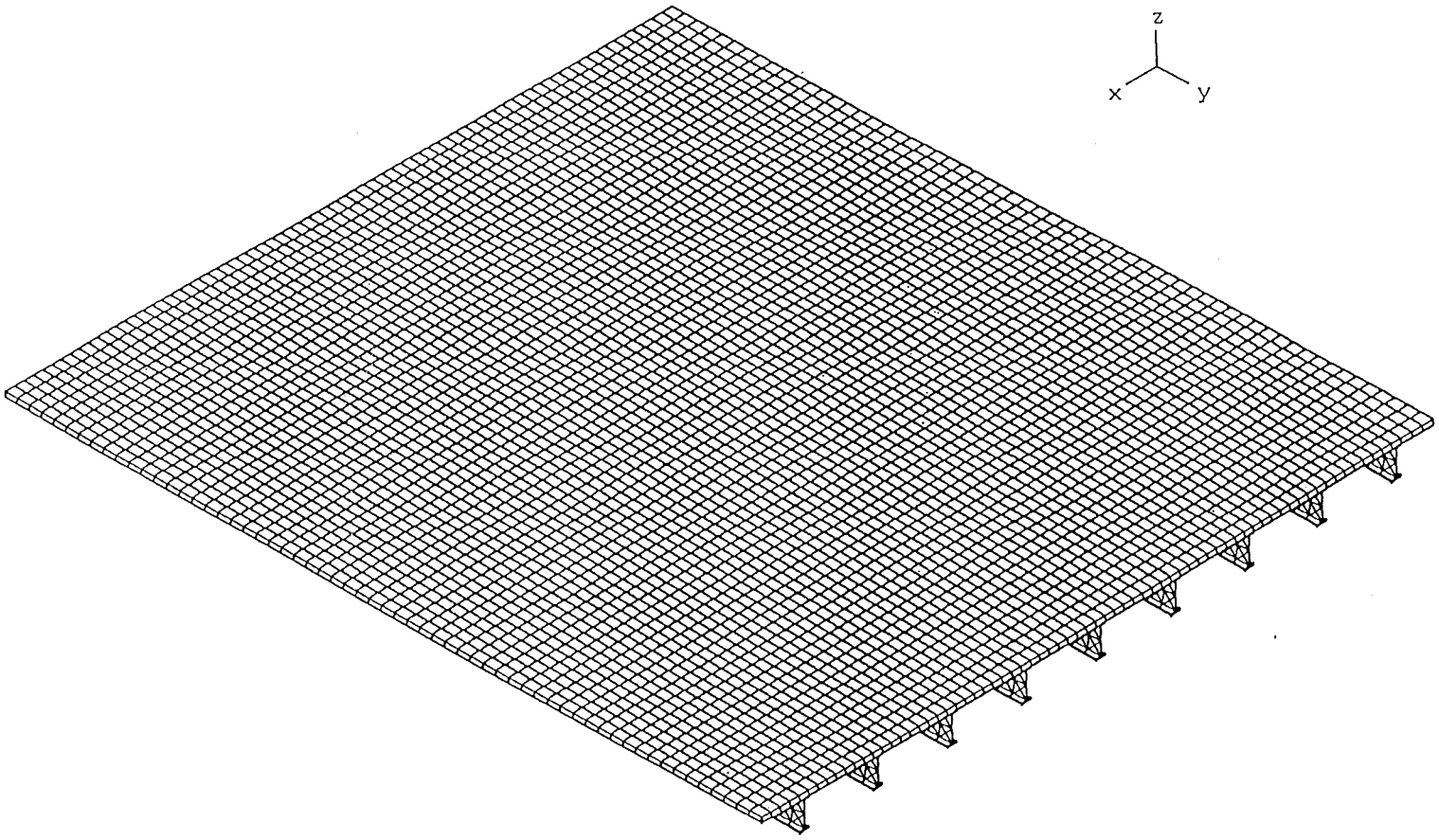

Figure 7.1. FEM Model of I-65 Bridge over Second Avenue

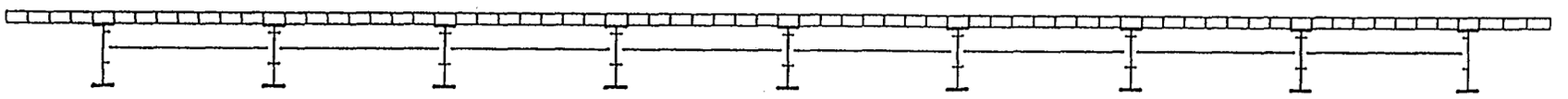

Figure 7.2. Typical Cross Section of FEM Model

width of the deck slab. The cracked moment of inertia of the deck slab was calculated using the reinforcement details from the bridge drawings.

The FEM analyses were conducted on the Alabama Supercomputer Authority (ASA) Cray C90 Supercomputer through implementation of the ADINA (ADINA, 1990) finite element computer programs. Three different dynamic analyses were performed for this case study. A frequency analysis was conducted first to establish the dynamic characteristics of the bridge and for comparison of the predicted free vibration response with recorded field data. The two remaining (transient) dynamic analyses corresponded to the passing of the test truck across the bridge.

To establish the dynamic characteristics of the bridge and determine an appropriate time step to use in the transient analyses, a frequency analysis was first conducted. Since the structure was symmetrical about midspan, only one half of the FEM model was employed in the frequency analysis. Sixteen frequencies and mode shapes were extracted in the frequency analysis by the subspace iteration technique (Bathe, 1996). The fundamental frequency was the flexural torsional mode exhibiting a natural period of 0.257 seconds. The mode shape corresponding to this vibration mode is illustrated in Figure 7.3. A time history for a strain gage located on the bottom flange of girder seven in the actual bridge structure is presented in Figure 7.4. This time history is a recording of the flexural strains on the tension flange of the girder as the test truck passed over the bridge. The natural period of vibration calculated from this trace is approximately 0.25 seconds, which agrees quite favorably with that predicted by the FEM model.

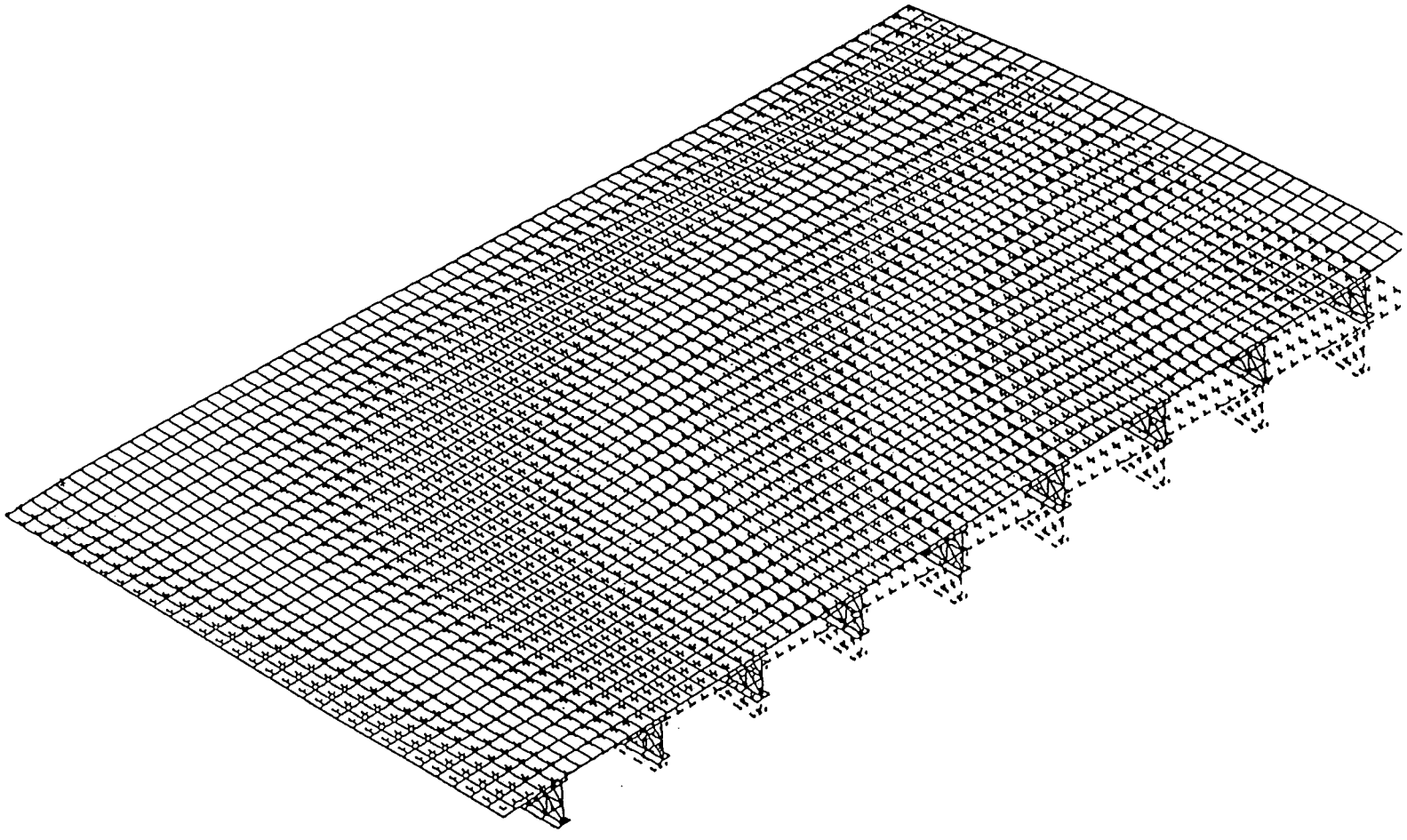

Figure 7.3. Flexural - Torsional Vibration Mode Shape

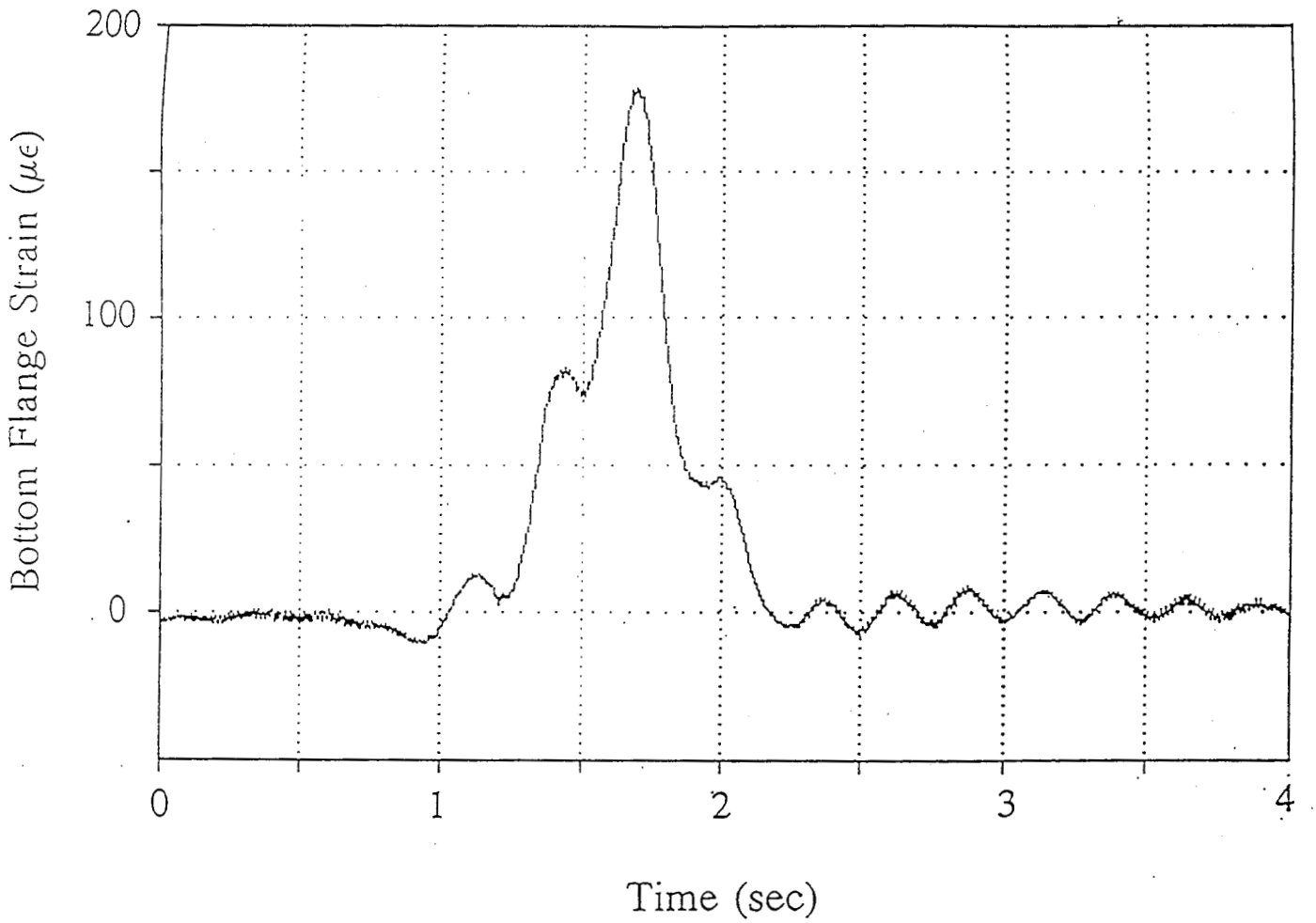

Figure 7.4. Field Measurement of Bottom Flange Strain in Girder G7

To further verify the accuracy of the FEM results, transient analyses were conduced with the ALDOT test truck passing over the bridge at a speed of 88 kph (55 MPH). The test truck was a three-axle truck loaded with concrete blocks having a total weight of 346.3 kN. An illustration of the test truck and its axle configuration are presented in Figure 2.11. The test truck itself was not modeled, the transient loads were simulated as a network of traveling loads and masses consistent with the truck configuration and its position on the bridge as a function of time. The results of the FEM analyses were then compared with corresponding results obtained from the actual field tests.

The transient dynamic analyses conduced on the FEM model utilized the Newmark method of direct numerical integration to evaluate the differential equations of motion, with Rayleigh damping. The amount of damping to implement into the FEM model was determined from analysis of the field results. A logarithmic decrement (Clough and Penzien, 1993) was applied to the amplitude decay of the free vibration strain traces of the field data (Figure 7.4) to obtain a damping factor. For all bridges examined the damping factor was in the range of 1.7% to 2.1% of critical damping. The Rayleigh damping coefficients were determined by using the observed damping at the fundamental frequency of the bridge, and 5% damping at a frequency of 20Hz. The damping factor of 5% at 20Hz was selected to decrease the effect of the higher modes in the model, which exist only in a mathematical sense.

Comparisons of the dynamic FEM results with field test data are presented in Tables 7.1 and 7.2. Table 7.1 illustrates the comparison of maximum bottom flange girder stresses at midspan for girder G4 with the test truck in lane two and for girder

Table 7.1. Maximum Bottom Flange Stresses in Girders at Midspan (MPa)

Girder	Field Measurements			FEM Results		
	With Diaphragms	Without Diaphragms	Percent Difference	With Diaphragms	Without Diaphragms	Percent Difference
G4	23.7	26.8	13.1%	23.1	24.6	6.5%
G6	15.5	15.1	-2.6%	12.9	12.6	-2.3%

Table 7.2. Maximum Girder Deflections at Midspan (mm)

Girder	Field Measurements			FEM Results		
	With Diaphragms	Without Diaphragms	Percent Difference	With Diaphragms	Without Diaphragms	Percent Difference
G4	8.5	9.0	5.9%	9.4	9.9	5.3%
G6	6.6	6.8	3.0%	6.3	6.5	3.2%

G6 with the test truck in lane three. Table 7.2 illustrates the comparison of girder midspan deflections for the same conditions described for Table 7.1. Excellent correlation with the FEM results and field test data is noted, thus again verifying the accuracy of the FEM results.

STATIC FEM ANALYSES

Although a more realistic method of analyzing FEM bridge models, dynamic analyses are much more computationally intensive than static analyses. In order to analyze as many different bridge types as possible, static analyses were employed for the parametric study of the load distribution effects of diaphragms in multi-girder steel bridges.

For each bridge investigated in the static analyses, the load truck was placed so that the greatest longitudinal moment was induced at midspan in the bridge. For the simple span bridges, this meant locating the second of the three axles of the truck at midspan. For multispan bridges, the location of the truck that produces maximum moment was determined by using the influence line for maximum moment at midspan. The location of the truck across the transverse dimension of the bridge was varied to insure obtaining the maximum flange stress and deflection in each girder. Multiple load cases were analyzed with the truck centered at eight points between each girder.

The results of these analyses are presented in influence line plots for each girder. The plots, such as Figure 7.5, depict the girder bottom flange stress at midspan versus the transverse location of the center of the truck. (Note that the girder numbering in Figures 7.5 through 7.9 is opposite that presented in Chapter Five.)

Similar influence lines generated for midspan girder deflections exhibited the same trends as the girder stress plots and therefore are not presented in this report.

The effect of diaphragm removal on slab deck bending moment in a typical simple span bridge was also investigated. Influence lines for transverse slab bending moment were generated for each panel across the midspan width of the bridge.

SIMPLE SPAN BRIDGES

A total of five simple span straight girder bridges were analyzed. The first bridge analyzed in this manner was the long, wide simple-span bridge A1 previously described in this chapter. The results of these analyses for girders G1 through G5 are presented in Figures 7.5 through 7.9, respectively. As shown in Figure 7.5, the exterior (fascia) girders exhibit little effect on the maximum stresses from the removal of the diaphragms. Girders 2 and 5 displayed increases in maximum stress (and deflection) of approximately 11%. The increase in girder 3 was approximately 9%, while the stresses for girder 4 increased about 10%. The center girder G5 exhibited an increase in bottom flange stress at midspan of approximately 9%, as shown in Figure 7.9.

As these figures clearly illustrate, removal of the diaphragms increases the bottom flange stress approximately 8% on average. The first interior girders tend to exhibit a slightly greater stress increase than the other interior girders, although the exterior girders showed essentially no increase in maximum stresses.

The second simple span bridge investigated, A2, was a modified version of bridge A1. The width of A1 was reduced to 12.2 m, allowing for only two lanes of traffic. The results of the FEM analyses for girders G1 through G3 are presented in

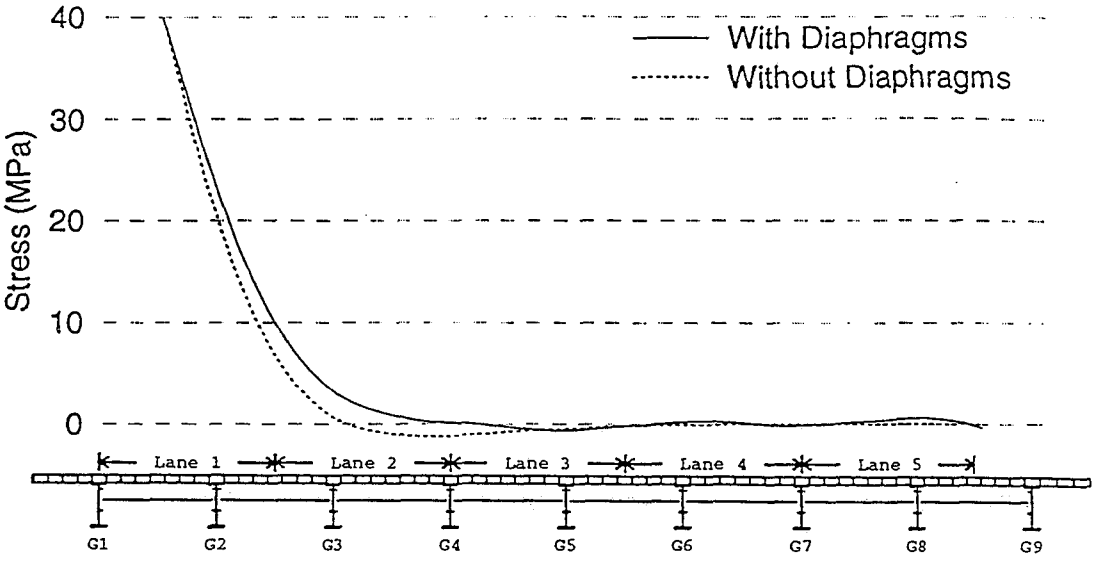

Figure 7.5. Influence Line for Bottom Flange Stress in Girder G1 of Bridge A1

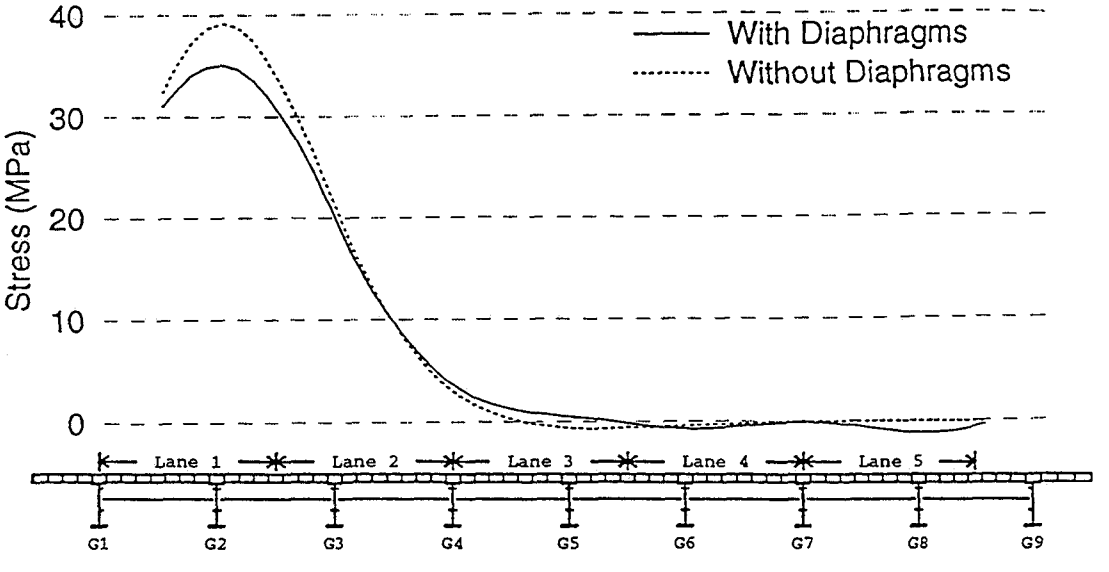

Figure 7.6. Influence Line for Bottom Flange Stress in Girder G2 of Bridge A1

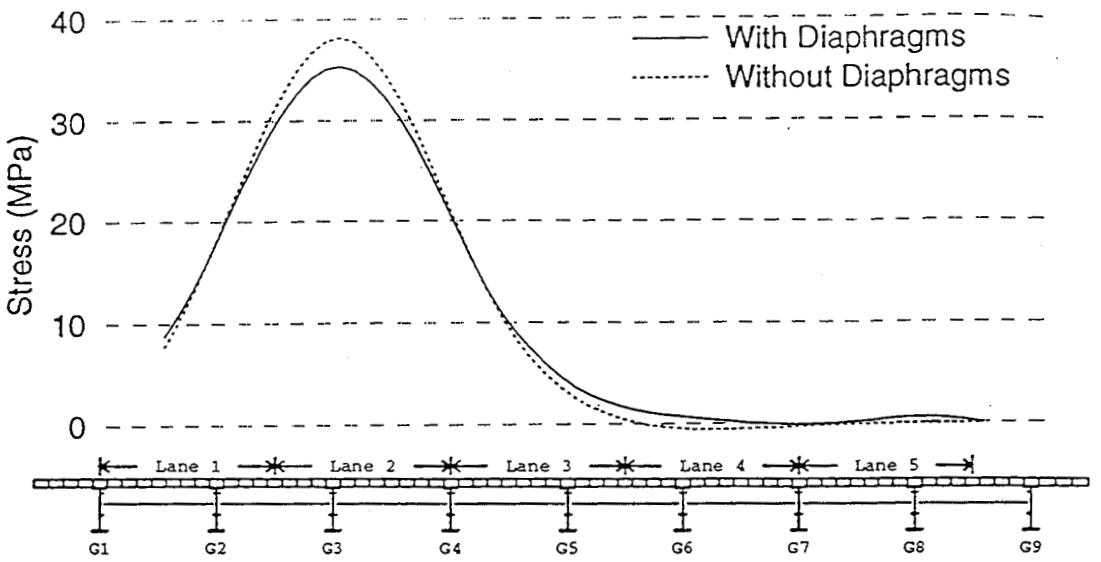

Figure 7.7. Influence Line for Bottom Flange Stress in Girder G3 of Bridge A1

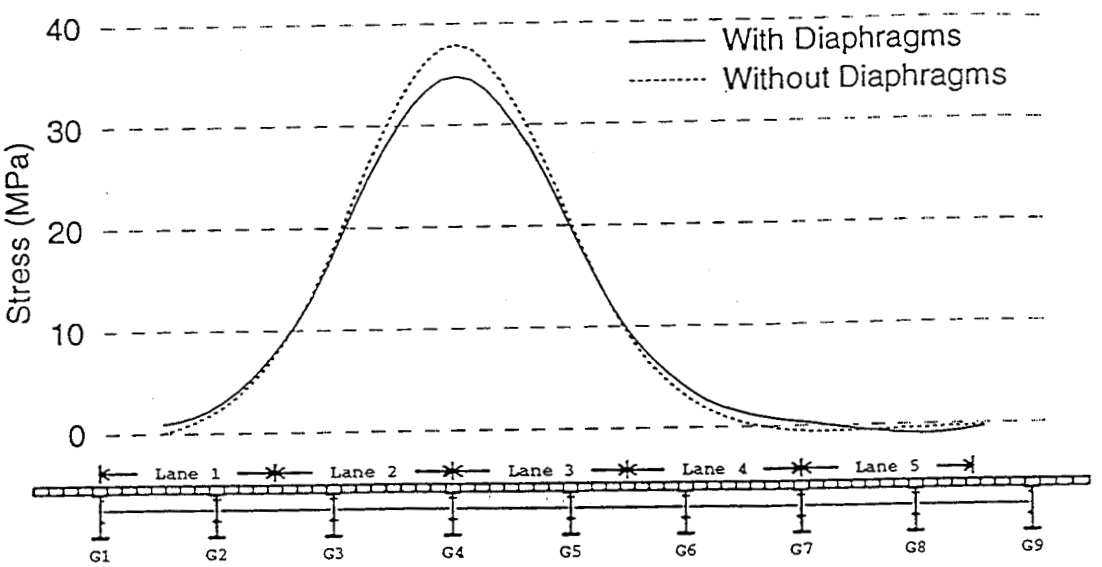

Figure 7.8. Influence Line for Bottom Flange Stress in Girder G4 of Bridge A1

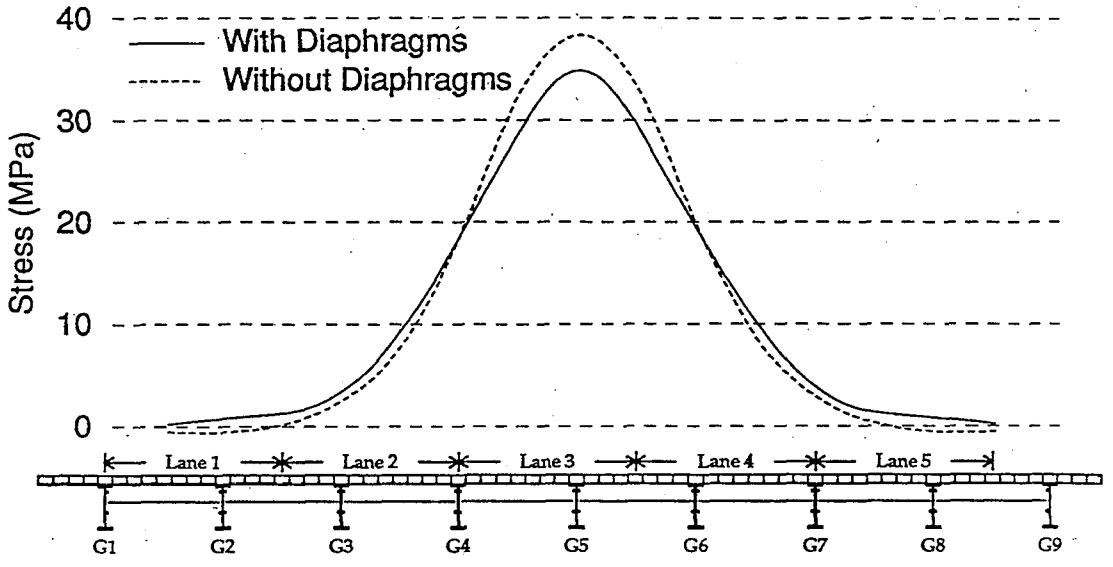

Figure 7.9. Influence Line for Bottom Flange Stress in Girder G5 of Bridge A1

Figures C.1 through C.3, respectively. Similar to the observation for bridge A1, the exterior girder exhibited little effect from diaphragm removal. The stresses in girder G2 increased 15% with diaphragm removal, while the center girder exhibited an increase of approximately 8%. Once again, the stress increase in the center girder G3 was slightly less than that in girder G2, with the exterior girder G1 experiencing very little effect.

To assess the effects of diaphragm removal on simple spans with fewer lines of diaphragms, a shorter span was also investigated in the static analysis. This 15.0 m span, referred to as A3, was located adjacent to span A1 in the northbound I-65 viaduct near Second Avenue South in Birmingham. The span consists of nine W840 x 176 (W33 x 118) girders with a 165 mm thick deck slab and has one line of MC460 x 63.5 (MC18 x 42.7) diaphragms. The results of the FEM analyses are presented in

Figures C.4 through C.8, for girders G1 through G5, respectively. The increases in flange stresses for the shorter span are consistently less than the corresponding increases in the longer span (bridge A1). The largest increases, approximately 5%, occurred in girder G2. The increase in girder G3 was minimal, around 3%, and the maximum stresses in the exterior girders were not affected by removal of the diaphragms.

Bridge A3 was also modified by reducing its width to 12.2 m with five girders and two lanes of traffic and is referred to as bridge A4. The results of the FEM analyses for girders G1 through G3 are presented in Figures C.9 through C.11, respectively. The exterior girders, again, experienced little effect from the removal of the diaphragms. As with bridge A3, the stresses in the middle girder, G3, increased very slightly, while the first interior girder (G2) had the largest increases, around 7%.

An additional, medium-sized simple span was also analyzed, referred to as bridge A5. This bridge was Span 84 of the Central Business District viaduct on I-20/59 South. The 20.2 m span has a 178 mm thick deck slab supported on eight W920 x 223 (W36 x 150) girders spaced at 2.65 m with three lines of diaphragms. The results of the FEM analyses for girders G1 through G4 are presented in Figures C.12 through C.15, respectively. The exterior girder exhibited no appreciable effect from the removal of the diaphragms. The interior girder, G3, experienced a stress increase of about 3%, while the increase in the first interior girder, G2, was slightly higher at about 5%.

The effect of diaphragm removal on the transverse bending moment in the deck slab of bridge A1 was also investigated. Of specific interest was the transverse section

of deck slab over the midspan diaphragm line. Influence lines for both positive and negative slab bending moments, in one exterior and three interior slab panels, are presented in Figures C.16 through C.27.

The largest increases in positive moment occurred in the center of the panels (Figures C.17, C.20, C.23, and C.26). The maximum increase in positive moment was approximately 15 - 20%, which was experienced by the exterior panels as illustrated in Figure C.17. There were only marginal increases in the positive moments at locations directly over the beams due to diaphragm removal. Conversely, diaphragm removal generally decreased the negative moments in the slab as illustrated in Figures C.18, C.19, C.21, C.22, C.24, and C.25.

In summary, the maximum positive slab moments, which occur midway between adjacent girders, increased approximately 15 to 20% due to diaphragm removal. The maximum positive slab moments are nearly three times as large as the maximum negative slab moments. These negative slab moments, which occur over the girders, exhibited a general decrease as a result of diaphragm removal.

SKEWED SIMPLE SPANS

The FEM analysis was extended to skewed simple span bridges. A total of four skewed simple spans were investigated. The first of the skewed simple spans analyzed, B1, was span 10 of the railroad viaduct on I-65 North in downtown Birmingham. The 30.2 m span is skewed 30.6 degrees with nine W920 x 417 (W36 x 280) girders with coverplates spaced at 2.44 m and five lines of diaphragms. The deck slab is 165 mm thick. The FEM results are presented in Figures 7.10 through 7.14 for girders G1 through G5, respectively. Again, the exterior girders were affected only

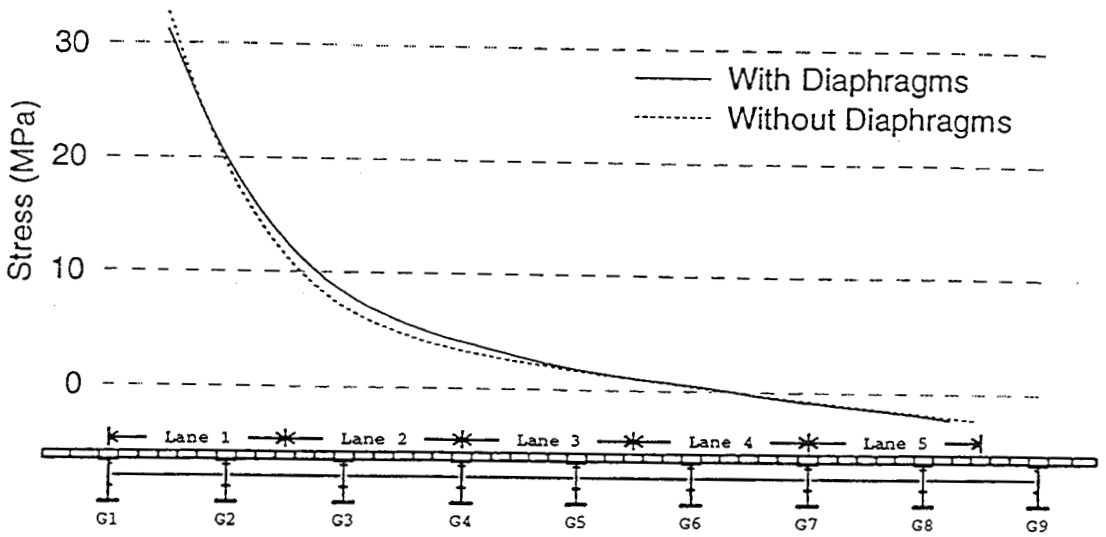

Figure 7.10. Influence Line for Bottom Flange Stress in Girder G1 of Bridge B1

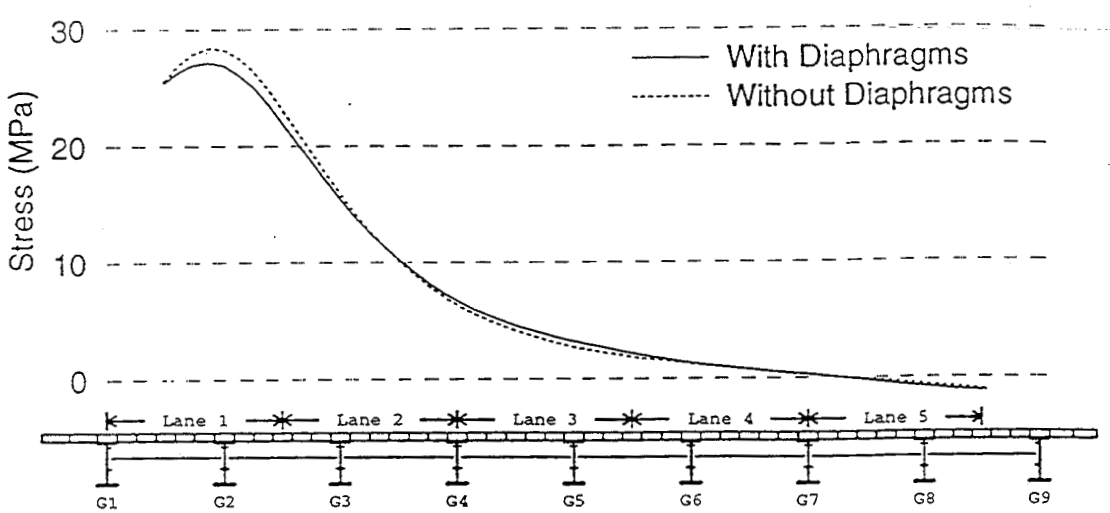

Figure 7.11. Influence Line for Bottom Flange Stress in Girder G2 of Bridge B1

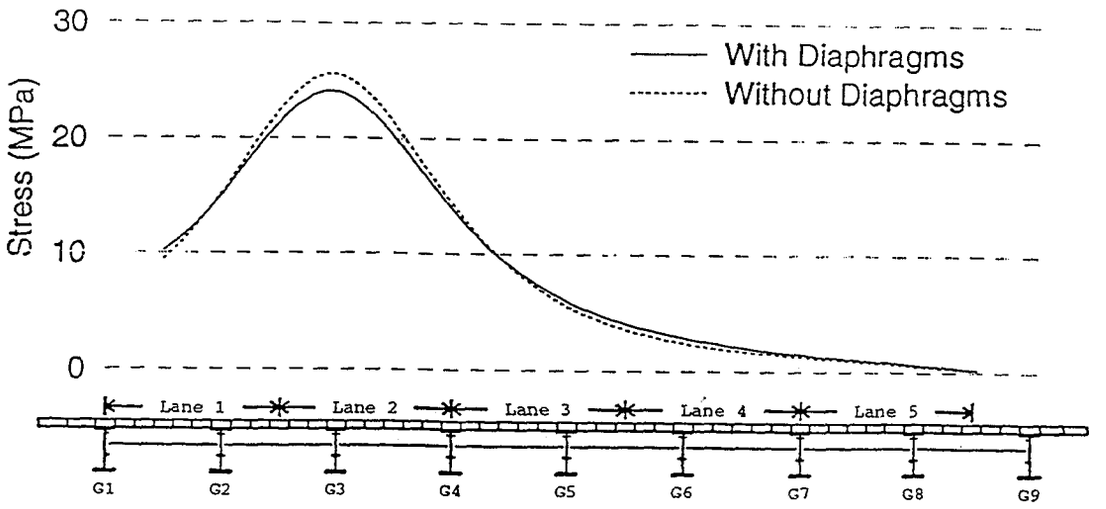

Figure 7.12. Influence Line for Bottom Flange Stress in Girder G3 of Bridge B1

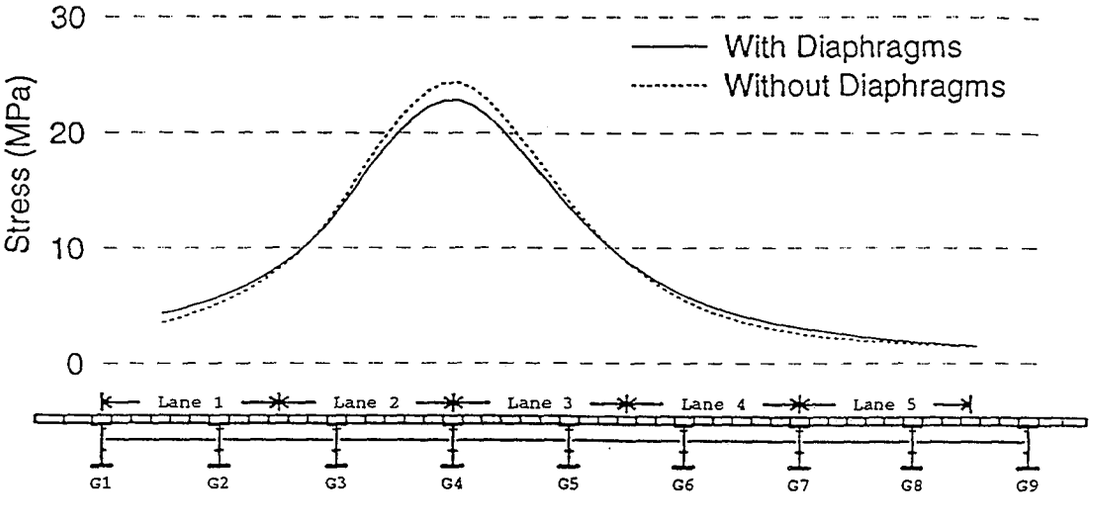

Figure 7.13. Influence Line for Bottom Flange Stress in Girder G4 of Bridge B1

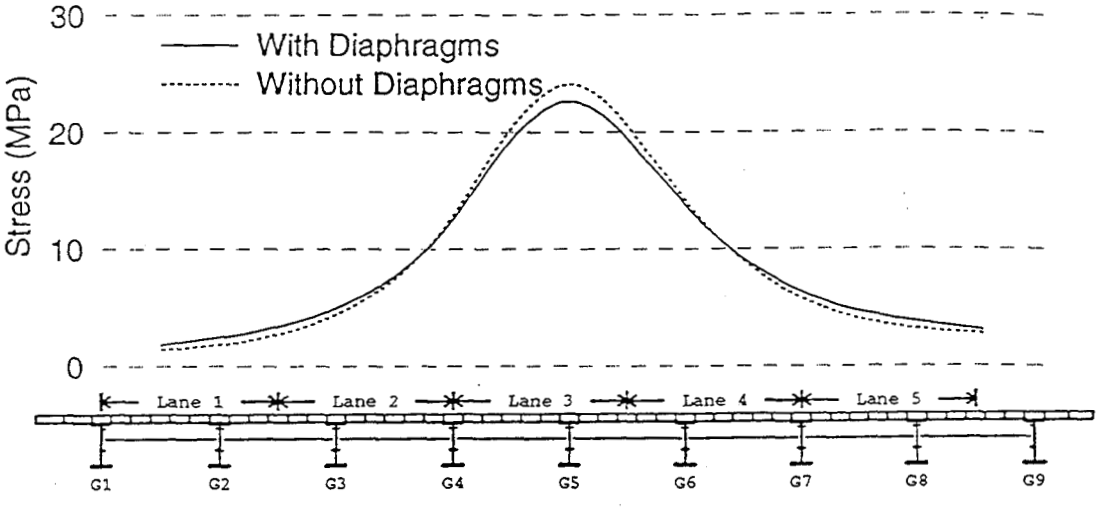

Figure 7.14. Influence Line for Bottom Flange Stress in Girder G5 of Bridge B1

slightly by removal of the diaphragms, and the bottom flange stresses in all of the interior girders increased approximately 5%.

As with the unskewed bridges, the nine girder span was modified to a five girder version and analyzed to investigate the effect of diaphragm removal on a narrow skewed bridge. This bridge is referred to as B2. Again, the spacing of the girders was maintained at 2.44 m, and the girder sizes remained the same. The results of the FEM analyses for girders G1, G2, and G3 are presented in Figures C.28 through C.30, respectively. Consistent with the previous analyses, the exterior girders experienced no effect from the diaphragm removal. The stresses in the interior girders increased about 4%.

To assess the effects of diaphragm removal on shorter span skew bridges, another bridge was chosen for analysis. This bridge, B3, carries the four northbound

lanes of I-65 over Eighth Street South and is located approximately 1 km south of spans A1, A3, and B1. The 21.7 m span is skewed 30.6 degrees and consists of a 165 mm thick slab on eight W920 x 201 (W36 x 135) girders with three lines of diaphragms. The results of the analyses for girders G1 through G4 are presented in Figures C.31 through C.34, respectively. These results were similar to the results of the previous analyses, B2, in that the exterior girders were not affected by diaphragm removal, and the stress increases in the interior girders were minimal. Also, the first interior girder, G2, experienced a slightly greater stress increase after removal of the diaphragms, about 4%.

Bridge B3 was also modified into a narrower version, referred to as Bridge B4, with five girders at the same 2.21 m spacing and a total width of 10.7 m. The FEM results for girders G1, G2, and G3 are presented in Figures C.35 through C.37, respectively. Comparison of the bottom flange stress and deflections at midspan displayed the same trends as previous analyses. The maximum stresses in the exterior girders were not affected by removal of the diaphragms; the interior girders experienced minimal increases. Furthermore, it is noted that the first interior girder G2 experienced a slightly larger stress increase (approximately 4%) than the center girder G3.

From the results of the static analyses of the right and skewed simple span bridges, several trends have appeared. First, the maximum stresses and deflections in the exterior girders were not significantly affected by diaphragm removal. Due to the amount of lateral clearance required for the load truck, it was never centered directly above the exterior girder. Therefore, the exterior girders never experienced the worst

case of loading, which would produce the greatest difference in results for the conditions with and without diaphragms. Second, the girders immediately adjacent to the exterior girders experienced the greatest increase in stress from removal of the diaphragms. This was because these girders were close enough to the edge of the bridge that the edge of the slab reduced the load distribution effect of the deck. Although this behavior would be even more pronounced in the exterior girders, the proximity of the curb precludes the worst case loading, as discussed previously.

Finally, inspection of these stress influence lines does indicate that the diaphragms distributed loads across the bridges to a certain extent. The influence lines for the models with diaphragms are somewhat smoother, while the models without diaphragms have influence lines with more noticeable peaks. When the truck was located away from a particular girder, the stresses in that girder were less in the no-diaphragm model. As the truck was moved closer to that girder, the difference in stress between the models decreased until the truck was centered about halfway between that girder and the adjacent girder. At that point, the stress in the no-diaphragm model exceeded the stress in the model with diaphragms. In most cases, the maximum increases in girder bottom flange stresses at midspan were less than 10%, with the largest increase of 15% occurring in the longest unskewed span.

CONTINUOUS SPAN BRIDGES

The FEM analyses were extended to include multi-girder, 3-span continuous bridges. Both composite and non-composite behavior was investigated. In each bridge the exterior spans, spans 1 and 3, are 22.3 m long; and the interior span, span 2, is 31.7 m in length. These continuous bridge models are based upon the 3-span

CBD bridge on I-65 located adjacent to the Birmingham Civic Center. Two variations of the bridge were investigated: (1) a wide eight girder four lane bridge, and (2) a narrow five girder two lane bridge.

For the static analyses conducted on these bridges, the test truck loading was placed at two different locations along the length of the bridge. At the first location, the second of the three truck axles was placed approximately 4.6 m before the second bent on span 1. This positioning created the largest midspan girder moments for span 1. The second location positioned the second axle of the test truck exactly at midspan of the center span (span 2). This condition created the largest positive midspan girder moment in span 2.

The first continuous bridge investigated, bridge C1, was a four lane non-composite bridge. Influence lines for midspan girder stresses for girders G1 through G4 are presented in Figures 7.15 through 7.18, respectively, for span 1 with the truck positioned on span 1. Similar results are presented in Figures C.38 through C.41 for span 2 with the truck positioned on span 2.

Similar to the simple span results, the exterior girders in this bridge showed no increase in the maximum stress. The interior girders all showed a consistent increase of approximately 5% in stress due to diaphragm removal, with the girders immediately adjacent to the exterior girders showing a little higher increase (approximately 6%). The relative increases in negative moment stresses at midspan (when the truck was placed on span 2) were more pronounced. However, the negative moments in span 1 girders were generally less than a fourth of the positive moments. Overall, the increases in girder stresses in the center span were higher than in span 1, but the

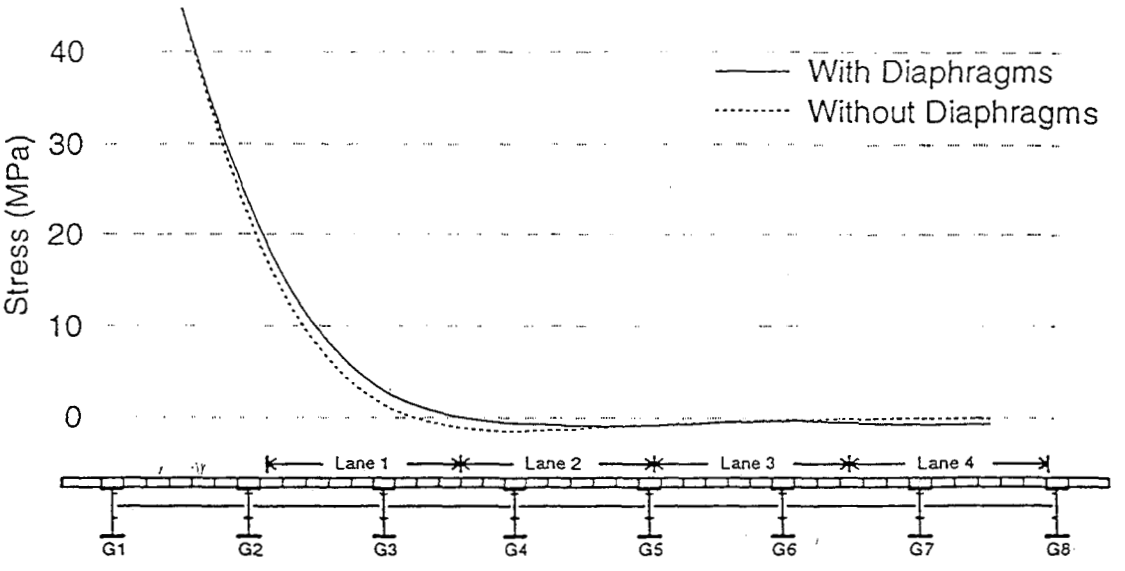

Figure 7.15. Influence Line for Bottom Flange Stress: Girder G1, Span 1, Bridge C1; Truck on Span 1

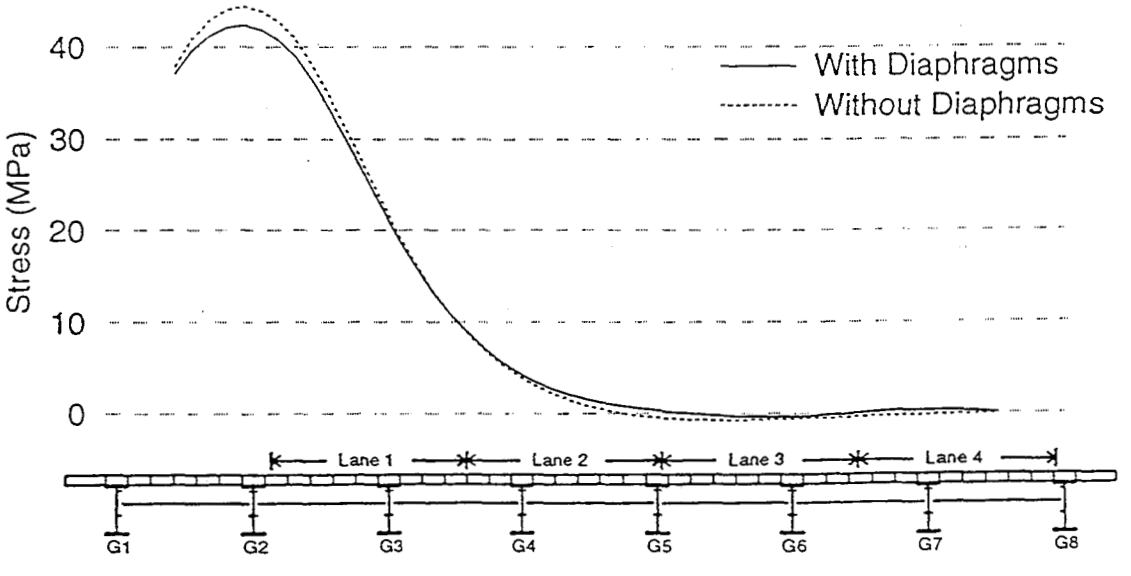

Figure 7.16. Influence Line for Bottom Flange Stress: Girder G2, Span 1, Bridge C1; Truck on Span 1

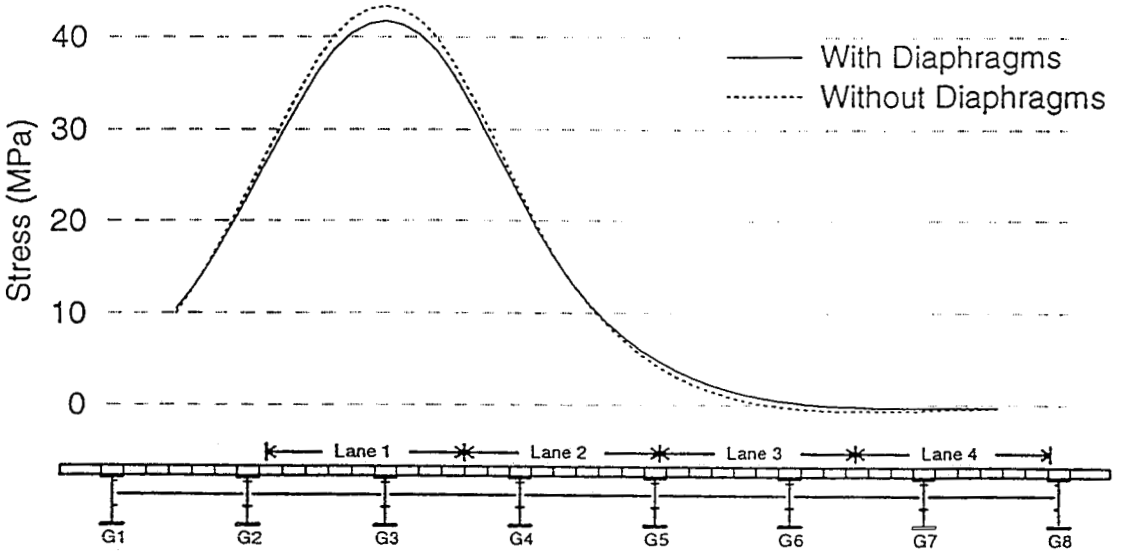

Figure 7.17. Influence Line for Bottom Flange Stress: Girder G3, Span 1, Bridge C1; Truck on Span 1

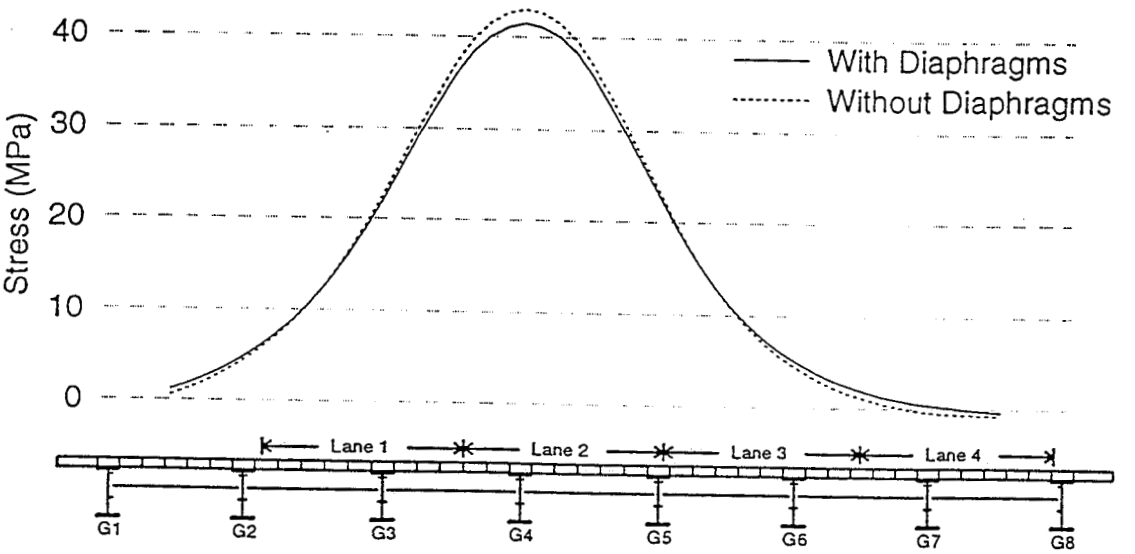

Figure 7.18. Influence Line for Bottom Flange Stress: Girder G4, Span 1, Bridge C1; Truck on Span 1

increases were still only about 7%. Also, the percent increase in negative moment girder stresses at midspan were higher, but the actual magnitude of the stress increases were insignificant.

The next continuous span bridge analyzed, C2, was the same as C1 except that bridge C2 was composite. The FEM results for girders G1 through G4 for span 1 with the truck positioned on span 1 are presented in Figures 7.19 through 7.22 respectively. Similar results for span 2 with the truck positioned on span 2 are presented in Figures C.42 through C.45.

In general, the increases in both the positive moment and negative moment girder stresses at midspan in the composite bridge were greater, about 8% in span 1 and 13% in span 2, than in the noncomposite counterparts. Because of composite action the tensile stresses in the flanges are less in bridge C2 than in bridge C1. The increased girder stiffness in the composite bridges is responsible for the larger relative increase in girder stresses. If the stiffness of the slab between the girders is the same in both bridge types, but the girder stiffness is increased by composite action, then more of the load is taken by the girder directly beneath the wheel, and less is distributed by the deck slab.

The next bridge analyzed, bridge C3, was a two lane, five girder, non-composite bridge. The span 1 results for girders G1 through G3, for the truck on span 1, are presented in Figures 7.23 through 7.25, respectively. The results for girders G1 through G3 in span 2 for the truck on span 2 are presented in Figures C.46 through C.48, respectively.

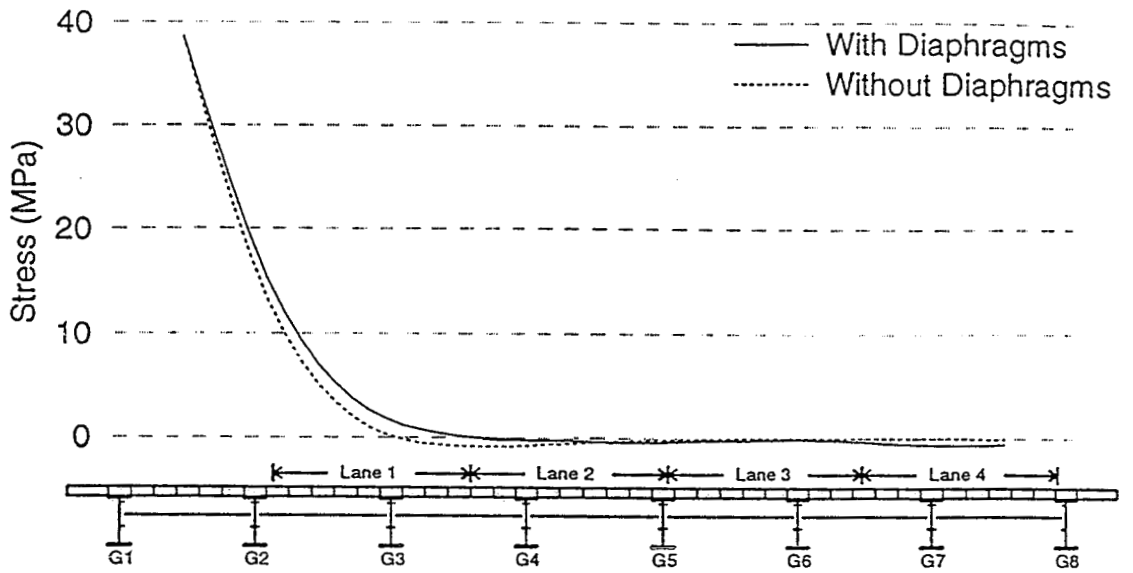

Figure 7.19. Influence Line for Bottom Flange Stress: Girder G1, Span 1, Bridge C2; Truck on Span 1

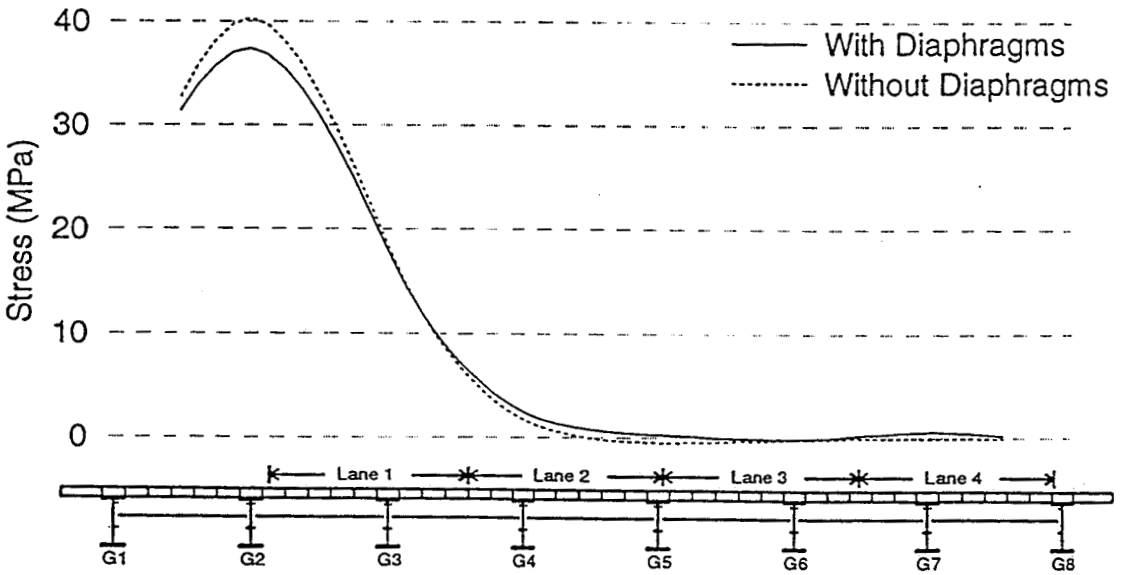

Figure 7.20. Influence Line for Bottom Flange Stress: Girder G2, Span 1, Bridge C2; Truck on Span 1

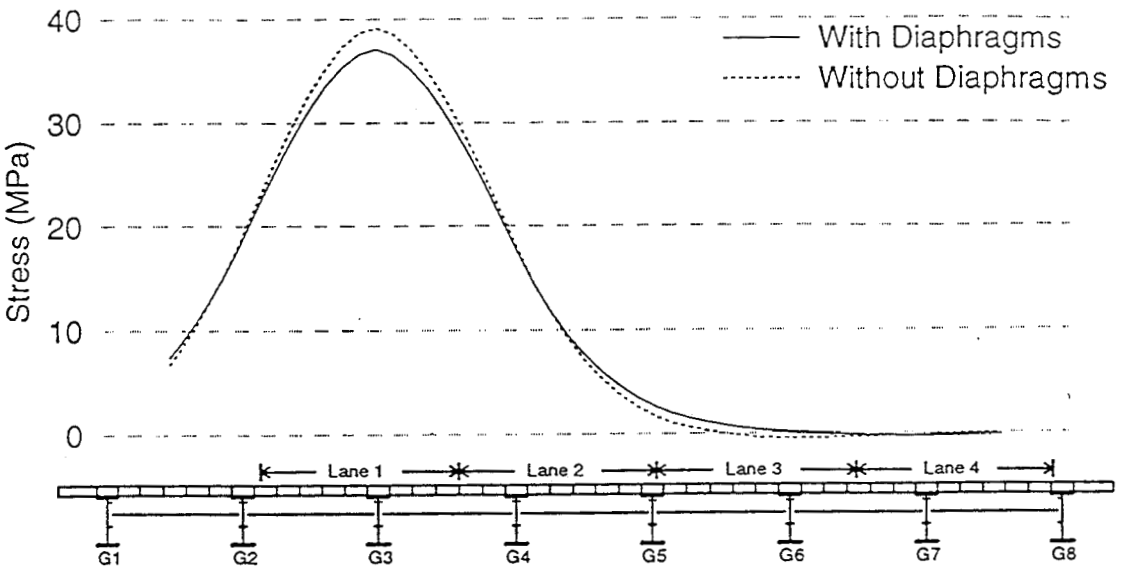

Figure 7.21. Influence Line for Bottom Flange Stress: Girder G3, Span 1, Bridge C2; Truck on Span 1

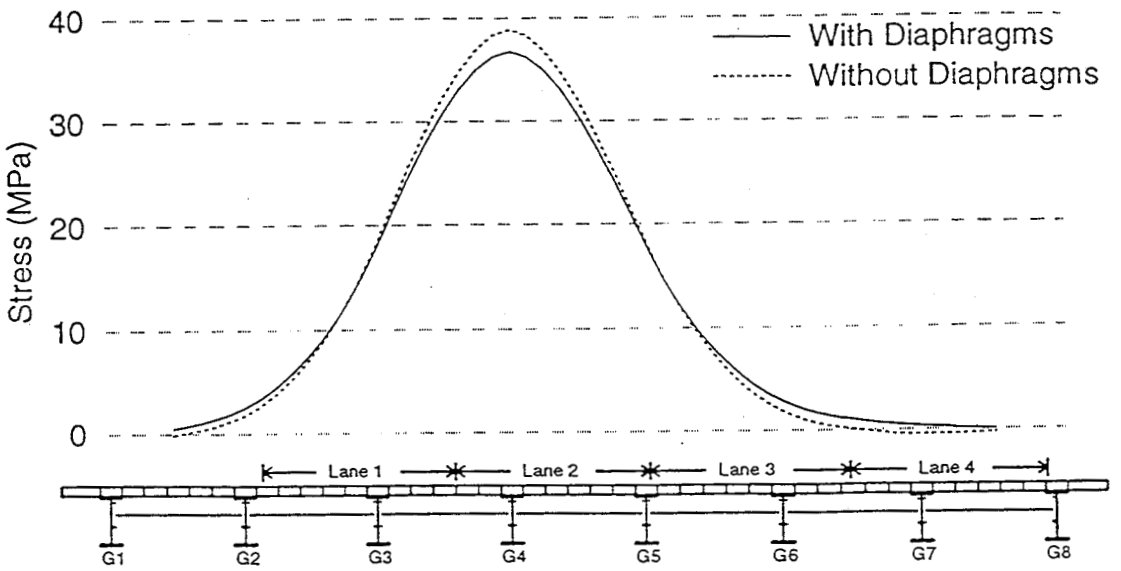

Figure 7.22. Influence Line for Bottom Flange Stress: Girder G4, Span 1, Bridge C2; Truck on Span 1

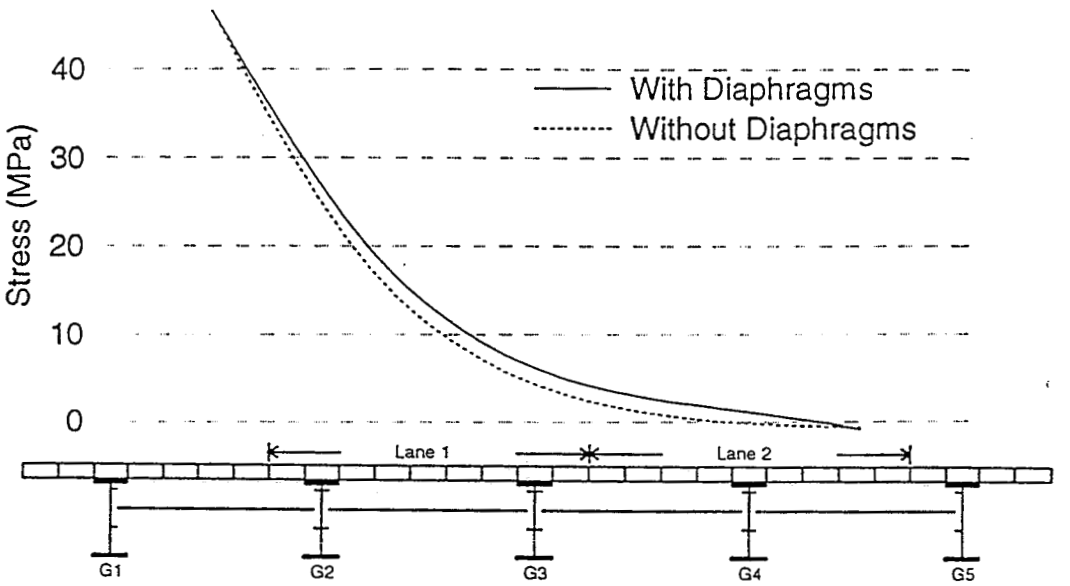

Figure 7.23. Influence Line for Bottom Flange Stress: Girder G1, Span 1, Bridge C3; Truck on Span 1

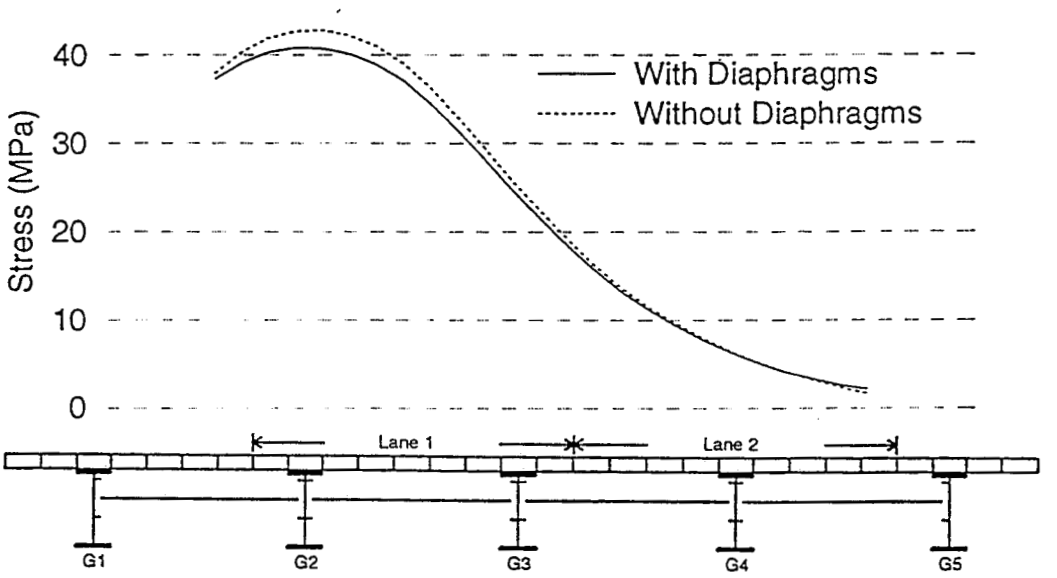

Figure 7.24. Influence Line for Bottom Flange Stress: Girder G2, Span 1, Bridge C3; Truck on Span 1

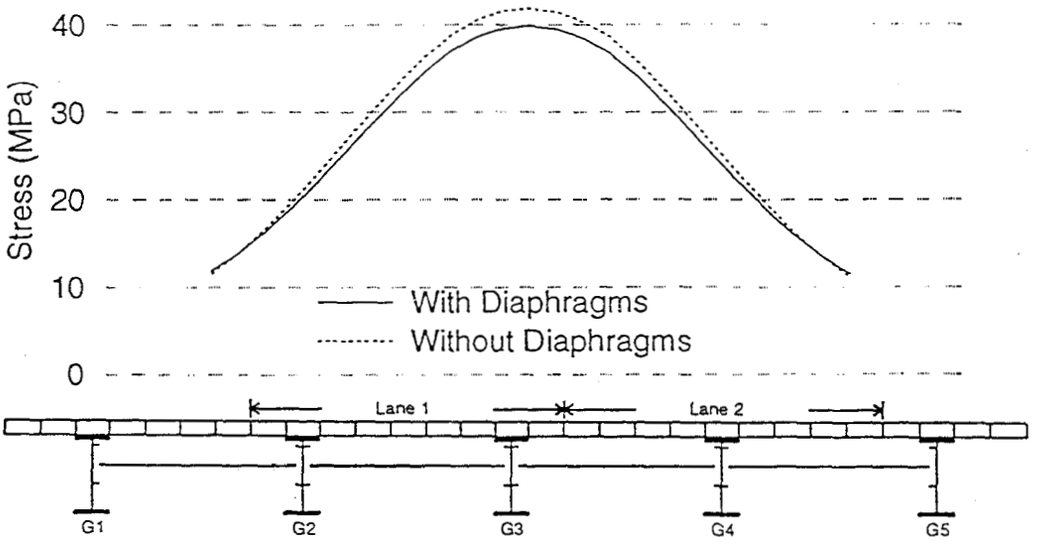

Figure 7.25. Influence Line for Bottom Flange Stress: Girder G3, Span 1, Bridge C3; Truck on Span 1

The narrower bridge exhibits a more pronounced edge effect on the second and fourth of the five girders, as was seen in the simple span bridges. These girders experience increases of approximately 8% in stress. The point of maximum influence for the model without diaphragms is directly above the girder, but in the model with diaphragms it is slightly outside of the girder. This illustrates that the diaphragm in the space between the exterior girders has the greatest effect on local load distribution than any other of the diaphragms. This is verified by the largest stress increases occurring at the first interior girder.

The last continuous bridge analyzed, bridge C4, was the composite version of bridge C3. The influence lines for midspan girder stresses for girders G1 through G3 are presented in Figures 7.26 through 7.28, respectively, for span 1 with the truck on

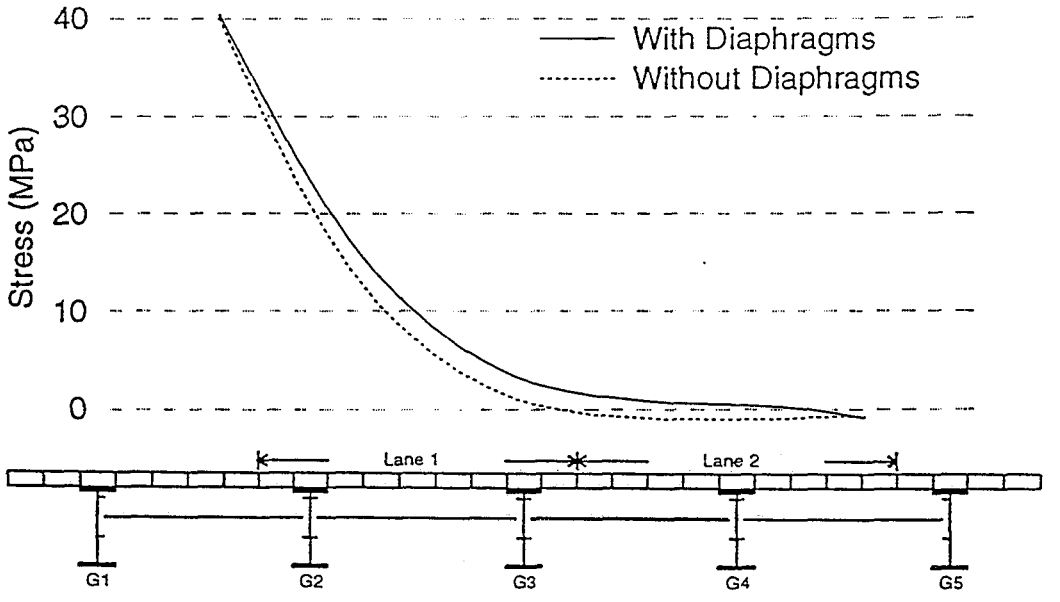

Figure 7.26. Influence Line for Bottom Flange Stress: Girder G1, Span 1, Bridge C4; Truck on Span 1

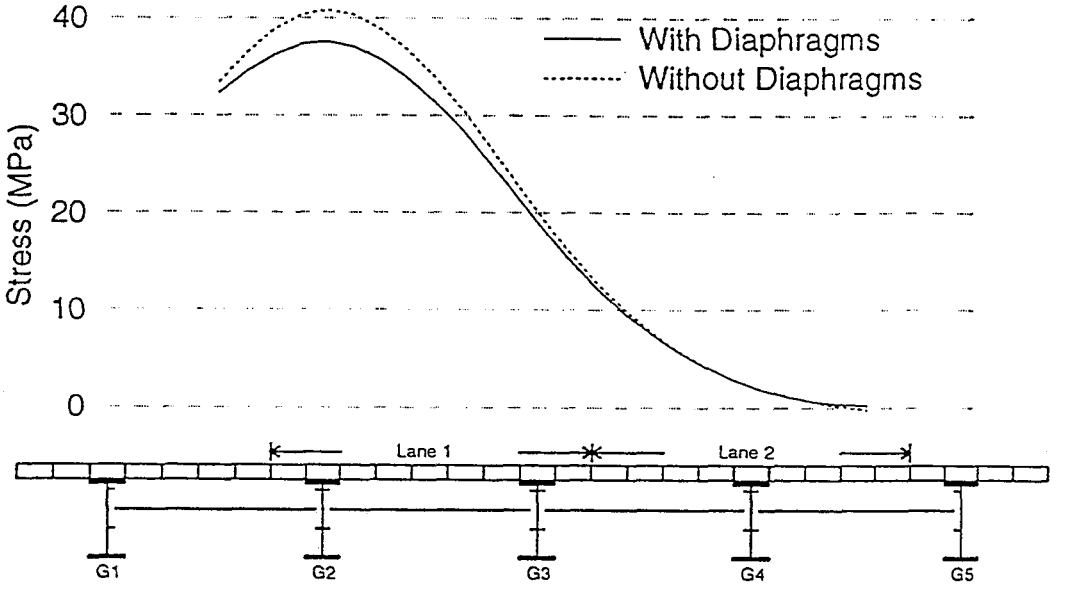

Figure 7.27. Influence Line for Bottom Flange Stress: Girder G2, Span 1, Bridge C4; Truck on Span 1

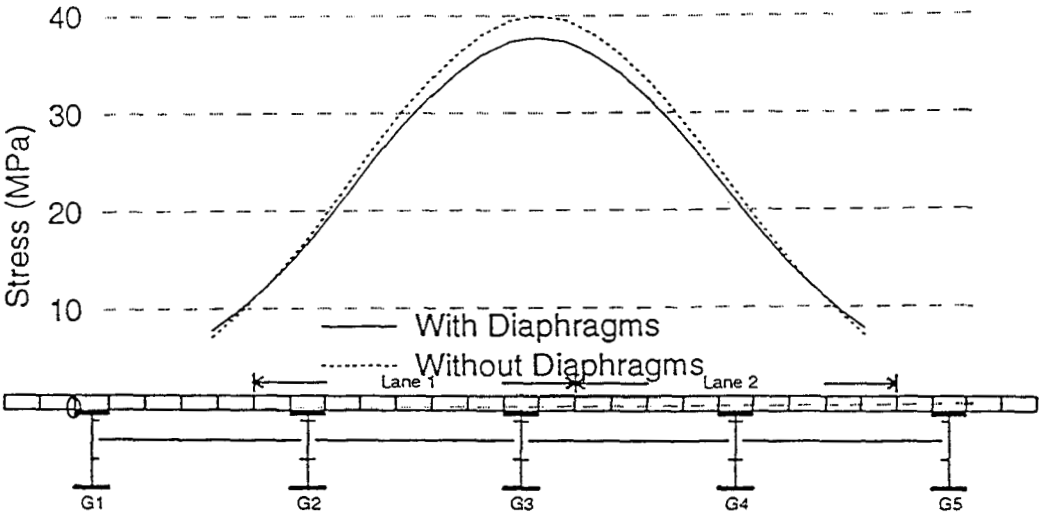

Figure 7.28. Influence Line for Bottom Flange Stress: Girder G3, Span 1, Bridge C4; Truck on Span 1

span 1. Similar results for span 2 with the truck on span 2 are presented in Figures C.49 through C.51. This model exhibited the highest stress increases due to a combination of the composite action and the narrow width. The increases in the first interior girders were approximately 10%, and the center girder showed an increase of about 7%.

For all composite bridges investigated, the exterior girders appeared to be relatively insensitive to diaphragm removal. The interior girders of the noncomposite bridges experienced increases in positive moment stresses of approximately 6 to 7 percent, with slightly higher increases in negative moment midspan girder stresses. For the composite bridges, the increases in girder stresses due to diaphragm removal

were slightly higher than those exhibited by their noncomposite counterparts, approximately 8 to 10 percent.

CONCLUSIONS

The overall effect of diaphragm removal on both simple span and continuous span bridges appears to be limited. The exterior girders are virtually insensitive to diaphragm removal. The increase in positive bending moment stress for an interior girder in a simple span bridge was 14%. However, the average increase was generally less than 8%. Simple span skewed bridges were even less sensitive to diaphragm removal.

Interior girders of continuous bridges experienced average increase in positive moment stresses of approximately 7% and 10%, respectively, for noncomposite and composite bridges percent. Increases in the negative bending moment stresses at midspan were just slightly greater, however, their actual magnitudes were substantially less than the positive moment stresses.

The most significant effect of diaphragm removal was on the deck slab transverse bending moments in the simple span bridges. The maximum positive slab moments increased approximately 15 to 20%. However, the negative slab moments generally decreased as a result of diaphragm removal.

CHAPTER EIGHT

CONCLUSIONS AND RECOMMENDATIONS

CONCLUSIONS

Field measurements of distortion-induced stresses were made at welded diaphragm-girder connections typical of the original bridge construction. The measured stresses were compared with laboratory test results of other researchers. These comparisons indicate the stress ranges at most connections are high enough that fatigue cracking is expected at additional connections and reinitiation of fatigue cracking is expected at some connections where hole drilling alone is used to repair fatigue cracks in the girder webs.

Fatigue cracking of bolted connection angles used to replace original welded connections was found to be strongly influenced by the gap between the leg of the connection angle and the girder web. The gap results from fit-up error, the installation procedure, and yielding of the angle due heavy trucks. A new angle design and installation procedure was proposed and tested in the laboratory and in the field. The new design performed better in the laboratory and field tests than the angle design most commonly used by ALDOT in previous repairs. The test results indicate that the likelihood of fatigue cracking of the new angle design is reduced but not eliminated. The new installation procedure was used to install four lines of diaphragms in an existing bridge, and the procedure appears practical.

Field installation and tests were performed using new diaphragms and connection angles installed at two different distances below the top girder flanges (web gap lengths). No significant difference resulted from the two different distances.

Hence, exiting holes in the girder webs for connection angle bolts drilled during previous repairs can be used for installing angles of the new design.

Removal of all interior diaphragms to eliminate fatigue damaged diaphragm-girder connections from composite simple span bridges is feasible. Field tests and Finite Element Method (FEM) analyses confirm that the increase in interior girder stresses resulting from complete diaphragm removal is approximately ten to 15 percent. Removal of all interior diaphragms from continuous span non-composite bridges is not feasible. For the bridges investigated, one line of diaphragms on each side of the interior supports is required for bracing against lateral-torsional buckling. The increase in stresses in typical interior girders is found to be approximately the same as for simple span bridges and does not represent a significant increase.

Changes in the live load stresses in the exterior girders in both simple and continuous span bridges are insignificant. This observation is important because the wind loading stresses on exterior girders are significantly increased by removal of interior diaphragms. Wind loading is not critical for the bridges investigated; however, the research results do show that a structural evaluation including loading combinations with wind loading must be investigated before removing all diaphragms from an existing bridge. An evaluation procedure is outlined in Chapter Four, Appendix A and Appendix B.

The increases in deck slab bending moments due to removing diaphragms are slightly greater (5 to 7 percent) than the stress increases experienced by the girders. From FEM analyses of a typical simple span bridge, the transverse positive bending moments midway between the girders increased approximately 15 to 20 percent. The

negative transverse moments over the girders decreased. These results are corroborated by theoretical results presented by Newmark (1946). Increased positive moments may shorten the remaining life of the deck, but are judged not to have a significant effect on the interstate highway bridges in Birmingham.

RECOMMENDATIONS

The following strategy for maintaining fatigue damaged diaphragm-girder connections in multi-girder bridges with rolled section girders and channel diaphragms is recommended based on the results of the research presented here.

Removal of interior diaphragms (not at supports) is recommended to eliminate unnecessary lines of interior diaphragms. Diaphragms at supports are necessary to resist transverse horizontal loads and should not be removed for any reason. The first line of diaphragms on each side of interior supports of continuous span girders are necessary for bracing against lateral-torsional buckling and should remain in-place. A structural evaluation should be performed on a candidate bridge to verify that combined dead load, live load and wind load stresses on the exterior girders are acceptable with the diaphragms removed. If these combined stresses are found unacceptable, removal of only some lines of diaphragms and/or all interior diaphragms except those between the exterior girder and first interior girder should be investigated.

Removal of only selected connections and diaphragms is desirable because maintenance costs are avoided, or delayed, at some connections. Removal of complete lines of diaphragms is not required. To repair fatigue cracking in parts of the connection other than the girder web, an individual diaphragm can be removed to eliminate the affected connection. To repair distortion-induced fatigue cracks in the

girder web, the diaphragms on both sides of the affected girder should be removed. The fatigue cracks in the girder web should be repaired by drilling a hole at the crack tips as in previous repairs.

Fatigue damaged connections at necessary lines of interior diaphragms should be replaced with a bolted connection of the new design proposed here. The connection angles should be installed by bolting to the girder web first then to the diaphragm to avoid creation of a gap between the connection angle and girder web. Connection angles should be installed with approximately a 90 mm gap between the top of the connection angle and the bottom of the top girder flange. This will allow existing holes from previous connection replacements to be utilized. Connections at both ends of an individual diaphragm should be replaced at the same time to avoid misalignment of the diaphragm. Fatigue cracks in the girder webs should be repaired by drilling a hole at the crack tips (as performed in previous repairs) before installing the new connections.

REFERENCES

American Association of State Highway and Transportation Officials (AASHTO). (1994). *LRFD Bridge Design Specifications.* First Edition. Washington, D.C.

American Association of State Highway and Transportation Officials (AASHTO). (1983). *Manual for Maintenance Inspection of Bridges.* 1989 Interims. Washington, D.C.

American Association of State Highway and Transportation Officials (AASHTO). (1992). *Standard Specifications for Highway Bridges.* Fifteenth Edition. Washington, D.C.

American Association of State Highway and Transportation Officials (AASHTO). (1944). *Standard Specifications for Highway Bridges.* Washington, D.C.

American Concrete Institute (ACI). (1989). Building Code Requirements for Reinforced Concrete. Detroit, Michigan.

American Institute of Steel Construction (AISC). (1994). *Load and Resistance Factor Design.* Second Edition. Chicago, Illinois.

American Institute of Steel Construction (AISC). (1986). *Highway Structures Design Handbook.* Pittsburgh, Pennsylvania.

Automatic Dynamic Incremental Nonlinear Analysis (ADINA). (1990). Report ARD 90-1. ADINA R&D, Inc. Watertown, MA.

Azizinamini, A., Kathol, S., and Beacham, M.W. (1994). "Steel Girder Bridge Design: Can it be Simplified?." *Modern Steel Construction.* Volume 34 (9). September. pp. 44-46.

Bakht, B., and Moses, F. (1988). "Lateral Distribution Factors for Highway Bridges." *Journal of Structural Engineering. ASCE.* 114(8). pp. 1785-1803.

Bathe, Klaus - Jürgen. (1996). Finite Element Procedures. Prentice Hall, Inc., Edgewood Cliffs, N.J.

Clough, Ray W. And Penzien, Joseph. (1993). Dynamics of Structures. Second Edition. McGraw-Hall, Inc., New York.

Davis, D.G. (1995). "Feasibility of Diaphragm Removal from Multi-girder Steel Bridges." Thesis presented to Auburn University in partial fulfillment of requirements for degree of Master of Science in Civil Engineering. 138 pages.

Fisher, J.W. (1978). "Fatigue Cracking in Bridges from Out-of-Plane Displacements." Canadian Journal of Civil Engineering, 5(4), 542-556.

Fisher, J.W. (1983). "Fatigue Cracking in Bridges." Civil Engineering Transactions, The Institute of Engineers, Australia, July: 223-235.

Fisher, J.W., Yen, B.T., and Wang, D. (1989). "Fatigue of Bridge Structures - A Commentary and Guide for Design, Evaluation, and Inspection of Cracking", ATLSS, Advanced Technology for Large Structural Systems, Lehigh University, July: 89-102.

Fisher, J.W., Jin, J., Wagner, D.C. and Yen, B.T. (1990). "Distortion Induced Cracking in Steel Bridge Members." *Center for Advanced Technology for Large Structural Systems Report No. 90-07.* Lehigh University. 101 pages.

Keating, P.B., and Crozier, A.R. (1992). "Evaluation and Repair of Fatigue Damage to Midland County Bridges." *Report No. TX-92/1313-1F.* Texas Department of Transportation. 157 p.

Keating, P.B. and Fisher, J.W. (1987). "Fatigue Behavior of Variable Loaded Bridge Details Near the Fatigue Limit." Transportation Research Record 1118, National Research Council, Washington, D.C., 56-64.

Kennedy, J.B., Grace, N.F., and Soliman, M. (1989). "Welded-versus Bolted-Steel I-Diaphragms in Composite Bridges." *Journal of Structural Engineering.* ASCE. 115(2). pp. 417-432.

Kostem, C.N., and deCastro, E.S. (1977). "Effects of Diaphragms on Lateral Load Distribution in Beam-slab Bridges." *Transportation Research Record No. 645.* Transportation Research Board. pp. 6-9.

Lower, D.A. (1995). "Field Tests of Distortion-Induced Fatigue Cracking in Diaphragm-Girder Connections for Multi-Girder Bridges." Thesis presented to Auburn University in partial fulfillment of requirements for degree of Master of Science in Civil Engineering, 328 pages.

Moore, M., Strand, K.A., Grubb, M.A., and Cayes, L.R. (1990). "Wheel-Load Distribution Results from the AISI-FHWA Model Bridge Study." *Transportation Research Record No. 1275.* Transportation Research Board. pp. 34-44.

Newmark, N. (1948). "Design of I-Beam Bridges." *Proceedings.* ASCE. Paper No. 2381.

Newmark, N. (1946). "Studies of Slab Beam Highway Bridges." University of Illinois Engineering Experiment Station. Bulletin Series No. 363.

OPTIM Electronics Corporation (1994). "Test Control Software, Version 5.1." OPTIM Electronics Corporation, Germantown, Maryland.

Stafford, T.E. (1996). "A Field Study of Diaphragm Behavior and Performance in Multigirder Steel Bridges." Thesis presented to Auburn University in partial fulfillment of requirements for degree of Master of Science in Civil Engineering. 167 pages.

Stallings, J.M. (1991). *FRAMEIO.* A Computer Program.

Stallings, J.M., Cousins, T.E., Rotto, R.K., and Reid, C.B. (1993). "Evaluation of Fatigue Cracking in I-65 Mobile Delta Crossing Bridges: Volume I, Floorbeam-Girder Connections." Auburn University Highway Research Center Report. 186 pages.

Stallings, J.M., Cousins, T.E. and Tedesco, J.W. (1995). "Fatigue of Diaphragm-Girder Connections." *Auburn University Highway Research Center Interim Report RP930-307.* 69 pages.

Taylor, A.C., and Ojalvo, M. (1966). "Torsional Restraint of Lateral Buckling." *Journal of the Structural Division.* ASCE. 92 (2). April. pp. 115-129.

Trahair, N.S. (1993). *Flexural-Torsional Buckling of Structures.* CRC Press, Inc. Boca Raton, Florida. 360 p.

Walker, W.H. (1987). "Lateral Load Distribution in Multi-Girder Bridges." *Engineering Journal.* American Institute of Steel Construction (AISC). First Quarter. pp. 21- 28.

Wang, Jow-Ying (1991). "Development of Bridge Analysis Tools." A Thesis Submitted to Auburn University in Partial Fulfillment of the Requirements for the Degree of Master of Science. 92 p.

Wilson, W. (1940). "Design of Connection Angles for Stringers of Railway Bridges." AREA, Vol. 41, pp. 889-903.

Wright, W., Nelson, R. and Chase, S. (1992). "I-64 Over Maury River Analysis of Fatigue Retrofit Procedures." Turner Fairbank Highway Research Center. McLean, Virginia. (December 8, 1992). 43 p.

Yamada, K. and Albrecht, P. (1976). "Fatigue Design of Welded Bridge Details for Service Stresses." Transportation Research Record 607, National Research Council, Washington, D.C., 25-30.

Yura, J.A. (1992). "Fundamentals of Beam Bracing." *Is Your Structure Suitably Braced?*. 1993 Conference. April 6-7,1993. Milwaukee, Wisconsin. Structural Stability Research Council. Lehigh University. Bethlehem, Pennsylvania.

Yura, J.A. (1984). "C_b Factors for LTB." University of Texas at Austin. Personal Correspondence.

Zokaie, T., Osterkamp, T.A., and Imbsen, R. A. (1991). "Distribution of Wheel Loads on Highway Bridges." *Final Report of NCHRP Project 12-26.* Transportation Research Board. Washington, D.C.

APPENDICES

APPENDIX A

NON-COMPOSITE BRIDGE ANALYSIS

PROCEDURE

Non-Composite Bridge

STEP 1: Identify bridge geometry.

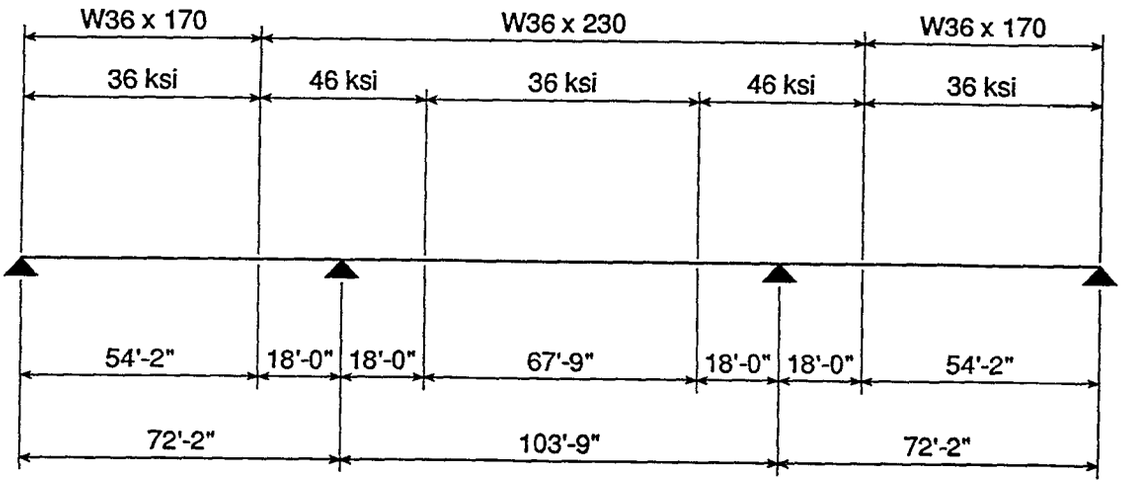

Figure A.1. Girder Details for 3-Span Continuous Bridge at CBD Interchange

Exterior Span

S = 7.57 ft
Section = W36x170
S_x = 580 in.^{3}
Slab thickness = 6.5 in.
n_g = 8 girders

Interior Span

S = 7.57 ft
Section = W36x230
S_x = 837 in.^{3}
Slab thickness = 6.5 in.
n_g = 8 girders

STEP 2: Determine the maximum factored moments for the governing load cases. (Here an interior girder is considered.)

Location	Load Case	Maximum Moment (k-in)
Exterior Span	Dead Load[1]	+ 4,830
Interior Bent	Dead Load[1]	- 13,470
Interior Span	Dead Load[1]	+ 8,200
Exterior Span	HS20-44 (14 ft)	**+17,370**
Interior Bent	HS20-44 (14 ft)	- 13,780
Interior Span	HS20-44 (14 ft)	**+ 22,220**
Exterior Span	HS20-44 (30 ft)	+ 12,830
Interior Bent	HS20-44 (30 ft)	- 12,440
Interior Span	HS20-44 (30 ft)	+ 18,140
Exterior Span	Lane Load (2 conc. load)	+ 6,060
Interior Bent	Lane Load (2 conc. load)	**- 19,960**
Interior Span	Lane Load (2 conc. load)	+ 12,840

[1] Dead load moments are based on a uniformly distributed factored loading of 1.34 k/ft.

STEP 3: Determine the lateral torsional buckling (LTB) moment capacity for the Exterior Span. Conservatively assume the entire exterior span is a W36x170.

LTB capacity from AASHTO Eq. 10-102c.

$$M_r = 91x10^3 C_b \left(\frac{I_{yc}}{L_b}\right)\left[0.772\left(\frac{J}{I_{yc}}\right) + 9.87\left(\frac{d}{L_b}\right)^2\right]^{1/2} \leq M_y$$

A) Calculate cross sectional parameters I_{yc}, J, D, D_c.

$I_{yc} = t_f b_f^3/12 = (1.10)(12.03)^3/12 = 160$ in.^{4}

$D = d - 2t_f = 36.17 - 2(1.10) = 33.97$ in.

$$D_c = \frac{D}{2} = \frac{33.97}{2} = 16.99 \text{ in.}$$

$$J = \frac{(2b_f t_f^3 + Dt_w^3)}{3} = \frac{[(2)(12.03)(1.10)^3 + (33.97)(0.68)^3]}{3}$$

J = 14.24 in.^{4}

B) Verify the conditional limits of Eq. 10 - 102c.

$$0.1 \leq \frac{I_{yc}}{I_y} \leq 0.9$$

$$\frac{I_{yc}}{I_y} = \frac{160}{320} = 0.5 \qquad \text{O.K.}$$

$$\frac{D_c}{t_w} \leq \frac{\lambda}{\sqrt{F_y}}$$

$$\frac{\lambda}{\sqrt{F_y}} = \frac{15400}{\sqrt{36000}} = 81.17$$

$$\frac{D_c}{t_w} = \frac{16.99}{0.68} = 24.99 < 81.17 \qquad \text{O.K.}$$

C) Calculate C_b and M_r. Try complete diaphragm removal.
Calculate C_b for top flange with continuous lateral bracing provided by deck.
Calculate M_r from AASHTO Eq. 10-102c.

$$C_b = 3.0 - \frac{2}{3}\left(\frac{M_1}{M_0}\right) + \frac{8}{3}\left(\frac{M_{CL}}{M_0 + M_1}\right)$$

M_0 = End moment that produces the largest compressive bottom flange stress. Positive for compression in the bottom flange.

M_1 = The other end moment. Positive for compression in the bottom flange.

M_{CL} = Moment at center line of the span. Positive for tension in the bottom flange.

NOTE 1: The moments used for the calculation of C_b should be those corresponding to the critical load case which is dead load plus HS20 lane loading for this span.

L_b = 72.17 ft or 866 in., full length of exterior span

M_1 = 0 k-in.

M_0 = 33,430 k-in.

M_{CL} = 9500 k-in.

$$C_b = 3.0 - \frac{2}{3}\left(\frac{0}{33{,}430}\right) + \frac{8}{3}\left(\frac{9500}{33{,}430 + 0}\right)$$

$C_b = 3.76$

$$M_r = 91\text{x}10^3\,(3.76)\left(\frac{160}{866}\right)\left[0.772\left(\frac{14.24}{160}\right) + 9.87\left(\frac{36.17}{866}\right)^2\right]^{1/2}$$

M_r = 18,530 k-in.

$M_y = (46\text{ ksi})(837\text{ in.}^3) = 38{,}500$ k-in.

$M_r < M_0 < M_y$

Therefore, complete diaphragm removal is not possible. An evaluation of partial removal is required. The moment capacity with bracing provided by only first line diaphragms of the interior bent is evaluated below.

C) Continued: For partial diaphragm removal the exterior span is broken into two unbraced lengths.

L_b = 24.13 ft or 290 in., from interior bent to diaphragm line

M_1 ≡ -688 k-in. (Creates tension in bottom flange.)

M_0 ≡ 33,430 k-in. (Creates compression in bottom flange.)

M_{CL} ≡ -14,010 k-in. (Creates compression in bottom flange.)

$$C_b = 3.0 - \frac{2}{3}\left(\frac{-688}{33,430}\right) + \frac{8}{3}\left(\frac{-14,010}{33,430 + -688}\right)$$

$C_b = 1.85$

$$M_r = 91x10^3\,(1.85)\left(\frac{160}{290}\right)\left[0.772\left(\frac{14.24}{160}\right) + 9.87\left(\frac{36.17}{290}\right)^2\right]^{1/2}$$

M_r = 43,790 k-in.

$M_y = (46\ ksi)(837\ in.^3) = 38,500$ k-in.

$M_r > M_y$

L_b = 48.04 ft or 576 in., from diaphragm line to end of girder

M_1 = 0 k-in. (Creates tension in bottom flange.)

M_0 = -688 k-in. (Creates compression in bottom flange.)

M_{CL} = 10,710 k-in. (Creates compression in bottom flange.)

Neither end moment for this unbraced length creates compression in the bottom flange, so LTB will not occur.

Therefore, the moment capacity is governed by the yield moment, as opposed to the LTB moment capacity, after all of the diaphragms are removed except the first line of diaphragms off the interior bent.

STEP 4: Determine the LTB moment capacity for the Interior Span. For this example the entire span is a W36x230.

A) Calculate cross section parameter I_{yc}, J, D, D_c.

$I_{yc} = t_f b_f^3/12 = (1.26)(16.47)^3/12 = 469$ in.^{4}

$D = d - 2t_f = 35.90 - 2(1.26) = 33.38$ in.

$$D_c = \frac{D}{2} = \frac{33.38}{2} = 16.69 \text{ in.}$$

$$J = \frac{(2bt_f^3 + Dt_w^3)}{3} = \frac{[(2)(16.47)(1.26)^3 + (33.38)(0.76)^3]}{3}$$

$J = 26.85$ in.^{4}

B) Verify the conditional limits of Eq. 10 - 102c.

$$0.1 \le \frac{I_{yc}}{I_y} \le 0.9$$

$$\frac{I_{yc}}{I_y} = \frac{469}{940} = 0.5 \qquad \text{O.K.}$$

$$\frac{D_c}{t_w} \le \frac{\lambda}{\sqrt{F_y}}$$

$$\frac{\lambda}{\sqrt{F_y}} = \frac{15400}{\sqrt{46000}} = 71.80$$

$$\frac{D_c}{t_w} = \frac{16.69}{0.76} = 21.96 < 71.80 \qquad \text{O.K.}$$

C) Calculate C_b and M_r. Try complete diaphragm removal.
Calculate C_b for top flange with continuous lateral bracing provided by deck.
Calculate M_r from AASHTO Eq. 10-102c.

$$C_b = 3.0 - \frac{2}{3}\left(\frac{M_1}{M_0}\right) + \frac{8}{3}\left(\frac{M_{CL}}{M_0 + M_1}\right)$$

NOTE 1: The moments used for the calculation of C_b should be those corresponding to the critical load case.

L_b = 103.75 ft for 1245 in., full length of interior span

M_1 = 22,270 k-in.

M_0 = 33,430 k-in.

M_{CL} = 20,990 k-in.

$$C_b = 3.0 - \frac{2}{3}\left(\frac{22{,}270}{33{,}430}\right) + \frac{8}{3}\left(\frac{20{,}990}{33{,}430 + 22{,}270}\right)$$

$C_b = 3.56$

$$M_r = 91x10^3\,(3.56)\left(\frac{469}{1245}\right)\left[0.772\left(\frac{26.85}{469}\right) + 9.87\left(\frac{35.90}{1245}\right)^2\right]^{1/2}$$

M_r = 27,940 k-in.

$M_y = (46\ \text{ksi})(837\ \text{in.}^3) = 38{,}500$ k-in.

$M_r < M_0 < M_y$

Therefore, complete diaphragm removal is not possible. An evaluation of partial removal is required. The moment capacity with bracing provided by only first line of diaphragms off the interior bent is evaluated below.

C) Continued: For partial diaphragm removal the interior span is broken into three unbraced lengths.

L_b = 20.79 ft or 250 in., from interior bent to diaphragm line.

M_1 = -115 k-in.

M_0 = 33,430 k-in.

M_{CL} = -15,930 k-in.

$$C_b = 3.0 - \frac{2}{3}\left(\frac{-115}{33{,}430}\right) + \frac{8}{3}\left(\frac{-15{,}930}{33{,}430 + -115}\right)$$

$C_b = 1.72$

$$M_r = 91x10^3\,(1.72)\left(\frac{469}{250}\right)\left[0.772\left(\frac{26.85}{469}\right) + 9.87\left(\frac{35.90}{250}\right)^2\right]^{1/2}$$

M_r = 146,150 k-in.

$M_y = (46\ ksi)(837\ in.^3) = 38{,}500$ k-in.

$M_r > M_y$

L_b = 62.37 ft or 748 in., between diaphragms lines.

M_1 = -115 k-in.

M_0 = -4700 k-in.

M_{CL} = 20,990 k-in.

Neither end moment for this unbraced length creates compression in the bottom flange, so LTB will not occur.

L_b = 20.79 ft or 250 in., from diaphragms line to interior bent.

M_1 = -4700 k-in.

M_0 = 22,270 k-in.

M_{CL} = -7660 k-in.

$$C_b = 3.0 - \frac{2}{3}\left(\frac{-4700}{22{,}270}\right) + \frac{8}{3}\left(\frac{-7660}{22{,}270 + -4700}\right)$$

C_b = 1.98

$$M_r = 91x10^3\,(1.98)\left(\frac{469}{250}\right)\left[0.772\left(\frac{26.85}{469}\right) + 9.87\left(\frac{35.90}{250}\right)^2\right]^{1/2}$$

M_r = 168,240 k-in.

$M_y = (46\ ksi)(837\ in.^3) = 38{,}500$ k-in.

$M_r > M_y$

Therefore, the moment capacity is governed by the yield moment, as opposed to the LTB moment capacity, when the first line diaphragms off the interior bents remain in place.

STEP 5: Wind load analysis for the exterior spans. Check bottom flange in the positive moment region only for partial diaphragm removal.

A) Limit stress.

Yielding of the bottom flange controls in the positive moment region; the limit is $F_y = 36$ ksi.

B) Wind load stress, F_W. $L_b = 48.04$ ft.

$$W = \left(\frac{3ft}{2}\right)\left(\frac{50psf}{1000}\right) = 0.075 \text{ k/ft on bottom flange}$$

$$M_W = 0.1\ W\ L_b^2 = 0.1\ (0.075)\ (48.04)^2\ (12 \text{ in./ft}) = 208 \text{ k-in.}$$

$$S_f = t_f b_f^2/6 = (1.10)\ (12.03)^2/6 = 26.5 \text{ in.}^3$$

$$F_W = \frac{M_w}{S_f} = \frac{208}{26.5} = 7.8 \text{ ksi}$$

C) Dead load stress, F_{DL}.

$M_{DL} = 4830$ k-in. maximum factored positive moment

$S_x = 580$ in.^{3} W36x170, non-composite

$$F_{DL} = \frac{4830}{(1.3)(580)} = 6.4 \text{ ksi service load stress}$$

D) Live load stress, F_{LL+I}.

$M_{LL+I} = 17{,}370$ k-in. maximum factored positive moment for an interior girder

$$DF_{int} = \frac{S}{5.5} = \frac{7.57}{5.5} = 1.38$$

$$DF_{ext} = \frac{S}{4 + 0.25S} = \frac{7.57}{4 + 0.25(7.57)} = 1.29$$

$$F_{LL+I} = \frac{DF_{int}}{DF_{ext}}\ \frac{M_{LL+I}}{2.171 S_x} = \left(\frac{1.29}{1.38}\right)\left(\frac{17{,}370}{2.171(580)}\right)$$

$F_{LL+I} = 12.9$ ksi service load stress for exterior girder.

D) Group load combinations II and III for exterior spans.

Group II: $F = 1.3(F_{DL} + F_W)$

$F = 1.3(6.4 + 7.8) = 18.5 \text{ ksi} < 36 \text{ ksi}$ O.K.

Group III: $F = 1.3(F_{DL} + F_{LL+I} + .3F_W)$

$F = 1.3(6.4 + 12.9 + .3(7.8)) = 28.1 \text{ ksi} < 36 \text{ ksi}$ O.K.

Stresses are within the limit for the exterior spans after partial diaphragm removal.

STEP 6: Wind load analysis for the interior span. Check bottom flange in positive moment region only for partial diaphragm removal.

A) Limit stress.

Yielding of the bottom flange controls in the positive moment region; the limit is $F_y = 36$ ksi.

B) Wind load stress, F_W. $L_b = 62.37$ ft between diaphragms.

$$W = \left(\frac{3ft}{2}\right)\left(\frac{50psf}{1000}\right) = 0.075 \text{ k/ft}$$

$$M_W = 0.1\ W\ L_b^2 = 0.1\ (0.075)(62.37)^2\ (12 \text{ in./ft}) = 350 \text{ k-in.}$$

$$S_f = t_f b_f^2/6 = (1.26)(16.47)^2/6 = 57.0 \text{ in.}^3$$

$$F_W = \frac{M_w}{S_f} = \frac{350}{57.0} = 6.1 \text{ ksi}$$

C) Dead load stress, F_{DL}.

$M_{DL} = 8200$ k-in. maximum factored positive moment

$S_x = 837$ in.^{3} W36x230, non-composite

$$F_{DL} = \frac{8200}{(1.3)(837)} = 7.5 \text{ ksi service load stress}$$

D) Live load stress, F_{LL+I}.

$M_{LL+I} = 22{,}200$ k-in. maximum factored positive moment for an interior girder

$$F_{LL+I} = \frac{DF_{int}}{DF_{ext}}\ \frac{M_{LL+I}}{2.171 S_x} = \left(\frac{1.29}{1.38}\right)\left(\frac{22{,}200}{2.171(837)}\right)$$

$F_{LL+I} = 11.4$ ksi service load stress for exterior girder

D) Group load combinations II and III for interior span.

Calculate the combined stresses.

Group II: $F = 1.3(F_{DL} + F_W)$

$$F = 1.3(7.5 + 6.1) = 17.7 \text{ ksi} < 36 \text{ ksi} \qquad \text{O.K.}$$

Group III: $F = 1.3(F_{DL} + F_{LL+I} + .3F_W)$

$$F = 1.3(7.5 + 11.4 + .3(6.1)) = 26.9 \text{ ksi} < 36 \text{ ksi} \quad \text{O.K.}$$

Stresses are within the limit for the interior span after partial diaphragm removal.

STEP 7: Torsional Brace Analysis

$M_{req'd}$ = 33,430 k-in. (interior bent)

STRENGTH

$$M_{br} = \frac{0.04LM_f^2}{nEI_{eff}C_{bb}^2} = \frac{0.04(72.17\ x\ 12)(33430)^2}{(7)(29000)(320)(1.0)^2} = 596 \text{ k-in.}$$

$$S_x)_{req'd} = \frac{596}{36} = 16.6 \text{ in.}^3$$

USING MC 18x42.7 $S_x = 61.6$ in.^{3} O.K.

Check LTB of Diaphragm

$$I_{yc} = \frac{b_f^3 t_f}{12} = \frac{(3.950)^3(0.625)}{12} = 3.21 \text{ in.}^4$$

$$J = \frac{2b_f t_f^3 + Dt_w^3}{3} = \frac{(2)(3.950)(0.625)^3 + (16.75)(0.450)^3}{3} = 1.15 \text{ in.}^4$$

$$M_r = 91x10^3 C_b \frac{I_{yc}}{L_b}\left[0.772\frac{J}{I_{yc}} + 9.87\left(\frac{d}{L_b}\right)^2\right]^{1/2}$$

$$M_r = (91x10^3)(2.3)\left(\frac{3.21}{91}\right)\left[(0.772)\left(\frac{1.15}{3.21}\right) + (9.87)\left(\frac{\pi(18)}{91}\right)^2\right]^{1/2}$$

M_r = 14927 k-in.

$M_y = (36 \text{ ksi})(61.6 \text{ in.}^3) = 2218$ k-in.

$M_r > M_y > M_{br} = 596$ k-in. O.K.

STIFFNESS

$$\beta_T)_{req'd} = \frac{2.4LM_f^2}{nEI_{eff}C_{bb}^2} = \frac{2.4(72.17\ x\ 12)(33430)^2}{(1)(29000)(320)(1.85)^2} = 73{,}140 \text{ k-in.}$$

$$\beta_b = \frac{6EI_{br}}{S} \quad \text{(Ext. Gird.)} \qquad \beta_b = \frac{12EI_{br}}{S} \quad \text{(Int. Gird.)}$$

$$\beta_b)_{avg} = \frac{(2x6 + 6x12)}{8} = \frac{10.5EI_{br}}{S}$$

$$\beta_b = \frac{10.5(29000)(554)}{(7.57 \times 12)} = 1{,}857{,}000 \text{ k-in.}$$

NOTE 3: Because the diaphragm-girder connections are or will be primarily bolted connections, the brace stiffness is assumed to be only 25% of this calculated value. However, additional research is required to accurately establish the stiffness of the bolted diaphragm-girder connections.

$\beta_b = 0.25\ (1{,}857{,}000) = 464{,}300$ k-in.

$$\beta_g = \frac{\left(\frac{24(n_g - 1)^2}{n_g}\right) S^2 EI_x}{L^3} = \frac{24(8-1)^2(91)^2(29000)(10500)}{8(72.17x12)^3} = 570{,}700 \text{ k-in.}$$

$$\beta_c, \beta_s, \beta_t = \frac{3.3E}{h_i}\left(\frac{h}{h_i}\right)^2 \left[\frac{(N + 1.5h_i)t_w^{\,3}}{12} + \frac{t_s b_s^{\,3}}{12}\right]$$

$$\beta_c = \frac{3.3(29000)}{7.0}\left(\frac{33.97}{7.0}\right)^2 \left[\frac{[8+1.5(7.0)](1.10)^3}{12}\right]$$

$\beta_c = 660{,}700$ k-in.

$$\beta_s = \frac{3.3(29000)}{19.0}\left(\frac{33.97}{19.0}\right)^2 \left[\frac{[8+1.5(19.0)](1.10)^3}{12} + \frac{(0.50)(2)(6.0)^3}{12}\right]$$

$\beta_s = 355{,}000$ k-in.

$$\beta_t = \frac{3.3(29000)}{7.97}\left(\frac{33.97}{7.97}\right)^2 \left[\frac{[8+1.5(7.97)](1.10)^3}{12}\right]$$

$\beta_T = 482{,}800$ k-in.

$$\frac{1}{\beta_{sec}} = \frac{1}{\beta_c} + \frac{1}{\beta_s} + \frac{1}{\beta_t} = \frac{1}{660{,}700} + \frac{1}{355{,}000} + \frac{1}{482{,}800}$$

β_{sec} = 156,200 k-in.

$$\frac{1}{\beta_T} = \frac{1}{\beta_b} + \frac{1}{\beta_{sec}} + \frac{1}{\beta_g} = \frac{1}{464{,}300} + \frac{1}{156{,}200} + \frac{1}{570{,}700}$$

β_T = 97,000 k-in. > $\beta_T)_{req'd}$ = 73,140 k-in. O.K.

APPENDIX B

COMPOSITE BRIDGE ANALYSIS

PROCEDURE

Composite Bridge

STEP 1: Identify bridge geometry.

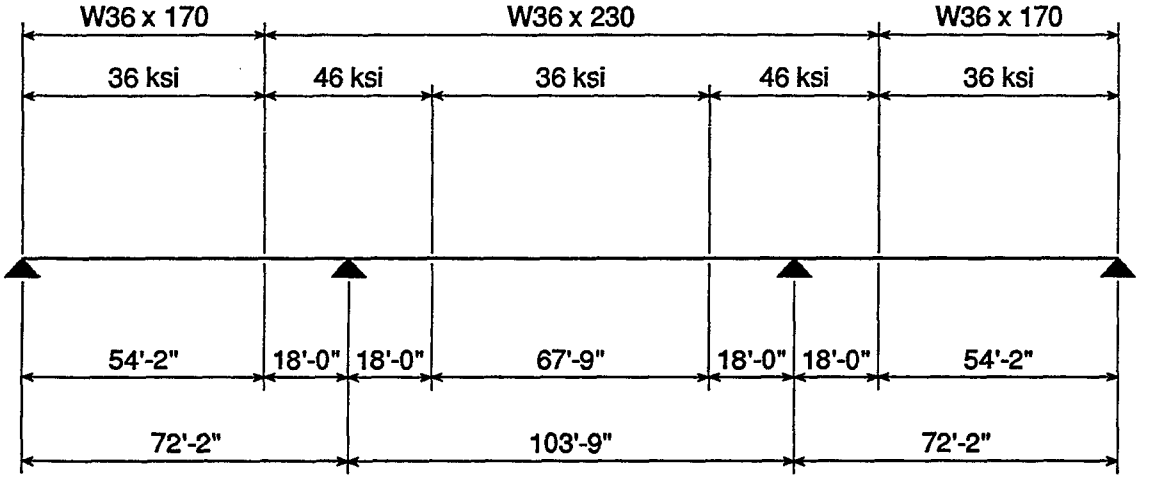

Figure B.2. Girder Details for 3-Span Continuous Bridge at CBD Interchange

Exterior Span

S = 7.57 ft
Section = W36x170
S_x = 580 in.^{3} (non-composite)
S_b = 781 in.^{3} (composite)
Slab thickness = 6.5 in.
n_g = 8 girders

Interior Span

S = 7.57 ft
Section = W36x230
S_x = 837 in.^{3} (non-composite)
S_b = 1062 in.^{3} (composite)
Slab thickness = 6.5 in.
n_g = 8 girders

STEP 2: Determine the maximum factored moments for the governing load cases. (An interior girder is considered here.)

Location	Load Case	Maximum Moment (k-in)
Exterior Span	Dead Load[1]	+ 5,630
Interior Bent	Dead Load[1]	- 11,200
Interior Span	Dead Load[1]	+ 10,460
Exterior Span	HS20-44 (14 ft)	**+ 18,720**
Interior Bent	HS20-44 (14 ft)	- 11,380
Interior Span	HS20-44 (14 ft)	**+ 24,580**
Exterior Span	HS20-44 (30 ft)	+ 13,990
Interior Bent	HS20-44 (30 ft)	- 10,400
Interior Span	HS20-44 (30 ft)	+ 20,180
Exterior Span	Lane Load (2 conc. load)	+ 7,790
Interior Bent	Lane Load (2 conc. load)	**- 15,930**
Interior Span	Lane Load (2 conc. load)	+ 15,420

[1] Dead load moments are based on a uniformly distributed factored loading of 1.34 k/ft on the non-composite steel girder.

STEP 3: Determine the lateral torsional buckling (LTB) moment capacity for the Exterior Span. Conservatively assume the entire exterior span is a W36x170.

LTB capacity from AASHTO Eq. 10-102c.

$$M_r = 91x10^3 C_b \left(\frac{I_{yc}}{L_b}\right)\left[0.772\left(\frac{J}{I_{yc}}\right) + 9.87\left(\frac{d}{L_b}\right)^2\right]^{1/2}$$

A) Calculate cross section parameters I_{yc}, J, D, D_c.

$I_{yc} = t_f b_f^3 / 12 = (1.10)(12.03)^3 / 12 = 160$ in.^{4}

$D = d - 2t_f = 36.17 - 2(1.10) = 33.97$ in.

$$D_c = \frac{D}{2} = \frac{33.97}{2} = 16.99 \text{ in.}$$

$$J = \frac{2b_f t_f^3 + Dt_w^3}{3} = \frac{[(2)(12.03)(1.10)^3 + (33.97)(0.68)^3]}{3}$$

$J = 14.24$ in.^{4}

B) Verify the conditional limits of Eq. 10 - 102c.

$$0.1 \le \frac{I_{yc}}{I_y} \le 0.9$$

$$\frac{I_{yc}}{I_y} = \frac{160}{320} = 0.5 \qquad \text{O.K.}$$

$$\frac{D_c}{t_w} \le \frac{\lambda}{\sqrt{F_y}}$$

$$\frac{\lambda}{\sqrt{F_y}} = \frac{15400}{\sqrt{36000}} = 81.17$$

$$\frac{D_c}{t_w} = \frac{16.99}{0.68} = 24.99 < 81.17 \qquad \text{O.K.}$$

C) Calculate C_b for top flange with continuous lateral bracing provided by deck. Try complete removal.

$$C_b = 3.0 - \frac{2}{3}\left(\frac{M_1}{M_0}\right) + \frac{8}{3}\left(\frac{M_{CL}}{M_0 + M_1}\right)$$

M_0 = End moment that produces the largest compressive bottom flange stress. Positive for compression in the bottom flange.

M_1 = The other end moment. Positive for compression in the bottom flange.

M_{CL} = Moment at center line of the span. Positive for tension in the bottom flange.

NOTE 1: The moments used for the calculation of C_b should be those corresponding to the critical load case.

L_b = 72.17 ft or 866 in., full length of exterior span

M_1 = 0 k-in.

M_0 = 29,400 k-in.

M_{CL} = 11,490 k-in.

$$C_b = 3.0 - \frac{2}{3}\left(\frac{0}{29{,}400}\right) + \frac{8}{3}\left(\frac{11{,}490}{29{,}400 + 0}\right)$$

C_b = 4.04

D) Calculate M_r.

$$M_r = 91 \times 10^3 \,(4.04)\left(\frac{160}{866}\right)\left[0.772\left(\frac{14.24}{160}\right) + 9.87\left(\frac{36.17}{866}\right)^2\right]^{1/2}$$

M_r = 19,910 k-in.

E) Calculate M_{cr}, LTB capacity including torsional bracing provided by deck. Calculate effective torsional brace stiffness.

$$\frac{1}{\beta_T} = \frac{1}{\beta_b} + \frac{1}{\beta_{sec}} + \frac{1}{\beta_g}$$

β_T = Effective torsional brace stiffness

β_b = Stiffness of the attached brace

β_{sec} = Cross sectional web stiffness

β_g = Girder system stiffness

NOTE 2: In the paper presented by Yura (1992), β_b is the stiffness of the attached brace, e.g., diaphragms, slab, etc. Since the objective of the procedure presented here is to verify that removing all diaphragms is possible, only the stiffness provided by the slab is considered.

$$\beta_b = \frac{6EI_s}{S} \text{ (exterior girder)}$$

$$\beta_b = \frac{12EI_s}{S} \text{ (interior girder)}$$

$$\beta_b)_{avg} = \frac{(2x6 + 6x12)}{8} \frac{EI_s}{S} = \frac{10.5EI_s}{S}$$

$$E = 57\sqrt{f'c} = 57\sqrt{4000} = 3604 \text{ ksi}$$

$$I_s = \frac{bt_s^3}{12} = \frac{(1.0)\ (6.5)^3}{12} = 22.8 \text{ in.}^4\text{/in.}$$

NOTE 3: For this case, I_s is the moment of inertia per unit length of the slab.

$$\beta_b = \frac{10.5(3604)(22.8)}{(7.57x12)} = 9494 \text{ (k-in./rad)/in.}$$

NOTE 4: Conservatively assume only half the span has shear studs.

$$\beta_b = \frac{1}{2}(9494) = 4747 \text{ (k-in./rad)/in.}$$

$$\beta_{sec} = \frac{3.3E}{h}\left[\frac{(N+1.5h)t_w^3}{12} + \frac{t_s b_s^3}{12}\right]$$

NOTE 5: For continuous bracing of the slab take (N+1.5h) as 1.0 in./in.

NOTE 6: For transverse stiffeners to be effective, the stiffeners must be attached to the flange that is braced by the torsional brace. Therefore, conservatively neglect the contribution provided by the stiffeners at the existing diaphragm connections.

$$\beta_{sec} = \frac{3.3(29x10^3)}{36.17}\left[\frac{(1.0)(0.68)^3}{12}\right] = 69.3 \text{ (k-in./rad)/in.}$$

$$\beta_g = \frac{\left(\frac{24(n_g-1)^2}{n_g}\right) S^2 E I_x}{L^3} = \frac{\left(\frac{24(8-1)^2}{8}\right) (7.57X12)^2(29x10^3)(10{,}500)}{(72.17x12)^3}$$

$$\beta_g = 568{,}650 \text{ (k-in./rad)/in.}$$

$$\frac{1}{\beta_T} = \frac{1}{\beta_b} + \frac{1}{\beta_{sec}} + \frac{1}{\beta_g} = \frac{1}{4747} + \frac{1}{69.3} + \frac{1}{568{,}650}$$

$$\beta_T = 68.3 \text{ (k-in./rad)/in.}$$

Calculate M_o, I_{eff}, C_T, C_{bb}.

$$M_o = \frac{M_r}{C_{bu}} = \frac{19{,}910}{4.04} = 4930 \text{ k-in.}$$

$$I_{eff} = I_{yc} + \frac{t}{c} I_{yt} = 320 \text{ in.}^4$$

$C_T = 1.2$ for top flange loading

Conservatively assume $C_{bb} = 1.0$

$C_{bu} = 4.04$

$$M_{cr} = \left(C_{bu}{}^2 M_o{}^2 + \frac{C_{bb}{}^2 \beta_T E I_{eff}}{2C_T} \right)^{1/2} \leq M_y$$

NOTE 7: The "2" in the denominator of the second term of the above equation is a factor of safety to account for, among other things, the initial-out-of-straightness of the girder. Hence, the torsional bracing is required to

be twice as stiff as theoretically required to produce the calculated moment capacity.

$$M_{cr} = \left[(4.04)^2(4930)^2 + \frac{(1.0)^2(68.3)(29x10^3)(320)}{2(1.2)}\right]^{1/2}$$

$M_{cr} = 25{,}700$ k-in.

$M_y = F_y S_x = (46 \text{ ksi})\ (837 \text{ in.}^3) = 38{,}500$ k-in.

$M_{cr} < M_{REQ'D} < M_Y$

Therefore, the section must be reevaluated using the weighted average approach suggested by Trahair. Only the equations which change are shown below.

Recalculate I_{yc}, J, and d. 75% of span is W36x170, 25% is W36x230. Properties are calculated for W36x230 in STEP 4.

$I_{yc} = (160)(.75) + (469)(.25) = 237 \text{ in.}^4$

$J = (14.24)(.75) + (26.85)(.25) = 17.39 \text{ in.}^4$

$d = (36.17)(.75) + (35.90)(.25) = 36.10$ in.

Recalculate M_r

$$M_r = 91x10^3(4.04)\left(\frac{237}{866}\right)\left[0.772\left(\frac{17.39}{237}\right) + 9.87\left(\frac{36.10}{866}\right)^2\right]^{1/2}$$

$M_r = 27{,}340$ k-in.

Recalculate t_w, β_{sec}, β_b, and β_T.

$t_w = (.68)(.75) + (.76)(.25) = 0.70$ in.

$$\beta_{sec} = \frac{3.3(29x10^3)}{36.10}\left[\frac{(1.0(0.70)^3}{12}\right] = 75.8 \text{ (k-in./rad)/in.}$$

$\beta_b = \frac{1}{2}\ (9494) = 4747$ (k-in./rad)/in.

$$\frac{1}{\beta_T} = \frac{1}{\beta_b} + \frac{1}{\beta_{sec}} + \frac{1}{\beta_g} = \frac{1}{4747} + \frac{1}{75.8} + \frac{1}{568{,}650}$$

$\beta_T = 74.6$ (k-in./rad)/in.

Recalculate M_o and I_{eff}.

$$M_o = \frac{M_r}{C_{bu}} = \frac{27{,}340}{4.04} = 6770 \text{ k-in.}$$

$I_{eff} = (320)(.75) + (940)(.25) = 475 \text{ in.}^4$

Recalculate M_{cr}.

$$M_{cr} = \left[(4.04)^2(6770)^2 + \frac{(1.0)^2(74.6)(29x10^3)(475)}{2(1.2)}\right]^{1/2}$$

$M_{cr} = 34{,}300$ k-in.

$M_y = 38{,}500$ k-in.

$M_{cr} > M_y$

$M_{cr} > M_{REQ'D} = 29{,}400$ k-in.

The moment capacity is below the yield moment but greater than required for an Inventory Rating factor of one.

STEP 4: Determine LTB moment capacity for the Interior Span.

A) Calculate cross section parameters I_{yc}, J, D, D_c.

$I_{yc} = t_f b_f^3/12 = (1.26)(16.47)^3/12 = 469$ in.^{4}

$D = d - 2t_f = 35.90 - 2(1.26) = 33.38$ in.

$$D_c = \frac{D}{2} = \frac{33.38}{2} = 16.69 \text{ in.}$$

$$J = \frac{(2b_f t_f^3 + Dt_w^3)}{3} = \frac{[(2)(16.47)(1.26)^3 + (33.38)(0.76)^3]}{3}$$

$J = 26.85$ in.^{4}

B) Check the conditional limits of Eq. 10-102c.

$$0.1 \le \frac{I_{yc}}{I_y} \le 0.9$$

$$\frac{I_{yc}}{I_y} = \frac{469}{940} = 0.5 \qquad \text{O.K.}$$

$$\frac{D_c}{t_w} \le \frac{\lambda}{\sqrt{F_y}}$$

$$\frac{\lambda}{\sqrt{F_y}} = \frac{15400}{\sqrt{46000}} = 71.80$$

$$\frac{D_c}{t_w} = \frac{16.69}{0.76} = 21.96 < 71.80 \qquad \text{O.K.}$$

C) Calculate C_b for top flange with continuous lateral bracing provided by deck. Try complete removal.

$L_b = 103.75$ ft or 1245 in., full length of interior span

$M_1 = 16{,}050$ k-in.

$M_o = 29{,}400$ k-in.

M_{CL} = 23,440 k-in.

$$C_b = 3.0 - \frac{2}{3}\left(\frac{16{,}050}{29{,}400}\right) = \frac{8}{3}\left(\frac{23{,}440}{29{,}400+16{,}050}\right)$$

C_b = 4.01

D) Calculate M_r.

$$M_r = 91x10^3(4.01)\left(\frac{469}{1245}\right)\left[0.772\left(\frac{26.85}{469}\right) + 9.87\left(\frac{35.90}{1245}\right)^2\right]^{1/2}$$

M_r = 31,500 k-in.

E) Calculate M_{cr}, LTB capacity including torsional bracing provided by deck.

Calculate effective torsional brace stiffness.

$$\beta_b)_{avg} = \frac{(2x6 + 6x12)}{8} = \frac{10.5EI_s}{S}$$

$$E = 57\sqrt{f'_c} = 57\sqrt{4000} = 3604 \text{ ksi}$$

$$I_s = \frac{bt_s^3}{12} = \frac{(1.0)(6.5^3)}{12} = 22.8 \text{ in.}^4\text{/in.}$$

$$\beta_b = \frac{10.5(3604)(22.8)}{(7.57x12)} = 9494 \text{ (k-in./rad)/in.}$$

Conservatively assume half of the span has shear studs.

β_b = ½(9494) = 4747 (k-in./rad)/in.

$$\beta_{sec} = \frac{3.3E}{h}\left[\frac{(N+1.5h)t_W^3}{12} + \frac{t_s b_s^3}{12}\right]$$

For continuous bracing of the slab take (N+1.5h) as 1.0 in.

$$\beta_{sec} = \frac{3.3(29x10^3)}{35.90}\left[\frac{(1.0)(0.76)^3}{12}\right] = 97.5 \text{ (k-in./rad)/in.}$$

$$\beta_g = \frac{\left(\frac{24(n_g-1)^2}{n_g}\right) S^2 E I_x}{L^3} = \frac{\left(\frac{24(8-1)^2}{8}\right)(7.57x12)^2(29x10^3)(15{,}000)}{(103.76x12)^3}$$

$\beta_g = 273{,}560$ (k-in./rad)/in.

$$\frac{1}{\beta_T} = \frac{1}{\beta_b} + \frac{1}{\beta_{sec}} + \frac{1}{\beta_g} = \frac{1}{4747} + \frac{1}{97.5} + \frac{1}{273{,}560}$$

$\beta_T = 95.5$ (k-in./rad)/in.

Calculate M_o, I_{eff}, C_T, C_{bb}.

$$M_0 = \frac{M_r}{C_{bu}} = \frac{31{,}500}{4.01} = 7850 \text{ k-in.}$$

$$I_{eff} = I_{yc} + \frac{t}{c} I_{yt} = 940 \text{ in.}^4$$

$C_T = 1.2$ for top flange loading

Conservatively assume $C_{bb} = 1.0$

$C_{bu} = 4.02$

$$M_{cr} = \left(C_{bu}{}^2 M_o{}^2 + \frac{C_{bb}{}^2 \beta_T E I_{eff}}{2C_T} \right)^{1/2} \leq M_y$$

$$M_{cr} = \left[(4.01)^2(7850)^2 + \frac{(1.0)^2(95.5)(29x10^3)(940)}{2(1.2)} \right]^{1/2}$$

$M_{cr} = 45{,}600$ k-in.

$M_y = F_y S_x = (46 \text{ ksi})\ (837 \text{ in.}^3) = 38{,}500$ k-in.

$M_{cr} < M_y$

Therefore, the moment capacity is governed by the yield moment, as opposed to the LTB moment, with all of the interior diaphragms removed.

STEP 5: Wind load analysis for the exterior spans. Check bottom flange stress at the support and near midspan.

Stress near midspan.

A) Limit stress.

Yielding controls in the positive moment region; the limit stress is $F_y = 36$ ksi.

B) Wind load stress, F_W. $L_b = 72.17$ ft. full span length.

$$W = \left(\frac{3ft}{2}\right)\left(\frac{50psf}{1000}\right) = 0.075 \text{ k/ft on bottom flange}$$

$$M_W = 0.125\ W\ L_b^2 = 0.125\ (0.075)\ (72.17)^2\ (12 \text{ in./ft}) = 586 \text{ k-in.}$$

$$S_f = t_f b_f^2/6 = (1.10)\ (12.03)^2/6 = 26.5 \text{ in.}^3$$

$$F_W = \frac{586}{26.5} = 22.1 \text{ ksi}$$

C) Dead load stress, F_{DL}. All dead load assumed non-composite.

$M_{DL} = 4830$ k-in. maximum factored positive moment

$S_x = 580$ in.^{3} W36x170, non-composite

$$F_{DL} = \frac{4830}{(1.3)(580)} = 6.4 \text{ ksi service load stress}$$

D) Live load stress, F_{LL+I}.

$M_{LL+I} = 18{,}720$ k-in. maximum factored positive moment for an interior girder

$S_x = 781$ in.^{3} composite cross section

$$DF_{int} = \frac{S}{5.5} = \frac{7.57}{5.5} = 1.38$$

$$DF_{ext} = \frac{S}{4 + 0.25S} = \frac{7.57}{4 + 0.25(7.57)} = 1.29$$

$$F_{LL+I} = \frac{DF_{int}}{DF_{ext}} \frac{M_{LL+I}}{2.171 S_x} = \left(\frac{1.29}{1.38}\right)\left(\frac{18{,}720}{2.171(781)}\right)$$

F_{LL+I} = 10.3 ksi service load stress for exterior girder.

E) Group load combinations II and III for exterior span near midspan.

Group II: $F = 1.3(F_{DL} + F_W)$

$F = 1.3(6.4 + 22.1) = 37.1$ ksi > 36 ksi N.G.

Group III: $F = 1.3(F_{DL} + F_{LL+I} + .3F_W)$

$F = 1.3(6.4 + 10.3 + .3(22.1)) = 30.3$ ksi < 36 ksi O.K.

Combined stress for Group II exceeds the limit.

Stresses at the support. For this structure F_W for the exterior span is larger than for interior span.

A) Limit stress.

Yielding $F = F_y = 36$ ksi

Local Buckling $b' = b_f/2 = 16.47/2 = 8.24$

$F = (2055\, t_f/b')^2/1000 = 99$ ksi

LTB $F = \frac{M_{cr}}{S_x} = \left(\frac{34{,}300}{837}\right) = 41$ ksi exterior span

B) Wind load stress, F_W. L_b = 72.17 ft full span length.

F_W = 22.1 ksi same as near midspan

C) Dead load stress, F_{DL}. All dead load non-composite.

M_{DL} = 13,470 k-in. maximum factored negative moment

S_x = 837 in.^{3} W36x230, non-composite

$$F_{DL} = \frac{13{,}470}{(1.3)(837)} = 12.4 \text{ ksi}$$

D) Live load stress, F_{LL+I}.

M_{LL+I} = 15,930 k-in. maximum factored negative moment for an interior girder.

S_x = 837 in.^{3} W36x230, non-composite at support

$$F_{LL+I} = \left(\frac{1.29}{1.38}\right)\left(\frac{15{,}930}{2.171(837)}\right) = 8.2 \text{ ksi for exterior girder}$$

E) Group load combinations II and III at support.

Group II: $F = 1.3\,(F_{DL} + F_W)$

$F = 1.3\,(12.4 + 22.1) = 44.9 \text{ ksi} > 41 \text{ ksi}$ N.G.

Group III: $F = 1.3\,(F_{DL} + F_{LL+I} + .3F_W)$

$F = 1.3\,(12.4 + 8.2 + .3(22.1)) = 35.4 \text{ ksi} < 41 \text{ ksi}$ O.K.

Combined stress for Group II exceeds the limit.

STEP 6: Wind load analysis for the interior span. Check the bottom flange stress near midspan.

A) Limit stress.

Yielding controls, limit stress in $F_y = 36$ ksi.

B) Wind load stress, F_W. $L_b = 103.75$ ft full span length.

$W = 0.075$ k/ft

$M_W = 0.125\ WL_b^2 = 0.125\ (0.075)\ (103.75)^2\ (12\ \text{in./ft}) = 1210$ k-in.

$S_f = t_f b_f^2/6 = 57.0\ \text{in.}^3$ W36x230

$$F_W = \frac{M_W}{S_f} = \frac{1210}{57.0} = 21.2 \text{ ksi}$$

C) Dead load stress, F_{DL}. All dead load assumed non-composite.

$M_{DL} = 8200$ k-in. maximum factored positive moment

$S_x = 837\ \text{in.}^3$ non-composite

$$F_{DL} = \frac{8200}{(1.3)(837)} = 7.5 \text{ ksi}$$

D) Live load stress, F_{LL+I}.

$M_{LL+I} = 24{,}580$ k-in. maximum factored positive moment for interior girder.

$S_x = 1062\ \text{in.}^3$ composite section.

$$F_{LL+I} = \frac{DF_{int}}{DF_{ext}} \frac{M_{LL+I}}{2.171 S_x} = \left(\frac{1.29}{1.38}\right)\left(\frac{22{,}980}{2.171(1062)}\right)$$

$F_{LL+I} = 9.3$ ksi for exterior girder

E) Group load combinations II and III for interior girder.

Group II: $F = 1.3(F_{DL} + F_W)$

$F = 1.3(7.5 + 21.2) = 37.3 \text{ ksi} > 36 \text{ ksi}$ N.G.

Group III: $F = 1.3(F_{DL} + F_{LL+I} + .3F_W)$

$F = 1.3(7.5 + 9.3 + .3(21.2)) = 30.1 \text{ ksi} < 36 \text{ ksi}$ O.K.

Combined stress for Group II exceeds limit.

APPENDIX C

FINITE ELEMENT ANALYSIS RESULTS

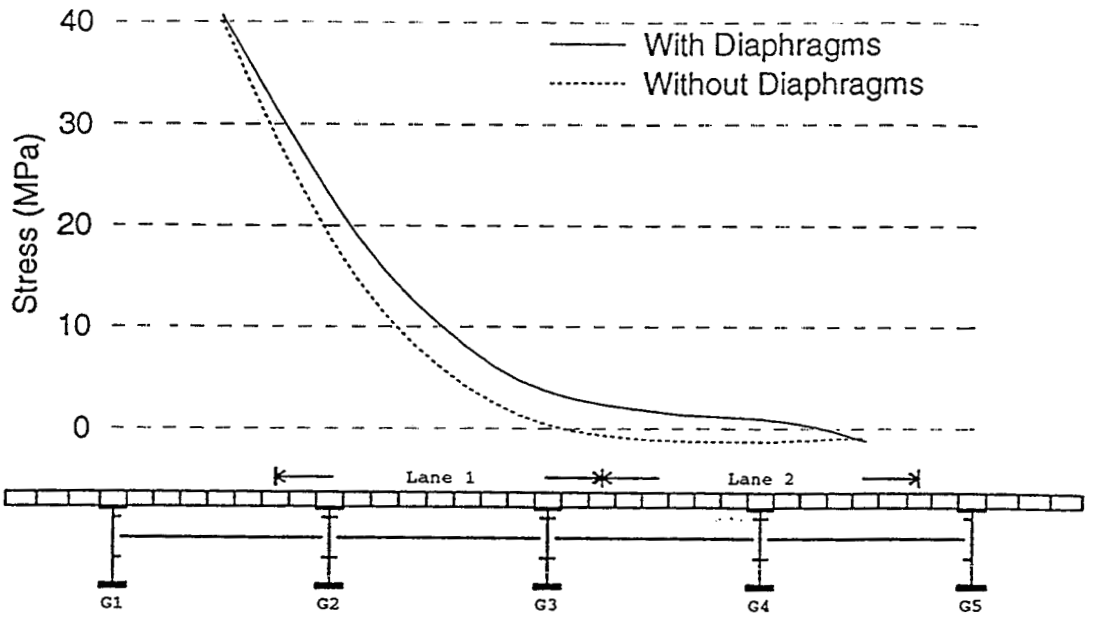

Figure C1. Influence line for bottom flange stress in girder G1 of bridge A2

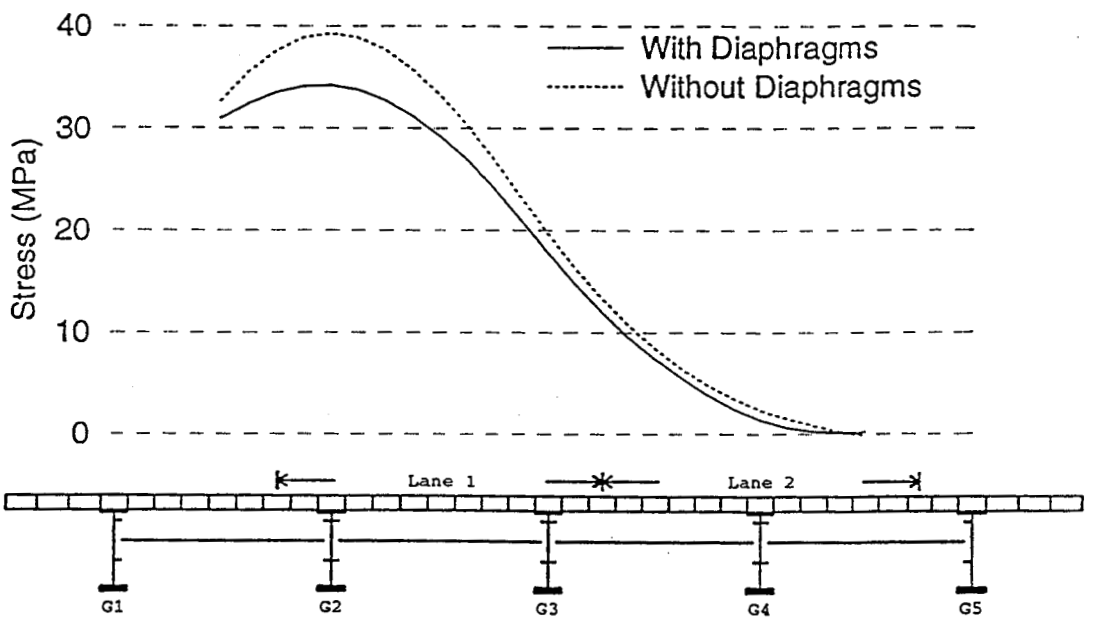

Figure C2. Influence line for bottom flange stress in girder G2 of bridge A2

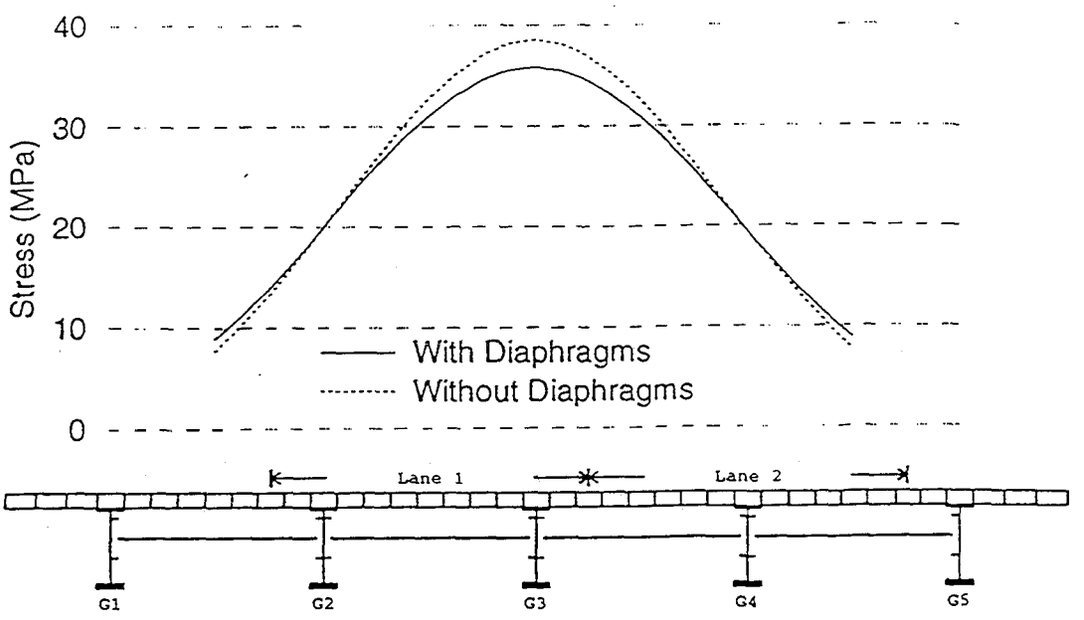

Figure C3. Influence line for bottom flange stress in girder G3 of bridge A2

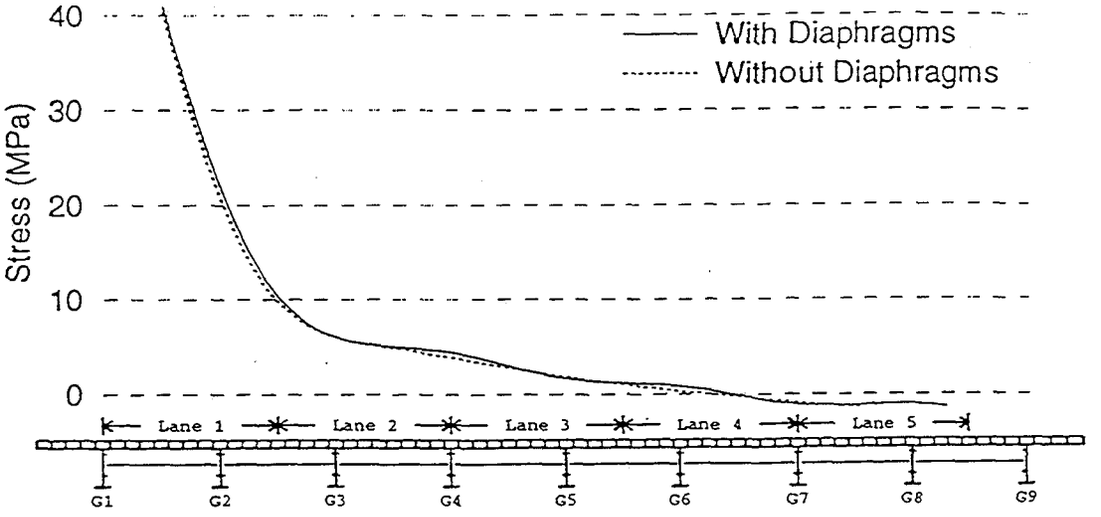

Figure C4. Influence line for bottom flange stress in girder G1 of bridge A3

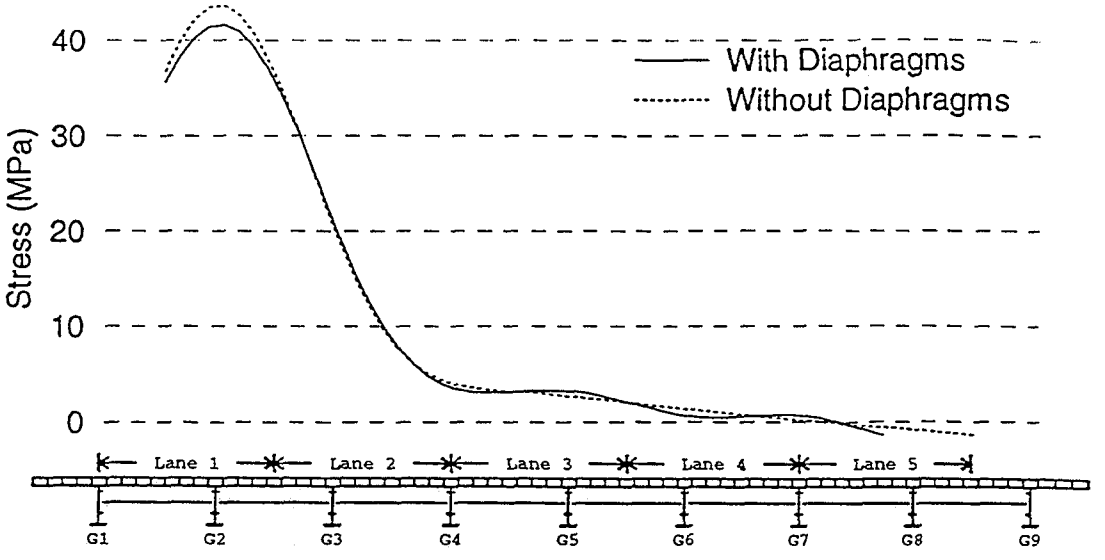

Figure C5. Influence line for bottom flange stress in girder G2 of bridge A3

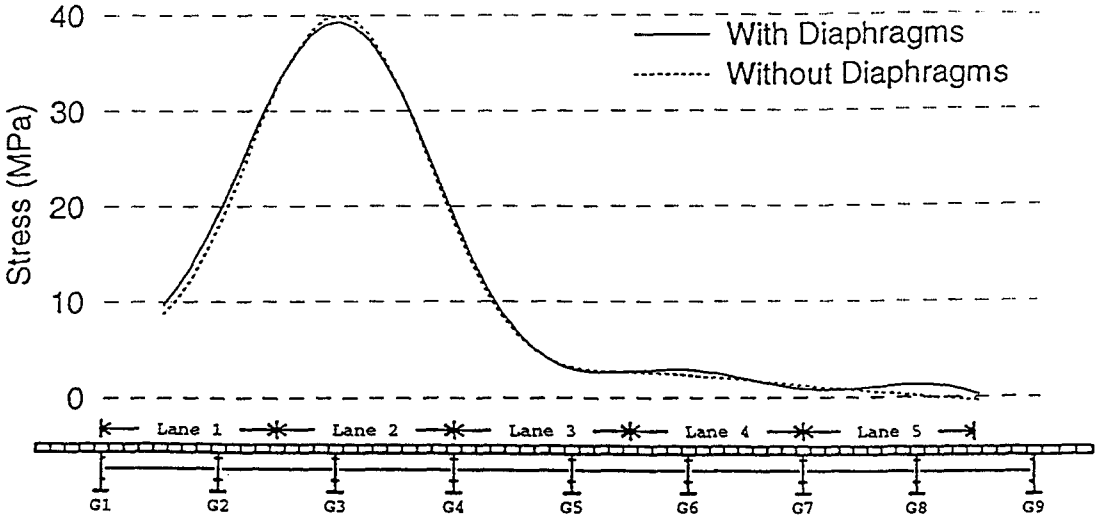

Figure C6. Influence line for bottom flange stress in girder G3 of bridge A3

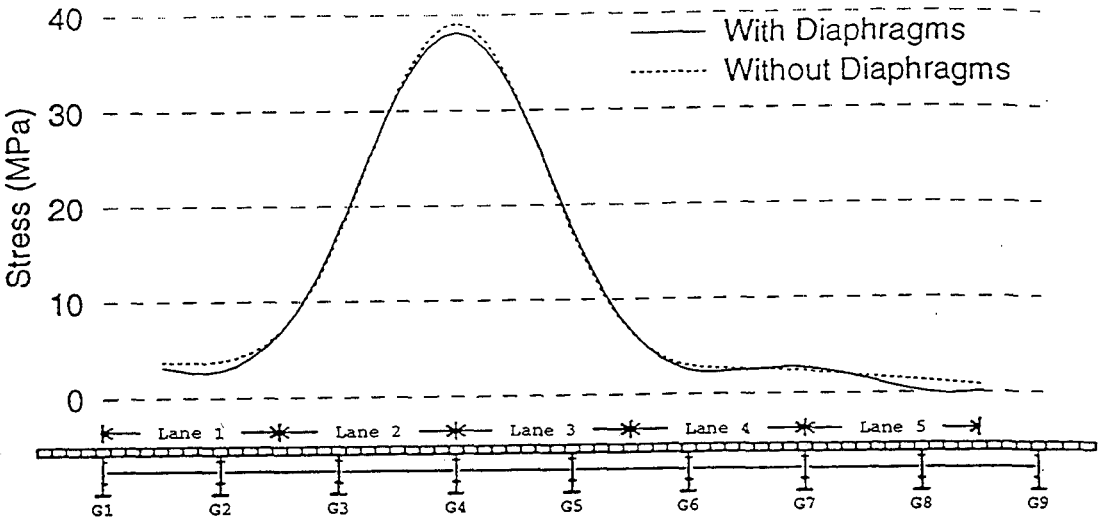

Figure C7. Influence line for bottom flange stress in girder G4 of bridge A3

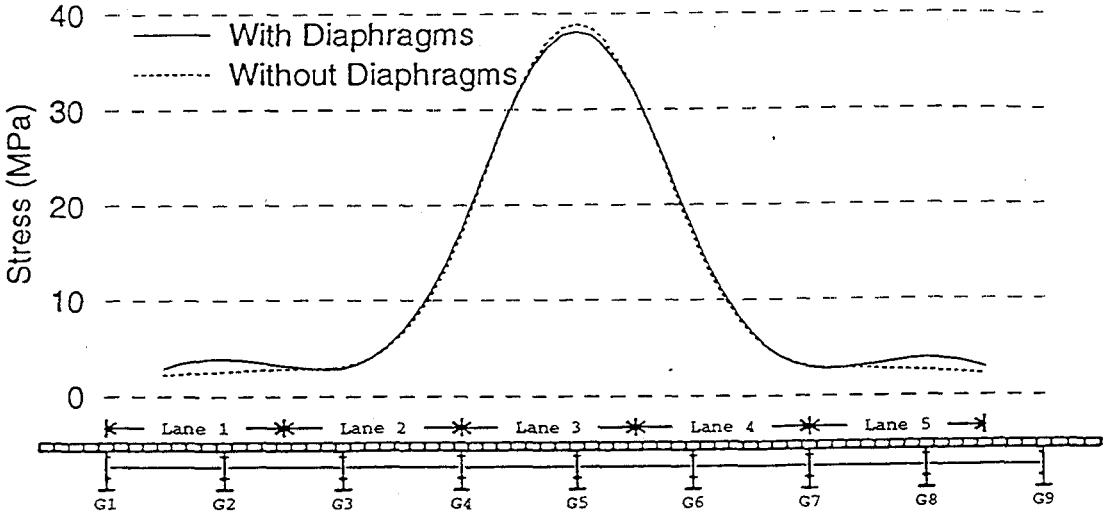

Figure C8. Influence line for bottom flange stress in girder G5 of bridge A3

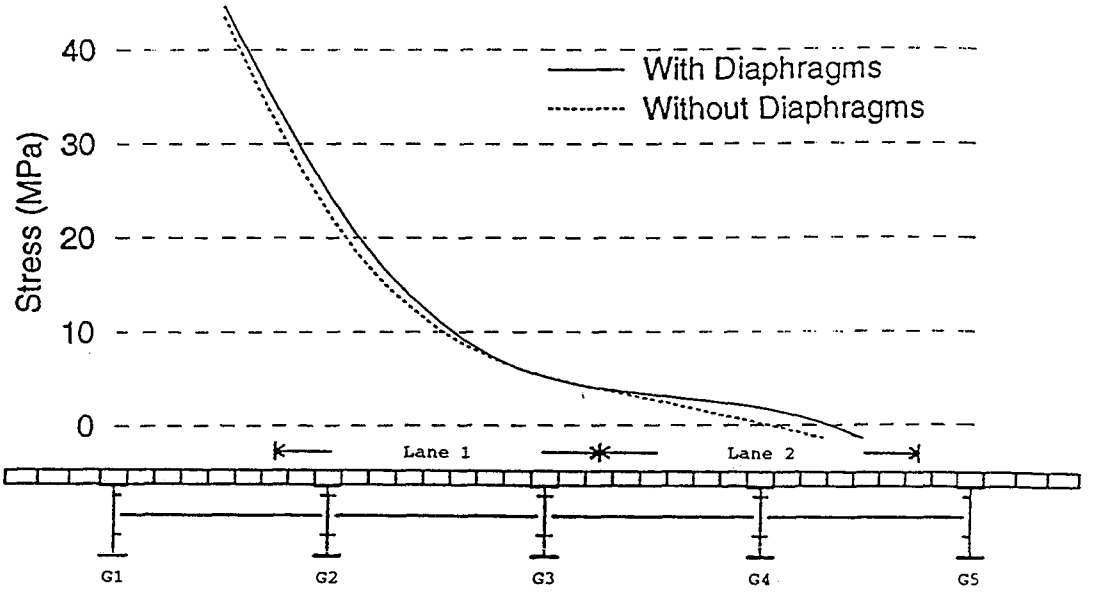

Figure C9. Influence line for bottom flange stress in girder G1 of bridge A4

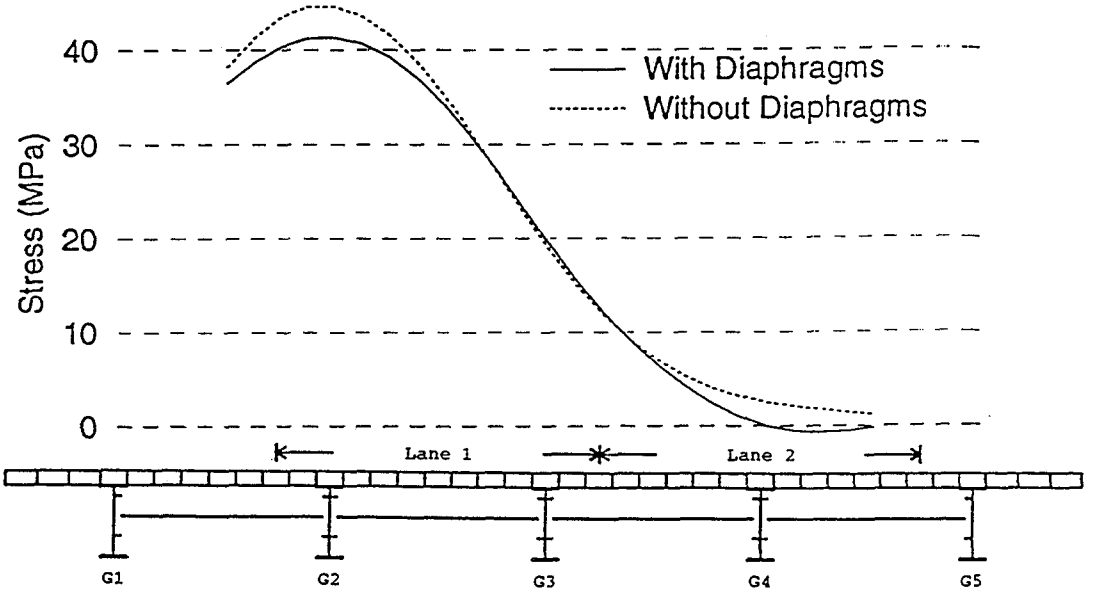

Figure C10. Influence line for bottom flange stress in girder G2 of bridge A4

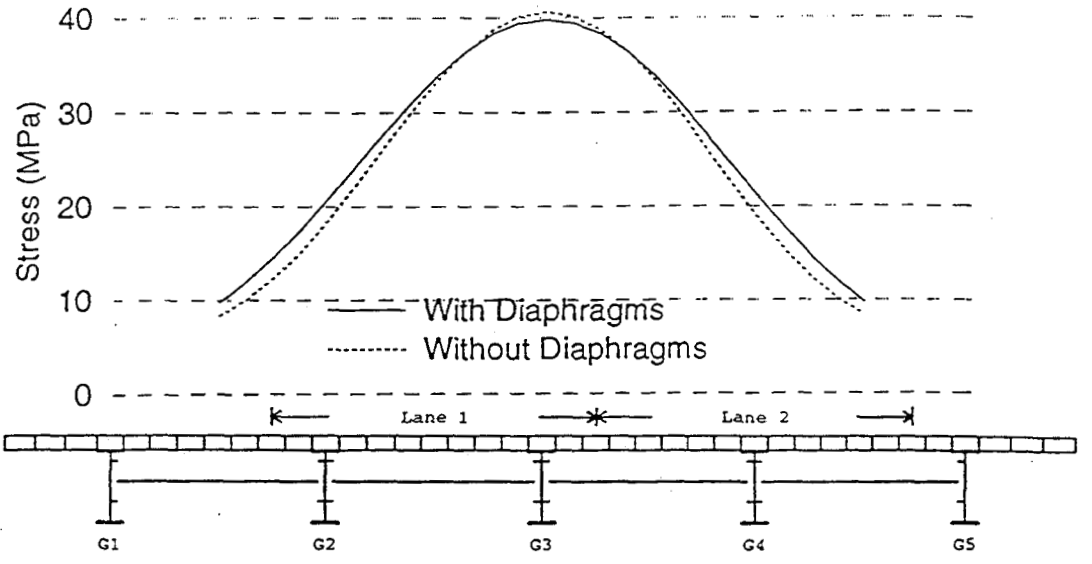

Figure C11. Influence line for bottom flange stress in girder G3 of bridge A4

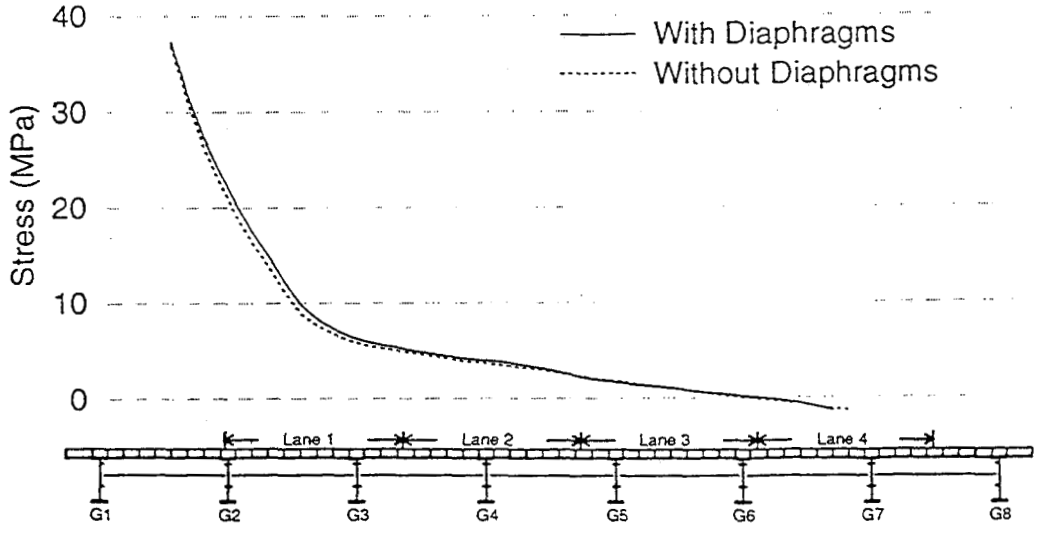

Figure C12. Influence line for bottom flange stress in girder G1 of bridge A5

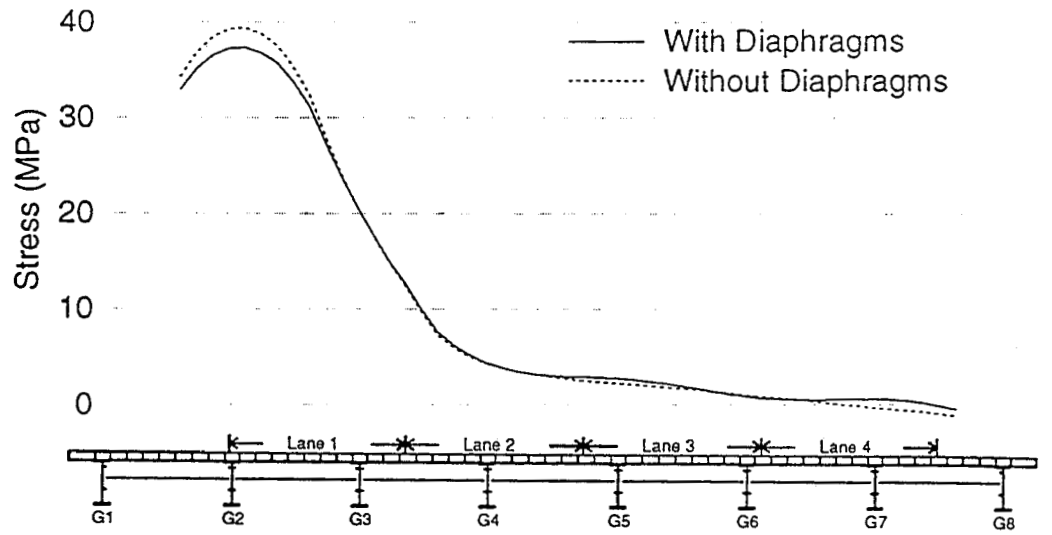

Figure C13. Influence line for bottom flange stress in girder G2 of bridge A5

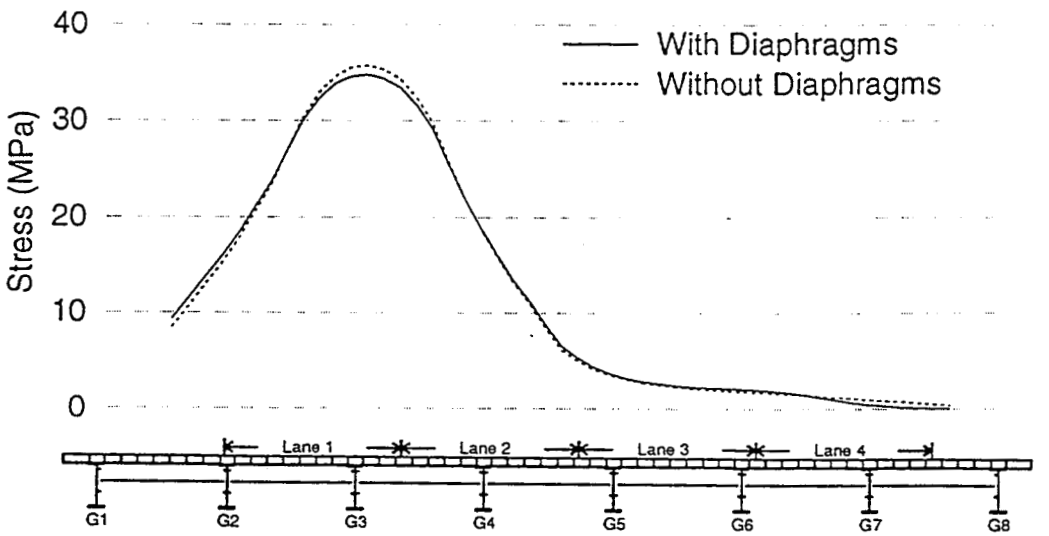

Figure C14. Influence line for bottom flange stress in girder G3 of bridge A5

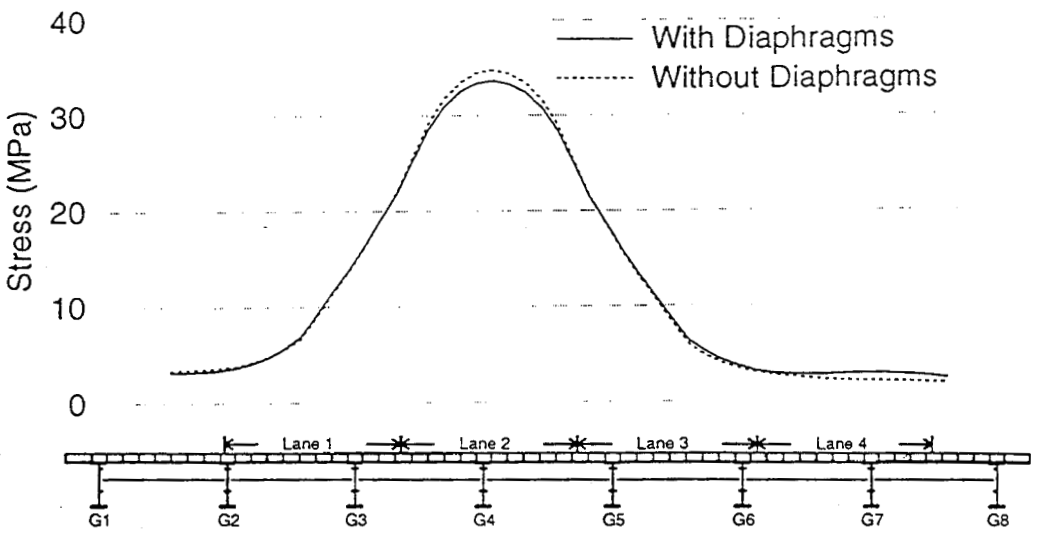

Figure C15. Influence line for bottom flange stress in girder G4 of bridge A5

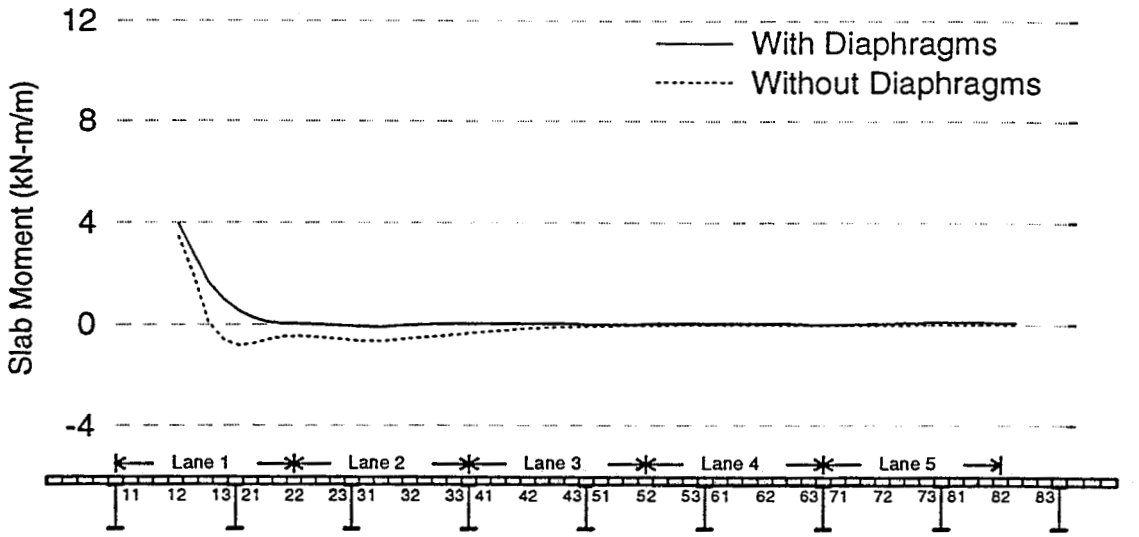

Figure C16. Deck slab bending moment influence line for bridge A1, panel 1

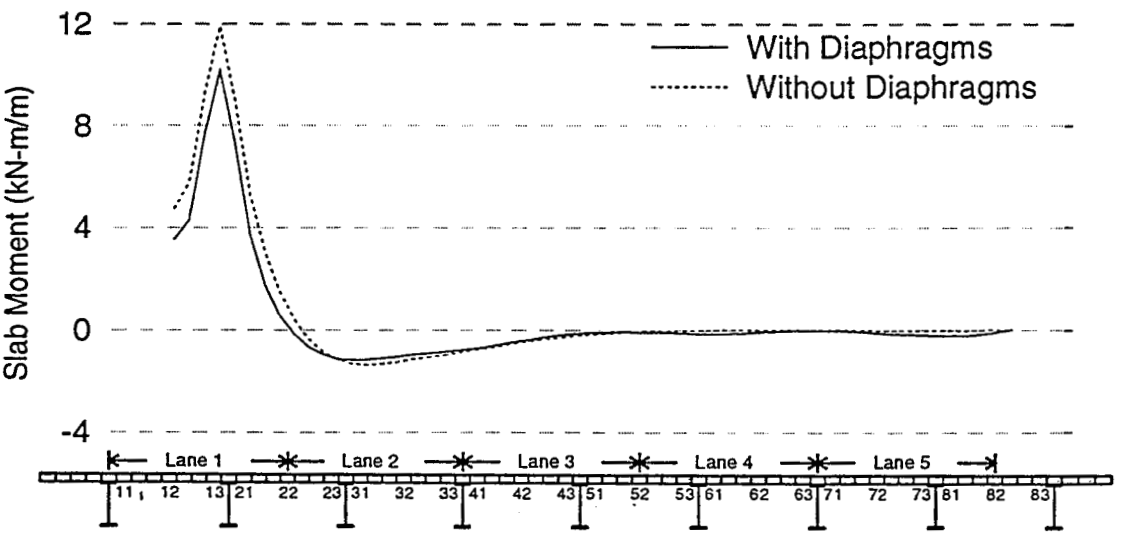

Figure C17. Deck slab bending moment influence line for bridge A2, panel 1

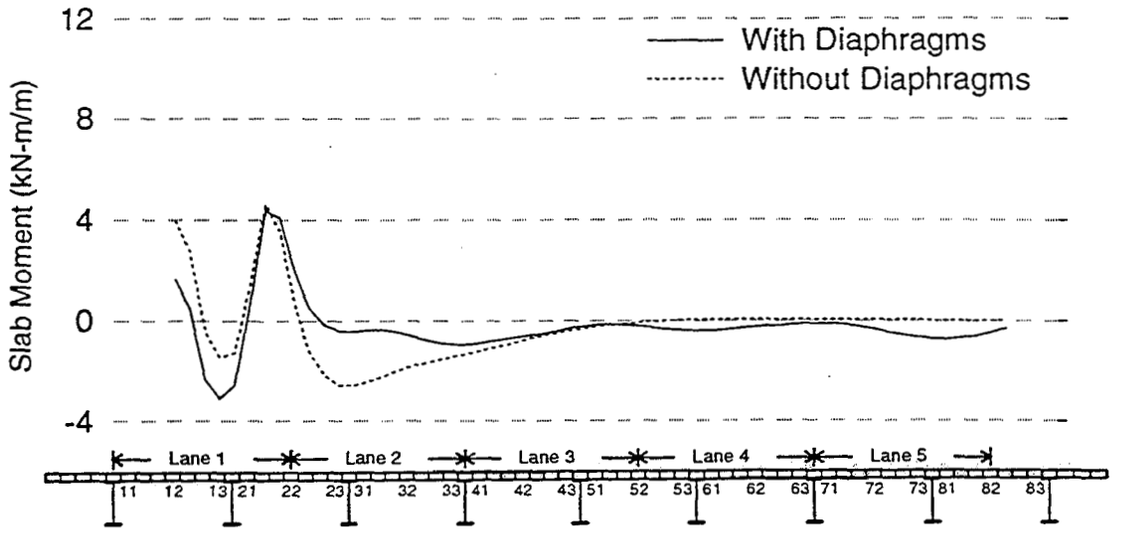

Figure C18. Deck slab bending moment influence line for bridge A3, panel 1

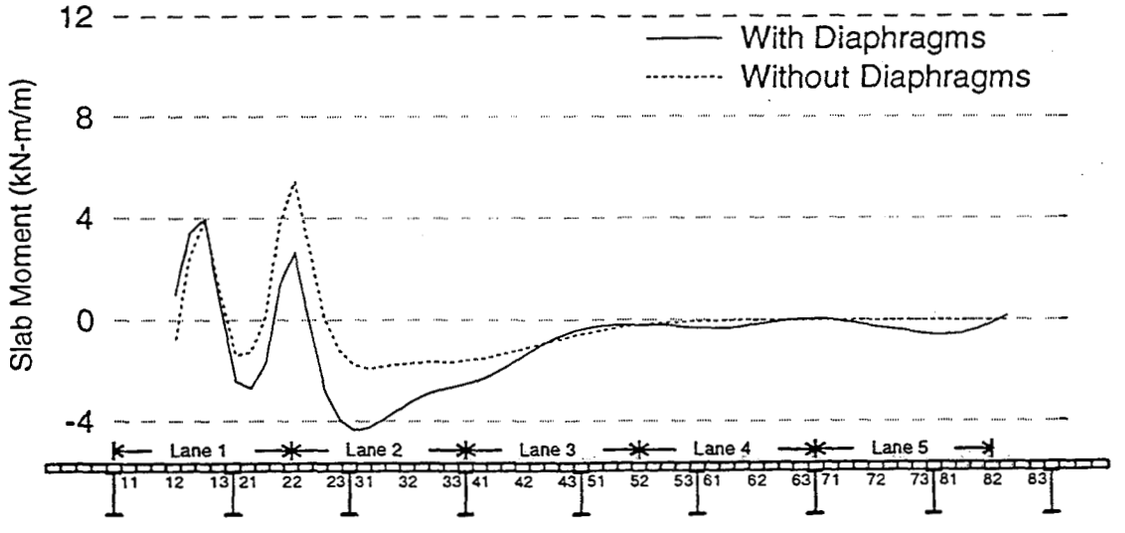

Figure C19. Deck slab bending moment influence line for bridge A1, panel 2

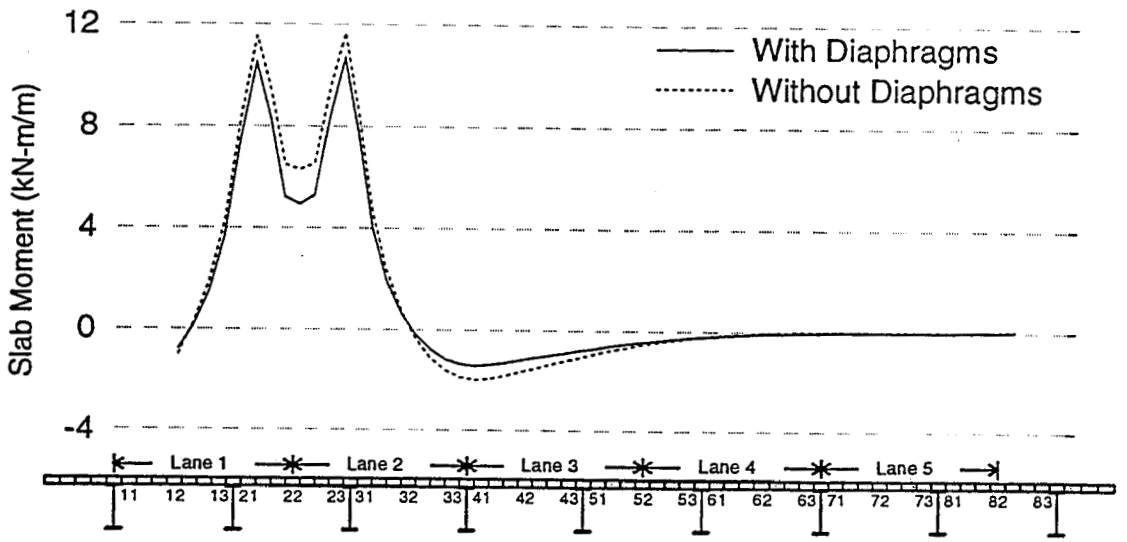

Figure C20. Deck slab bending moment influence line for bridge A2, panel 2

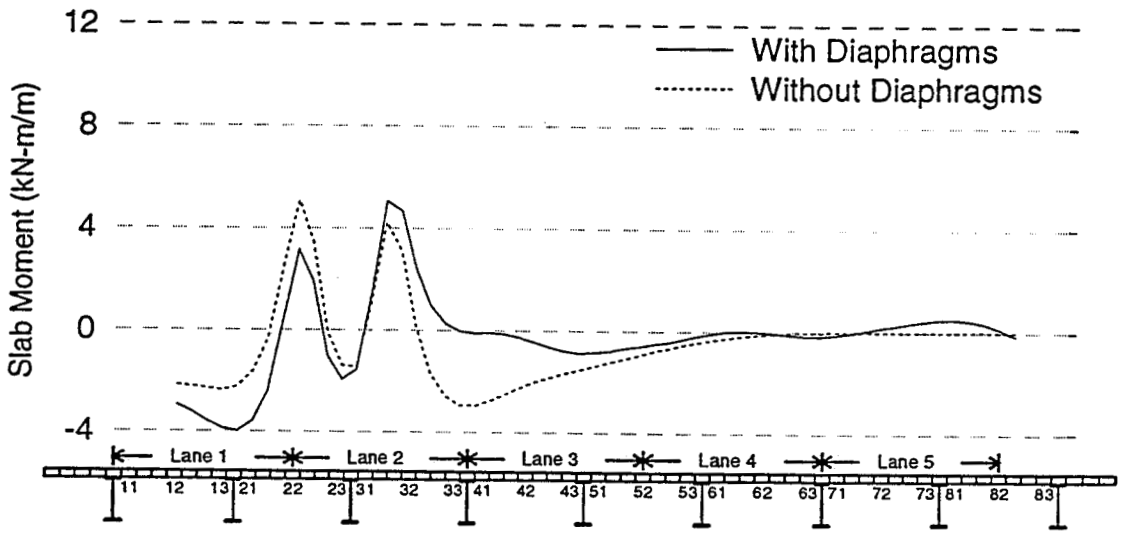

Figure C21. Deck slab bending moment influence line for bridge A3, panel 2

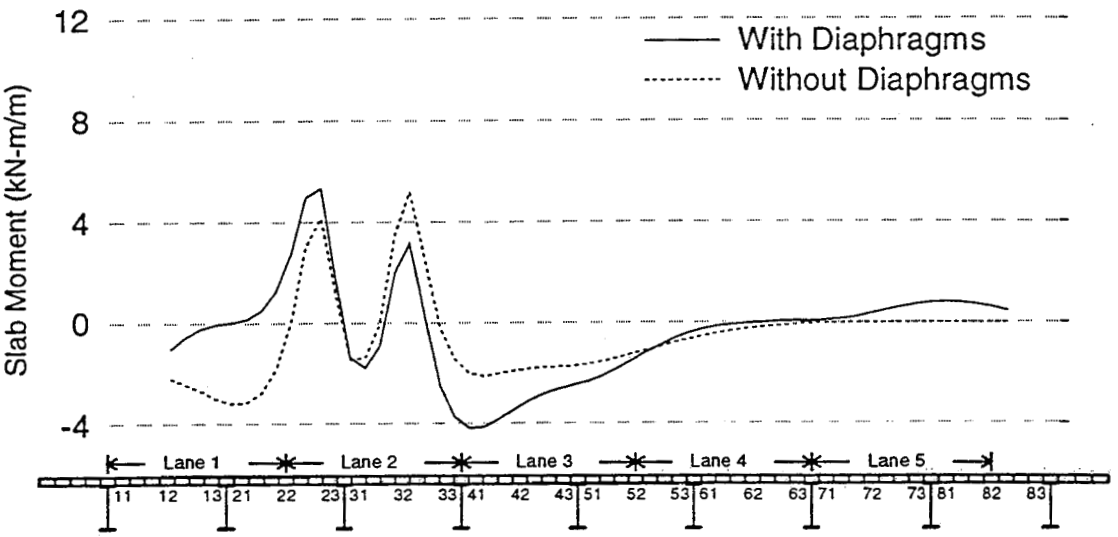

Figure C22. Deck slab bending moment influence line for bridge A1, panel 3

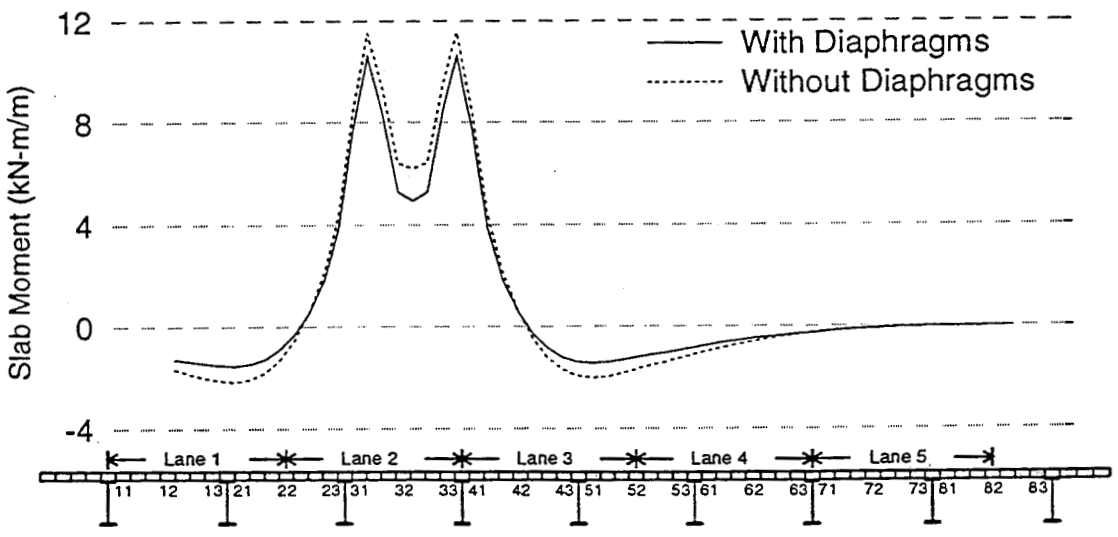

Figure C23. Deck slab bending moment influence line for bridge A2, panel 3

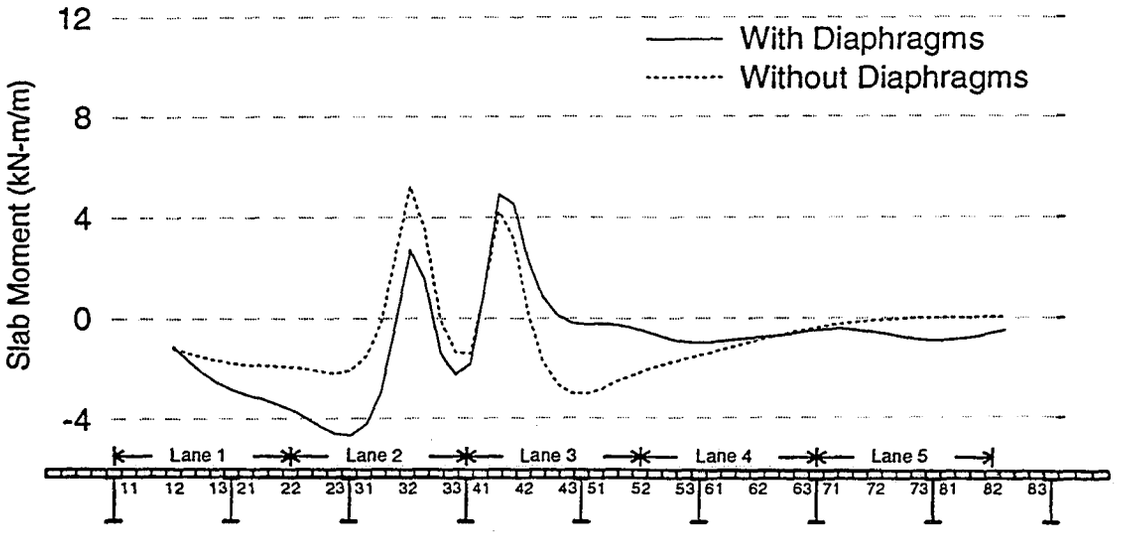

Figure C24. Deck slab bending moment influence line for bridge A3, panel 3

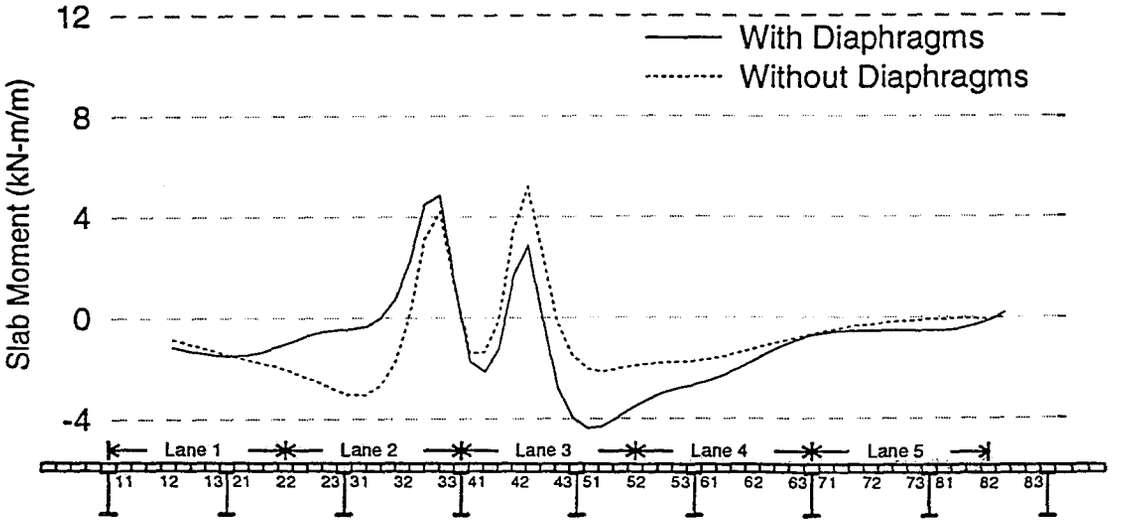

Figure C25. Deck slab bending moment influence line for bridge A1, panel 4

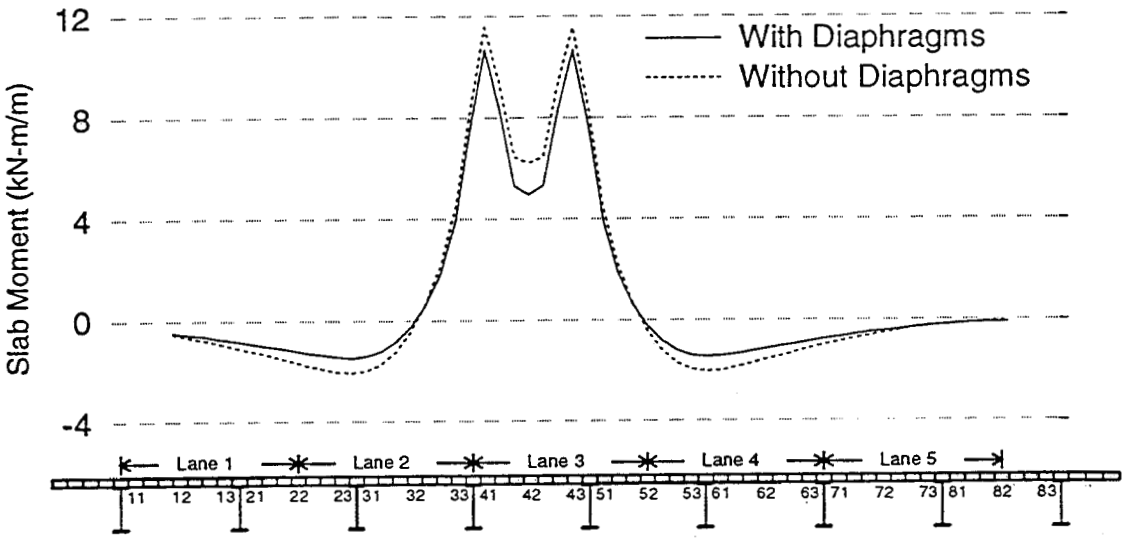

Figure C26. Deck slab bending moment influence line for bridge A2, panel 4

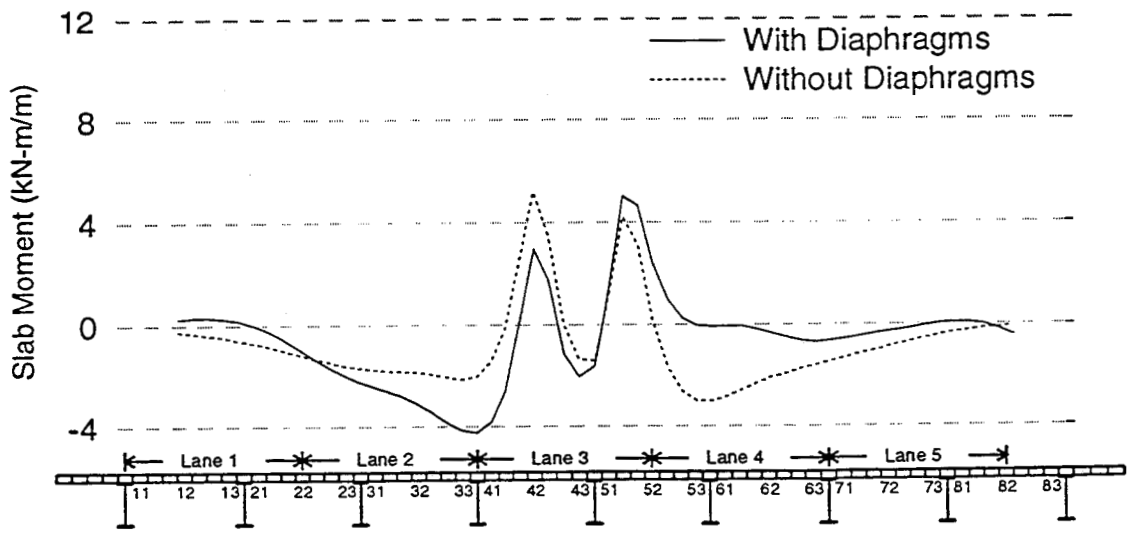

Figure C27. Deck slab bending moment influence line for bridge A3, panel 4

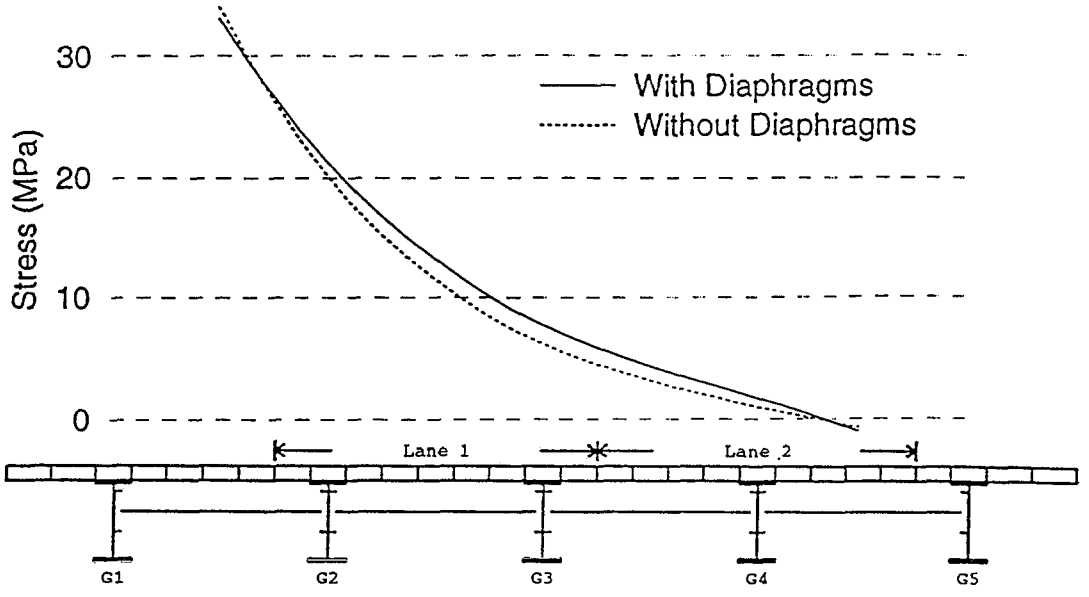

Figure C28. Influence line for bottom flange stress in girder G1 of bridge B2

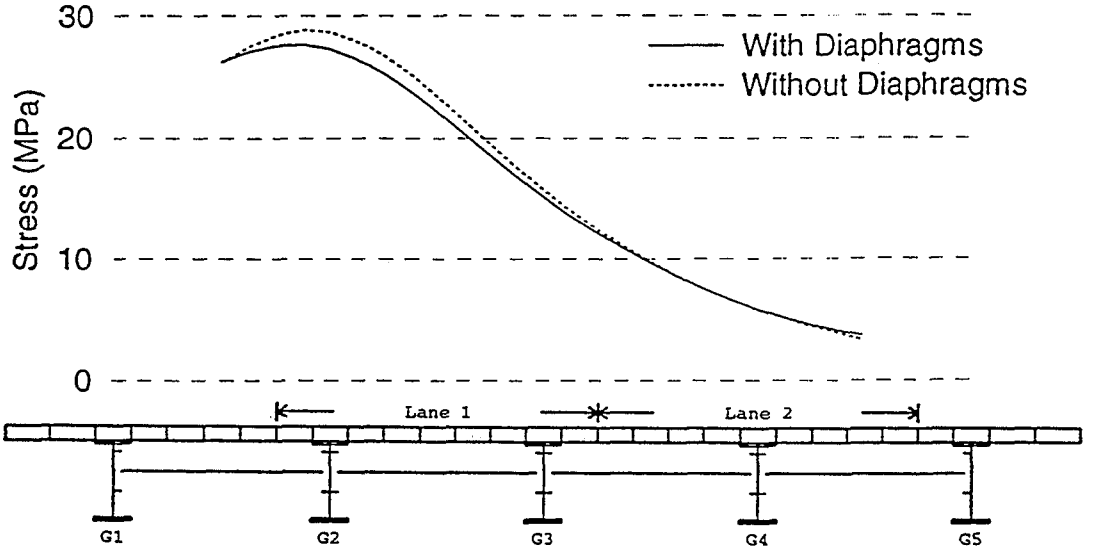

Figure C29. Influence line for bottom flange stress in girder G2 of bridge B2

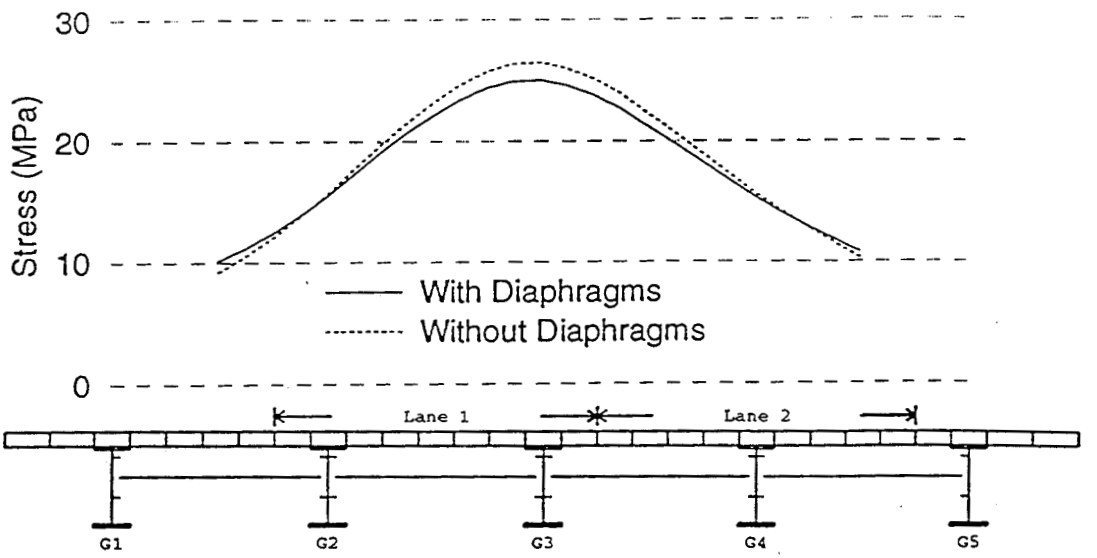

Figure C30. Influence line for bottom flange stress in girder G3 of bridge B2

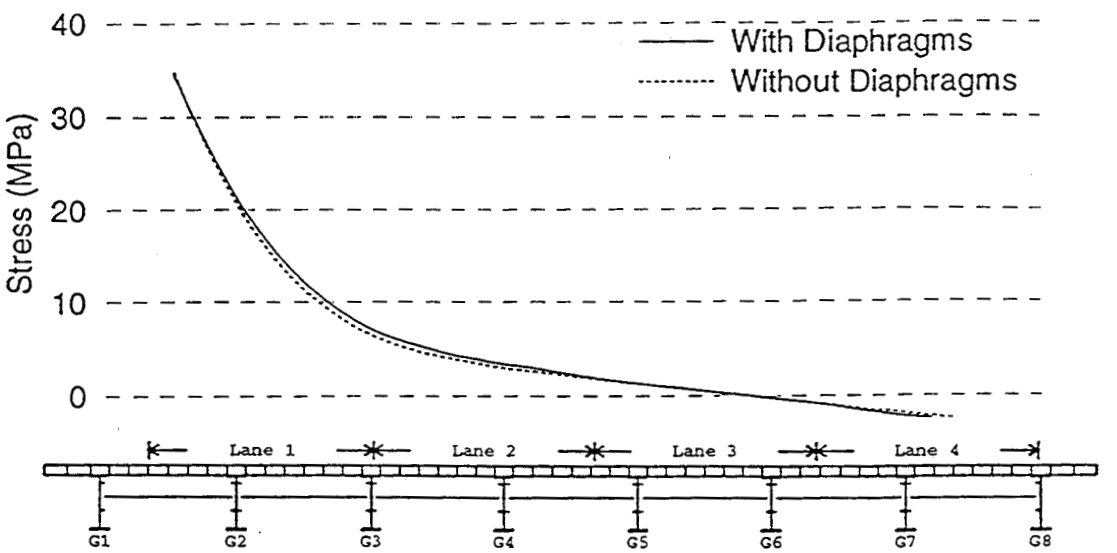

Figure C31. Influence line for bottom flange stress in girder G1 of bridge B3

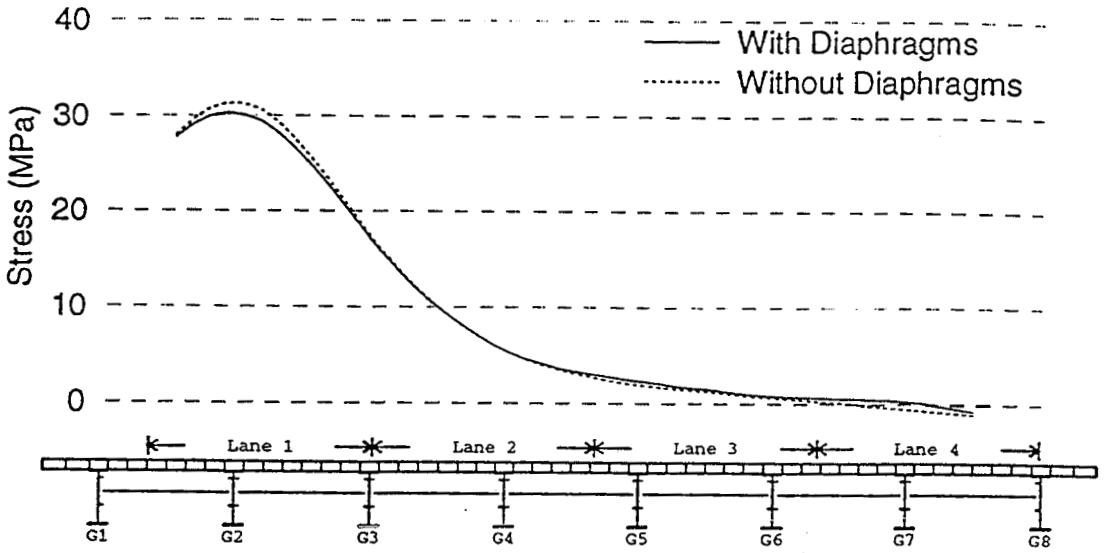

Figure C32. Influence line for bottom flange stress in girder G2 of bridge B3

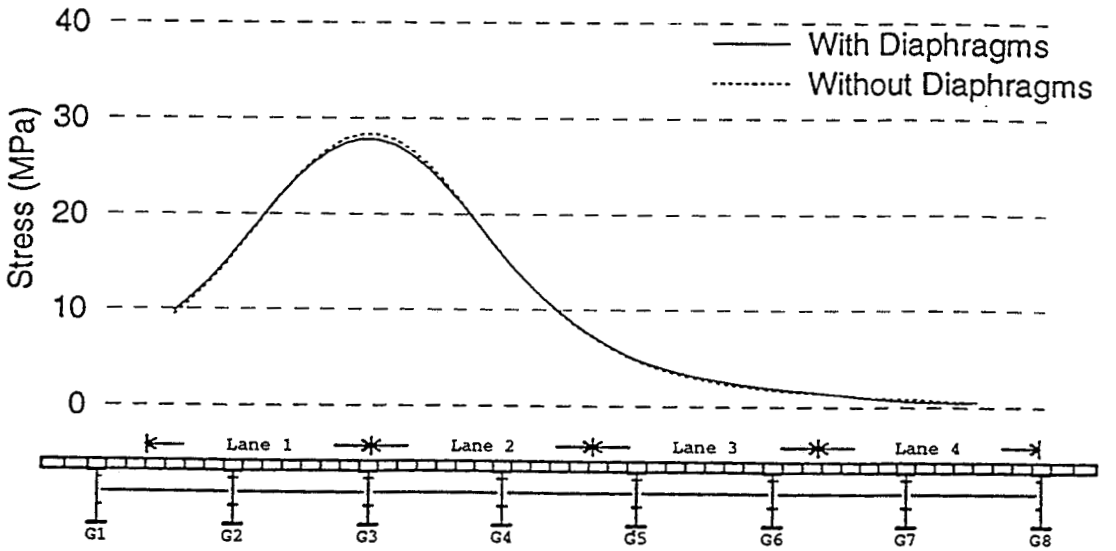

Figure C33. Influence line for bottom flange stress in girder G3 of bridge B3

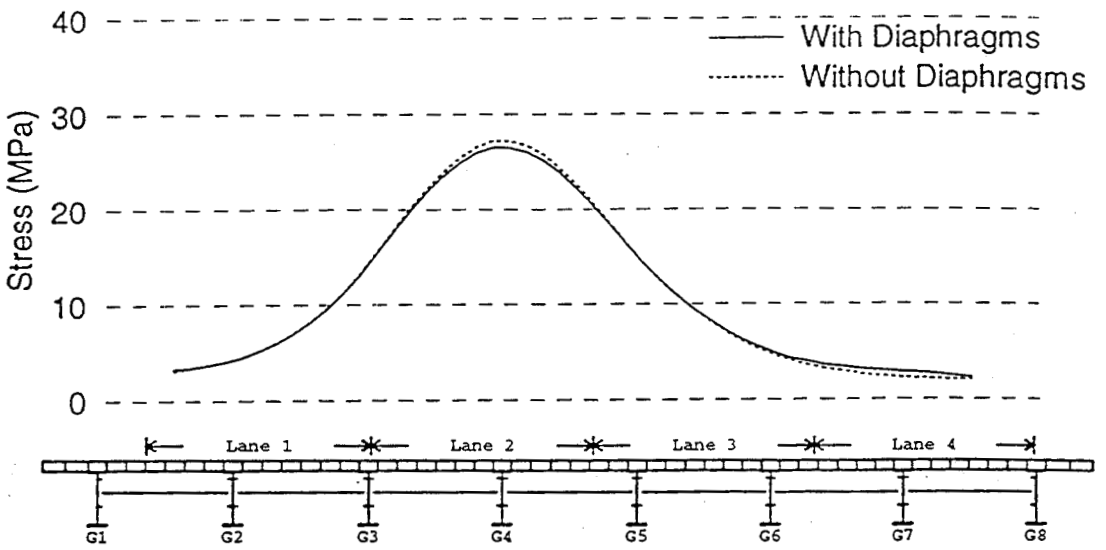

Figure C34. Influence line for bottom flange stress in girder G4 of bridge B3

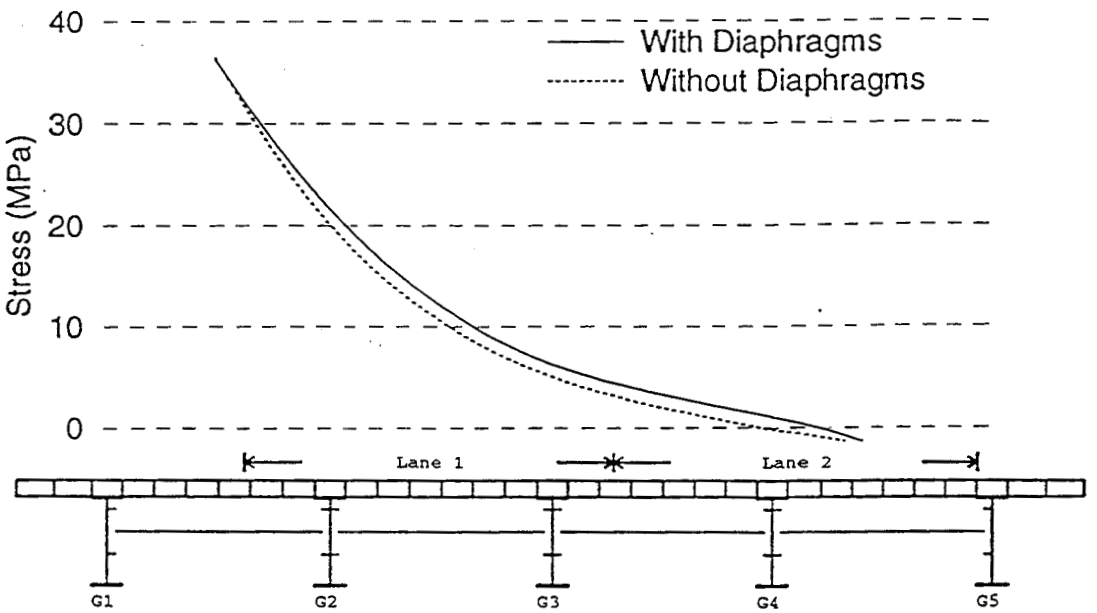

Figure C35. Influence line for bottom flange stress in girder G1 of bridge B4

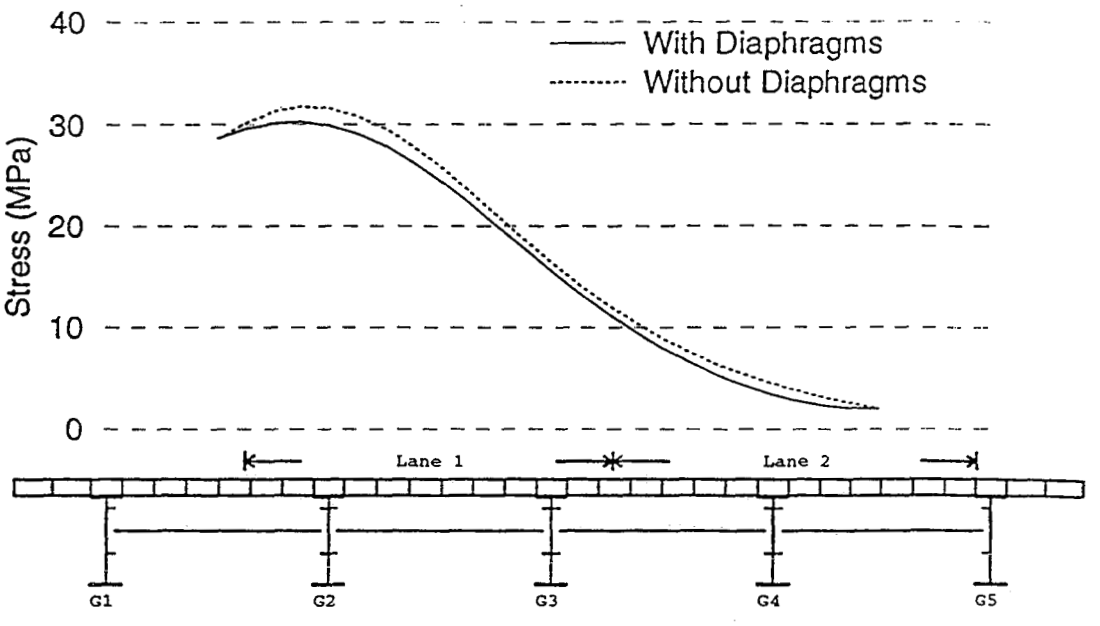

Figure C36. Influence line for bottom flange stress in girder G2 of bridge B4

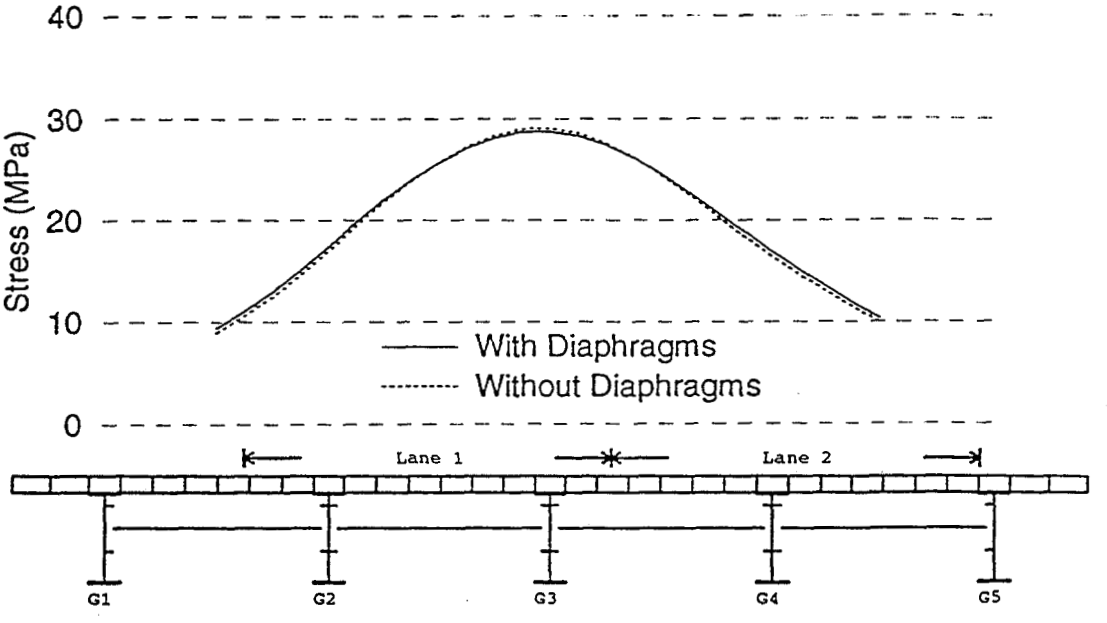

Figure C37. Influence line for bottom flange stress in girder G3 of bridge B4

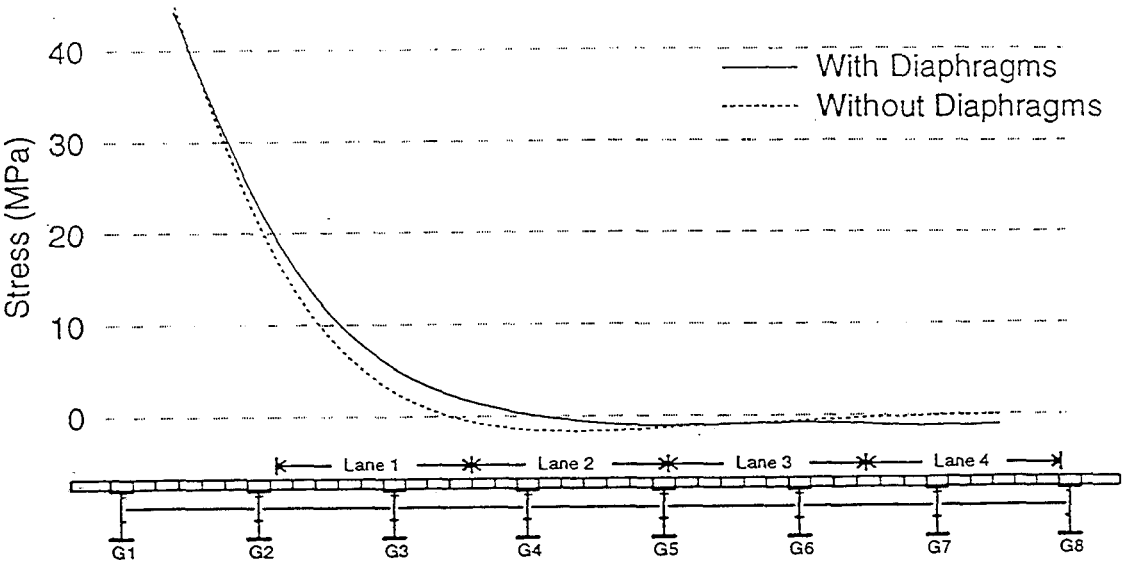

Figure C 38. Influence line for bottom flange stress in girder G1 span 2, bridge C1; truck on span 2

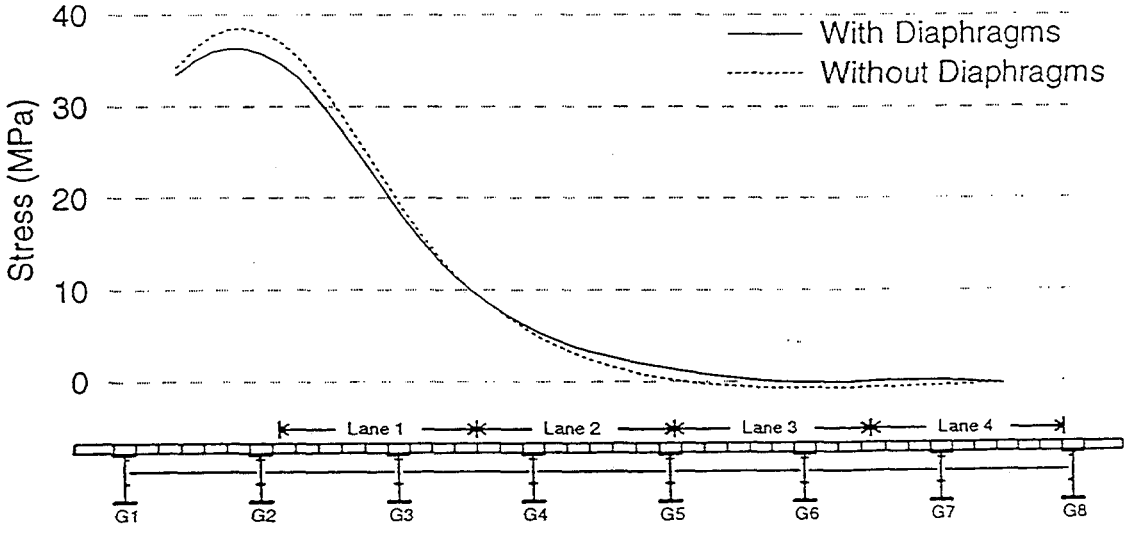

Figure C 39. Influence line for bottom flange stress in girder G2 span 2, bridge C1; truck on span 2

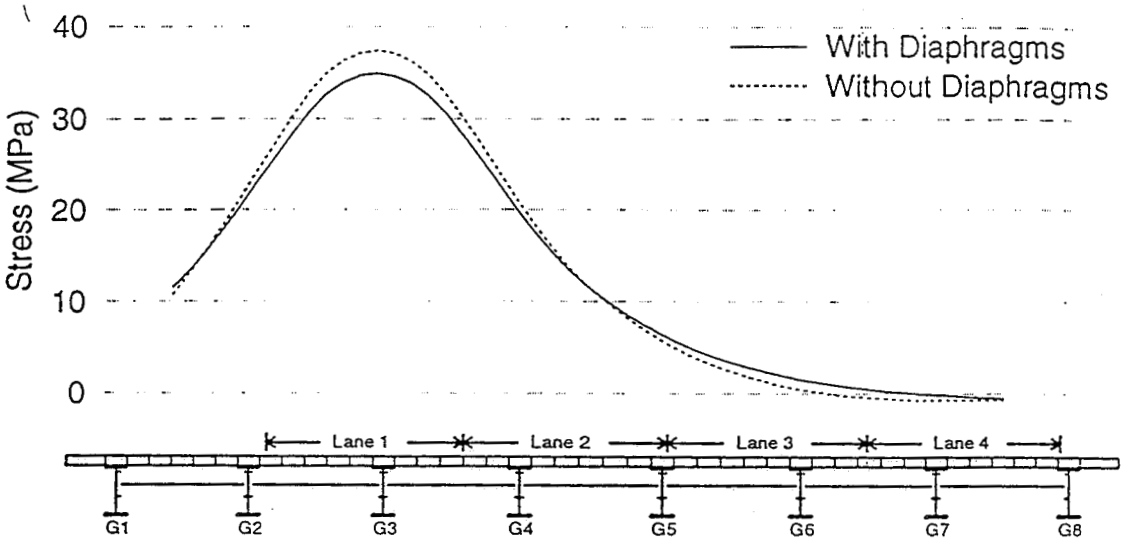

Figure C 40. Influence line for bottom flange stress in girder G3 span 2, bridge C1; truck on span 2

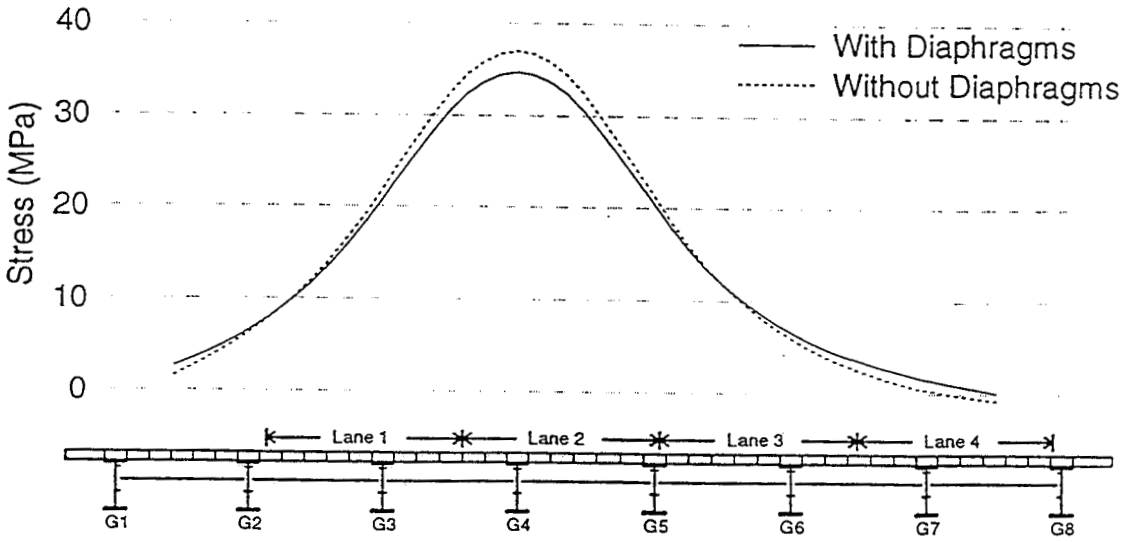

Figure C 41. Influence line for bottom flange stress in girder G4 span 2, bridge C1; truck on span 2

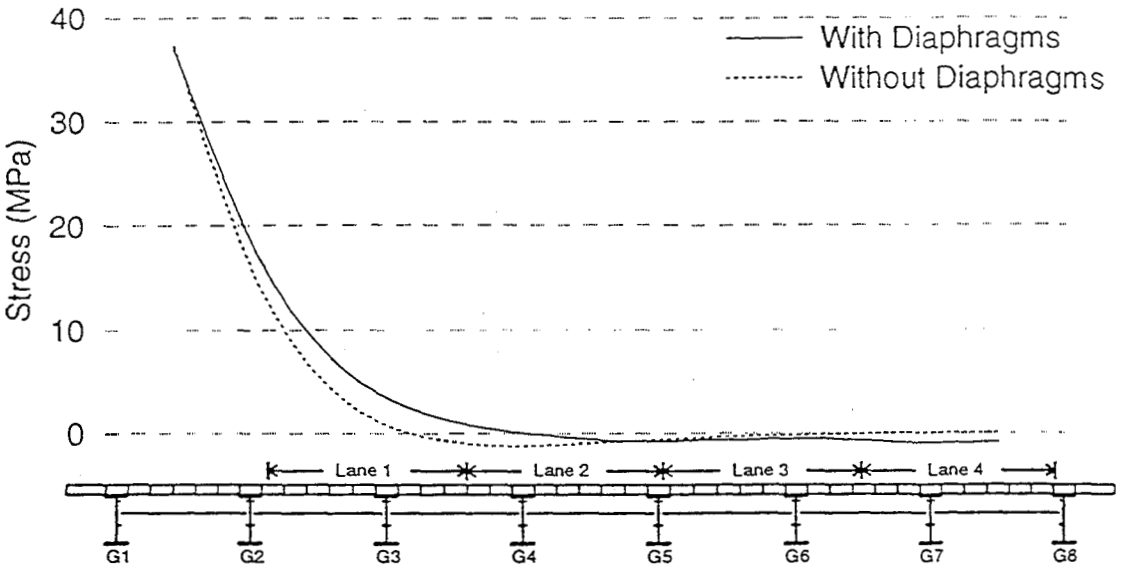

Figure C 42. Influence line for bottom flange stress in girder G1 span 2, bridge C2; truck on span 2

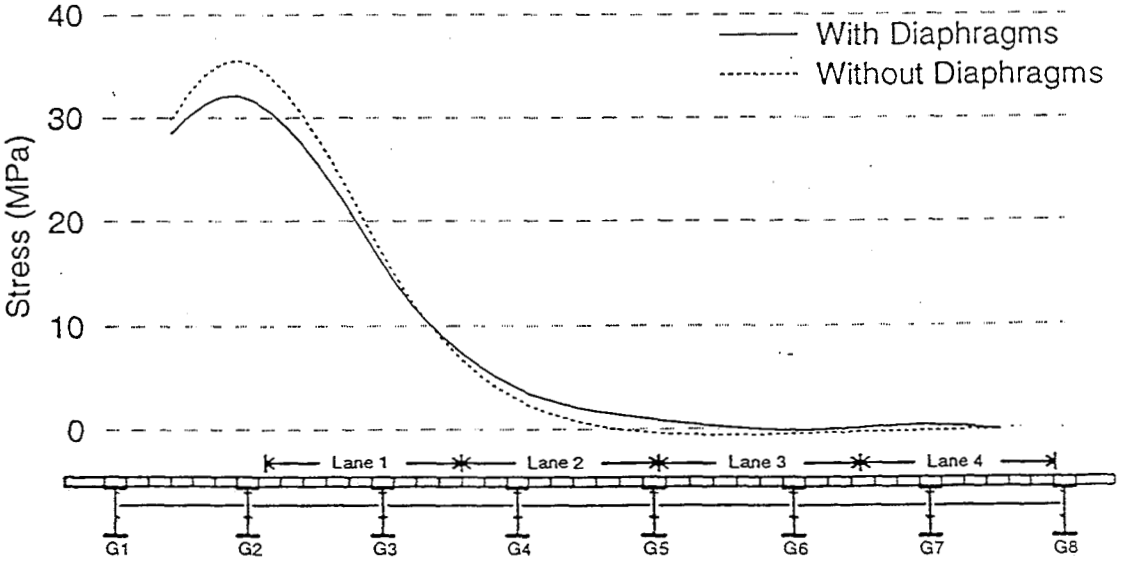

Figure C 43. Influence line for bottom flange stress in girder G2 span 2, bridge C2; truck on span 2

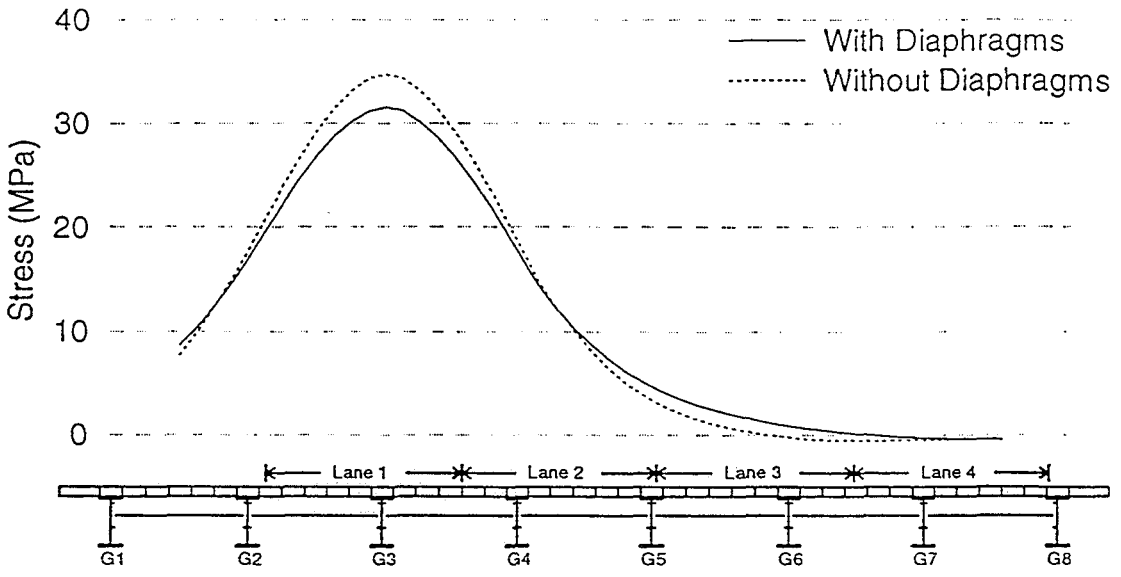

Figure C 44. Influence line for bottom flange stress in girder G3 span 2, bridge C2; truck on span 2

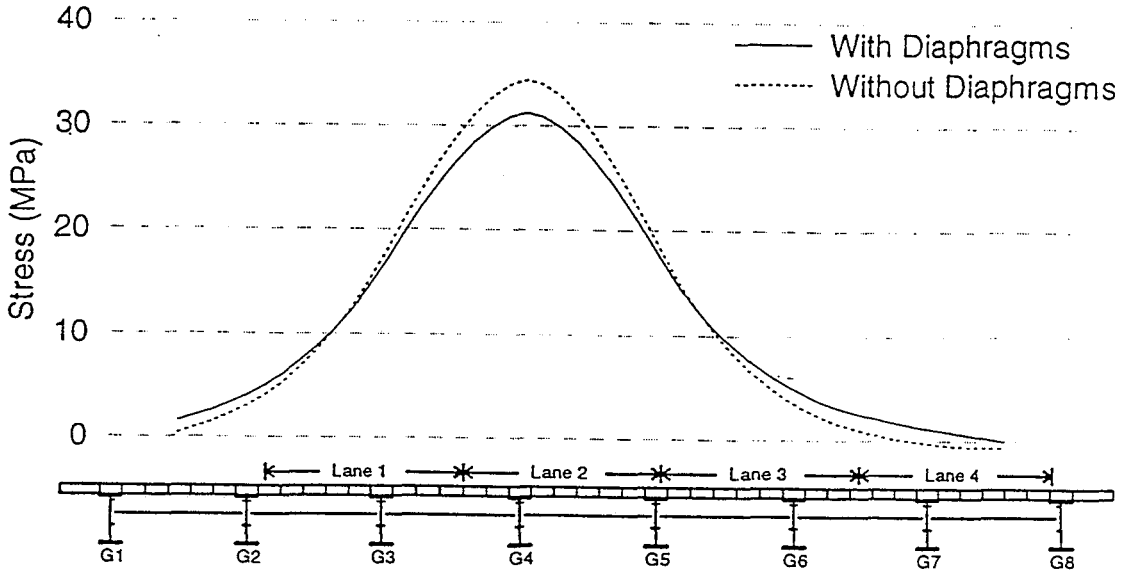

Figure C 45. Influence line for bottom flange stress in girder G4 span 2, bridge C2; truck on span 2

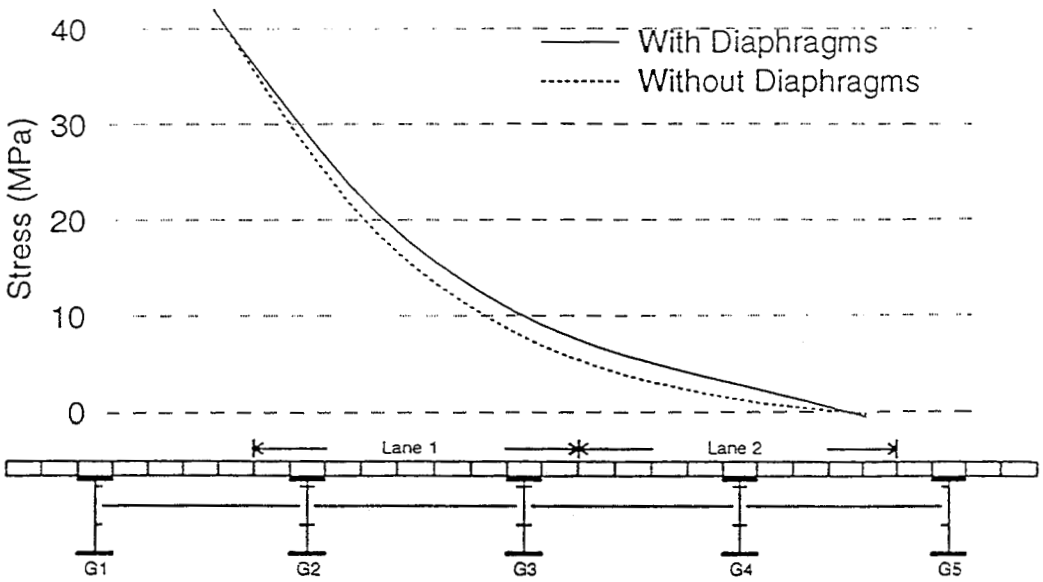

Figure C 46. Influence line for bottom flange stress in girder G1 span 2, bridge C3; truck on span 2

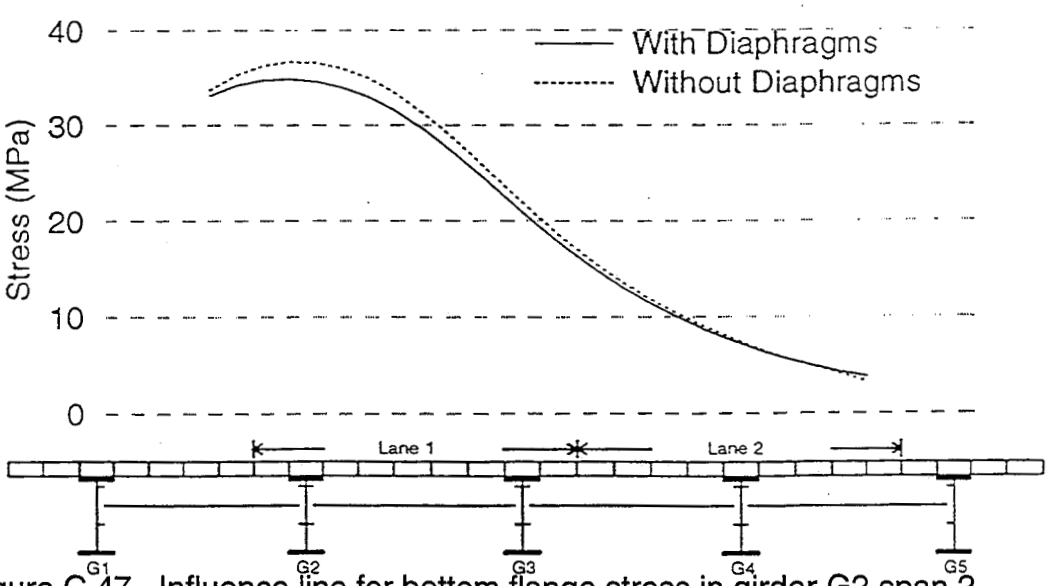

Figure C 47. Influence line for bottom flange stress in girder G2 span 2, bridge C3; truck on span 2

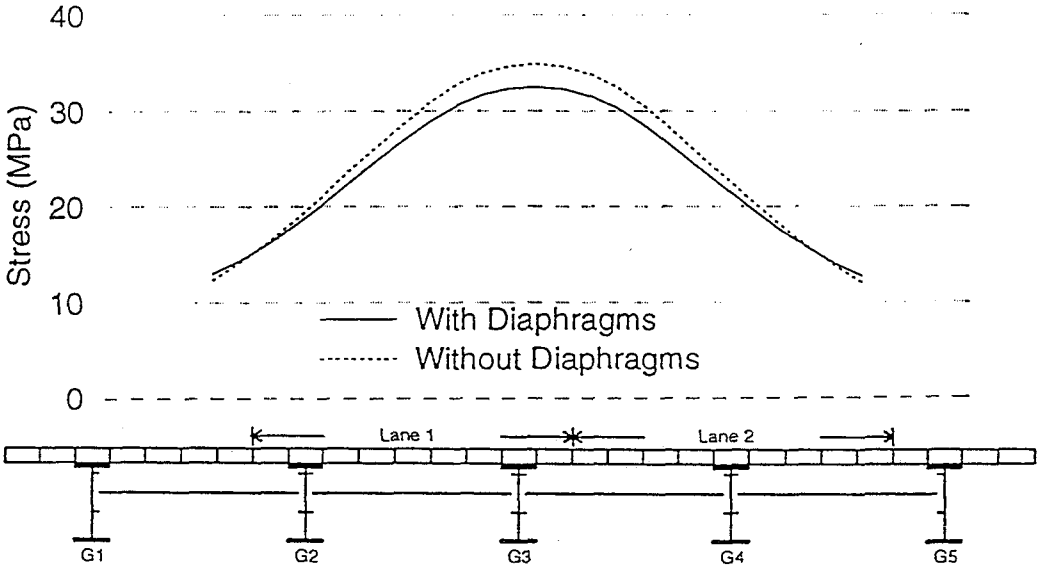

Figure C 48. Influence line for bottom flange stress in girder G3 span 2, bridge C3; truck on span 2

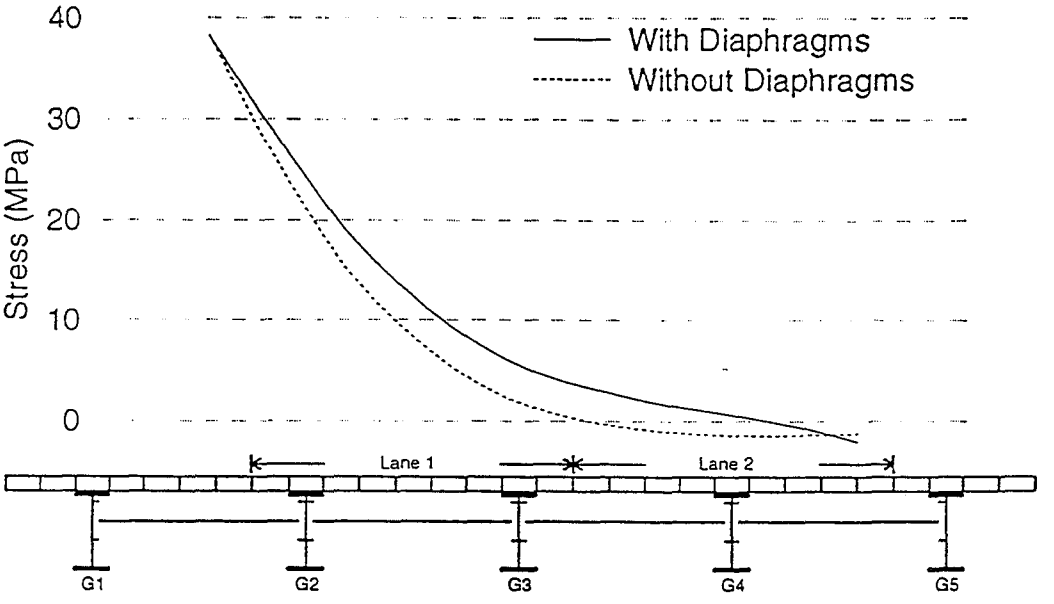

Figure C 49. Influence line for bottom flange stress in girder G1 span 2, bridge C4; truck on span 2

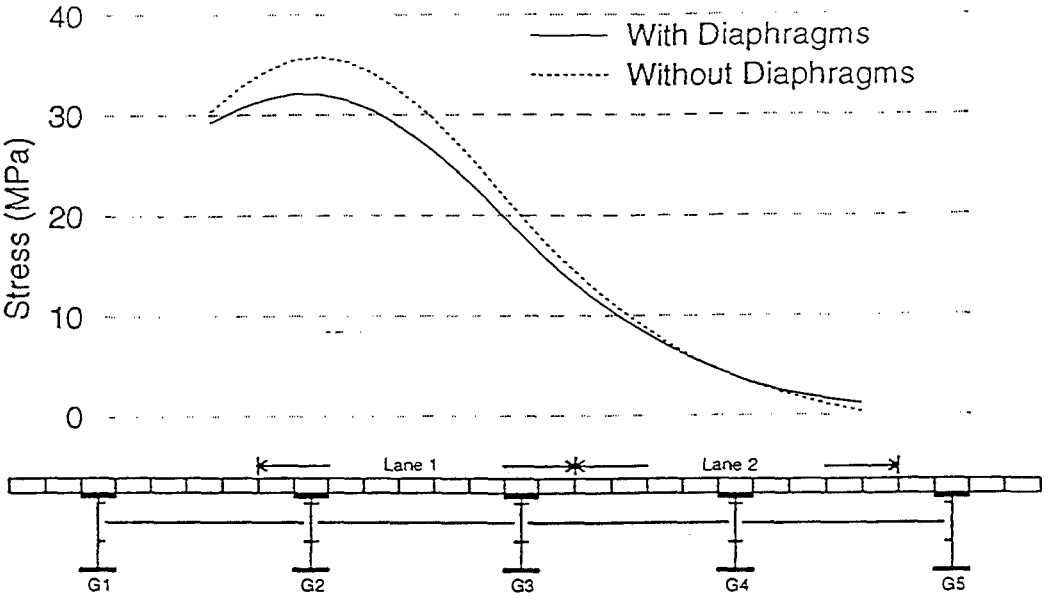

Figure C 50. Influence line for bottom flange stress in girder G2 span 2, bridge C4; truck on span 2

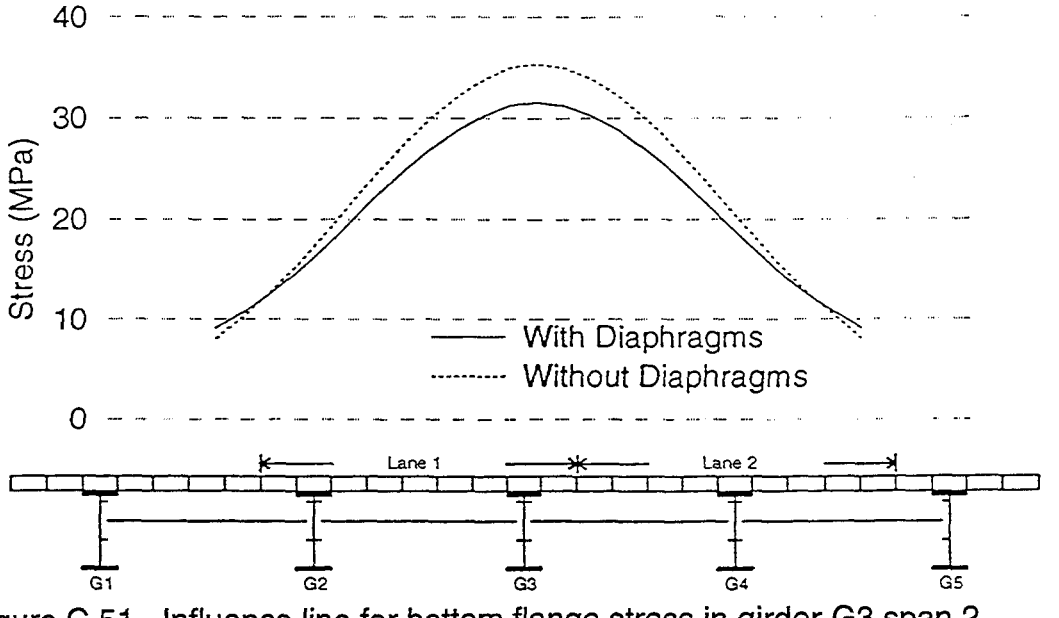

Figure C 51. Influence line for bottom flange stress in girder G3 span 2, bridge C4; truck on span 2